Oxidative Medicine and Cellular Longevity

Aging, Metabolic, and Degenerative Disorders: Biomedical Value of Antioxidants

Lead Guest Editor: Mohamed M. Abdel-Daim
Guest Editors: Nadia I. Zakhary, Lotfi Aleya, Simona G. Bungău, Raghvendra A. Bohara, and Nikhat J. Siddiqi

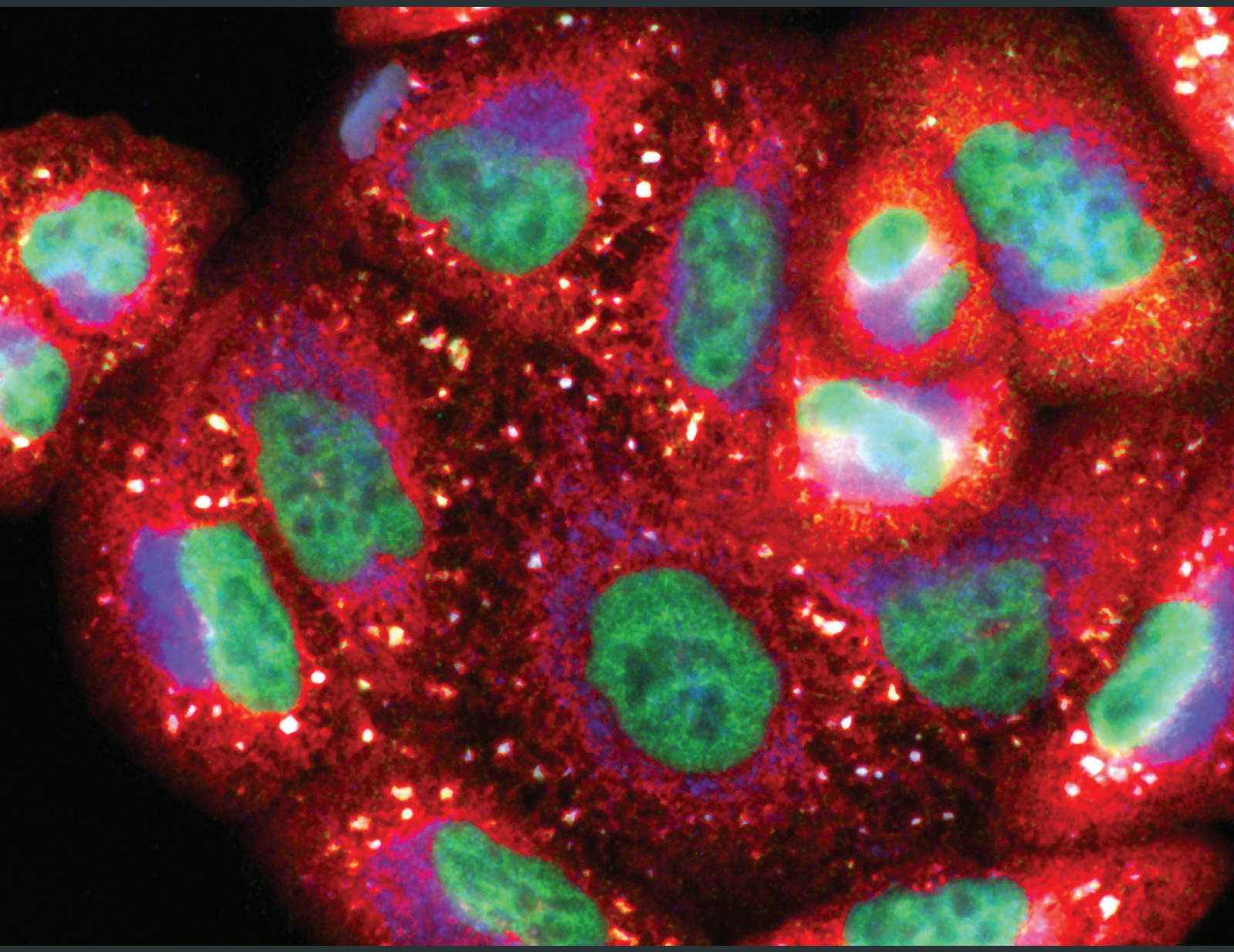

Aging, Metabolic, and Degenerative Disorders: Biomedical Value of Antioxidants

Oxidative Medicine and Cellular Longevity

Aging, Metabolic, and Degenerative Disorders: Biomedical Value of Antioxidants

Lead Guest Editor: Mohamed M. Abdel-Daim
Guest Editors: Nadia I. Zakhary, Lotfi Aleya, Simona G. Bungau, and Raghvendra A. Bohara

Editorial Board

Contents

Hindawi
Oxidative Medicine and Cellular Longevity
Volume 2018, Article ID 2098123, 2 pages
https://doi.org/10.1155/2018/2098123

Editorial

Aging, Metabolic, and Degenerative Disorders: Biomedical Value of Antioxidants

Mohamed M. Abdel-Daim,[1,2] **Nadia I. Zakhary**,[3] **Lotfi Aleya**,[4] **Simona G. Bungău**,[5] **Raghvendra A. Bohara**,[6] **and Nikhat J. Siddiqi**[7]

[1]*Pharmacology Department, Faculty of Veterinary Medicine, Suez Canal University, Ismailia 41522, Egypt*
[2]*Department of Ophthalmology and Micro-Technology, Yokohama City University, Yokohama, Japan*
[3]*Cancer Biology Department, National Cancer Institute, Cairo University, Cairo 11796, Egypt*
[4]*Chrono-Environment Laboratory, Bourgogne Franche-Comté University, UMR CNRS 6249, 25030 Besançon Cedex, France*
[5]*Pharmacy Department, Faculty of Medicine and Pharmacy, University of Oradea, Oradea, Romania*
[6]*Centre for Interdisciplinary Research, D. Y. Patil University, Kolhapur 416006, India*
[7]*Department of Biochemistry, College of Science, King Saud University, Riyadh 11495, Saudi Arabia*

Correspondence should be addressed to Mohamed M. Abdel-Daim; abdeldaim.m@vet.suez.edu.eg

Received 7 March 2018; Accepted 7 March 2018; Published 10 April 2018

Oxidative stress is a common aetiological factor in aging, metabolic diseases, and degenerative disorders. The body contains an endogenous antioxidant system to help neutralize reactive oxygen species and mitigate oxidative damage. Every living cell survives when there is a balance between the oxidative stress generated and the counter antioxidant system present. Once this harmony is disrupted, the generated stress loads on the cell and starts to exert pathological, metabolic, and degenerative effects. Antioxidants have been proven to ameliorate drug toxicity [1], carcinogenesis [2], and neurodegenerative processes [3, 4]. In this special issue, several articles have proposed different molecular mechanisms to mitigate oxidative stress and prevent aging, metabolic, and degenerative disorders.

For example, S. M. Ahmed et al. searched and analyzed previous animal studies to develop a conclusive systematic review discussing the use of different types of mesenchymal stromal cells (MSCs) for the treatment of acute and chronic pancreatitis and pancreatic fibrosis. They concluded that bone marrow and umbilical cord MSCs were the most frequently administered cell types. In addition, they did not recommend clinical trials to investigate the use of MSCs as therapy for pancreatitis due to the insufficiency of published data.

In cardiovascular research, S. I. Khan et al. evaluated the effects of febuxostat and allopurinol on a rat model of ischemia-reperfusion (IR) injury and concluded that febuxostat had more potent protective activities than allopurinol against IR injury by inhibiting apoptosis (MAPK) and inflammation (NF-κBp65/TNF-α) pathways. In another study, N. M. Al-Rasheed et al. investigated the potential cardioprotective effect of simvastatin on a diabetic cardiomyopathy (DCM) rat model and suggested that simvastatin ameliorates DCM by attenuating inflammation, oxidative stress, and apoptosis, induced by hyperglycemia and hyperlipidemia.

In the field of diabetes research, B. Assefa et al. investigated the mechanisms underlying insulin-like growth factor binding protein-2- (IGFBP-2-) stimulated glucose uptake in adipocytes and concluded that the potentiating effects of IGFBP-2 on 3T3-L1 adipocyte GU are independent of its binding to IGF-1 and might occur, which was mediated through the activation of PI3K/Akt, AMPK/TBC1D1, and PI3K/PKCζ/λ/GLUT-4 signaling. In addition, H. M. A.

Abdelrazek et al. evaluated the protective role of black seed oil (NSO) active constituent in streptozotocin-induced diabetic rats and showed that NSO improved oxidative stress, hepatic glycogen storage, and pancreatic islet insulin secretion.

Another study in oncology, performed by E. A. Toraih et al., examined the expression of miR-34a and miR-11 of its bioinformatically selected target genes and proteins to test their potential dysregulation in renal cell carcinoma tumorigenesis and cancer progression. Moreover, Z. You et al. evaluated the alleviating role of fermented papaya extracts (FPEs) in estrogen- and progestogen-induced mammary gland hyperplasia via their antioxidant activities and inhibition of DNA damage.

T.-Y. Song et al. showed the possible protective effects of ergothioneine and hispidin on methylglyoxal-induced neuronal cell hyperglycemic damage in rat pheochromocytoma cells through inhibition of oxidative stress and the NF-κB transcription pathway, which adds to the rich neuroscience literature. Further, B. Pietrucha et al. compared the antioxidant status and major lipophilic antioxidants in patients with ataxia-telangiectasia (AT) and Nijmegen breakage syndrome (NBS) and confirmed the irregularities in redox homeostasis, and reduction of coenzyme Q10 in AT and NBS patients could be used as potential diagnostic tools in these diseases. In addition, M. S. Fawzy et al. examined the expression of longevity-related transcriptional factors (SOX2, OCT3/4, and NANOG) to evaluate them as diagnostic tools as well as to treat glioblastoma multiforme.

Finally, A. B. Abdel-Naim et al. isolated rutin isolated from *Chrozophora tinctoria* along with other five flavonoids and found that rutin enhanced bone cell proliferation and ossification markers using human osteosarcoma cell lines (SAOS-2 and MG-63). We hope that the readers of this special issue will find it enlightening about the potential benefits of antioxidants, which may help them fill the knowledge gaps in the prevention and treatment of aging, metabolic, and degenerative disorders.

Mohamed M. Abdel-Daim
Nadia I. Zakhary
Lotfi Aleya
Simona G. Bungău
Raghvendra A. Bohara
Nikhat J. Siddiqi

References

[1] K. I. Block, A. C. Koch, M. N. Mead, P. K. Tothy, R. A. Newman, and C. Gyllenhaal, "Impact of antioxidant supplementation on chemotherapeutic toxicity: a systematic review of the evidence from randomized controlled trials," *International Journal of Cancer*, vol. 123, no. 6, pp. 1227–1239, 2008.

[2] L. Milkovic, W. Siems, R. Siems, and N. Zarkovic, "Oxidative stress and antioxidants in carcinogenesis and integrative therapy of cancer," *Current Pharmaceutical Design*, vol. 20, no. 42, pp. 6529–6542, 2014.

[3] M. S. Uddin, A. Stachowiak, A. A. Mamun et al., "Autophagy and Alzheimer's disease: from molecular mechanisms to therapeutic implications," *Frontiers in Aging Neuroscience*, vol. 10, p. 4, 2018.

[4] J. K. Candlish and N. P. Das, "Antioxidants in food and chronic degenerative diseases," *Biomedical and Environmental Sciences*, vol. 9, no. 2-3, pp. 117–123, 1996.

Hindawi
Oxidative Medicine and Cellular Longevity
Volume 2018, Article ID 8753063, 12 pages
https://doi.org/10.1155/2018/8753063

Research Article

Longevity-Related Gene Transcriptomic Signature in Glioblastoma Multiforme

Manal S. Fawzy[1,2] **Dahlia I. Badran**[1,3] **Essam Al Ageeli,**[4] **Saeed Awad M. Al-Qahtani,**[5] **Saleh Ali Alghamdi,**[6] **Ghada M. Helal,**[7] **and Eman A. Toraih**[3,8]

[1]*Department of Medical Biochemistry, Faculty of Medicine, Suez Canal University, Ismailia 41522, Egypt*
[2]*Department of Medical Biochemistry, Faculty of Medicine, Northern Border University, Arar, Saudi Arabia*
[3]*Center of excellence in Molecular and Cellular Medicine, Faculty of Medicine, Suez Canal University, Ismailia, Egypt*
[4]*Department of Clinical Biochemistry (Medical Genetics), Faculty of Medicine, Jazan University, Jazan, Saudi Arabia*
[5]*Department of Physiology, Faculty of Medicine, Taibah University, Almadinah Almunawwarah, Saudi Arabia*
[6]*Medical Genetics, Clinical Laboratory Department, College of Applied Medical Sciences, Taif University, Taif, Saudi Arabia*
[7]*Department of Medical Biochemistry, Faculty of Medicine, Mansoura University, Mansoura, Egypt*
[8]*Genetics Unit, Histology and Cell Biology Department, Faculty of Medicine, Suez Canal University, Ismailia, Egypt*

Correspondence should be addressed to Manal S. Fawzy; manal2_khashana@ymail.com
and Eman A. Toraih; emantoraih@gmail.com

Received 2 October 2017; Accepted 11 December 2017; Published 21 March 2018

Academic Editor: Simona G. Bungău

Glioblastoma multiforme (GBM) (grade IV astrocytoma) has been assumed to be the most fatal type of glioma with low survival and high recurrence rates, even after prompt surgical removal and aggressive courses of treatment. Transcriptional reprogramming to stem cell-like state could explain some of the deregulated molecular signatures in GBM disease. The present study aimed to quantify the expression profiling of longevity-related transcriptional factors *SOX2*, *OCT3/4*, and *NANOG* to evaluate their diagnostic and performance values in high-grade gliomas. Forty-four specimens were obtained from glioblastoma patients (10 females and 34 males). Quantitative real-time polymerase chain reaction was applied for relative gene expression quantification. In silico network analysis was executed. *NANOG* and *OCT3/4* mRNA expression levels were significantly downregulated while that of *SOX2* was upregulated in cancer compared to noncancer tissues. Receiver operating characteristic curve analysis showed high diagnostic performance of *NANOG* and *OCT3/4* than *SOX2*. However, the aberrant expressions of the genes studied were not associated with the prognostic variables in the current population. In conclusion, the current study highlighted the aberrant expression of certain longevity-associated transcription factors in glioblastoma multiforme which may direct the attention towards new strategies in the treatment of such lethal disease.

1. Introduction

Tumors of the brain were considered one of the ten most common causes of cancer-related mortality [1]. According to the World Health Organization (WHO) classification, the primary brain tumors are categorized into glial tumors (e.g., glioblastoma, astrocytomas, oligodendroglial tumors, and ependymal tumors), embryonic tumors (e.g., medulloblastomas), tumors of the meninges, tumors of the hematopoietic system, and tumors of the sellar region [2]. The most fatal type of glioma has been reported to be the glioblastoma multiforme (GBM) [3] which represents up to 50% of almost all primary brain gliomas [4] with poor prognosis [5] and median survival rate of nearly 25 months after treatment [6]. The recurrence of the tumor after prompt surgical removal despite the aggressive courses of radio- and chemotherapy denotes the limited understanding of the disease biology [7]. Dell'Albani has stated that "new insights into the causes and the potential treatment of CNS tumors have come from disclosing relations with genes that regulate cell

growth, proliferation, differentiation, and death during normal development" [7]. These genes may represent a new target for GBM treatment by ameliorating the survival rate and preventing or minimizing disease recurrence.

Several emerging evidences support the reactivation of pluripotent transcription factors in many types of cancer [8–12]. As a normal biological phenomenon, these factors are expressed in embryonic stem cells (ESCs) and somatic cells where they imply the self-renewal [13] and the pluripotency characteristics [14]. As cancer development is a multistep process in which differentiated cells transform into immature ones, these factors could participate in cancer biogenesis and/or progress.

Among these pluripotent transcription factors overexpressed in high-grade gliomas are "sex-determining region Y-Box (SOX2), octamer-binding transcription factor 4 (OCT 4), and Nanog homeobox (NANOG)" [13, 15].

SOX2 gene encodes a transcriptional factor (TF) of 317 amino acids which contains a high-mobility group DNA-binding domain (Figure 1(a)) [16]. It implicated in embryonic development regulation, cell fate determination, and embryonic stem cell pluripotency. More specifically, it was reported to control the neural stem cell proliferation and differentiation into neurons, astrocytes, or oligodendrocytes [17]. *SOX2* is expressed in stem cells of endoderm-derived organs such as the liver, pancreas, and stomach [18], and its aberrant expression has been found to support self-renewal and inhibit neuronal differentiation [19]. Additionally, *SOX2* knockout in glioblastoma stem cells isolated from human glioma tumor inhibits cell proliferation and tumorigenicity in immunodeficient mice [20].

OCT3/4 is a member of a transcription POU family (Figure 1(b)) which has to react with other TFs in order to stimulate or inhibit gene expression [21] in ESCs through heterodimerization with SOX2. It was implicated in embryonic development regulation, cell fate determination, and embryonic stem cell pluripotency [22]. Finally, NANOG (Figure 1(c)) is involved in gene regulation with the aforementioned two transcription factors through their binding to the promoters of several genes which mediates the pluripotency, inhibits embryonic stem cell differentiation, and autorepresses its own expression in differentiating cells [22]. It has been found to be localized mainly in the nuclei of high-grade glioma cells than lower grades [15]. Despite the fact that OCT3/4 and NANOG have shown a direct relationship with the tumor grade, their oncogenic nature in brain tumorigenesis has not been established yet [23].

Up to our knowledge, there were no previous studies that relate the expression of the aforementioned longevity-related transcription factors in GBM patients among the Arab population. Hence, the present study for the first time aimed to quantify the expression levels of these markers in GBM sample of Egyptian patients and to correlate their expressions with the available clincopathological features. A thorough understanding of the relevance of each biomarker in GBM will be in need not only for reliable diagnosis of the disease but also to participate in future drug design for this fetal tumor.

2. Materials and Methods

2.1. Study Participants and Tissue Samples. The current study included 44 glioblastoma patients (10 females and 34 males, aged 38 to 62 years) assessed retrospectively from archived formalin-fixed paraffin-embedded section (FFPE) specimens of the Pathology Department, Mansoura University Hospitals, Egypt, from 2010 to 2013. They had glioblastoma multiforme grade 4, subjected to surgical removal and postoperative irradiation, and followed up for more than 36 months. Specimens were collected before receiving chemotherapy or radiotherapy prior to surgery. They were compared to 10 FFPE noncancerous brain specimens obtained from patients undergoing brain tissue resection for other reasons collected from the same hospital. Guidelines in the Declaration of Helsinki were followed, and an approval by the Medical Research Ethics Committee of Faculty of Medicine, Suez Canal University, was obtained before taking part. Written informed consent was obtained from all participants before providing the archived tissue samples as part of their routine register in our University Teaching Hospitals.

2.2. RNA Extraction. Extraction of total RNA from FFPE specimens was done using RNeasy FFPE Kit (Qiagen, 52304) according to the protocol of the manufacturer. RNA concentration and purity were assessed with NanoDrop ND-1000 spectrophotometer (NanoDrop Tech. Inc., Wilmington, DE, USA), followed by agarose gel electrophoresis (1%) check for RNA integrity.

2.3. Reverse Transcription (RT). Complementary DNA (cDNA) was obtained by total RNA conversion using the High-Capacity cDNA Reverse Transcription Kit (Applied Biosystems, P/N 4368814) with RT random primers on T-Professional Basic, Biometra PCR System (Biometra, Goettingen, Germany), as previously described [12]. Appropriate negative and positive controls were included in each experiment.

2.4. Gene Expression Profiling. The Minimum Information for Publication of Quantitative Real-Time PCR Experiments (MIQE) guidelines were followed for the real-time PCR reactions. Pluripotent gene relative expressions were assessed using "Universal PCR master mix II, No UNG (2×)" (TaqMan®, Applied Biosystems, P/N 4440043), TaqMan assay (Applied Biosystems, assay ID Hs02387400_g1 for NANOG, Hs01053049_s1 for SOX2, and Hs03005111_g for OCT3/4) and compared to the endogenous control TATA box binding protein (*TBP*) (Hs00427620_m1) which has been proved in our previous work [24] to be uniformly and stably expressed with no significant difference between GBM and noncancer tissues for gene expression normalization. PCRs were done in 20 μl total volume using "StepOne™ Real-Time PCR System (Applied Biosystems)" as previously described in details [25].

2.5. Statistical Analysis. Data analysis was done using PC-ORD ver. 5 software package and Statistical Package for the Social Sciences (SPSS) for windows software (version 22.0). Two-tailed statistical tests were used for continuous and

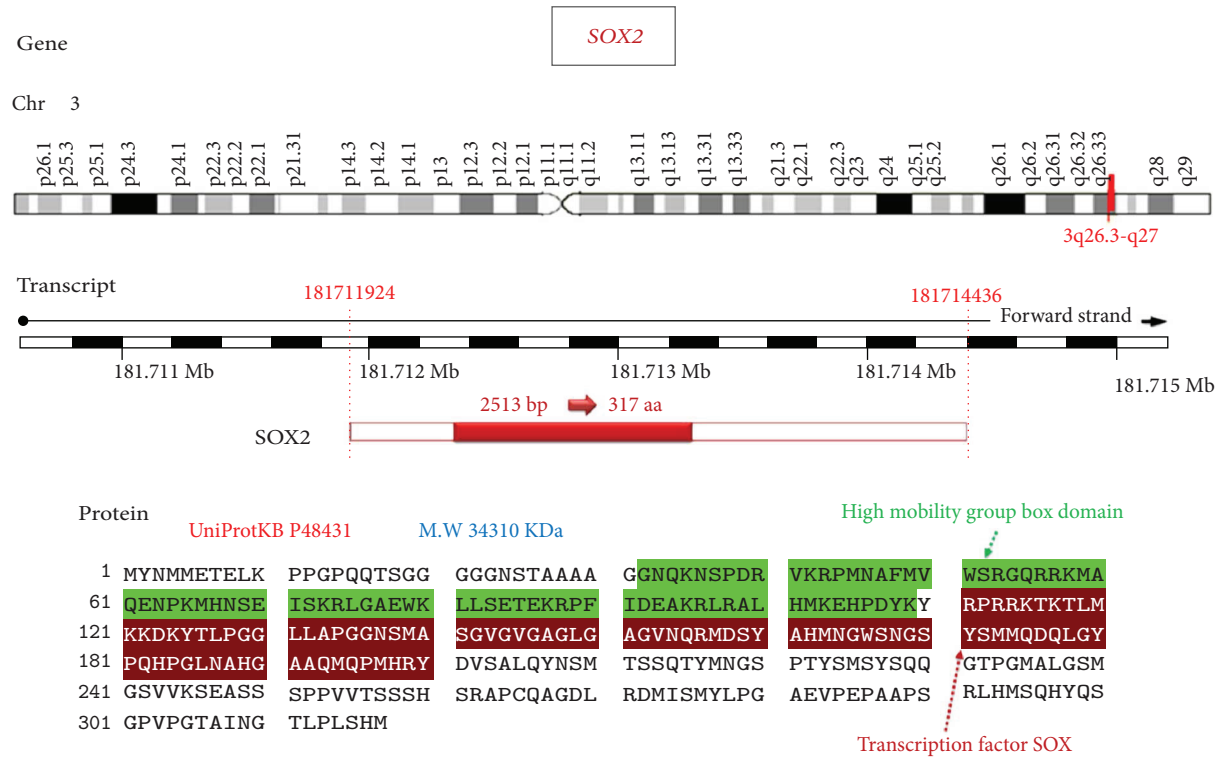

(a)

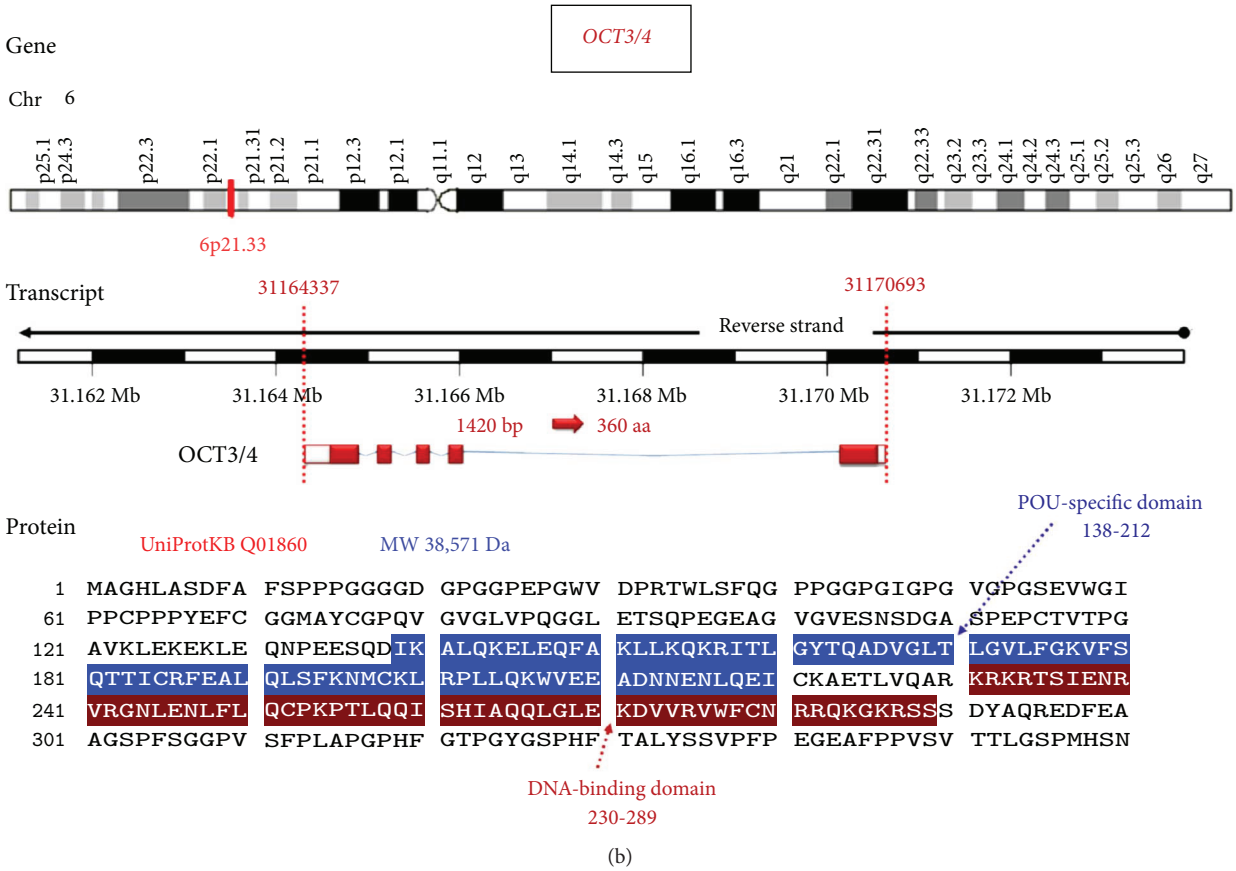

(b)

Figure 1: Continued.

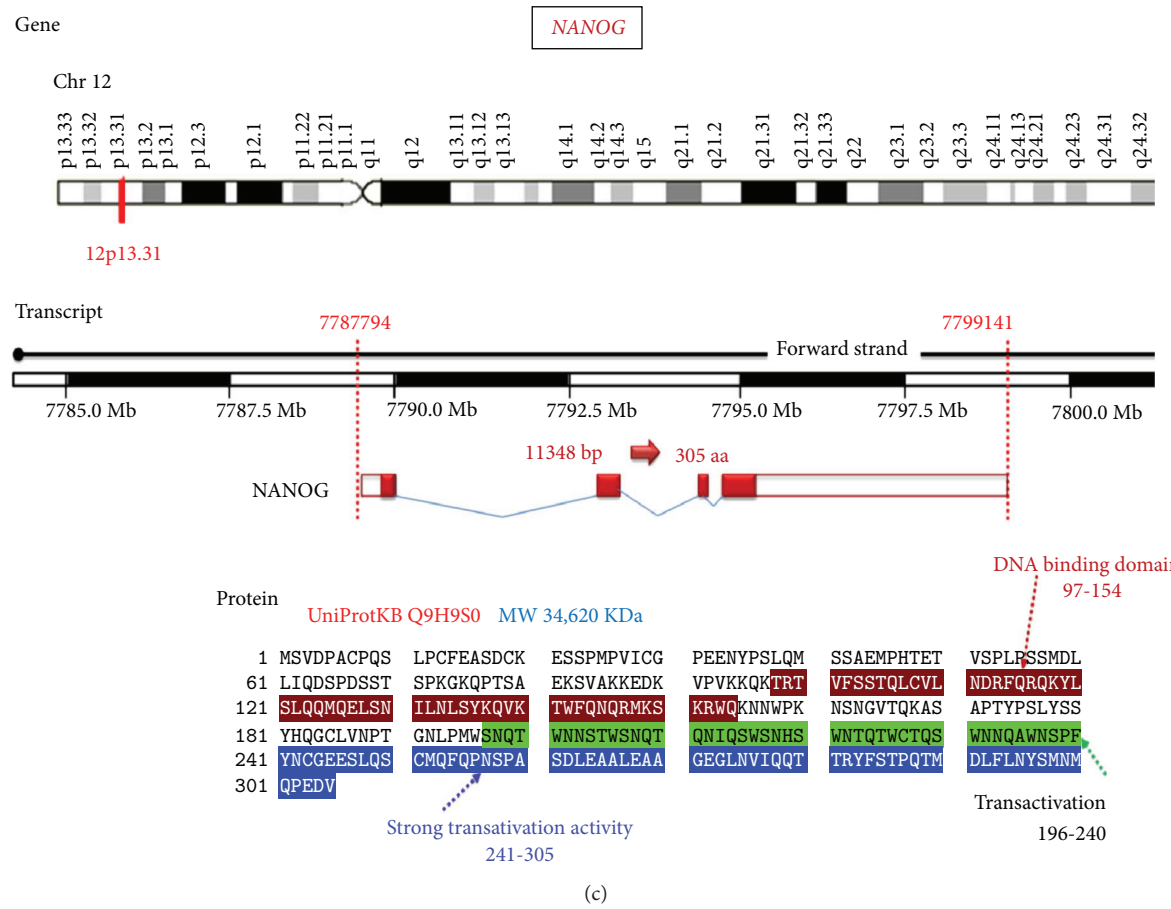

(c)

Figure 1: Structural analysis of the studied longevity-related genes. (a) *SOX2* gene (OMIM 184429) location in chromosome 3q26.33. The complete gene spans 2513 bases of genomic DNA (NC_000003.12; Chr 3: 181,711,924 to 181,714,436, plus strand; human genome assembly GRCh38). This intronless gene encodes a member of the SRY-related HMG-box family of transcription factors (translation length: 317 amino acids). *SOX2* refers to the primary and predominant transcript of the *SOX2* gene. The high-mobility group box domain amino acid sequence in the SOX2 transcription factor is highlighted by green color and the DNA-binding domain sequences are brown colored. (b) *NANOG* gene (OMIM: 607937) location in chromosome 12p13.31. The complete gene spans 11,348 bases of genomic DNA (NC_000012.12; Chr 12: 7,787,794 to 7,799,141, plus strand). The encoded protein (305 amino acids). (c) *OCT3/4* gene (OMIM: 164177) location in chromosome 6p21.33. The gene spans 1420 bases of genomic DNA (NC_00006.12; genomic coordinates (GRCh38): 6: 31,164,337-31,170,693, minus strand). The gene encodes a transcription factor (360 amino acids) containing a POU-specific homeodomain (blue amino acid sequences) and DNA-binding domain (brown amino acid sequences). MW: molecular weight; Da: Dalton; aa: amino acids (data source: http://Genecards.org, http://Ensembl.org and UniProtKB).

categorical variables. Correlation analysis between the variables was performed via Pearson's correlation coefficient. p value < 0.05 was considered significant. The fold change of mRNA expression in each patient cancer tissue relative to the mean of controls was calculated using Livak method that depends on the quantitation cycle (C_q) value with the following equation: relative quantity $= 2^{-\Delta\Delta C_q}$ [26]. The diagnostic performance of pluripotent genes was evaluated by receiver operating characteristic (ROC) analysis. Kaplan–Meier estimator was generated for survival analysis, and log-rank test was applied for different Kaplan–Meier curve (stratified by clinicopathological features) comparisons. Linear regression analysis using ENTER method was performed to evaluate potential factors affecting the overall survival of patients. Two-way Hierarchical cluster analysis was run for exploratory multivariate analysis. Ward's method and Euclidean (Pythagorean) were adjusted for linkage method and distance measure, respectively, with a beta value of −0.75 to reach the minimum % of chaining. Principal Component Ordination analysis was used to visualize clustering of patients according to their clinicopathological characteristics [27].

3. Results

3.1. Expression Profile of Pluripotent Genes. Baseline clinical features of the study participants are illustrated in Table 1. Relative expression analyses of pluripotent genes in brain cancer specimens were compared to *TBP*. Our results revealed that the expression levels of *NANOG* and *OCT3/4* were significantly downregulated ($p < 0.001$ and $= 0.001$, resp.) while that of *SOX2* was significantly upregulated ($p = 0.0027$) in tumor specimens compared to noncancer tissues (Figures 2(a) and 2(b)). Both NANOG

Table 1: Characteristics of GBM patients.

Variables	Number (%) or mean ± SE
Age	
Mean ± SE	51.4 ± 0.97
Age categories	
35–50 y	18 (40.9)
>50 y	26 (59.1)
Gender	
Female	10 (22.7)
Male	34 (77.3)
Tumor site	
Frontal	22 (50)
Frontotemporal	4 (9.1)
Temporoparietal	18 (40.9)
Recurrence	
Nonrecurrent	36 (81.8)
Recurrent	8 (18.2)
Disease-free survival (months)	
Mean ± SE	15.1 ± 0.85
Range	6–27
Prolonged DFS (>1 y)	28 (63.6)
Short DFS (≤1 y)	16 (36.4)
Overall survival (months)	
Mean ± SE	15.6 ± 0.86
Range	8–27
High survival (>1 y)	30 (68.2)
Low survival (≤1 y)	14 (31.8)

and OCT3/4 mRNAs showed high diagnostic values as biomarkers for GBM (AUC = 0.886 ± 0.054 and 0.736 ± 0.078, resp.) (Figure 3).

3.2. Association with Clinicopathological Characteristics and Survival Analysis. Higher *OCT3/4* gene expression was noted in elder GBM patients ($p = 0.036$). No statistically significant association was found with any other parameters (Figure 4). Correlation analysis revealed moderate correlation between *NANOG* and *SOX2* gene expression profile ($r = 0.484$, $p = 0.023$). In addition, elder age of patients was associated with poor overall survival (OS) ($r = -0.479$, $p = 0.024$) and disease-free survival (DFS) ($r = -0.481$, $p = 0.023$) (Figure 5).

Linear regression analysis was performed to evaluate potential factors affecting overall survival of patients. None of the genes or clinicopathological variables was determined as a good prognostic marker for patients' survival in the study population (Table 2). However, survival analysis in GBM by log-rank and Tarone-Ware tests showed poor OS among elder patients (Figure 6 and Table S1).

3.3. Multivariate Analysis. Exploratory multivariate analysis by principle component and hierarchical cluster analyses classified patients into 3 groups based on the relative expression of the combined genes (Figure 7). However, there was no clear demarcation found between patients according to age, gender, tumor site, and recurrence (Figure S1).

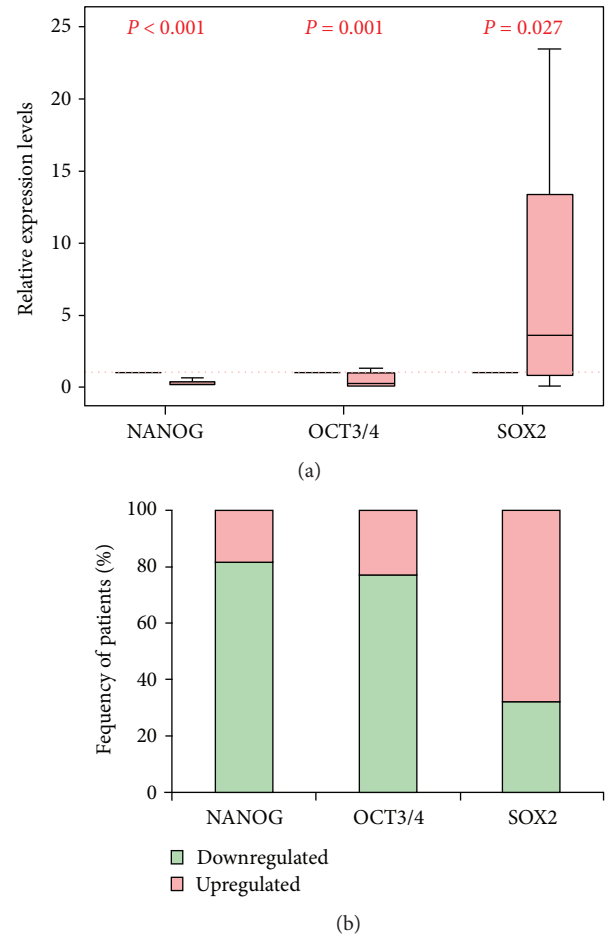

Figure 2: Expression profile of pluripotent genes in GBM patients compared to controls. (a) Values are presented as medians and quartiles of fold change relative to controls. The box defines upper and lower quartiles (25% and 75%, resp.) and the Whisker bars indicate upper and lower adjacent limits. *TBP* was used as an internal control. Noncancer tissues was set to have a relative expression value of 1.0. Mann–Whitney *U* test was used for comparison. p value < 0.05 was considered statistically significant. (b) Frequency of patients with up- and downregulated genes.

4. Discussion

The presence of a significant heterogeneity in certain types of solid tumors including GBM is becoming obvious. Hence, it will be rational to search for and evaluate specific molecular markers that could assist in diagnosis and/or prognosis of these tumors and could act as targeted molecular markers for personalized therapy [7]. Here, we attempted to investigate the presence of a molecular signature of longevity-related genes (*SOX2*, *NANOG*, and *OCT3/4*) by examining their mRNA expression in GBM tissues relative to noncancer tissues. Our analyses revealed that the expression level of SOX2 was significantly upregulated. This finding was consistent with several independent cohorts [28–30] and in part with Guo et al., [13] who detected an overexpression of

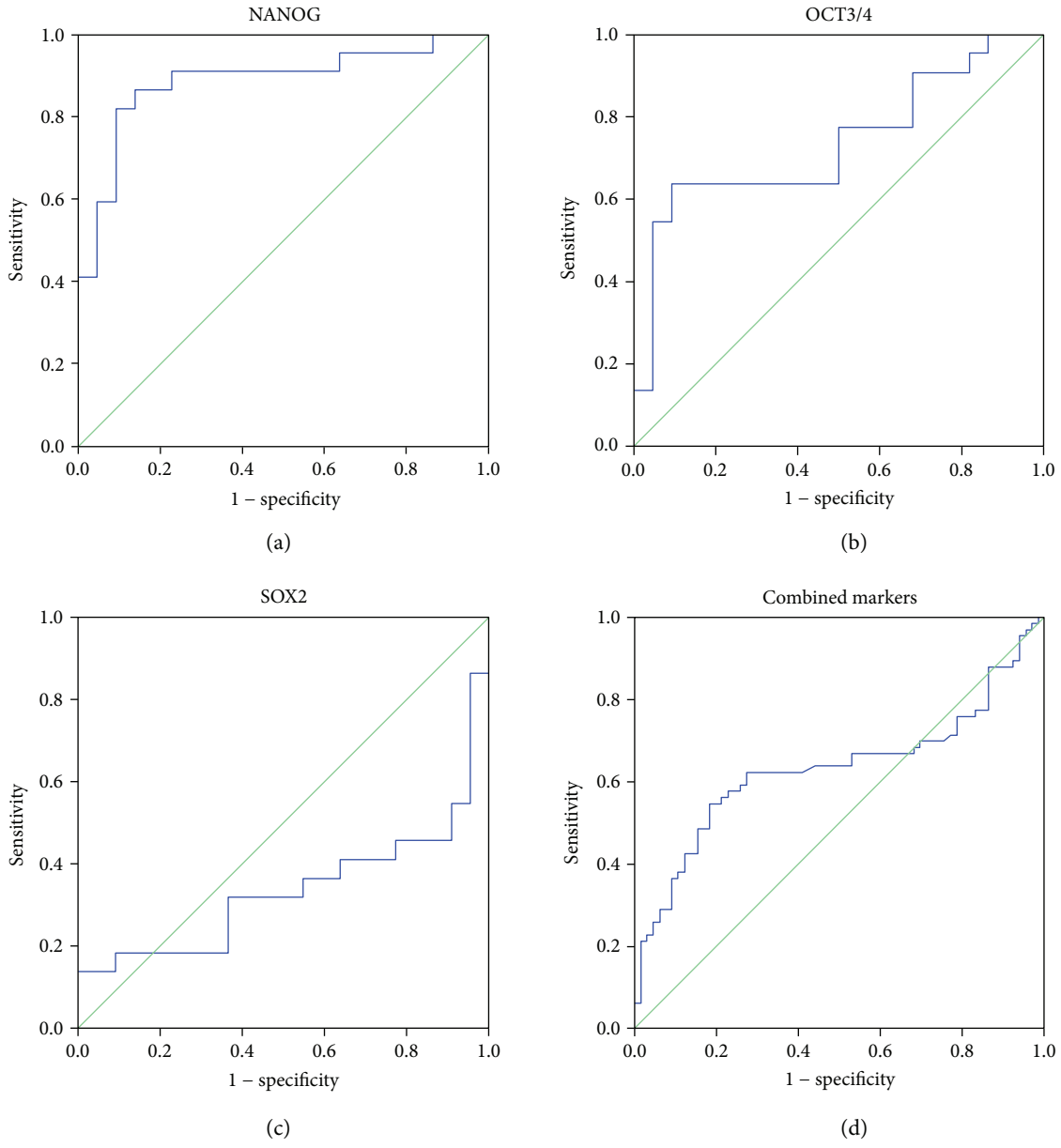

Area under the curve

Markers	AUC	SE	*P* values	95% confidence internal	
				Lower bound	Upper bound
NANOG	0.886	0.054	0.000	0.780	0.992
OCT3/4	0.736	0.078	0.007	0.582	0.889
SOX2	0.335	0.087	0.060	0.164	0.505
Combined	0.631	0.051	0.009	0.531	0.731

Figure 3: Diagnostic performance of pluripotent genes to discriminate between GBM and noncancer samples. NANOG and OCT3/4 showed high diagnostic values as biomarkers for GBM.

SOX2 mRNA in grade IV gliomas compared to grade II. Of the three longevity-related factors, SOX2 seems to be the playmaker in the development of brain tumors [18]. When overexpressed, it promotes cell cycle progression into S phase and proliferation [3, 20, 28, 31], which were attenuated by application of SOX2-RNAi (RNA interference) therapy [32]. At the cellular level, Garros-Regulez et al. [33] proposed SOX2 upregulation via activation of GBM-specific signaling pathways that maintain the overexpression of SOX2 via transforming growth factor-beta (TGF-β), Sonic Hedgehog (SHH), epidermal growth factor receptor (EGFR), and fibroblast growth factor receptor (FGFR)

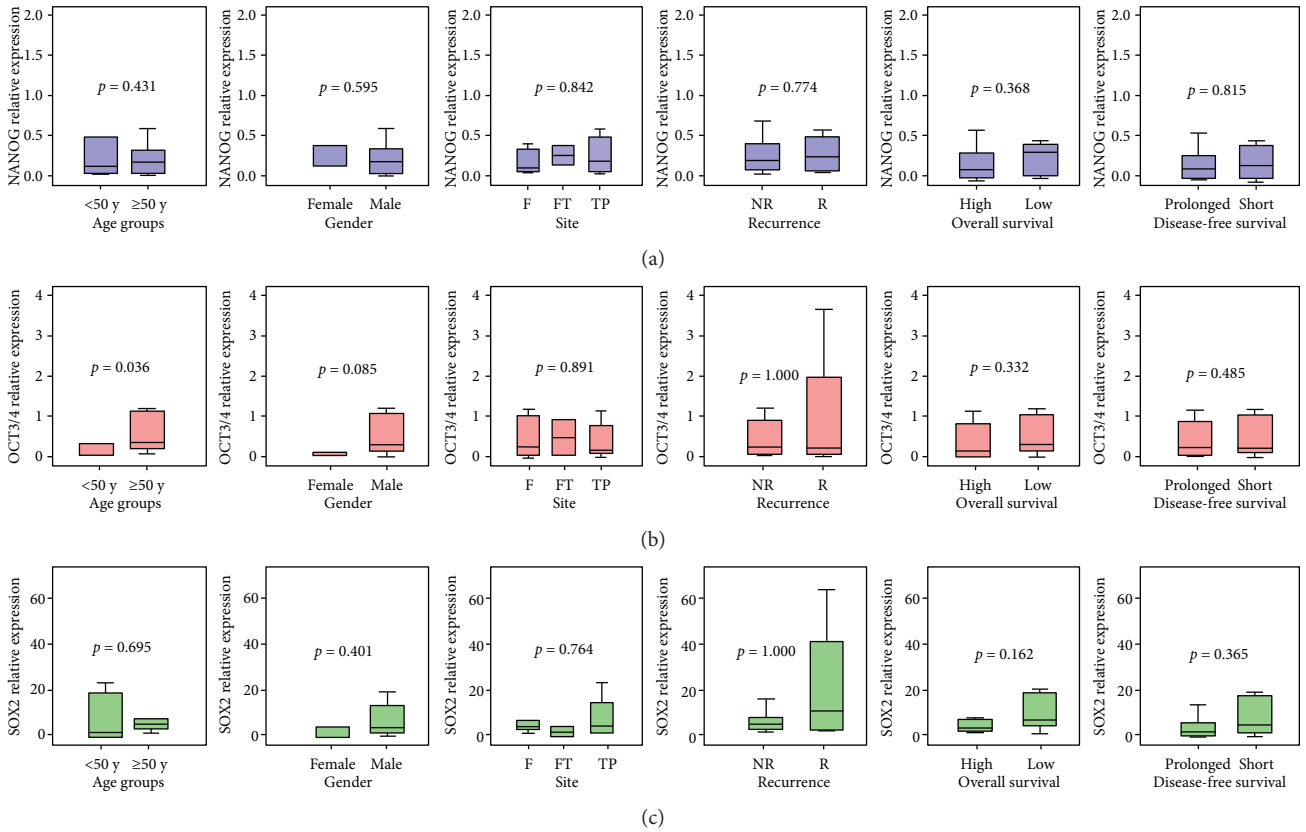

Figure 4: Association between gene expression and the clinicopathological features. Values are presented as medians and quartiles of fold change relative to controls. The box defines upper and lower quartiles (25% and 75%, resp.) and the whisker bars indicate upper and lower adjacent limits. TBP was used as an internal control. Noncancer tissues were set to have a relative expression value of 1.0. Mann–Whitney U and Kruskal-Wallis tests were used for comparison. p value < 0.05 was considered statistically significant. F: frontal tumor site; FT: frontotemporal; TP: temporoparietal; R: recurrent; NR: nonrecurrent.

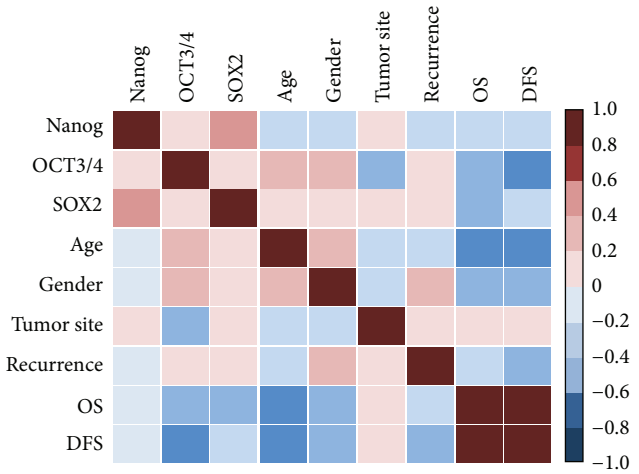

Figure 5: Correlation matrix between transcriptomic signature and the clinicopathological features. Pearson's correlation analysis was performed and represented as color gradient.

pathways. In addition, *SOX2* gene amplification and DNA promoter hypomethylation have been reported in a group of GBM patients to expand the mechanism responsible for SOX2 upregulation [34].

Despite that our in silico analysis revealed that the expression of the studied stem-related factors has similar colocalization and physical interactions with each other [12], they seem to be differentially expressed independently in the current samples. We found that *NANOG* and *OCT3/4* were significantly downregulated in GBM tissues. Our finding might seem contradictory to the stemness role these pluripotent transcription factors play; however, it is worth to emphasize that the mechanistic functions of SOX2, OCT4, and NANOG in cancer cells are a little different in each stage of tumor progress. Kallas et al. reported high levels of SOX2, OCT4, and NANOG transcription factor expressions at the beginning of their tested human embryonic stem cell differentiation. However, on progress of the differentiation process, a decline in OCT4 and NANOG expression levels was observed, while expression of SOX2 was kept at a high level [35]. They suggested that the pluripotency is maintained by a transcriptional network that is harmonized by the aforementioned core transcription factors. During differentiation, the epigenetic modifications could play a role in level modulation of these factors.

The other possible reasons for inconsistency of gene expression for the three stem cell marker studies could be sampling bias and/or relatively low expression levels of these

Table 2: Linear regression analysis to determine predictors for survival.

	Unstandardized coefficients		Standardized coefficients			95% confidence interval for B	
	B	Std. error	Beta	t	Sig.	Lower bound	Upper bound
(Constant)	34.675	10.593		3.273	0.006	11.955	57.395
Age	−0.318	0.220	−0.363	−1.448	0.170	−0.790	0.153
Gender	−2.142	3.510	−0.170	−0.610	0.551	−9.671	5.387
Tumor site	0.079	1.498	0.014	0.053	0.959	−3.134	3.292
Recurrence	0.501	3.635	0.036	0.138	0.892	−7.295	8.296
NANOG	0.374	3.095	0.033	0.121	0.905	−6.263	7.011
OCT3/4	−0.943	1.339	−0.173	−0.705	0.493	−3.815	1.928
SOX2	−0.085	0.123	−0.214	−0.691	0.501	−0.348	0.178

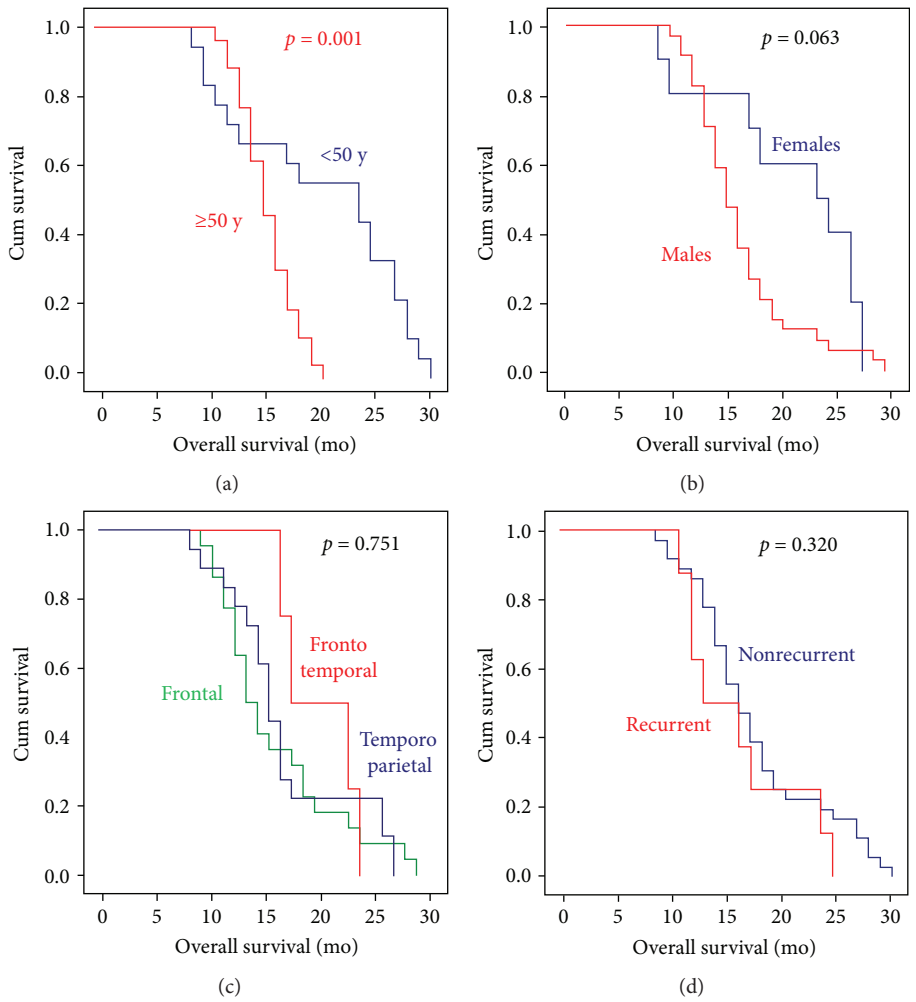

Figure 6: Kaplan–Meier survival curve in GBM patients. Log-rank (Mantel-Cox) test was used for comparison. Statistical significance at $p < 0.05$.

factors within the individual GBM tissue examined in the current study [36]. This could be explained by the unique stem cell signature that has been implied by each tumor due to the inherent intratumor heterogeneity within GBM tissues [37–39]. Our multivariate analysis and the hierarchical cluster analysis confirmed the previous suggestions by revealing classification of the study population into 3 groups based on the combined gene expression that confirm a specific protumorigenic profile. Similar to other combinations of cancer stem cell markers in other types of cancer [40, 41], previous studies revealed that cancer stem cells which were isolated using different markers in the same

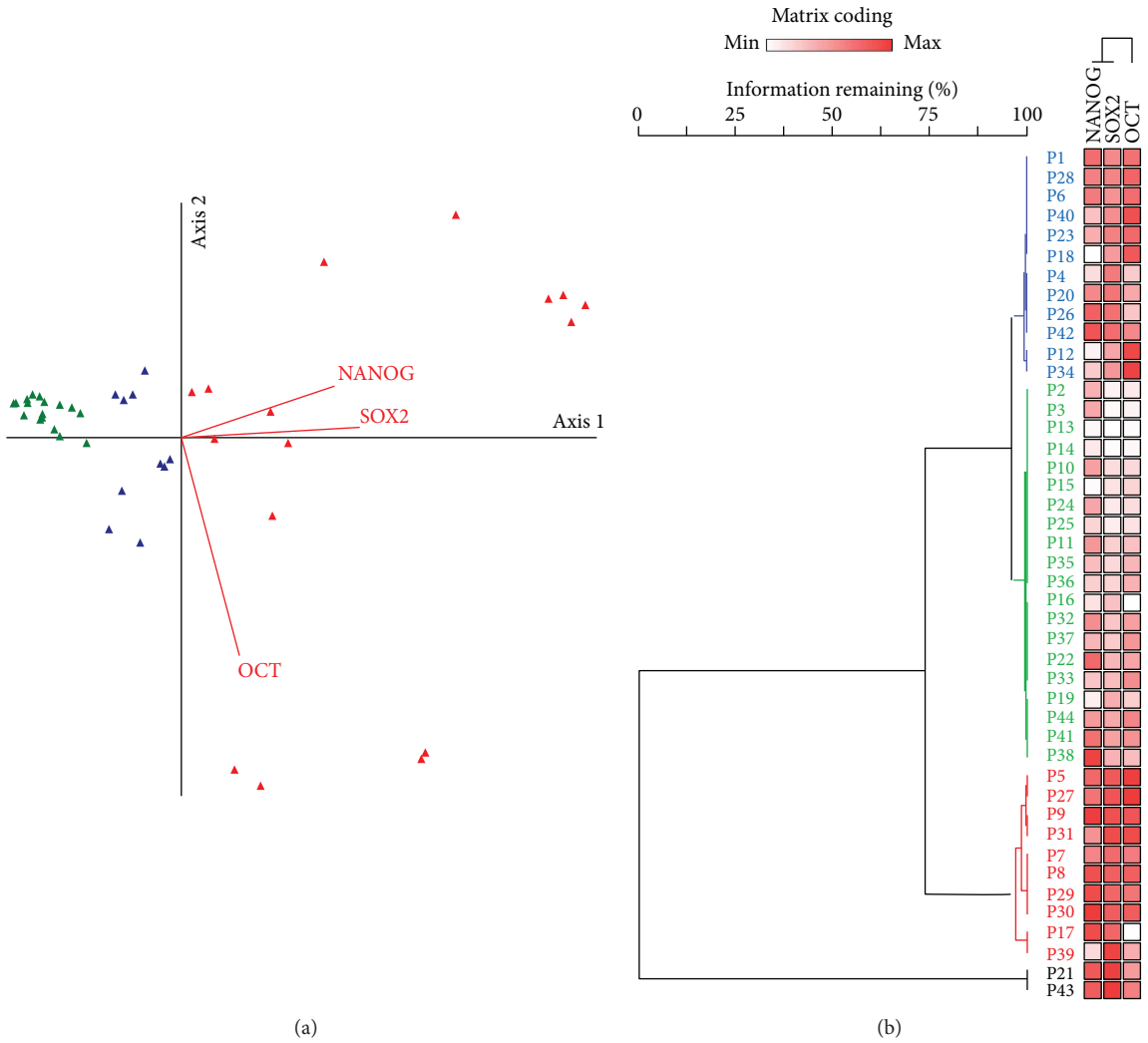

Figure 7: Multivariate analyses cluster GBM patients according to transcriptomic signature. PC-ORD v5.0 was used for exploratory multivariate analysis. Data set was profiled by the program. There was no need for transformation as beta diversity was zero and there was no outlier. (a) Ordination graph by PCO and (b) two-way hierarchical cluster analysis. The following parameters were adjusted: linkage method; Ward's method; distance method; Euclidean method; relativizing matrix by column maximum; and matrix coding percentile by column. Percent chaining = 7.38. Clustering identified three patient groups according to their gene expression. The red clade for overexpression of the three pluripotent genes, the green clade discriminates patients with gene downregulation, and the blue clade has variable degrees of expression. Two samples (black clade) were out-group from the other clusters.

cancer phenotype had different expression profiles quantified by real-time PCR. Combined expression analysis might more accurately identify true cancer stem cells for each type of cancer [40], including GBM tumors.

Ji et al. reported that unlike normal stem cells, OCT4 could be dispensable for self-renewal, survival, and differentiation of transformed cells. They provided direct evidence for the functional divergence of OCT4 from the pluripotent state following the cancer tissue transformation [42]. This could support the downregulation of this stem-related marker noted in the current advanced stages of GBM cases. Additionally, Bradshaw et al. [36] reported low OCT4 relative expressions at the transcription and protein levels within their FFPE GBM samples. They speculated that the relatively OCT4-expressing cell low number could indicate the most primitive stem cell population within GBM which may possibly bring about the rest of downstream cells within the GBM tumor. Otherwise, the SOX2 ubiquitous redundancy is more likely to be expressed in the more differentiated cells reflecting its usefulness as a potential progenitor cell marker within the GBM tissues [36].

In contrast to the finding of Zbinden et al. [43] that NANOG was essential for GBM tumourigenicity in orthotopic xenografts, we found downregulation of this marker in the current GBM samples. We speculated that this difference could be due to either the low NANOG-expressing cell number within the study samples as mentioned above for the OCT4 marker or the type of NANOG transcript that has been quantified by the available quantitative PCR analysis at the time of the current work which preferentially recognized the varying levels of NANOG expression. As NANOG is coded by two genes (i.e., *NANOG* and *NANOGP8*) in

human, it has been found that *NANOGP8* is the most abundantly expressed of the two NANOG-encoding genes in GBMs, accounting for more than ninety percent of all NANOG-encoding mRNAs in a number of previously tested cases [43]. However, future lineage analyses will be required for unravelling the high NANOG-expressing cell nature and NANOG expression stability as recommended by the latter researchers.

Correlating the available clincopathological features including the survival data of GBM cases with the gene expression results revealed that poor overall survival and disease-free survival were found significantly among patients as reported by previous studies [44, 45]. Despite that GBM can occur in individuals of any age according to the previous population-based studies, the median age is nearly above 60 years. Additionally, primary GBMs have been reported to develop commonly in older individuals (mean, 55 years), whereas secondary ones were found in middle-aged subjects (39 year olds) [4].

5. Conclusion

The current study findings highlighted the dysregulated longevity-related gene expression in GBM Egyptian cases that could have a potential role in carcinogenesis and procuration of stemness-like properties in this type of tumors. The current study could be limited by the relatively small sample size and the fact that all patients have grade IV gliomas, although this last issue increases the specificity of the study results that confined to one stage of GBM. Additional large-scale studies including different glioma grades are recommended to evaluate the relation of the studied longevity-related gene expression with different WHO grades as well as to confirm their putative role as diagnostic and/or prognostic biomarkers. These could be an interesting era for future individualized molecular-targeted therapy for GBM patients.

Abbreviations

C_q: Quantitation cycle
DFS: Disease-free survival
ESCs: Embryonic stem cells
GBM: Glioblastoma multiforme
MIQE: Minimum Information for Publication of Quantitative Real-Time PCR Experiments
NANOG: Nanog homeobox
OCT: Octamer-binding transcription factor
OS: Overall survival
ROC: Receiver-operating characteristic
RT: Reverse transcription
SOX2: Sex-determining region Y-Box.

Conflicts of Interest

The authors declare that they have no competing of interests.

Acknowledgments

The authors thank the Oncology Diagnostic Unit and the Center of Excellence in Molecular and Cellular Medicine, Suez Canal University, Ismailia, Egypt, for providing the facilities for performing the research work.

Supplementary Materials

Table S1: Kaplan–Meier curves comparing survival of patients with different clinical variables. Figure S1: multivariate analysis stratified by clinicopathological features. *(Supplementary Materials)*

References

[1] American Cancer Society, *Cancer Facts & Figures 2015*, American Cancer Society, Atlanta, 2015.

[2] D. N. Louis, A. Perry, G. Reifenberger et al., "The 2016 World Health Organization classification of tumors of the central nervous system: a summary," *Acta Neuropathologica*, vol. 131, no. 6, pp. 803–820, 2016.

[3] M. Schmitz, A. Temme, V. Senner et al., "Identification of SOX2 as a novel glioma-associated antigen and potential target for T cell-based immunotherapy," *British Journal of Cancer*, vol. 96, no. 8, pp. 1293–1301, 2007.

[4] X. Zhang, W. Zhang, W.-D. Cao, G. Cheng, and Y.-Q. Zhang, "Glioblastoma multiforme: molecular characterization and current treatment strategy (review)," *Experimental and Therapeutic Medicine*, vol. 3, no. 1, pp. 9–14, 2012.

[5] R. Stupp, W. P. Mason, M. J. van den Bent et al., "Radiotherapy plus concomitant and adjuvant temozolomide for glioblastoma," *The New England Journal of Medicine*, vol. 352, no. 10, pp. 987–996, 2005.

[6] R. R. Lonser, S. Walbridge, A. O. Vortmeyer et al., "Induction of glioblastoma multiforme in nonhuman primates after therapeutic doses of fractionated whole-brain radiation therapy," *Journal of Neurosurgery*, vol. 97, no. 6, pp. 1378–1389, 2002.

[7] P. Dell'Albani, "Stem cell markers in gliomas," *Neurochemical Research*, vol. 33, no. 12, pp. 2407–2415, 2008.

[8] I. Ben-Porath, M. W. Thomson, V. J. Carey et al., "An embryonic stem cell-like gene expression signature in poorly differentiated aggressive human tumors," *Nature Genetics*, vol. 40, no. 5, pp. 499–507, 2008.

[9] M. Schoenhals, A. Kassambara, J. De Vos, D. Hose, J. Moreaux, and B. Klein, "Embryonic stem cell markers expression in cancers," *Biochemical and Biophysical Research Communications*, vol. 383, no. 2, pp. 157–162, 2009.

[10] J. Matsuoka, M. Yashiro, K. Sakurai et al., "Role of the stemness factors Sox2, Oct3/4, and Nanog in gastric carcinoma," *Journal of Surgical Research*, vol. 174, no. 1, pp. 130–135, 2012.

[11] W. Luo, S. Li, B. Peng, Y. Ye, X. Deng, and K. Yao, "Embryonic stem cells markers SOX2, OCT4 and Nanog expression and their correlations with epithelial-mesenchymal transition in nasopharyngeal carcinoma," *PLoS One*, vol. 8, no. 2, article e56324, 2013.

[12] E. A. Toraih, M. S. Fawzy, A. I. El-Falouji et al., "Stemness-related transcriptional factors and homing gene expression profiles in hepatic differentiation and cancer," *Molecular Medicine*, vol. 22, no. 1, pp. 653–663, 2016.

[13] Y. Guo, S. Liu, P. Wang, S. Zhao, F. Wang, and L. Bing, "Expression profile of embryonic stem cell-associated genes Oct4, Sox2 and Nanog in human gliomas," *Histopathology*, vol. 59, no. 4, pp. 763–775, 2011.

[14] T. Seymour, A. J. Twigger, and F. Kakulas, "Pluripotency genes and their functions in the normal and aberrant breast and brain," *International Journal of Molecular Sciences*, vol. 16, no. 11, pp. 27288–27301, 2015.

[15] C. S. Niu, D. X. Li, Y. H. Liu, X. M. Fu, S. F. Tang, and J. Li, "Expression of NANOG in human gliomas and its relationship with undifferentiated glioma cells," *Oncology Reports*, vol. 26, no. 3, pp. 593–601, 2011.

[16] F. Doetsch, L. Petreanu, I. Caille, J. M. Garcia-Verdugo, and A. Alvarez-Buylla, "EGF converts transit-amplifying neurogenic precursors in the adult brain into multipotent stem cells," *Neuron*, vol. 36, no. 6, pp. 1021–1034, 2002.

[17] D. Maric, A. Fiorio Pla, Y. H. Chang, and J. L. Barker, "Self-renewing and differentiating properties of cortical neural stem cells are selectively regulated by basic fibroblast growth factor (FGF) signaling via specific fgf receptors," *The Journal of Neuroscience*, vol. 27, no. 8, pp. 1836–1852, 2007.

[18] R. Favaro, I. Appolloni, S. Pellegatta, A. B. Sanga, P. Pagella, and E. Gambini, "Sox2 is required to maintain cancer stem cells in a mouse model of high-grade oligodendroglioma," *Cancer Research*, vol. 74, no. 6, pp. 1833–1844, 2014.

[19] G. Thiel, "How Sox2 maintains neural stem cell identity," *Biochemical Journal*, vol. 450, no. 3, pp. e1–e2, 2013.

[20] R. M. Gangemi, F. Griffero, D. Marubbi et al., "*SOX2* silencing in glioblastoma tumor-initiating cells causes stop of proliferation and loss of tumorigenicity," *Stem Cells*, vol. 27, no. 1, pp. 40–48, 2009.

[21] M. Pesce and H. R. Scholer, "Oct-4: gatekeeper in the beginnings of mammalian development," *Stem Cells*, vol. 19, no. 4, pp. 271–278, 2001.

[22] L. A. Boyer, T. I. Lee, M. F. Cole, S. E. Johnstone, S. S. Levine, and J. P. Zucker, "Core transcriptional regulatory circuitry in human embryonic stem cells," *Cell*, vol. 122, no. 6, pp. 947–956, 2005.

[23] T. Seymour, A. Nowak, and F. Kakulas, "Targeting aggressive cancer stem cells in glioblastoma," *Frontiers in Oncology*, vol. 5, no. 159, 2015.

[24] M. S. Fawzy, E. A. Toraih, and H. Y. Abdallah, "Long noncoding RNA metastasis-associated lung adenocarcinoma transcript 1 (MALAT1): a molecular predictor of poor survival in glioblastoma multiforme in Egyptian patients," *Egyptian Journal of Medical Human Genetics*, vol. 18, no. 3, pp. 231–239, 2017.

[25] E. A. Toraih, M. S. Fawzy, E. A. Mohammed, M. H. Hussein, and M. M. EL-Labban, "MicroRNA-196a2 biomarker and targetome network analysis in solid tumors," *Molecular Diagnosis & Therapy*, vol. 20, no. 6, pp. 559–577, 2016.

[26] K. J. Livak and T. D. Schmittgen, "Analysis of relative gene expression data using real-time quantitative PCR and the $2^{-\Delta\Delta C}{}_{T}$ method," *Methods*, vol. 25, no. 4, pp. 402–408, 2001.

[27] M. S. Fawzy, E. A. Toraih, N. M. Aly, A. Fakhr-Eldeen, D. I. Badran, and M. H. Hussein, "Atherosclerotic and thrombotic genetic and environmental determinants in Egyptian coronary artery disease patients: a pilot study," *BMC Cardiovascular Disorders*, vol. 17, no. 1, p. 26, 2017.

[28] L. Annovazzi, M. Mellai, V. Caldera, G. Valente, and D. Schiffer, "SOX2 expression and amplification in gliomas and glioma cell lines," *Cancer Genomics & Proteomics*, vol. 8, no. 3, pp. 139–147, 2011.

[29] C. W. Brennan, R. G. Verhaak, A. McKenna et al., "The somatic genomic landscape of glioblastoma," *Cell*, vol. 155, no. 2, pp. 462–477, 2013.

[30] A. M. de la Rocha, N. Sampron, M. M. Alonso, and A. Matheu, "Role of SOX family of transcription factors in central nervous system tumors," *American Journal of Cancer Research*, vol. 4, no. 4, pp. 312–324, 2014.

[31] K. Weina and J. Utikal, "SOX2 and cancer: current research and its implications in the clinic," *Clinical and Translational Medicine*, vol. 3, no. 1, p. 19, 2014.

[32] F. Oppel, N. Müller, G. Schackert et al., "SOX2-RNAi attenuates S-phase entry and induces RhoA-dependent switch to protease-independent amoeboid migration in human glioma cells," *Molecular Cancer*, vol. 10, no. 1, p. 137, 2011.

[33] L. Garros-Regulez, I. Garcia, E. Carrasco-Garcia et al., "Targeting SOX2 as a therapeutic strategy in glioblastoma," *Frontiers in Oncology*, vol. 6, no. 222, 2016.

[34] M. M. Alonso, R. Diez-Valle, L. Manterola et al., "Genetic and epigenetic modifications of Sox2 contribute to the invasive phenotype of malignant gliomas," *PLoS One*, vol. 6, no. 11, article e26740, 2011.

[35] A. Kallas, M. Pook, A. Trei, and T. Maimets, "SOX2 is regulated differently from NANOG and OCT4 in human embryonic stem cells during early differentiation initiated with sodium butyrate," *Stem Cells International*, vol. 2014, Article ID 298163, 12 pages, 2014.

[36] A. Bradshaw, A. Wickremsekera, S. T. Tan, L. Peng, P. F. Davis, and T. Itinteang, "Cancer stem cell hierarchy in glioblastoma multiforme," *Frontiers in Surgery*, vol. 3, 2016.

[37] D. Stieber, A. Golebiewska, L. Evers et al., "Glioblastomas are composed of genetically divergent clones with distinct tumourigenic potential and variable stem cell-associated phenotypes," *Acta Neuropathologica*, vol. 127, no. 2, pp. 203–219, 2014.

[38] A. Morokoff, W. Ng, A. Gogos, and A. H. Kaye, "Molecular subtypes, stem cells and heterogeneity: implications for personalised therapy in glioma," *Journal of Clinical Neuroscience*, vol. 22, no. 8, pp. 1219–1226, 2015.

[39] A. R. Safa, M. R. Saadatzadeh, A. A. Cohen-Gadol, K. E. Pollok, and K. Bijangi-Vishehsaraei, "Glioblastoma stem cells (GSCs) epigenetic plasticity and interconversion between differentiated non-GSCs and GSCs," *Genes & Diseases*, vol. 2, no. 2, pp. 152–163, 2015.

[40] J. Skoda, M. Hermanova, T. Loja, P. Nemec, J. Neradil, and P. Karasek, "Co-expression of cancer stem cell markers corresponds to a pro-tumorigenic expression profile in pancreatic adenocarcinoma," *PLoS One*, vol. 11, no. 7, article e0159255, 2016.

[41] G. S. Wilson, Z. Hu, W. Duan et al., "Efficacy of using cancer stem cell markers in isolating and characterizing liver cancer stem cells," *Stem Cells and Development*, vol. 22, no. 19, pp. 2655–2664, 2013.

[42] J. Ji, T. E. Werbowetski-Ogilvie, B. Zhong, S.-H. Hong, and M. Bhatia, "Pluripotent transcription factors possess distinct roles in normal versus transformed human stem cells," *PLoS One*, vol. 4, no. 11, article e8065, 2009.

[43] M. Zbinden, A. Duquet, A. Lorente-Trigos, S.-N. Ngwabyt, I. Borges, and A. Ruiz i Altaba, "NANOG regulates glioma stem cells and is essential in vivo acting in a cross-functional

network with GLI1 and p53," *The EMBO Journal*, vol. 29, no. 15, pp. 2659–2674, 2010.

[44] D. Xie, Y. X. Zeng, H. J. Wang et al., "Amplification and overexpression of epidermal growth factor receptor gene in glioblastomas of Chinese patients correlates with patient's age but not with tumor's clinicopathological pathway," *Acta Neuropathologica*, vol. 110, no. 5, pp. 481–489, 2005.

[45] M. Vand Rajabpour, H. Yahyazadeh, and M. Beheshti, "Prognostic factors and survival of glioblastoma multiform (GBM) in Iranian patients," *International Journal of Cancer Management*, vol. 10, article e6260, 2017.

Hindawi
Oxidative Medicine and Cellular Longevity
Volume 2018, Article ID 3250864, 14 pages
https://doi.org/10.1155/2018/3250864

Review Article

Mesenchymal Stromal Cell Therapy for Pancreatitis: A Systematic Review

Sara M. Ahmed,[1] Mahmoud Morsi,[2] Nehal I. Ghoneim,[1] Mohamed M. Abdel-Daim,[3,4] and Nagwa El-Badri[1]

[1]*Center of Excellence for Stem Cells and Regenerative Medicine, Zewail City of Science and Technology, 6th of October, Giza, Egypt*
[2]*Faculty of Medicine, Menoufia University, Shebin El Kom, Menoufia, Egypt*
[3]*Pharmacology Department, Faculty of Veterinary Medicine, Suez Canal University, Ismailia 41522, Egypt*
[4]*Department of Ophthalmology and Micro-Technology, Yokohama City University, Yokohama, Japan*

Correspondence should be addressed to Nagwa El-Badri; nelbadri@zewailcity.edu.eg

Received 26 October 2017; Accepted 31 December 2017; Published 18 March 2018

Academic Editor: Tullia Maraldi

Background. Based on animal studies, adult mesenchymal stromal cells (MSCs) are promising for the treatment of pancreatitis. However, the best type of this form of cell therapy and its mechanism of action remain unclear. *Methods*. We searched the PubMed, Web of Science, Scopus, Google Scholar, and Clinical Trials.gov websites for studies using MSCs as a therapy for both acute and chronic pancreatitis published until September 2017. *Results*. We identified 276 publications; of these publications, 18 met our inclusion criteria. In animal studies, stem cell therapy was applied more frequently for acute pancreatitis than for chronic pancreatitis. No clinical trials were identified. MSC therapy ameliorated pancreatic inflammation in acute pancreatitis and pancreatic fibrosis in chronic pancreatitis. Bone marrow and umbilical cord MSCs were the most frequently administered cell types. Due to the substantial heterogeneity among the studies regarding the type, source, and dose of MSCs used, conducting a meta-analysis was not feasible to determine the best type of MSCs. *Conclusion*. The available data were insufficient for determining the best type of MSCs for the treatment of acute or chronic pancreatitis; therefore, clinical trials investigating the use of MSCs as therapy for pancreatitis are not warranted.

1. Background

Pancreatitis is characterized by the release of pancreatic digestive enzymes from damaged exocrine cells and presents clinically in the following two forms: acute and chronic. Acute pancreatitis is a common cause of acute abdomen, which is self-limited in most cases; only 10–15% of patients with acute abdomen present with severe acute pancreatitis [1, 2]. Severe acute pancreatitis causes pancreatic tissue necrosis and organ failure with a mortality rate of up to 30–47% [1, 2]. Acute pancreatitis is induced by the acute activation of proenzymes in the pancreatic acinar cells leading to the lysis of the pancreatic tissue [3]. Inflammatory pancreatitis is associated with the local production of inflammatory cytokines, such as interleukin (IL)-1, IL-6, tumour necrosis factor-α (TNF-α), and interferon-γ (IFN-γ) [4, 5]. Remote organ failure results from the production of certain inflammatory chemokines, such as monocyte chemoattractant protein-1 (MCP-1) and fractalkine (FKN) [4, 6, 7]. Treatment strategies for acute pancreatitis remain lacking and are mainly conservative; in most cases, treatment is limited to fluid therapy and antibiotics in cases of infection. Nutritional support and prophylactic therapy are administered to prevent further pancreatic damage by inhibiting pancreatic enzyme synthesis and secretion [8, 9].

Chronic pancreatitis is a progressive condition that leads to damage in both the endocrine and exocrine pancreatic tissues and is complicated by diabetes (Type III) and exocrine pancreatic insufficiency. Alcohol consumption, genetic mutations, and pancreatic duct obstruction are the most

common risk factors for chronic pancreatitis [10]. Chronic pancreatitis is associated with chronic inflammation, leading to pancreatic fibrosis, acinar gland atrophy, and pancreatic duct obstruction [11]. Because pancreatic damage cannot be reversed, the treatment of chronic pancreatitis is mainly conservative.

Stem cell therapy has been considered for the treatment of many intractable diseases. MSCs are adult stem cells primarily isolated from bone marrow [12]. MSCs can self-renew and undergo multilineage differentiation [12]. According to the definition provided by the International Society for Cell Therapy, MSCs are characterized as plastic-adherent in standard culture conditions and can be differentiated in vitro into osteoblasts, chondroblasts, and adipocytes [13–15]. MSCs express specific surface markers, such as CD105, CD90, and CD73, but do not express CD45, CD34, CD14, CD11b, CD79 alpha, CD19, or HLA-DR. MSC-like cells have been isolated from other tissues, including the human placenta [16], peripheral blood [17], umbilical cord [18], adipose tissue [19], endometrium [20], and pancreas [12, 21, 22]. MSCs have been used for the treatment of wound injury and acute inflammation because they engraft into wounds and contribute to the remodelling of injured tissues [12, 15]. MSCs reduce the acute inflammatory response via their immunomodulatory effect by secreting anti-inflammatory cytokines, suppressing proinflammatory cytokines, and regulating immune cell activation [23–25]. MSCs suppress T cell proliferation and B cell maturation and activate regulatory T cells to further suppress the immune response in vitro [26, 27]. MSCs decrease chronic inflammation and subsequent fibrosis via multiple mechanisms, including the downregulation of the expression of TGF-β1, which is a major regulator of chronic inflammation and fibrosis [28, 29]. MSCs also attenuate local hypoxia and oxidative stress [30, 31]. MSCs decrease the secretion of collagen, which is the main constituent of the extracellular matrix (ECM), to ameliorate the excessive secretion of the ECM and its degradation during fibrosis [32, 33]. MSCs exert their immunosuppressive effect by decreasing the levels of anti-inflammatory cytokines and inhibiting the production of immunoglobulins and active immune cells [34, 35]. Furthermore, MSCs have been shown to specifically translocate to injured tissues and induce angiogenesis in ischaemic tissues [36–38]. Given these advantages, MSCs are promising candidates for cell replacement therapy for tissue inflammation. Due to the lack of effective therapies for both acute and chronic pancreatitis and the high mortality rate associated with severe acute pancreatitis, a new therapeutic approach is highly desirable. Due to their accessibility, relative safety, and lack of ethical considerations, MSC therapy is the most common approach used in experimental stem cell therapy. Here, we review studies that investigated the effects of MSC transplantation in acute and chronic pancreatitis.

2. Method

2.1. Eligibility Criteria for Systematic Search. The eligibility of the studies was assessed by two independent reviewers in duplicate. We included all studies describing in vivo experiments in which MSC transplantation was performed as the therapeutic approach for either acute or chronic pancreatitis. Review articles, hypotheses, conference abstracts, editorials, and studies describing only in vitro data were excluded. We also excluded in vitro studies using MSC therapy in an in vitro model of pancreatitis, studies using cell-free MSC derivatives, and articles written in languages other than English.

2.2. Search Strategy and Study Selection. A systematic search was conducted following the recommendations by the Preferred Reporting Items for Systematic Reviews and Meta-Analyses (PRISMA) [39]. We searched PubMed, Scopus, Google Scholar, Web of Science, and Clinical trials.gov for articles published until September 2017. In addition, we manually searched the reference lists of relevant review articles for any study that may have been missed during the database search. The following keywords were used: pancreatitis, mesenchymal stromal cells, mesenchymal stem cells, acute pancreatitis, chronic pancreatitis, bone marrow mesenchymal stromal cells, umbilical cord mesenchymal cells, pancreatitis therapy, and stem cells. Three investigators independently screened the titles and abstracts of the studies identified in the systematic search to determine their relevance. After the initial screening, we retrieved the relevant articles and assessed the articles according to the eligibility criteria.

2.3. Data Extraction, Synthesis, and Analysis. Two researchers independently extracted the data using a standardized Excel sheet. Discrepancies were resolved by consensus. We classified the studies according to the type of pancreatitis, that is, acute or chronic. The primary outcome measures included signs of pancreatic damage after the infusion of MSCs, changes in the serum amylase and lipase levels, and histological changes in the pancreatic tissue. Pancreatic tissue fibrosis was the primary outcome assessed in chronic pancreatitis studies using MSC therapy. The secondary outcome measures included the type of MSCs used, the mechanism by which the MSC therapy was effective in treating pancreatitis, and the effect of the cell infusion on mortality following acute pancreatitis. The extracted data included the inclusion criteria; exclusion criteria; MSC type; route, source and dose of therapy; and outcome measures. Due to the heterogeneity of the data, conducting a meta-analysis was not feasible.

2.4. Risk of Bias Assessment. Two investigators assessed the risk of bias in individual studies using the Cochrane Risk of Bias tool [40]. The risk of bias was assessed as "low risk," "high risk," or "unclear risk." The main items of bias were as follows: (1) sequence generation, (2) allocation concealment, (3) blinding of participants and personnel, (4) blinding of outcome assessors, (5) incomplete outcome data, (6) selective outcome reporting, (7) source of funding, (8) conflicts of interest, and (9) sample size calculations. We used additional domains from the SYRCLE Risk of Bias Tool, which is a tool used to assess the risk of bias in preclinical animal

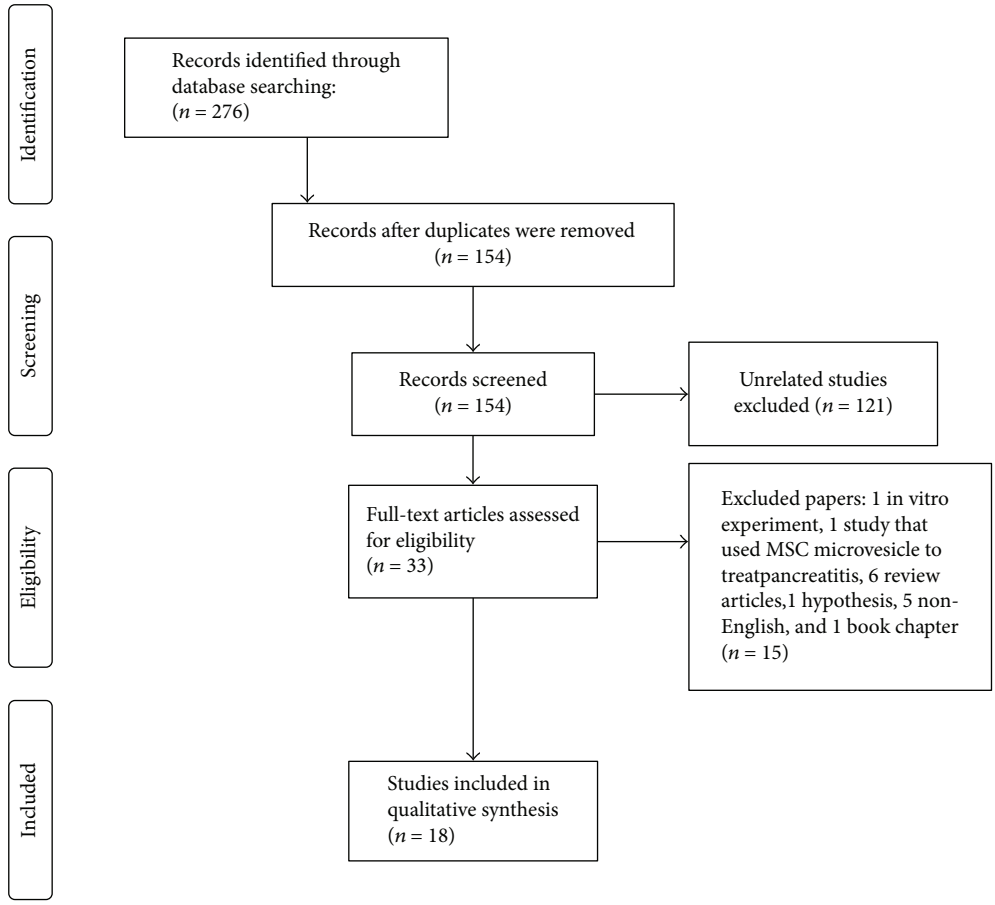

Figure 1: A flow chart to show the eligible studies for inclusion in the review.

studies [41]. These domains included the following: (1) similarity of experimental groups, (2) random housing of animals, and (3) random animal selection for outcome assessment. Disagreements between the investigators were resolved by consensus.

3. Results

We identified 276 publications; of these publications, 122 were duplicates and were removed. After reviewing the titles and abstracts, we excluded 121 unrelated studies. Thirty-two papers were eligible for a full-text review. We further excluded 15 studies as follows: one study involved an in vitro experiment, one study used MSC microvesicles to treat pancreatitis, 6 publications were review articles, one article was a hypothesis paper, 5 papers were written in a language other than English, and one publication was a book chapter. After the full-text review, only 18 studies met our inclusion criteria (flow chart: Figure 1).

Of the 18 included studies, 16 studies used MSCs for acute pancreatitis, while only 3 eligible studies used MSCs as a therapy for chronic pancreatitis (one study used MSCs for both acute and chronic pancreatitis) [42]. No previously published or currently ongoing clinical trials investigating MSC therapy for pancreatitis were identified. All included studies involved experimental animals. The most commonly used types of MSC in the included studies were bone marrow and umbilical cord MSCs. Bone marrow MSCs (BM-MSCs) were administered to animals in 12 studies; of these studies, 11 studies used BM-MSCs for the treatment of acute pancreatitis, and only one study used BM-MSCs for the treatment of chronic pancreatitis. Umbilical cord MSCs (UCMSCs) were examined in four studies; of these studies, 3 applied UCMSCs for the treatment of acute pancreatitis, and one applied UCMSCs for the treatment of chronic pancreatitis (Figure 2). The included studies used either rat or human MSCs, while one study used canine MSCs [43]. MSCs from rats were the most commonly used to treat pancreatitis ($N = 11$ studies; 8 investigating acute pancreatitis and 2 investigating chronic pancreatitis). Only 7 studies used human MSC for pancreatitis therapy (6 studies investigating acute pancreatitis and one study investigating chronic pancreatitis) (Figure 3). Among the 7 studies using human MSCs, 3 studies administered BM-MSCs to investigate acute pancreatitis, 3 other studies administered UCMSCs to investigate acute pancreatitis, and 1 study administered foetal membrane MSCs to investigate chronic pancreatitis.

3.1. MSC Therapy for Acute Pancreatitis. In 16 studies, MSCs were administered for the treatment of acute pancreatitis. Eleven studies used BM-MSCs [44–54], while 3 studies used UCMSCs [55–57]. Of the 11 studies, one study administered

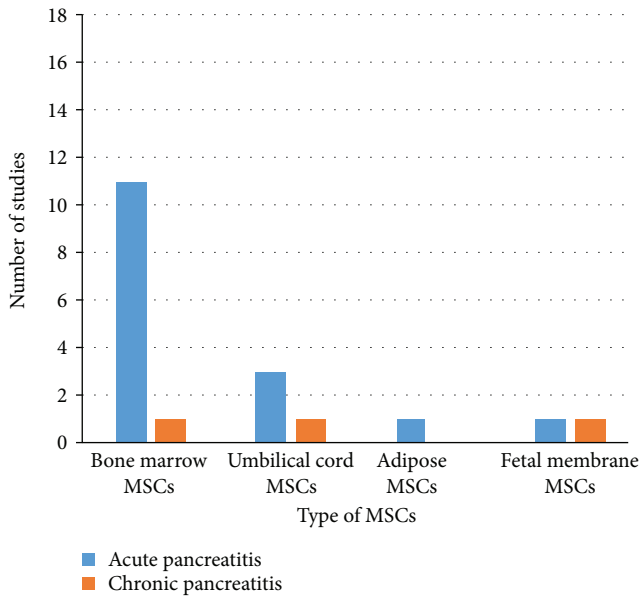

Figure 2: Number of studies according to the type of MSCs used to treat pancreatitis.

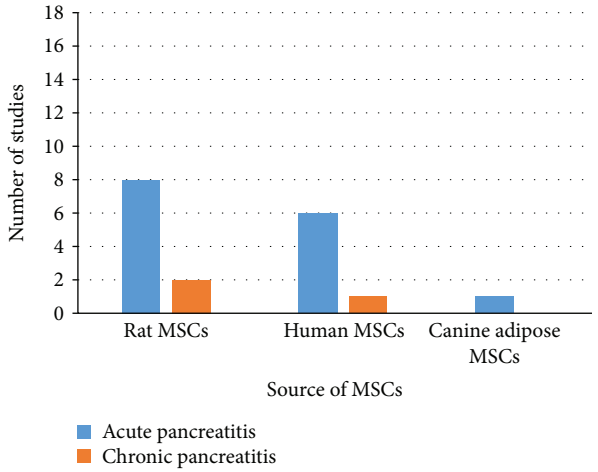

Figure 3: Number of studies according to the source of MSCs used to treat pancreatitis.

adipose-derived MSCs [43], and one study administered foetal membrane MSCs [42] (Table 1). Since acute pancreatitis is a self-limited condition and pancreatic tissue damage occurs only following severe acute pancreatitis, all included studies investigated the effect of MSC therapy in severe acute pancreatitis. Multiple methods of inducing severe acute pancreatitis were used: injection of Na-taurocholate (7 studies) [44, 46, 47, 49, 50, 52], intraperitoneal injections of caerulein (2 studies) [29, 30], L-arginine-induced acute pancreatitis (one study) [33], and deoxy-STC injection under the pancreatic capsule (1 study) [51]. All 16 studies showed a reduction in pancreatic tissue damage, necrosis, inflammation, and oedema compared to those of the untreated groups. In all 16 studies, the serum amylase and lipase levels were lower than those in the control groups. Fourteen of the 16 studies investigated the mechanism of action of the MSCs in alleviating the acute inflammation and tissue damage following acute pancreatitis. The studies evaluated the effect of MSC transplantation on immunomodulation, angiogenesis, and apoptosis as well as the antioxidant effect and the homing of infused cells (Figure 4).

Eleven of the 16 studies used BM-MSCs as therapy for severe acute pancreatitis [44–52]. Except for two studies [51, 52], well-characterized MSCs were infused into animals using defined surface markers and mesodermal differentiation according to the criteria of the International Society for Cell Therapy. Nine of the 11 studies further evaluated the mechanism of action of BM-MSCs following severe acute pancreatitis [44–49, 52]. Eight of the nine studies examined the immunomodulatory mechanism of the infused BM-MSCs. In 2 of the 8 studies, the infused BM-MSCs downregulated the expression of proinflammatory markers, including nuclear transcription factor kappa B p65 (NF-κB p65), IL-1β, IL-6, TNF-α, TGF-β, NOS2, COX2, SPHK1 IL-15, and IL-17 [44, 49]. One study showed that human clonal BM-MSCs suppressed T cell proliferation and increased the expression of Foxp3 regulatory T cells in pancreatic tissue with mild or severe acute pancreatitis [44]. One study showed that the infusion of rat BM-MSCs increased the expression of anti-inflammatory cytokines, such as IL-10, following acute pancreatitis [48]. Another study demonstrated that microRNA-9-modified BM-MSCs (pri-miR-9-BM-MSCs) could further ameliorate pancreatic damage in severe acute pancreatitis [54]. The pri-miR-9-BM-MSCs decreased the local and serum proinflammatory response (TNF-α, IL-1β, IL-6, HMGB1, MPO, and CD68), increased the levels of anti-inflammatory cytokines (IL-4, IL-10, and TGF-β), and enhanced the regeneration of the damaged pancreas. Furthermore, these pri-miR-9-BM-MSCs could deliver miR-9 to the damaged pancreas and peripheral blood mononuclear cells (PBMCs) and inhibit the NF-κB signalling pathway [54]. Three of the eleven studies administered BM-MSCs as therapy for severe acute pancreatitis, and the BM-MSCs increased antioxidant activities, such as superoxide dismutase (SOD) and glutathione peroxidase (GPx) [45, 51, 54]. In one study, human clonal BM-MSCs decreased the levels of malondialdehyde (MDA), which is a product of lipid peroxidation that increases during acute pancreatitis [45]. Two of the eleven studies administered BM-MSCs as a therapy for severe acute pancreatitis and showed that human BM-MSCs used as a therapy for acute pancreatitis enhance neovascularization and angiogenesis [46, 47]. After the administration of BM-MSCs pretreated with stromal-cell-derived factor 1α (SDF-1α), the expression of angiogenesis markers (CD31, VEGF, and vWF) was increased in the pancreatic tissue [46]. Compared with untreated BM-MSCs, the supernatant from human BM-MSCs pretreated with SDF-1α significantly promoted angiogenesis in vitro [46]. In one study, human BM-MSCs transfected with TSG-6 were infused to treat severe acute pancreatitis based on the premise that

Table 1: Summary of studies addressed MSCs in acute pancreatitis. L-arg: L-arginine; Na TCA: sodium taurocholate solution; TCA: taurocholic acid solution; LPS: lipopolysaccharide; rBM-MSCs: rat bone marrow mesenchymal stromal cells; hBM-MSCs: human bone marrow mesenchymal stromal cells; UCMSCs: umbilical cord mesenchymal stromal cells; hUCMSCs: human umbilical cord mesenchymal stromal cells; rFMMSCs: rat fetal membrane mesenchymal stromal cells; SD rats: Sprague Dawley rats; mir-9: microRNA-9; N/A: not applicable; PBS: phosphate buffer saline.

Author	Pancreatitis induction method	Source of MSCs	Dose of MSCs	Route of MSC infusion	Timeline of MSC therapy		Specific treatment of MSCs	Outcome		
					Treatment time point	Scarification timeline		Serum amylase and lipase	Histological feature of pancreas	Mechanism of action of infused MSCs
Qu et al., [53]	L-arg	rBM-MSCs	1 ml cell suspension: 1×10^7 cells/ml	Tail vein of SD rats	4 days	After 7, 14, and 21 days	N/A	Decreased	Decreased	(i) Pancreatic lineage differentiation
Qian et al., [54]	Na TCA and Caerulein	rBM-MSCs	1×10^7cells/kg	Tail vein of SD rats	24 hrs.	After 3 days	miR-9 modified BM-MSCs	Decreased	Decreased	(i) Immunomodulatory effect (ii) Antiapoptotic effect (iii) Antioxidant effect (iv) Enhancement of regeneration of damaged pancreas (v) Deliver miR-9 to the injured pancreas or peripheral blood mononuclear cell (PBMC), which can target the NF-κB1/p50 gene and inhibit the NF-κB signaling pathway
He et al., [47]	Na TCA	hBM-MSCs	2.0×10^6 cells	Tail vein of C57BL/6 mice	6 hrs.	N/A	hBM-MSCs transfected with TSG-6 siRNA	Decreased	Decreased	(i) Immunomodulatory effect
Jung et al., [45]	Cerulein and sequential LPS	hBM-MSCs	1×10^6 cells	Tail vein of SD rats	24 hrs	After 3 days	N/A	Decreased	Decreased	(i) Immunomodulatory effect (ii) Antioxidant effect
Yin et al., [48]	L-arg	rBM-MSCs	1×10^6 cells	Tail vein of SD rats	3 hrs.	After 1, 2, and 3 days	N/A	Decreased	Decreased	(i) Immunomodulatory effect
Qian et al., [46]	Na TCA	rBM-MSCs	1×10^7 cells/ml/kg	Tail vein of SD rats	1, 5, 7, and 10 days	N/A	BM-MSCs pretreated with SDF-1α	Decreased	Decreased	(i) Immunomodulatory effect (ii) Angiogenesis-enhancing effect
Tu et al., [52]	Na TCA	rBM-MSCs	2×10^6 cells/ml	Dorsal penile vein of SD rats	1 hr.	After 6, 12, 24, and 48 hrs.	N/A	Decreased	Decreased	N/A

Table 1: Continued.

Author	Pancreatitis induction method	Source of MSCs	Dose of MSCs	Route of MSC infusion	Timeline of MSC therapy		Specific treatment of MSCs	Outcome		
					Treatment time point	Scarification timeline		Serum amylase and lipase	Histological feature of pancreas	Mechanism of action of infused MSCs
Chen et al., [50]	Na TCA	BM-MSCs (source not specified)	1×10^6 cells	Tail vein of SD rats	0 hr. 0, 6 hrs. 0, 6, and 12 hrs.	After 6 hrs. After 12 hrs. After 24 hrs.	N/A	Decreased	Decreased	N/A
Tu et al., [51]	Deoxy-STC	rBM-MSCs	2 ml cell suspension: 1×10^6 cells/ml	Tail vein of SD rats	N/A	After 6, 24, and 72 hrs.	N/A	Decreased	Decreased	(i) Immunomodulatory effect (ii) Antioxidant effect
Zhao et al., [49]	TCA	rBM-MSCs	$5–7 \times 10^7$ cells	Tail vein of SD rats	24 hrs.	After 72 hrs.	N/A	Decreased	Decreased	(i) Immunomodulatory effect
Jung et al., [44]	Mild acute pancreatitis: cerulein Severe acute pancreatitis: Na TCA	hBM-MSCs	N/A	Tail vein of SD rats	N/A	After 3 days	N/A	Decreased	Decreased	(i) Immunomodulatory effect (ii) Antiapoptotic effect (apoptosis of acinar cells was reduced in severe acute pancreatitis than in mild acute pancreatitis)
Hua et al., [57]	Na TCA	hUCMSCs	1×10^6 cells in 200 μl saline	Tail vein of SD rats	12 hrs	After 3 days	ANGPT1-transfected hUCMSCs	Decreased	Decreased	(i) Immunomodulatory effect (ii) Angiogenesis-enhancing effect
Yang et al., [56]	Na TCA	hUCMSCs	5×10^6 cells/kg 5×10^4, 5×10^6, and 1×10^7 cells/kg 5×10^6	Tail vein of SD rats	0, 1, 6, and 12 hrs 1 hr 6 hrs	After 48 hrs.	N/A	Decreased	Decreased	(i) Immunomodulatory effect
Meng et al., [55]	Na TCA	hUSMSCs	1×10^7 cells/kg	Tail vein of SD rats	12 hrs	After 1, 3, and 5 days	N/A	Decreased	Decreased	(i) Antiapoptotic effect (reduce acinar cell apoptosis) (ii) Immunomodulatory effect
Kim et al., [43]	Na TCA	Canine adipose tissue-derived MSCs	2×10^6 cells/kg in 200 μl PBS	Tail vein of SD rats	N/A	After 3 days	N/A	Decreased	Decreased	(i) Immunomodulatory effect
K et al., 2016	TCA	rFMMSCs	1×10^6 cells in 200 ul PBS	Penile vein of August Copenhagen Irish rats	N/A	After 4 days	N/A	Decreased	Decreased	(i) Immunomodulatory effect

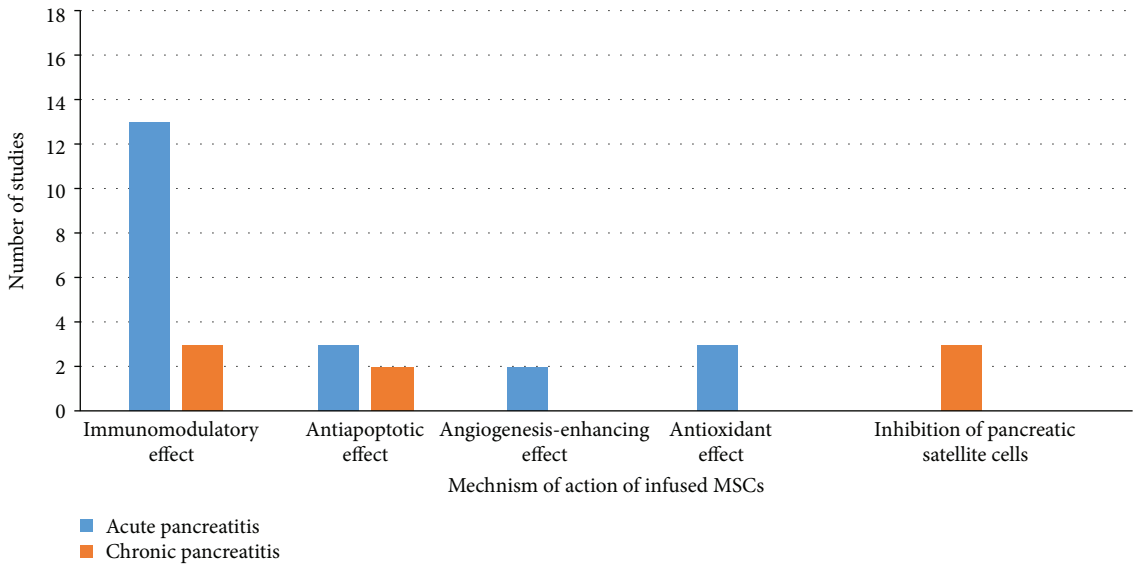

Figure 4: Mechanism of action of infused MSCs in acute and chronic pancreatitis.

the effect of MSCs was partially due to activation by signals from injured tissues and the secretion of multifunctional anti-inflammatory protein tumour necrosis factor-α-stimulated gene/induced protein 6 (TSG-6/TNAIP6), leading the authors to hypothesize that infused MSCs exerted their key effects primarily via the secretion of TSG-6 [47]. These studies showed that MSCs could significantly inhibit the activation and release of proinflammatory cytokines (TNF-α, IL-1β, and IL-6) and increase the production of anti-inflammatory cytokines (IL-4 and IL-10). In addition, the infused MSCs significantly reduced the serum level of MCP-1, which is a vital chemokine in the pathogenesis of pancreatitis [47]. Another study showed that pancreatic tissue damage could be further improved following MSC transplantation along with granulocyte colony stimulating factor (G-CSF) therapy [53]. In addition to its role in the mobilization of haematopoietic stem cells, G-CSF enhanced the proliferation of transplanted BM-MSCs by binding to G-CSF receptors [53, 58]. This study showed that G-CSF promoted BM-MSC homing and enhanced the ability of the BM-MSCs to differentiate into cells of the pancreatic lineage as evidenced by the expression of the pancreatic markers Nkx6, Ngn3, and Pax4 [53].

Five of 11 studies examined BM-MSC homing to the injured pancreas after the induction of acute pancreatitis by tracking the infused BM-MSCs [44, 48, 49, 53, 54]. In only 4 of these 5 studies, the human BM-MSCs homed to the damaged pancreatic tissue after the induction of severe acute pancreatitis [44, 49, 53, 54]. Interestingly, none of the studies that used BM-MSC as a therapy for severe acute pancreatitis reported the effect of the transplanted BM-MSCs on mortality in the animal models used for severe acute pancreatitis.

Three studies investigated the effect of umbilical cord-derived mesenchymal stem cells (UCMSCs) on severe acute pancreatitis [55–57]. All 3 studies used well-characterized MSCs as defined by surface markers and the mesodermal differentiation potential according to the criteria of the International Society for Cell Therapy. The UCMSC injection reduced pancreatic tissue damage in all 3 studies. Necrosis, inflammation, and oedema were ameliorated, and the levels of serum amylase and lipase were decreased. Similarly, in these same studies, the UCMSCs reduced the serum levels of proinflammatory cytokines (TNF-α, IFN-γ, IL-1β, and IL-6) and increased the levels of anti-inflammatory cytokines (IL-4 and IL-10) [55–57]. In one of these studies, the infusion of UCMSCs reduced pancreatic acinar cell apoptosis compared to that observed in the control group [55]. One study used modified UCMSCs and examined their effect on angiogenesis. The UCMSCs were transfected with Angiopoietin-1 (ANGPT1), which plays an important role in the regulation of endothelial cell survival, vascular stabilization, and angiogenesis. The administration of the ANGPT1-transfected UCMSCs resulted in further reductions in pancreatic injury and serum levels of proinflammatory cytokines and promoted pancreatic angiogenesis. Of the three studies that administered UCMSCs as therapy for severe acute pancreatitis, only one reported the mortality rate after the administration of UCMSCs and showed that the infusion decreased mortality after the induction of severe acute pancreatitis [56].

The administration of canine adipose-derived MSCs reduced the serum levels of proinflammatory cytokines (TNF-α, IFN-γ, IL-1β, and IL-6) while increasing the levels of anti-inflammatory cytokines (IL-4 and IL-10). In addition, the canine adipose-derived MSCs decreased the percentage of $CD3^+$ T cells while simultaneously increasing the percentage of $FoxP3^+$ regulatory T cells in the damaged pancreatic tissue [43]. However, this study did not show the effect of the adipose-derived MSC infusion on mortality following acute pancreatitis.

Compared to the untreated group, the administration of rat foetal membrane-derived mesenchymal stem cells (rat FM-MSC) into the rat penile vein after the induction of severe acute pancreatitis reduced the serum levels of proinflammatory cytokines (TNF-α and IL-6) [42]. The

rat FM-MSCs also reduced the number of $CD68^+$ cells [42]. However, this study did not show the effect of MSC infusion on mortality following acute pancreatitis.

Due to heterogeneity in the administered MSCs, their dose, the frequency of administration, the sources and types of MSCs, and the method of the induction of pancreatitis, a valid comparison among the different protocols is challenging. We could not statistically compare the different types of MSCs to determine the superiority of any one type of MSCs in achieving a favourable therapeutic outcome in acute pancreatitis.

3.2. MSC Therapy for Chronic Pancreatitis. The literature search resulted in only 3 studies in which MSCs were administered for the treatment of chronic pancreatitis. In the three studies, chronic pancreatitis was induced in Sprague Dawley rats by an intravenous injection of dibutyltin dichloride via the penile vein [42, 59, 60]. The sources of the MSCs included rat umbilical cord MSCs [60], human amnion-derived MSCs (hAMSCs) [42], and rat BM-MSCs [59] (Table 2). All three studies showed reduced pancreatic damage and decreased fibrosis after the administration of the stem cells [42, 59, 60]. In all studies, this effect was considered a result of the inhibition of the pancreatic satellite cells. The injection of rat UCMSCs lowered the expression of monocyte chemoattractant protein 1 (MCP-1), vascular cell adhesion molecule 1 (VCAM-1), intercellular adhesion molecule 1 (ICAM-1), IL-6, and TNF-α [60]. The tracking of the infused rat UCMSCs using carboxyfluorescein succinimidyl ester (CFSE) dye revealed that these cells homed to and engrafted the damaged pancreatic tissue [60]. In another study, nuclear factor kappa B (NF-kB), which is an important regulator of the inflammatory response and apoptosis, was inactivated in rat UCMSCs using the inhibitor IκBαM. The modified UCMSCs, called IκBαM-MSCs, were then infused to treat chronic pancreatitis in a rat model. IκBαM-MSCs reduced the levels of proinflammatory cytokines, such as IL-1, IL-6, IL-8, FN, TIMP-1, TIMP-2, TNF-α, CTGF, ICAM-1, and TGF-β1; increased the levels of anti-inflammatory cytokines, such as IL-10; and promoted apoptosis in pancreatic stellate cells [59]. This effect was greater than that achieved by injection of rat UCMSCs alone [59].

3.3. Assessment of Risk of Bias and Methodological Quality. By assessing the methodological quality and risk of bias in each included study (Figure 5), we found that allocation concealment was not performed in any of the reported studies. In addition, a description of the blinding of the personnel who conducted the animal experiments was not included in any of the studies. Seven of the 18 studies (38.9%) blinded the assessors of the outcome (27.8% of the studies investigating acute pancreatitis, $N = 5$ and 11.1% of the studies investigating chronic pancreatitis, $N = 2$). The remaining studies were evaluated in an unclear manner due to the lack of data regarding their method of blinding. Only 2 of the 18 studies (11.1%) (both were used for the treatment of acute pancreatitis) were assessed as having a low risk for bias for incomplete outcome data, since the number of animals reported was consistent between the methods and results. The studies addressing chronic pancreatitis were evaluated as unclear for the risk of bias since the number of animals was not reported in either Method or Results; thus, sufficient data were not available to assess this feature. Sixteen of the 18 studies (88.9%) (72.2%, $N = 13$ in which MSC therapy was applied for acute pancreatitis and 2 studies, 11.1% in which MSC therapy was applied for chronic pancreatitis) were assessed as having a low risk of bias for selective reporting of the data. In Method, the serum amylase and lipase levels along with the histological scoring or pancreatic fibrosis (in case of chronic pancreatitis) as the prespecified outcome measure were reported. In only one study (using MSCs as a therapy for chronic pancreatitis), the serum amylase and lipase levels, along with the histological scoring, were presented in Results but unmentioned as an outcome in Method.

Only 5 of the 18 studies (27.7%) reported that the baseline severity of the disease was equal between the test and control groups (16.7%, $N = 3$ for MSC therapy for acute pancreatitis, and 11.1%, $N = 2$ using MSC therapy for chronic pancreatitis). Fourteen of the 18 studies (77.8%) had nonindustry sources of funding (61.1%, $N = 11$ for therapy for acute pancreatitis, 16.7%, $N = 3$ for chronic pancreatitis). Eleven of the 18 studies (61.1%) reported no conflicts of interest (50%, $N = 9$ for therapy for acute pancreatitis, and 11.1%, $N = 2$ for chronic pancreatitis), while 6 of the 18 studies reported a potential conflict of interest (all 6 were studies investigating acute pancreatitis, $N = 4$ BM-MSC therapy for acute pancreatitis, and $N = 2$ UCMSC therapy for acute pancreatitis). Only 6 studies (33.3%) (22.2%, $N = 4$ for acute pancreatitis, and 11.1%, $N = 2$ for chronic pancreatitis) reported a justification for their sample size selection (22.2%, $N = 4$ for acute pancreatitis, and 11.1%, $N = 2$ for chronic pancreatitis), while in the remaining studies, no calculation of sample size was performed. Only 2 studies (11.1%) reported that the animals used in the study were randomized ($N = 2$ for MSC therapy for acute pancreatitis). Due to the limited number of studies that reported internal validity practices, we could not proceed with an analysis to identify the effects of high versus low risks of bias on the effect size.

4. Discussion and Conclusion

In this study, we systematically reviewed studies investigating the effect of MSC therapy on acute and chronic pancreatitis. The impetus of this study was the absence of therapeutic strategies for pancreatitis and the promising therapeutic effect of MSCs. The current conservative therapy used for pancreatitis is effective in relieving the acute process of the disease and reducing patient mortality. However, this conservative therapy does not ensure a complete cure. Indeed, resistant chronic pancreatitis is often a sequela of the disease. The benefits of MSC therapy for pancreatitis include the amelioration of the local inflammatory process and damage to acinar cells in acute pancreatitis, and hence MSC therapy may limit the extent of fibrosis in chronic

Table 2: Summary of studies addressed MSCs in chronic pancreatitis. hFMMSCs: human fetal membrane mesenchymal stromal cells; rBM-MSCs: rat bone marrow mesenchymal stromal cell; rUCMSCs: rat umbilical cord mesenchymal stromal cells; PBS: phosphate buffer saline; SD rats: Sprague Dawley rats; N/A: not applicable

Author	Method of induction of pancreatitis	Source of MSCs	Dose of infused MSCs	Route of MSC infusion	Timeline of MSC therapy		Specific treatment of MSCs	Outcome	
					Infusion time point	Scarification time point		Pancreatic fibrosis	Mechanism of action of infused MSCs
K et al., 2016	Dibutyltin dichloride	hFMMSCs	1×10^6 cells in 200 μl PBS	Penile vein of SD rats	On day 5	Day 14	N/A		(i) Immunomodulatory effect (ii) Inhibition of activation of pancreatic satellite cells
Qin et al., [59]	N/A	rBM-MSCs	N/A	N/A	Group 1: 4 hrs. before chronic pancreatitis Group 2: during chronic pancreatitis Group 3: 4 hrs. after chronic pancreatitis	N/A	BM-MSCs were transfected with IkBαM	Decreased	(i) Immunomodulatory effect (ii) Antiapoptotic effect: reduced acinar cell apoptosis (iii) Inhibition of activation of pancreatic satellite cells
Zhou et al., [60]	Dibutyltin dichloride	rUCMSCs	1×10^6 cells/ml	Jugular vein of SD rats	On day 5	On days 14 and 28	rUCMSCs injected through jugular vein		(i) Immunomodulatory effect (ii) Antiapoptotic effect: reduced acinar cell apoptosis (iii) Inhibition of activation of pancreatic satellite cells

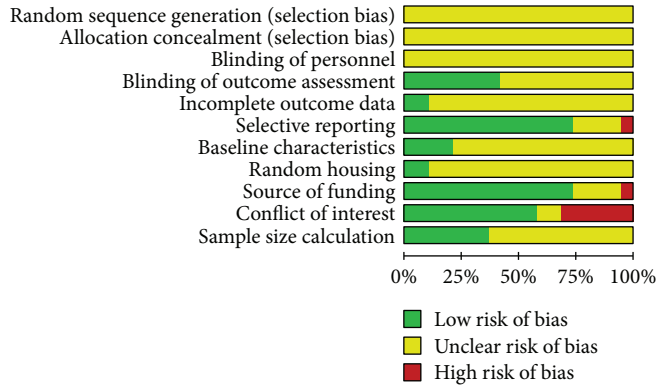

Figure 5: Risk of bias assessment for included studies.

pancreatitis. Recently, MSCs have been shown to be capable of replacing damaged pancreatic cells [53].

All studies were performed in rodents and showed pronounced heterogeneity in the outcome assessment; hence, conducting a meta-analysis was not feasible. Heterogeneity was observed in the technique used to induce pancreatitis, the type of MSCs used, the time of therapy after the disease onset, the source of the MSCs (human or murine), and the dose of the MSCs. Due to the lack of consistency, determining the most effective form of MSC therapy for pancreatitis is challenging. Similarly, none of the studies investigating chronic pancreatitis evaluated the efficacy of MSC therapy in a dose-dependent manner or followed up on the disease progression.

The included studies failed to address selection bias and detection bias using techniques such as randomization, blinding, and sample size calculations. These limitations in the study methodologies may have led to an exaggeration of the reported therapeutic effect [61–65]. Thus, these factors should be evaluated in future preclinical studies to ensure the validity of these studies because the currently available data do not sufficiently warrant the use of MSCs in clinical trials.

The mechanism of action of MSC therapy in both types of pancreatitis was confined to immunomodulatory effects mediated by the secretion of pro- and anti-inflammatory cytokines (Figure 4). No sufficient data were available regarding the interaction between MSCs and local immune cells. CD4+ T cells have been found to play a critical role in the development of tissue injury during acute pancreatitis in mice since the severity of pancreatitis is ameliorated by CD4+ T cell depletion [66]. MSCs have indeed been shown to suppress CD4+ T cell proliferation via multiple soluble factors or in a cell contact-dependent manner [67]. The favourable role of MSCs in the suppression of CD4+ T cell proliferation in acute pancreatitis warrants further investigation.

Necrosis of acinar cells, which is accompanied by the release of digestive enzymes, is the basic mechanism underlying the pathology of severe acute pancreatitis. In total, 3 studies showed that MSCs reduce oxidative stress, accounting for most of the damage to acinar cells [45, 51, 68]. In two other studies, the antiapoptotic effect of MSCs on acinar cells was documented [44, 55]. However, the mechanism by which MSCs exert this effect on acinar cells during acute pancreatitis remains unknown. Recent reports suggest that MSCs exert their antiapoptotic effect by secreting the antiapoptotic chemokine XCL1 [69]. Mouse skeletal myoblasts cocultured with MSCs showed very high resistance to apoptosis. This mechanism was mediated by the secretion of XCL1 by MSCs [69].

The tracking of the infused MSCs was important for determining their possible mechanism of action, particularly since numerous reports suggest that MSCs exert their regenerative effect via a paracrine, immunosuppressive effect rather than by directly differentiating into tissue-specific cells (in this case, pancreatic cells) [70]. A substantial body of literature reports that most intravenously infused MSCs become trapped in the lungs, raising many questions regarding their direct role in tissue regeneration [25, 44, 46, 47]. A study by Gong et al. showed that SDF-1, a critical regulator for MSC migration, is upregulated in injured pancreas following acute pancreatitis. SDF-1 enhanced BM-MSC migration in vitro as well as in vivo to injured pancreas during acute pancreatitis through their receptor: CXC chemokine receptor-4 (CXCR-4). BM-MSCs treated with anti CXCR-4 antibody showed less migration in vitro and less capability to migrate and to heal injured pancreas in comparison to untreated group, suggesting that SDF/CXCR4 axis may be important in regulation of MSC migration following acute pancreatitis [71].

Both marrow MSCs and UCMSCs lead to reduction in inflammation associated with acute pancreatitis along with enhanced angiogenesis when administered intravenously to affected rats. These MSCs ameliorate inflammation, which is likely one of the most obvious applications of MSC therapy in pancreatitis. In He et al. study, BM-MSCs were transfected with TSG-6 resulting in a significantly enhanced immunomodulatory function and improved effectiveness in treating severe acute pancreatitis [47]. TSG-6 has a potent anti-inflammatory effect with no apparent toxicity [72–74] and is thus a potentially effective therapy for severe acute pancreatitis. Human adipose-derived stem cells (HADSCs) may have potential to reduce inflammation through their immunomodulatory [75–77] and angiogenesis-enhancing effect [78] in addition to the secretion of growth factors

that promote repair [79]. Although these data suggest that HADSCs have a therapeutic potential in acute pancreatitis [80], no sufficient studies investigating the effect of HADSC therapy in acute pancreatitis have been reported.

In addition to morbidity, mortality is an important parameter in evaluating new therapies, particularly in a debilitating diagnosis, such as severe acute pancreatitis. Mortality is a frequent sequela (may reach up to 30–47%) of acute pancreatitis due to the complications of organ failure and tissue necrosis [1, 2]. Most evaluated studies did not assess mortality after the MSC infusion. Because the first 24 hours after the onset of acute pancreatitis are critical for prognosis [81], the therapeutic effect of the injected MSCs should be evaluated within this time frame. Studies investigating MSC therapy have shown that the time frame for the maximum therapeutic effect is an important determining factor, and early intervention is almost always necessary [82]. Indeed, only a few studies evaluated the outcome of MSC administration within 24 hours of the induction of severe acute pancreatitis [47, 50, 52, 55–57].

Unlike acute pancreatitis, very few (only 3) studies evaluated MSC therapy in chronic pancreatitis [42, 59, 60]. Interestingly, all 3 studies showed the promising potential of MSCs in decreasing the fibrosis that complicated chronic inflammation. MSCs appeared to exert their immunomodulatory effect on profibrotic factors, such as oxidative stress, hypoxia, and the transforming growth factor-β1 pathway [83].

Due to the significant therapeutic effect of MSCs and the lack of treatments for pancreatitis, the currently available data suggest that MSCs may be an attractive source of cell therapy for both acute and chronic pancreatitis. The relative safety of the protocol, particularly using autologous stem cells, coupled with the lack of effective traditional therapeutic approaches, merit clinical trials. However, the standardization of the therapy in the experimental setting is clearly lacking.

Disclosure

This work was presented as an oral presentation at 21st Pan Arab Conference on Diabetes, March 21–24, 2017.

Conflicts of Interest

Authors declare no competing financial interests.

Authors' Contributions

Sara M. Ahmed and Nagwa El-Badri conceived the idea; determined the inclusion and exclusion criteria, systematic search plan, and literature screening for eligibility; prepared the data extraction excel sheet and data extraction; and wrote and revised the whole paper. Mohamed M. Abdel-Daim critically revised the paper. Mahmoud Morsi helped in data extraction and literature screening for eligibility, prepared graphs, prepared risk assessment graph, revised the paper, and shared in writing Results and tables. Nehal I. Ghoneim helped in literature screening for eligibility, prepared risk of assessment graph, and revised the paper.

Acknowledgments

This work has been supported by Grant no. 5300 from the Science and Technology Development Fund.

References

[1] M. S. Petrov, S. Shanbhag, M. Chakraborty, A. R. J. Phillips, and J. A. Windsor, "Organ failure and infection of pancreatic necrosis as determinants of mortality in patients with acute pancreatitis," *Gastroenterology*, vol. 139, no. 3, pp. 813–820, 2010.

[2] C. E. Forsmark and J. Baillie, "AGA Institute technical review on acute pancreatitis," *Revista de Gastroenterología de México*, vol. 72, no. 3, pp. 257–285, 2007.

[3] Y. C. Chan and P. S. Leung, "Acute pancreatitis: animal models and recent advances in basic research," *Pancreas*, vol. 34, no. 1, pp. 1–14, 2007.

[4] T. Ishibashi, H. Zhao, K. Kawabe et al., "Blocking of monocyte chemoattractant protein-1 (MCP-1) activity attenuates the severity of acute pancreatitis in rats," *Journal of Gastroenterology*, vol. 43, no. 1, pp. 79–85, 2008.

[5] J. L. Frossard, M. L. Steer, and C. M. Pastor, "Acute pancreatitis," *Lancet*, vol. 371, no. 9607, pp. 143–152, 2008.

[6] L. Huang, P. Chen, L. Xu, Y. Zhou, Y. Zhang, and Y. Yuan, "Fractalkine upregulates inflammation through CX3CR1 and the Jak–Stat pathway in severe acute pancreatitis rat model," *Inflammation*, vol. 35, no. 3, pp. 1023–1030, 2012.

[7] L. Huang, J. Ma, Y. Tang et al., "siRNA-based targeting of fractalkine overexpression suppresses inflammation development in a severe acute pancreatitis rat model," *International Journal of Molecular Medicine*, vol. 30, no. 3, pp. 514–520, 2012.

[8] J. Baillie, "AGA Institute medical position statement on acute pancreatitis," *Gastroenterology*, vol. 132, no. 5, pp. 2019–2021, 2007.

[9] C. Y. Wang and Y. P. Zhao, "The guidelines interpretation for diagnosis and treatment of severe acute pancreatitis," *Zhonghua Wai Ke Za Zhi*, vol. 51, no. 3, pp. 198–200, 2013.

[10] E. Afghani, "Introduction to pancreatic disease: chronic pancreatitis," in *Pancreapedia: Exocrine Pancreas Knowledge Base*, The Exocrine Pancreas Knowledge Base, USA, 2015.

[11] M. W. Büchler, H. Freiss, and W. Uhl, *Chronic Pancreatitis: Novel Concepts in Biology and Therapy*, Blackwell Publishing, Oxford, UK, 2002.

[12] K. L. Seeberger, J. M. Dufour, A. M. J. Shapiro, J. R. T. Lakey, R. V. Rajotte, and G. S. Korbutt, "Expansion of mesenchymal stem cells from human pancreatic ductal epithelium," *Laboratory Investigation*, vol. 86, no. 2, pp. 141–153, 2006.

[13] M. Dominici, K. Le Blanc, I. Mueller et al., "Minimal criteria for defining multipotent mesenchymal stromal cells. The International Society for Cellular Therapy position statement," *Cytotherapy*, vol. 8, no. 4, pp. 315–317, 2006.

[14] B. J. Herdrich, R. C. Lind, and K. W. Liechty, "Multipotent adult progenitor cells: their role in wound healing and the treatment of dermal wounds," *Cytotherapy*, vol. 10, no. 6, pp. 543–550, 2008.

[15] J. L. Spees, M. J. Whitney, D. E. Sullivan et al., "Bone marrow progenitor cells contribute to repair and remodeling of the

lung and heart in a rat model of progressive pulmonary hypertension," *The FASEB Journal*, vol. 22, no. 4, pp. 1226–1236, 2008.

[16] V. L. Battula, P. M. Bareiss, S. Treml et al., "Human placenta and bone marrow derived MSC cultured in serum-free, b-FGF-containing medium express cell surface frizzled-9 and SSEA-4 and give rise to multilineage differentiation," *Differentiation*, vol. 75, no. 4, pp. 279–291, 2007.

[17] N. J. Zvaifler, L. Marinova-Mutafchieva, G. Adams et al., "Mesenchymal precursor cells in the blood of normal individuals," *Arthritis Research & Therapy*, vol. 2, no. 6, pp. 477–488, 2000.

[18] A. Erices, P. Conget, and J. J. Minguell, "Mesenchymal progenitor cells in human umbilical cord blood," *British Journal of Haematology*, vol. 109, no. 1, pp. 235–242, 2000.

[19] K. Morizono, D. A. De Ugarte, M. Zhu et al., "Multilineage cells from adipose tissue as gene delivery vehicles," *Human Gene Therapy*, vol. 14, no. 1, pp. 59–66, 2003.

[20] R. Dimitrov, T. Timeva, D. Kyurkchiev et al., "Characterization of clonogenic stromal cells isolated from human endometrium," *Reproduction*, vol. 135, no. 4, pp. 551–558, 2008.

[21] R. M. Baertschiger, D. Bosco, P. Morel et al., "Mesenchymal stem cells derived from human exocrine pancreas express transcription factors implicated in beta-cell development," *Pancreas*, vol. 37, no. 1, pp. 75–84, 2008.

[22] J. Kim, M. J. Breunig, L. E. Escalante et al., "Biologic and immunomodulatory properties of mesenchymal stromal cells derived from human pancreatic islets," *Cytotherapy*, vol. 14, no. 8, pp. 925–935, 2012.

[23] K. Sato, K. Ozaki, I. Oh et al., "Nitric oxide plays a critical role in suppression of T-cell proliferation by mesenchymal stem cells," *Blood*, vol. 109, no. 1, pp. 228–234, 2007.

[24] L. A. Ortiz, M. DuTreil, C. Fattman et al., "Interleukin 1 receptor antagonist mediates the antiinflammatory and antifibrotic effect of mesenchymal stem cells during lung injury," *Proceedings of the National Academy of Sciences of the United States of America*, vol. 104, no. 26, pp. 11002–11007, 2007.

[25] R. H. Lee, A. A. Pulin, M. J. Seo et al., "Intravenous hMSCs improve myocardial infarction in mice because cells embolized in lung are activated to secrete the anti-inflammatory protein TSG-6," *Cell Stem Cell*, vol. 5, no. 1, pp. 54–63, 2009.

[26] I. Rasmusson, O. Ringden, B. Sundberg, and K. Le Blanc, "Mesenchymal stem cells inhibit lymphocyte proliferation by mitogens and alloantigens by different mechanisms," *Experimental Cell Research*, vol. 305, no. 1, pp. 33–41, 2005.

[27] S. Aggarwal and M. F. Pittenger, "Human mesenchymal stem cells modulate allogeneic immune cell responses," *Blood*, vol. 105, no. 4, pp. 1815–1822, 2005.

[28] C. Linard, E. Busson, V. Holler et al., "Repeated autologous bone marrow-derived mesenchymal stem cell injections improve radiation-induced proctitis in pigs," *Stem Cells Translational Medicine*, vol. 2, no. 11, pp. 916–927, 2013.

[29] P. C. Tsai, T. W. Fu, Y. M. A. Chen et al., "The therapeutic potential of human umbilical mesenchymal stem cells from Wharton's jelly in the treatment of rat liver fibrosis," *Liver Transplantation*, vol. 15, no. 5, pp. 484–495, 2009.

[30] C. K. Sun, C. H. Yen, Y. C. Lin et al., "Autologous transplantation of adipose-derived mesenchymal stem cells markedly reduced acute ischemia-reperfusion lung injury in a rodent model," *Journal of Translational Medicine*, vol. 9, no. 1, p. 118, 2011.

[31] J. Niu, A. Azfer, O. Zhelyabovska, S. Fatma, and P. E. Kolattukudy, "Monocyte chemotactic protein (MCP)-1 promotes angiogenesis via a novel transcription factor, MCP-1-induced protein (MCPIP)," *The Journal of Biological Chemistry*, vol. 283, no. 21, pp. 14542–14551, 2008.

[32] L. Song, Y. J. Yang, Q. T. Dong et al., "Atorvastatin enhance efficacy of mesenchymal stem cells treatment for swine myocardial infarction via activation of nitric oxide synthase," *PLoS One*, vol. 8, no. 5, article e65702, 2013.

[33] L. Li, Y. Zhang, Y. Li et al., "Mesenchymal stem cell transplantation attenuates cardiac fibrosis associated with isoproterenol-induced global heart failure," *Transplant International*, vol. 21, no. 12, pp. 1181–1189, 2008.

[34] A. Corcione, F. Benvenuto, E. Ferretti et al., "Human mesenchymal stem cells modulate B-cell functions," *Blood*, vol. 107, no. 1, pp. 367–372, 2006.

[35] P. A. Sotiropoulou, S. A. Perez, A. D. Gritzapis, C. N. Baxevanis, and M. Papamichail, "Interactions between human mesenchymal stem cells and natural killer cells," *Stem Cells*, vol. 24, no. 1, pp. 74–85, 2006.

[36] J. Wu, Z. Sun, H. S. Sun et al., "Intravenously administered bone marrow cells migrate to damaged brain tissue and improve neural function in ischemic rats," *Cell Transplantation*, vol. 16, no. 10, pp. 993–1005, 2008.

[37] Z. Cheng, L. Ou, X. Zhou et al., "Targeted migration of mesenchymal stem cells modified with CXCR4 gene to infarcted myocardium improves cardiac performance," *Molecular Therapy*, vol. 16, no. 3, pp. 571–579, 2008.

[38] J. Xu, J. Qu, L. Cao et al., "Mesenchymal stem cell-based angiopoietin-1 gene therapy for acute lung injury induced by lipopolysaccharide in mice," *The Journal of Pathology*, vol. 214, no. 4, pp. 472–481, 2008.

[39] D. Moher, L. Shamseer, M. Clarke et al., "Preferred reporting items for systematic review and meta-analysis protocols (PRISMA-P) 2015 statement," *Systematic Reviews*, vol. 4, no. 1, 2015.

[40] J. P. Higgins and S. Green, Eds., *Cochrane Handbook for Systematic Reviews of Interventions*, John Wiley & Sons, New Jersey, USA, 2011, The Cochrane Collaboration.

[41] C. R. Hooijmans, M. M. Rovers, R. B. M. de Vries, M. Leenaars, M. Ritskes-Hoitinga, and M. W. Langendam, "SYRCLE's risk of bias tool for animal studies," *BMC Medical Research Methodology*, vol. 14, no. 1, p. 43, 2014.

[42] K. Kawakubo, S. Ohnishi, H. Fujita et al., "Effect of fetal membrane-derived mesenchymal stem cell transplantation in rats with acute and chronic pancreatitis," *Pancreas*, vol. 45, no. 5, pp. 707–713, 2016.

[43] H. W. Kim, W. J. Song, Q. Li et al., "Canine adipose tissue-derived mesenchymal stem cells ameliorate severe acute pancreatitis by regulating T cells in rats," *Journal of Veterinary Science*, vol. 17, no. 4, pp. 539–548, 2016.

[44] K. H. Jung, S. U. Song, T. Yi et al., "Human bone marrow–derived clonal mesenchymal stem cells inhibit inflammation and reduce acute pancreatitis in rats," *Gastroenterology*, vol. 140, no. 3, pp. 998–1008.e4, 2011.

[45] K. H. Jung, T. G. Yi, M. K. Son, S. U. Song, and S. S. Hong, "Therapeutic effect of human clonal bone marrow-derived mesenchymal stem cells in severe acute pancreatitis," *Archives of Pharmacal Research*, vol. 38, no. 5, pp. 742–751, 2015.

[46] D. Qian, J. Gong, Z. He et al., "Bone marrow-derived mesenchymal stem cells repair necrotic pancreatic tissue and promote angiogenesis by secreting cellular growth factors involved in the SDF-1α/CXCR4 Axis in rats," *Stem Cells International*, vol. 2015, Article ID 306836, 20 pages, 2015.

[47] Z. He, J. Hua, D. Qian et al., "Intravenous hMSCs ameliorate acute pancreatitis in mice via secretion of tumor necrosis factor-α stimulated gene/protein 6," *Scientific Reports*, vol. 6, no. 1, article 38438, 2016.

[48] G. Yin, G. Hu, R. Wan et al., "Role of bone marrow mesenchymal stem cells in L-arg-induced acute pancreatitis: effects and possible mechanisms," *International Journal of Clinical and Experimental Pathology*, vol. 8, no. 5, pp. 4457–4468, 2015.

[49] H. Zhao, Z. He, D. Huang et al., "Infusion of bone marrow mesenchymal stem cells attenuates experimental severe acute pancreatitis in rats," *Stem Cells International*, vol. 2016, Article ID 7174319, 10 pages, 2016.

[50] Z. Chen, F. Lu, H. Fang, and H. Huang, "Effect of mesenchymal stem cells on renal injury in rats with severe acute pancreatitis," *Experimental Biology and Medicine*, vol. 238, no. 6, pp. 687–695, 2013.

[51] X. H. Tu, J. X. Song, X. J. Xue et al., "Role of bone marrow-derived mesenchymal stem cells in a rat model of severe acute pancreatitis," *World Journal of Gastroenterology*, vol. 18, no. 18, pp. 2270–2279, 2012.

[52] X.-H. Tu, S.-X. Huang, W.-S. Li, J.-X. Song, and X.-L. Yang, "Mesenchymal stem cells improve intestinal integrity during severe acute pancreatitis," *Molecular Medicine Reports*, vol. 10, no. 4, pp. 1813–1820, 2014.

[53] B. Qu, Y. Chu, F. Zhu et al., "Granulocyte colony-stimulating factor enhances the therapeutic efficacy of bone marrow mesenchymal stem cell transplantation in rats with experimental acute pancreatitis," *Oncotarget*, vol. 8, no. 13, pp. 21305–21314, 2017.

[54] D. Qian, G. Wei, C. Xu et al., "Bone marrow-derived mesenchymal stem cells (BMSCs) repair acute necrotized pancreatitis by secreting microRNA-9 to target the NF-κB1/p50 gene in rats," *Scientific Reports*, vol. 7, no. 1, p. 581, 2017.

[55] H. B. Meng, J. Gong, B. Zhou, J. Hua, L. Yao, and Z. S. Song, "Therapeutic effect of human umbilical cord-derived mesenchymal stem cells in rat severe acute pancreatitis," *International Journal of Clinical and Experimental Pathology*, vol. 6, no. 12, pp. 2703–12, 2013.

[56] B. Yang, B. Bai, C. X. Liu et al., "Effect of umbilical cord mesenchymal stem cells on treatment of severe acute pancreatitis in rats," *Cytotherapy*, vol. 15, no. 2, pp. 154–162, 2013.

[57] J. Hua, Z. G. He, D. H. Qian et al., "Angiopoietin-1 gene-modified human mesenchymal stem cells promote angiogenesis and reduce acute pancreatitis in rats," *International Journal of Clinical and Experimental Pathology*, vol. 7, no. 7, pp. 3580–3595, 2014.

[58] S. A. Wexler, C. Donaldson, P. Denning-Kendall, C. Rice, B. Bradley, and J. M. Hows, "Adult bone marrow is a rich source of human mesenchymal "stem" cells but umbilical cord and mobilized adult blood are not," *British Journal of Haematology*, vol. 121, no. 2, pp. 368–374, 2003.

[59] T. Qin, C. J. Liu, H. W. Zhang et al., "Effect of the IkBα mutant gene delivery to mesenchymal stem cells on rat chronic pancreatitis," *Genetics and Molecular Research*, vol. 13, no. 1, pp. 371–385, 2014.

[60] C. H. Zhou, M. L. Li, A. L. Qin et al., "Reduction of fibrosis in dibutyltin dichloride–induced chronic pancreatitis using rat umbilical mesenchymal stem cells from Wharton's jelly," *Pancreas*, vol. 42, no. 8, pp. 1291–1302, 2013.

[61] J. A. Hirst, J. Howick, J. K. Aronson et al., "The need for randomization in animal trials: an overview of systematic reviews," *PLoS One*, vol. 9, no. 6, article e98856, 2014.

[62] S. C. Landis, S. G. Amara, K. Asadullah et al., "A call for transparent reporting to optimize the predictive value of preclinical research," *Nature*, vol. 490, no. 7419, pp. 187–191, 2012.

[63] N. A. Crossley, E. Sena, J. Goehler et al., "Empirical evidence of bias in the design of experimental stroke studies: a metaepidemiologic approach," *Stroke*, vol. 39, no. 3, pp. 929–934, 2008.

[64] E. D. M. Rooke, H. M. Vesterinen, E. S. Sena, K. J. Egan, and M. R. Macleod, "Dopamine agonists in animal models of Parkinson's disease: a systematic review and meta-analysis," *Parkinsonism & Related Disorders*, vol. 17, no. 5, pp. 313–320, 2011.

[65] National Institutes of Health, *Principles and Guidelines for Reporting Preclinical Research*, National Institutes of Health, Bethesda, Maryland, USA, 2015.

[66] A. Demols, O. Le Moine, F. Desalle, E. Quertinmont, J. L. van Laethem, and J. Devière, "$CD4^+$ T cells play an important role in acute experimental pancreatitis in mice," *Gastroenterology*, vol. 118, no. 3, pp. 582–590, 2000.

[67] M. M. Duffy, T. Ritter, R. Ceredig, and M. D. Griffin, "Mesenchymal stem cell effects on T-cell effector pathways," *Stem Cell Research & Therapy*, vol. 2, no. 4, p. 34, 2011.

[68] A. S. Gukovskaya, I. Gukovsky, Y. Jung, M. Mouria, and S. J. Pandol, "Cholecystokinin induces caspase activation and mitochondrial dysfunction in pancreatic acinar cells. Roles in cell injury processes of pancreatitis," *Journal of Biological Chemistry*, vol. 277, no. 25, pp. 22595–22604, 2002.

[69] S. J. Kwon, S. M. Ki, S. E. Park et al., "Anti-apoptotic effects of human Wharton's jelly-derived mesenchymal stem cells on skeletal muscle cells mediated via secretion of XCL1," *Molecular Therapy*, vol. 24, no. 9, pp. 1550–1560, 2016.

[70] S. Chiesa, S. Morbelli, S. Morando et al., "Mesenchymal stem cells impair in vivo T-cell priming by dendritic cells," *Proceedings of the National Academy of Sciences of the United States of America*, vol. 108, no. 42, pp. 17384–17389, 2011.

[71] J. Gong, H.-B. Meng, J. Hua et al., "The SDF-1/CXCR4 axis regulates migration of transplanted bone marrow mesenchymal stem cells towards the pancreas in rats with acute pancreatitis," *Molecular Medicine Reports*, vol. 9, no. 5, pp. 1575–1582, 2014.

[72] D. J. Prockop and J. Youn Oh, "Mesenchymal stem/stromal cells (MSCs): role as guardians of inflammation," *Molecular Therapy*, vol. 20, no. 1, pp. 14–20, 2012.

[73] H. Choi, R. H. Lee, N. Bazhanov, J. Y. Oh, and D. J. Prockop, "Anti-inflammatory protein TSG-6 secreted by activated MSCs attenuates zymosan-induced mouse peritonitis by decreasing TLR2/NF-κB signaling in resident macrophages," *Blood*, vol. 118, no. 2, pp. 330–338, 2011.

[74] H. G. Wisniewski and J. Vilcek, "Cytokine-induced gene expression at the crossroads of innate immunity, inflammation and fertility: TSG-6 and PTX3/TSG-14," *Cytokine & Growth Factor Reviews*, vol. 15, no. 2-3, pp. 129–146, 2004.

[75] E. W. Choi, I. S. Shin, H. W. Lee et al., "Transplantation of CTLA4Ig gene-transduced adipose tissue-derived mesenchymal stem cells reduces inflammatory immune response and

improves Th1/Th2 balance in experimental autoimmune thyroiditis," *The Journal of Gene Medicine*, vol. 13, no. 1, pp. 3–16, 2011.

[76] G. M. Spaggiari, A. Capobianco, H. Abdelrazik, F. Becchetti, M. C. Mingari, and L. Moretta, "Mesenchymal stem cells inhibit natural killer–cell proliferation, cytotoxicity, and cytokine production: role of indoleamine 2,3-dioxygenase and prostaglandin E2," *Blood*, vol. 111, no. 3, pp. 1327–1333, 2008.

[77] X. X. Jiang, Y. Zhang, B. Liu et al., "Human mesenchymal stem cells inhibit differentiation and function of monocyte-derived dendritic cells," *Blood*, vol. 105, no. 10, pp. 4120–4126, 2005.

[78] L. Cai, B. H. Johnstone, T. G. Cook et al., "IFATS collection: human adipose tissue-derived stem cells induce angiogenesis and nerve sprouting following myocardial infarction, in conjunction with potent preservation of cardiac function," *Stem Cells*, vol. 27, no. 1, pp. 230–237, 2009.

[79] A. Banas, T. Teratani, Y. Yamamoto et al., "IFATS collection: in vivo therapeutic potential of human adipose tissue mesenchymal stem cells after transplantation into mice with liver injury," *Stem Cells*, vol. 26, no. 10, pp. 2705–2712, 2008.

[80] Z. Wen, Q. Liao, Y. Hu, S. Liu, L. You, and Y. Zhao, "Human adipose-derived stromal/stem cells: a novel approach to inhibiting acute pancreatitis," *Medical Hypotheses*, vol. 80, no. 5, pp. 598–600, 2013.

[81] B. U. Wu, "Prognosis in acute pancreatitis," *Canadian Medical Association Journal*, vol. 183, no. 6, pp. 673–677, 2011.

[82] S. Li, X. Wang, J. Li et al., "Advances in the treatment of ischemic diseases by mesenchymal stem cells," *Stem Cells International*, vol. 2016, Article ID 5896061, 11 pages, 2016.

[83] B. Usunier, M. Benderitter, R. Tamarat, and A. Chapel, "Management of fibrosis: the mesenchymal stromal cells breakthrough," *Stem Cells International*, vol. 2014, Article ID 340257, 26 pages, 2014.

Hindawi
Oxidative Medicine and Cellular Longevity
Volume 2018, Article ID 8104165, 10 pages
https://doi.org/10.1155/2018/8104165

Research Article

Black Seed Thymoquinone Improved Insulin Secretion, Hepatic Glycogen Storage, and Oxidative Stress in Streptozotocin-Induced Diabetic Male Wistar Rats

Heba M. A. Abdelrazek,[1] **Omnia E. Kilany**,[2] **Muhammad A. A. Muhammad**,[3] **Hend M. Tag**,[4] **and Aaser M. Abdelazim**[5,6]

[1]*Department of Physiology, Faculty of Veterinary Medicine, Suez Canal University, Ismailia, Egypt*
[2]*Department of Clinical Pathology, Faculty of Veterinary Medicine, Suez Canal University, Ismailia, Egypt*
[3]*Department of Pathology, Faculty of Medicine, Suez Canal University, Ismailia, Egypt*
[4]*Zoology Department, Faculty of Sciences, Suez Canal University, Ismailia, Egypt*
[5]*Department of Biochemistry, Faculty of Veterinary Medicine, Zagazig University, Zagazig, Egypt*
[6]*Department of Basic Medical Sciences, College of Applied Medical Sciences, University of Bisha, Bisha, Saudi Arabia*

Correspondence should be addressed to Heba M. A. Abdelrazek; hebaabdelrazekvet@gmail.com

Received 28 October 2017; Accepted 19 December 2017; Published 4 March 2018

Academic Editor: Lotfi Aleya

Diabetes mellitus is one of the metabolic diseases having several complications. *Nigella sativa* oil (NSO) might have beneficial effects in the treatment of diabetic complications. Thirty-two mature male Wistar rats were equally divided into four experimental groups: control, control NSO 2 mL/kg, streptozotocin- (STZ-) induced diabetic, and diabetic (STZ-induced) treated with oral NSO 2 mg/kg for 30 days. Fasting blood glucose (FBG), insulin, and lipid profile levels were determined. Pancreatic and hepatic tissues were used for catalase and GSH. Histopathology, hepatic glycogen contents, insulin immunohistochemistry, and pancreatic islet morphometry were performed. NSO 2 mL/kg was noticed to decrease ($P < 0.05$) FBG and increase ($P < 0.05$) insulin levels in diabetic rats than in diabetic nontreated animals. Lipid profile showed significant ($P < 0.5$) improvement in diabetic rats that received NSO 2 mL/kg than in the diabetic group. Both pancreatic and hepatic catalase and GSH activities revealed a significant ($P < 0.05$) increment in the diabetic group treated with NSO than in the diabetic animals. NSO improved the histopathological picture and hepatic glycogen contents of the diabetic group as well as increased ($P < 0.05$) insulin immunoreactive parts % and mean pancreatic islet diameter. NSO exerts ameliorative and therapeutic effects on the STZ-induced diabetic male Wistar rats.

1. Introduction

Diabetes mellitus (DM) is considered as one of the most common chronic metabolic diseases characterized by increased blood glucose due to insulin resistance, insulin deficiency, or both [1]. Mostly, DM is associated with vascular, metabolic, neuropathic, and nephropathic disorders. Hyperglycemia and lipid profile abnormalities are the main clues for diagnosis of DM metabolic disorders [2]. Hyperglycemia is a consequence of the inability of the cells to utilize glucose and/or skeletal muscles and liver are not capable of glycogen storage [3]. Moreover, the persistent hyperglycemia in DM promoted oxidative stress through the formation or release of reactive oxygen species (ROS) and depletion of antioxidant reserve. Oxidative stress is the main cause of cardiovascular disease that results in mortalities [4, 5].

Insulin is the primary hormone which is involved in blood glucose control. Once insulin is released into the blood, it stimulates the entrance of glucose into skeletal muscles and, to a lesser extent, liver and adipose tissue via special

transporters, thus controlling glucose homeostasis [6]. Insulin binding mediates much action through interaction with insulin receptors (IR) [7].

The efficient management of diabetes requires continuous control to blood sugar level to minimize the risks of diabetic complications [8]. Thus, natural and therapeutic antioxidants are one of the strategies for diabetic remedy. Although there are various categories of antidiabetic drugs, these drugs possibly possess significant side effects or are very expensive [9, 10]. In comparison to the synthetic drug, natural plants have lesser toxicity and are devoid of any side effects [11].

Nigella sativa (NS), a dicotyledon plant species of the family Ranunculaceae, has been used since long eras in medical and culinary fields [12]. Its plant seeds are called black cumin or black seeds [13]. Thymoquinone (2-isopropyl-5-methyl-1,4-benzoquinone) is considered the chief active principle in the NS seeds and its volatile oily extract [14]. NS has several physiological and pharmacological properties such as hepatoprotective [15, 16], immunomodulatory [17], nephroprotective [18, 19], neuroprotective [20], antimutagenic, anticancer [21], and anticonvulsant [22] effects. Moreover, it is known for its hypotensive [23] properties.

The current study aimed to investigate the potential protective actions of NSO in streptozotocin- (STZ-) induced diabetic male Wistar rats. This was done via the manipulation of blood biochemical parameters, oxidative stress, histopathology, and pancreatic insulin immunoreactive parts.

2. Material and Methods

2.1. Experimental Rats. Thirty-two adult male Wistar rats, weighing 195–205 g, were kept in metallic cages (4/cage) at Laboratory Animal House, Faculty of Veterinary Medicine, Suez Canal University, Egypt. They were kept under standard natural day-light rhythm with a temperature of 25°C (±1°C) and allowed to ad libitum diet and water supply. The animals were handled and cared according to the ethical guidelines described by Faculty of Veterinary Medicine, Suez Canal University.

2.2. Experiment Design. After 14 days of acclimatization, animals were divided into four equal groups:

(i) Control group ($n = 8$): They were normal nondiabetic rats and gavaged daily with distilled water for one month.

(ii) *Nigella* group ($n = 8$): They were normal nondiabetic rats that were gavaged with 2 mL/kg cold-pressed NSO (Amazing Herbs Co., Turkey) containing 0.95% thymoquinone, as determined via HPLC, by gavage tube for one month.

(iii) Diabetic group: They were STZ-induced diabetic rats and given daily oral dose of distilled water by gavage tube for one month.

(iv) Diabetic *Nigella*-treated group: They were STZ-induced diabetic rats that were given a daily oral dose of 2 mL/kg cold-pressed NSO (Amazing Herbs Co., Turkey) containing 0.95% thymoquinone, as determined via HPLC, by gavage tube for one month.

2.3. Induction of Diabetes. Experimental rats from diabetic and diabetic treated with NSO groups were induced to diabetes after 16 h fasting by a sole STZ (TUKU-E Company, USA), intraperitoneal (i.p.) injection, in a dose of 45 mg/kg. STZ was freshly prepared in 0.1 M citrate buffer (pH 4.5). The STZ-inoculated rats were allowed ad libitum 20% glucose solution for a duration of 24 h to avoid the occurrence of hypoglycemia. Rats of the control and NSO groups were injected with citrate buffer only [24]. The occurrence of diabetes was ascertained after 48 h post-STZ injection by determination of blood glucose level. The animals that possessed blood glucose values of over 250 mg/dL were supposed to be diabetic [25].

2.4. Sampling. After 30 days of treatments, overnight fasted rats were decapitated under effect of anesthesia, and blood samples were obtained in sterile plain tubes. The sera were stored at −20°C. Pancreas and liver of each experimental animal were excised, rinsed in cold phosphate buffered saline, and dried with filter paper. Pancreas and liver of each rat was divided into 2 parts: one part was kept at −80°C until preparation of pancreatic homogenate for reduced glutathione (GSH) and catalase assay. The remaining part of pancreas and liver was immersed in 10% neutral buffered formalin for histopathological and immunohistochemical examination.

2.5. Body Weight. Experimental rats were weighed weekly during the experimental period.

2.6. Blood Glucose Value and Insulin Level. Fasting blood glucose level was estimated using reagent strips (Accu-Chek®, Roche). The levels of insulin in serum were estimated by commercial rat enzyme-linked immunosorbent assay (ELISA) kit (Abnova, Germany) according to enclosed manufacturer's protocol.

2.7. Lipid Profile. The high-density lipoprotein cholesterol (HDL-c), low-density lipoprotein cholesterol (LDL-c), total cholesterol (TC), and triglycerides (TG) were measured in sera using enzymatic colorimetric kits (Stanbio Laboratory, USA, and ELITechGroup, France) according to Tietz [26].

2.8. Catalase and Reduced Glutathione Activity (GSH). Catalase and GSH activities in pancreatic and hepatic homogenates were determined using colorimetric kits from Biodiagnostic (Egypt) and BioVision (USA), respectively, according to methods of Aebi [27] and Tietez [28], respectively.

2.9. Histopathology. Formalin-fixed pancreases and livers were put in paraffin wax, and several 5 μm sections were sliced and then subjected to hematoxylin and eosin (H&E) stain according to Bancroft and Gamble [29]. Livers of 5 μm sections were subjected to periodic acid Schiff (PAS) stain for glycogen demonstration [30].

Table 1: The effect of NSO 2 mL/kg on weekly body weight (g) of STZ-induced diabetic rats.

	Groups	Control	*Nigella*	Diabetic	Diabetic *Nigella* treated
Body weight (g)	Week 1	200.50 ± 1.48^{a}	200.33 ± 1.60^{a}	201.17 ± 1.72^{a}	201.50 ± 2.08^{a}
	Week 2	212.50 ± 3.23^{a}	211.25 ± 2.46^{a}	205.50 ± 2.10^{a}	203.25 ± 4.59^{a}
	Week 3	220.00 ± 4.56^{a}	228.75 ± 4.92^{a}	195.00 ± 3.19^{b}	200.75 ± 4.91^{b}
	Week 4	226.75 ± 5.27^{a}	239.00 ± 3.56^{a}	$160.00 \pm 4.^{c}$	188.50 ± 3.12^{b}

Values are presented as mean ± SE. ^{abc}Different letters on numbers in each row represent a significant difference at $P < 0.05$.

Table 2: Effect of NSO 2 mL/kg on FBG (mg/dL), insulin (pmol/L), HDL-c (mg/dL), LDL-c (mg/dL), TG (mg/dL), and TC (mg/dL) in STZ-induced diabetic rats.

Groups	Control	*Nigella*	Diabetic	Diabetic *Nigella* treated
FBG (mg/dL)	98.40 ± 7.00^{c}	93.60 ± 3.80^{c}	313.00 ± 5.19^{b}	187.40 ± 19.91^{a}
Insulin (pmol/L)	5.78 ± 0.49^{a}	6.25 ± 0.47^{a}	3.41 ± 0.29^{b}	5.36 ± 0.27^{a}
HDL-c (mg/dL)	44.73 ± 1.82^{b}	53.37 ± 2.02^{a}	22.31 ± 2.45^{d}	33.60 ± 2.26^{c}
LDL-c (mg/dL)	56.91 ± 2.86^{c}	47.09 ± 2.60^{d}	109.28 ± 4.18^{a}	84.52 ± 2.99^{b}
TG (mg/dL)	58.28 ± 3.47^{c}	52.07 ± 4.14^{c}	105.92 ± 3.19^{a}	84.25 ± 2.81^{b}
TC (mg/dL)	109.96 ± 4.08^{c}	89.84 ± 4.77^{d}	161.28 ± 8.54^{a}	139.54 ± 3.92^{b}

Values are presented as mean ± SE. ^{abcd}Different letters on numbers in each row represent a significant difference at $P < 0.05$.

2.10. Immunohistochemistry. Paraffin-embedded pancreases were sliced into 4 μm sections on the positively charged slides. Sections were subjected to xylene deparaffinization and then rehydrated with descending series of ethanol, followed by water. The sections were incubated with primary monoclonal anti-insulin antibody (catalog no. 13-9769-80, Thermo Fisher Scientific, Canada) at a rate of 0.5 μg/mL for 2 h at 25°C in a humidified chamber. Then the steps according to the method of Adewole and Ojewole [31] were followed.

2.11. Image Analysis and Islet Size. Measurements of pancreatic islet size were performed via ImageJ program. Insulin-positive islet immunostaining intensity and area % were determined from each slide of each experimental group using ImageJ program after subtracting light background. Seven fields of pancreatic islets were randomly chosen. The intensity of immunohistochemistry (IHC) staining and the percentages of IHC stained regions were obtained by ImageJ program and calculated according to Elgawish et al. [32]. The diameters of the pancreatic islet were measured by selecting seven of pancreatic islets/animal in all groups using ImageJ program by the aid of a calibrated micrometer.

2.12. Statistical Analysis. The data were presented as the mean ± standard error of mean (SEM). Statistically significant differences between groups were calculated using one-way analysis of variance (ANOVA) followed by Duncan's post hoc multiple comparison test (SPSS software, version 16.0; SPSS Inc., Chicago, IL, USA). The criterion for significance was set at $P < 0.05$.

3. Results

3.1. Body Weight. The body weights of the STZ-induced diabetic group rats reduced significantly ($P < 0.05$) than did those of the control nondiabetic rats at the 3rd and 4th weeks of the experiment. However, NSO 2 mL/kg treatment of diabetic rats increased their body weights ($P < 0.05$) compared to those of diabetic nontreated rats at the 4th week of the experimental period (Table 1).

3.2. Fasting Blood Glucose Value and Insulin Level. The injection of experimental rats with single i.p. dose of STZ induced a significant ($P < 0.05$) elevation in FBG levels compared to those of the control rats. Administration of NSO 2 mL/kg to the diabetic rats, for one month, induced a significant ($P < 0.05$) reduction in the levels of FBG compared to those of the diabetic group. Insulin level revealed a significant ($P < 0.05$) decrement in the STZ diabetic group than in the control one. Meanwhile treatment of the diabetic rats with NSO 2 mL/kg, for 1 month, significantly ($P < 0.05$) improved insulin to a level comparable to that of the control group (Table 2).

3.3. Lipid Profile. Oral administration of NSO 2 mL/kg to the nondiabetic rats for one month induced a significant ($P < 0.05$) increment in HDL-c level compared to that of the control group. However, HDL-c level revealed a significant ($P < 0.05$) decrement in the diabetic group than in the control. Meanwhile, administration of 2 mL/kg NSO to the diabetic rats increased HDL-c significantly ($P < 0.05$) compared to that of diabetic nontreated rats. Treatment of the control rats with NSO 2 mL/kg for one month induced a significant ($P < 0.05$) decrement in TC and LDL-c levels compared to those in the control. The diabetic rats revealed elevation in TC, TG, and LDL-c ($P < 0.05$) than did the control group. However, 30 days' treatment with NSO 2 mL/kg of the diabetic rats induced a significant ($P < 0.05$) decrement in TC, TG, and LDL-c values compared to those of the diabetic group (Table 2).

3.4. Pancreatic and Hepatic Oxidative Stress. Current data revealed that both hepatic and pancreatic catalase as well

Table 3: Effect of NSO 2 mL/kg on catalase (U/g) and GSH (mg/g) in pancreas and liver of STZ-induced diabetic rats.

Groups	Control	*Nigella*	Diabetic	Diabetic *Nigella* treated
Pancreatic catalase (U/g)	84.27 ± 5.56^{a}	86.66 ± 4.91^{a}	38.25 ± 2.30^{c}	69.00 ± 1.22^{b}
Hepatic catalase (U/g)	27.49 ± 2.26^{b}	34.73 ± 2.09^{a}	10.51 ± 1.31^{d}	18.19 ± 1.09^{c}
Pancreatic GSH (mg/g)	36.45 ± 2.80^{a}	42.71 ± 4.49^{a}	13.49 ± 3.12^{c}	23.00 ± 0.95^{b}
Hepatic GSH (mg/g)	85.71 ± 9.57^{a}	84.92 ± 6.33^{a}	35.95 ± 6.32^{b}	62.89 ± 6.63^{a}

Values are presented as mean ± SE. ^{abcd}Different letters on numbers in each row represent a significant difference at $P < 0.05$.

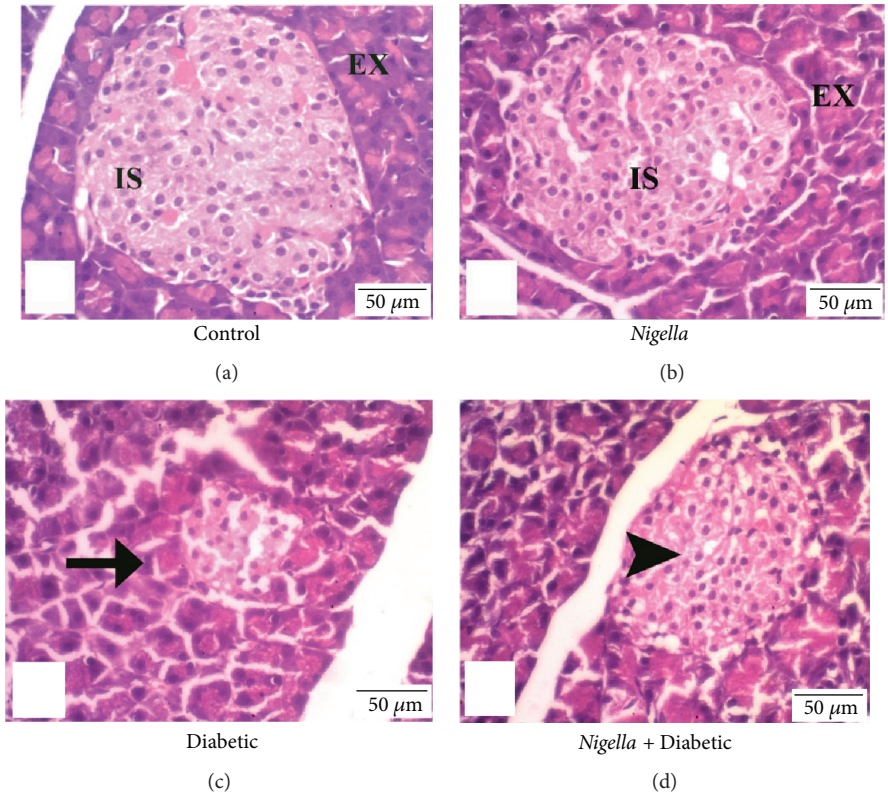

Figure 1: *Nigella* seed oil extract effect on pancreatic histopathology in normal and STZ-induced diabetic rats. (a and b) Control- and NSO- (2 mL/kg) treated control groups: normal control rat displayed healthy islets of Langerhans. (c) Diabetic control: arrow displays the atrophied islets of Langerhans. (d) NSO- (2 mL/kg) treated diabetic rats display bigger islets of Langerhans than do diabetic untreated group (arrowhead). Scale bar represents 50 μm.

as GSH activities were decreased significantly ($P < 0.05$) in the STZ-induced diabetic rats than in the control. Administration of NSO 2 mL/kg, for one month, to the diabetic rats significantly ($P < 0.05$) elevated hepatic and pancreatic catalase and GSH activities compared to those in the diabetic group (Table 3).

3.5. Histopathology and Islet Size. Examination of pancreatic sections from the control group and the *Nigella*-treated group showed abundant and scattered pancreatic islets of Langerhans between the exocrine parenchyma throughout the pancreas. The islets were large, well defined, and composed of groups of compact cells arranged in branching, irregular, and anastomosing cords separated by blood capillaries (Figures 1(a) and 1(b)).

On the other hand, examination of pancreases of the diabetic rats yielded an observable decrement in the number of islets. They were shrunken and irregular, and some of the islet cells showed hydropic degeneration while others were necrotized with deeply stained pyknotic nuclei. Few lymphocytes were seen attacking the islet cells (Figure 1(c)).

The diabetic group treated with oral NSO 2 mL/kg showed marked increase in number of islets throughout the pancreas, and most of them demonstrated recovery of their normal morphologic features comparable to those of the islets of the control group (Figure 1(d)).

Analysis of the mean diameter of pancreatic Langerhans islets among the studied groups showed a significant ($P < 0.05$) reduction in the mean diameter in the diabetic rats. Oral treatment with NSO (2 mL/kg), for one month, significantly ($P < 0.05$) increased the mean diameter of Langerhans islets compared to that in the diabetic nontreated group (Table 4).

The results obtained from histological sections of livers with hematoxylin and eosin staining for the control and *Nigella*-treated rats were similar. Liver histological

Table 4: The effect of NSO 2 mL/kg on mean pancreatic islet size (μm), insulin-positive islet area %, and insulin immunostaining intensity (integrated density) in STZ-induced diabetic rats.

Groups	Control	*Nigella*	Diabetic	Diabetic *Nigella* treated
Mean islet size (μm)	233.90 ± 24.71^{a}	247.52 ± 35.27^{a}	$29.83.36 \pm 83.17^{b}$	170.61 ± 26.63^{a}
Insulin-positive islet area (%)	65.79 ± 9.81^{a}	68.52 ± 9.58^{a}	18.01 ± 3.42^{c}	43.05 ± 5.57^{b}
Insulin immunostaining intensity (integrated density)	92.50 ± 3.05^{a}	99.34 ± 2.23^{a}	60.93 ± 4.31^{c}	76.15 ± 1.92^{b}

Values are presented as mean ± SE. [abc]Different letters on numbers in each row represent a significant difference at $P < 0.05$.

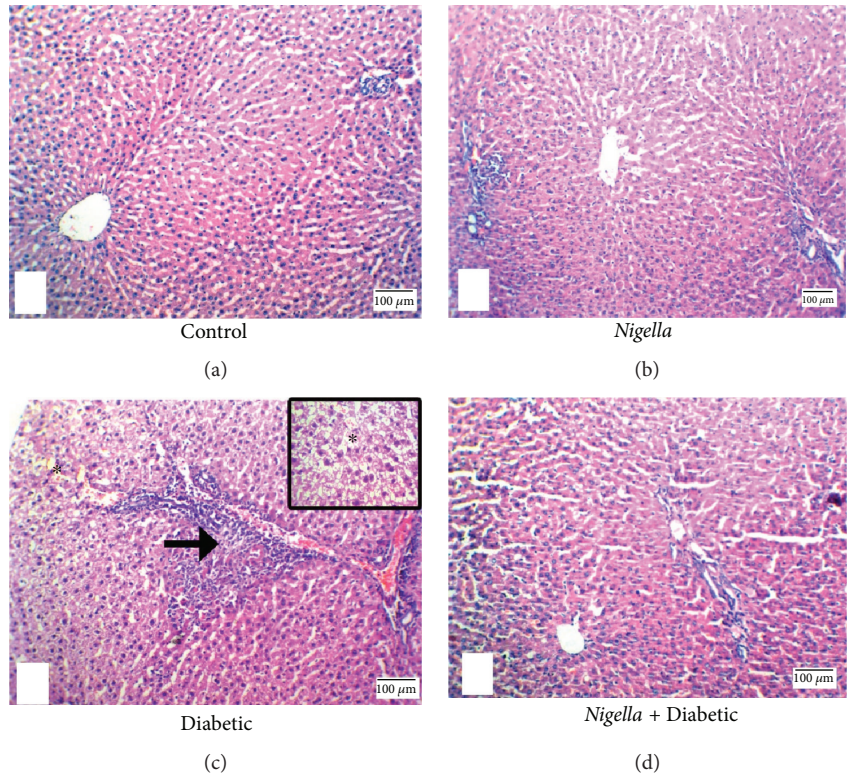

Figure 2: H&E stain of liver: (a) control group and (b) *Nigella*-treated rats demonstrate normal hepatic architecture showing the classic lobule with the central vein at the center and portal tracts at the periphery; each one is separated from the others by a similar distance, 100x. (c) Diabetic group showing ballooning degeneration of the hepatocyte (*, 40x), and interface hepatitis (arrow), 100x. (d) NSO-treated diabetic group showing restoration of normal architecture, 100x. Scale bar represents 100 μm.

observations of the control and *Nigella*-treated rats showed normal hepatic architecture showing the classic lobule with the central vein as its center and portal tracts at the periphery. Embedded in the portal tract were portal venule, hepatic arteriole, and interlobular bile ductule (Figures 2(a) and 2(b)). The livers of the diabetic animals showed ballooning degeneration, mild portal inflammation, and interface hepatitis (Figure 2(c)). Sections of liver tissues from diabetic animals treated with *Nigella* showed restoration of the normal hepatic architecture with marked reduction of portal inflammation and absence of interface hepatitis (Figure 2(d)).

The PAS-stained liver sections demonstrated abundant cytoplasmic contents of glycogen in the control and NSO-treated control (Figure 3(a) and (b)). The diabetic group showed marked depletion of glycogen contents in hepatocytes cytoplasm than did the control ones (Figure 3(c)). Treatment of diabetic rats with 2 mL/kg NSO improved glycogen contents in hepatocytes cytoplasm compared to those in the diabetic rats (Figure 3(d)).

3.6. Immunohistochemistry. Positive insulin expression was visualized as dark-brown cytoplasmic granules in the pancreatic islets' β cells. The quantitative analysis of insulin immunoreaction in the pancreatic islets showed significant ($P < 0.05$) variations among the study groups. Regarding the percentage of insulin-positive islet area, the analysis showed a significant ($P < 0.05$) decrement in the percentage of insulin-positive area in the diabetic group than in the control group. However, NSO treatment of the diabetic rats significantly ($P < 0.05$) improved positive islet area % compared to that of the diabetic ones (Table 4).

The immunostaining intensity of pancreatic islets' insulin was assessed in a quantitative fashion according to the microdensitometric method. The staining intensities of insulin in the pancreatic islets among different study groups are

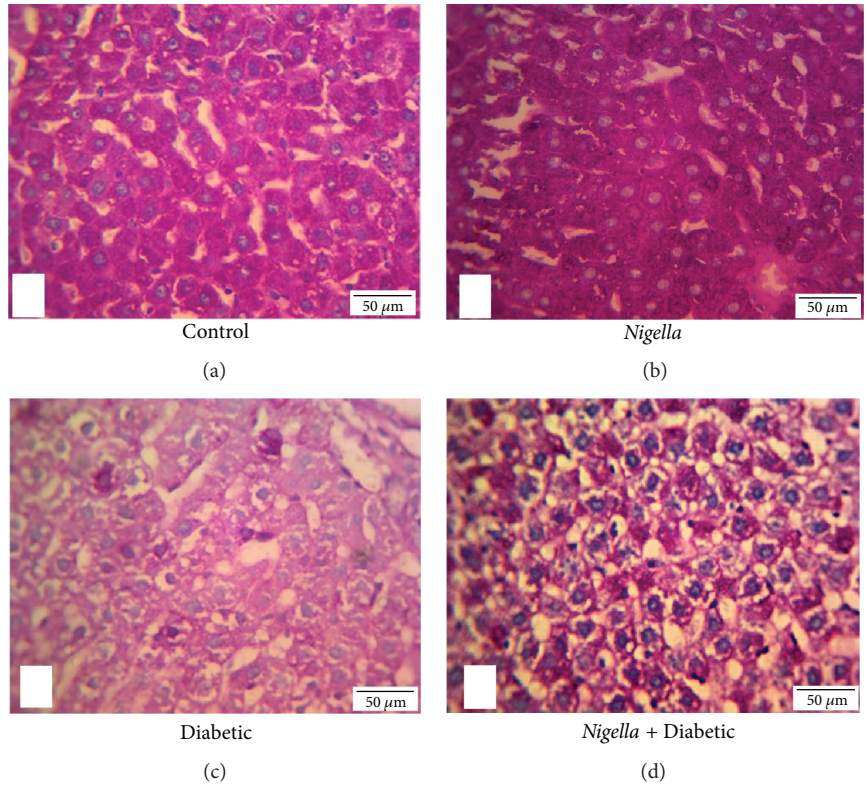

Figure 3: PAS stain of liver: (a) control group and (b) NSO- (2 mL/kg) treated control rats demonstrate abundant glycogen, which is present within the cytoplasm of the hepatocytes (magenta-colour granules), 400x. (c) Diabetic group demonstrates marked reduction in PAS positivity (few scattered glycogen granules), 400x. (d) NSO- (2 mL/kg) treated diabetic group demonstrates restoration of PAS positivity, 400x. Scale bar represents 50 μm.

shown in Figure 4 and Table 4. The *Nigella*-treated group exhibited pancreatic islets with the highest insulin staining intensity followed by the control with no significance between both of them compared to the diabetic group treated with NSO. On the other hand, the diabetic untreated animals showed the lowest ($P < 0.05$) insulin staining intensity.

4. Discussion

Diabetes mellitus is considered as one of the systemic, endocrine, and metabolic diseases, which is diagnosed by hyperglycemia. This could be considered with alterations in carbohydrate, lipid, and protein metabolism. This is considered to be due to reduction and/or impairment in antioxidant mechanisms inside the body leading to weight loss [33, 34].

Therefore the usage of antioxidants is considered as one of the strategies used for resetting the normal homeostasis in diabetic patients [35, 36]. Numerous plant extracts and compounds from these extracts are known to possess antidiabetic properties that could be used in the remedy of diabetes mellitus [11, 37]. *Nigella sativa* thymoquinone is considered as an antioxidant and hypoglycemic compound that could counteract the high cost and the adverse effects of pharmacological drugs [38], which confirms the antidiabetic effects of NSO.

The current study demonstrated that STZ produced a significant ($P < 0.05$) decrement in body weights at the 3rd and 4th weeks of experiment. These results are considered to be consistent with Wong and Tzeng [39] and Doğan and Çelik [40]. This could be due to reduction in glucose availability as well as amino acids to the body cells, which creates a lack in the substrates that are necessary for cellular biosynthesis and can affect linked cellular metabolism that causes muscle wasting [39]. Oral administration of NSO (2 mL/kg) containing 5% thymoquinone to the diabetic rats led to a marked increment in the body weights of these animals compared to diabetic nontreated rats. The current results were in accordance with those of Kanter et al. [41] and Kaleem et al. [42]. This may confirm the effect of NSO on diabetes-induced muscle wasting due to carbohydrate inaccessibility, which confirms the antidiabetic effect of NSO [42].

The serum level of insulin was reduced in the diabetic rats than in the control, while FBG level was increased ($P < 0.05$) in the diabetic group than in the control one. These results are considered to be consistent with those of Houcher et al. [43] and Mahmoud et al. [24]. This effect is due to the alkylating toxic action of STZ on β cells of pancreatic islets, which blocks insulin secretion leading to hyperglycemia [44]. NSO thymoquinone induced a marked decrease and a marked increase at $P < 0.05$ in both FBG and insulin levels, respectively, than in those in the diabetic group. These results were consistent with those of Fararh et al. [45], Rchid et al. [46],

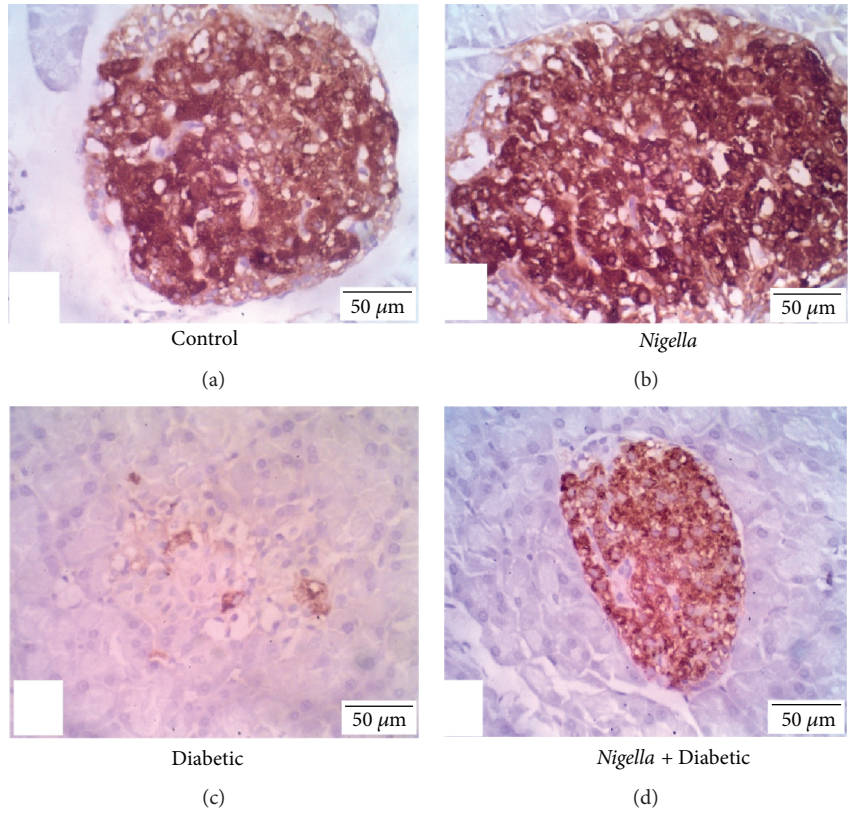

Figure 4: Immunohistochemical staining for insulin expression in pancreatic islets from different experimental groups. (a) Control, (b) NSO- (2 mL/kg) treated group, (c) diabetic group, and (d) diabetic group treated with NSO (2 mL/kg). Scale bar represents 50 μm.

Mahmoud et al. [24], and Balbaa et al. [25]. The FBG-lowering effect of NSO thymoquinone may illustrate its insulinotropic action [47] where it can make partial regeneration to β cells of pancreatic islets, thus leading to improvement in their insulin production [48] as well as its peripheral utilization [49]. Thymoquinone has a downregulating effect on the gluconeogenic enzymes expression and the production of hepatic glucose besides its ability for diminishing intestinal absorption for glucose [23]. Moreover, it can activate adenosine monophosphate-activated protein kinase (AMPK) in muscles and liver, thus inhibiting gluconeogenesis [50].

As clarified in the current study, STZ-induced dyslipidemia in the diabetic group (decreased HDL-c and increased TC, TG, and LDL-c). These results were parallel to those obtained by Doğan and Çelik [40]. Diabetic dyslipidemia occurs as a consequence to insulin deficiency and hyperglycemia, which increases lipolysis and fatty acids release from adipose tissue into circulation with alteration in their metabolism [51], thus increasing TC, TG, and LDL-c levels that predispose cardiovascular pathology [52]. Administration of NSO has positive effects on diabetes-induced abnormal lipid profile, which coincides with the results of Kaleem et al. [42], Kocyigit et al. [53], and Balbaa et al. [25]. The ameliorating effects of NSO thymoquinone on diabetic dyslipidemia may be due to its promoting effect on hepatic arylesterase activity, regulatory effects on cholesterol metabolism-influencing genes (Apo-A1, Apo-B100, and LDL-receptor genes) [54], and its antioxidant properties [55, 56].

In the current study, the influence of NSO on pancreatic and hepatic oxidative stress was examined in the STZ-induced diabetic male rats. The underlying mechanisms behind the oxidative stress and the free radicals generated by diabetes have been extensively investigated [41, 57]. The diabetic rats exhibited significantly reduced pancreatic and hepatic catalase and GSH activities due to the recorded hyperglycemia and hyperlipidemia [58], which exhaust the activities of natural antioxidants and promotes free radicals formation [59]. Treatment with NSO thymoquinone improved the antioxidant reserve of GSH and catalase activities in pancreatic and hepatic tissues, which was in agreement with the findings of Meral et al. [60], Kanter et al. [41], and Adewole et al. [61]. The antioxidant potential of thymoquinone molecule is confirmed by the presence of quinine in its structure [62]. Quinine facilitates the efficient access to the cellular and subcellular structures, making the ROS elimination easier [63]. Thymoquinone can also inhibit nonenzymatic lipid peroxidation [54] that protects hepatic and pancreatic antioxidant enzymes and reduces oxidative stress [15]. Moreover, the hypoglycemic influence of NSO potentiates its antioxidant effect via modulating hyperglycemia-induced ROS.

Parallel to the results of hepatic and pancreatic antioxidant enzymes, the hepatic and pancreatic histopathology showed deleterious effects on the STZ-induced diabetic rats. These changes include hepatic congestion, fibrosis, centrilobular hepatocyte swelling, and incidence of inflammatory cell infiltration, which were ameliorated by NSO. Pancreatic

pathology revealed severe atrophy, necrosis of acinar cells, and severe reduction in islet area %, which were greatly improved by NSO administration. The present results were in accordance with those of Kanter et al. [41], Widodo et al. [64], and Tuhin et al. [65]. The improvement in both pancreatic and hepatic histopathology could be attributed to the antioxidant potential of thymoquinone in NSO. Thymoquinone improves diabetic depletion of antioxidant reserves of catalase and GSH, thus keeping the integrity of both hepatic and pancreatic cells.

The depletion of hepatic glycogen contents in the diabetic rats was due to depletion of insulin that led to increased gluconeogenesis rather than glycogenesis [66]. Administration of NSO 2 mL/kg to the diabetic rats markedly improved hepatic glycogen contents due to the promotion of pancreatic insulin secretion, which activates glycogen synthase enzyme, thus reducing circulating glucose level [67].

The increment in pancreatic islet immunostained area % by NSO treatment in the diabetic rats, as a result of its antioxidant effect, was in agreement with the findings of Omar and Atia [38] and Widodo et al. [64]. The improvement of insulin immunoreactivity as well as pancreatic islet morphology and diameter could elucidate the upregulation of serum insulin level and the decrease in FBG, thus improving hyperlipidemia in diabetic rats.

5. Conclusion

Based on the current results, NSO was found to be an effective protection against the adverse consequences of STZ-induced diabetes in Wistar rats. NSO exerts its effect through thymoquinone antioxidant potential, which improved pancreatic and hepatic integrity, thus increasing pancreatic islet immunoreactivity, therefore increasing the serum insulin level, increasing hepatic glycogen content, reducing the elevated blood glucose level, and counteracting diabetic dyslipidemia.

Conflicts of Interest

The authors declare that there are no conflicts of interest to disclose.

References

[1] P. Kumar and M. Clark, "Diabetes mellitus and other disorders of metabolism," *Clinical Medicine*, vol. 2, pp. 1069–1071, 2002.

[2] American Diabetes Association, "Economic costs of diabetes in the U.S. in 2012," *Diabetes Care*, vol. 36, no. 4, pp. 1033–1046, 2013.

[3] D. Luis-Rodríguez, A. Martínez-Castelao, J. L. Górriz, F. De-Álvaro, and J. F. Navarro-González, "Pathophysiological role and therapeutic implications of inflammation in diabetic nephropathy," *World Journal of Diabetes*, vol. 3, no. 1, pp. 7–18, 2012.

[4] A. Sturza, O. M. Duicu, A. Vaduva et al., "Monoamine oxidases are novel sources of cardiovascular oxidative stress in experimental diabetes," *Canadian Journal of Physiology and Pharmacology*, vol. 93, no. 7, pp. 555–561, 2015.

[5] B. S. Karam, A. Chavez-Moreno, W. Koh, J. G. Akar, and F. G. Akar, "Oxidative stress and inflammation as central mediators of atrial fibrillation in obesity and diabetes," *Cardiovascular Diabetology*, vol. 16, no. 1, p. 120, 2017.

[6] A. Zorzano, W. Wilkinson, N. Kotliar et al., "Insulin-regulated glucose uptake in rat adipocytes is mediated by two transporter isoforms present in at least two vesicle populations," *Journal of Biological Chemistry*, vol. 264, no. 21, pp. 12358–12363, 1989.

[7] A. Belfiore, F. Frasca, G. Pandini, L. Sciacca, and R. Vigneri, "Insulin receptor isoforms and insulin receptor/insulin-like growth factor receptor hybrids in physiology and disease," *Endocrine Reviews*, vol. 30, no. 6, pp. 586–623, 2009.

[8] S. S. Schwartz, "Optimizing glycemic control and minimizing the risk of hypoglycemia in patients with type 2 diabetes," *Drugs in Context*, vol. 2013, article 212255, 8 pages, 2013.

[9] H. Nasri, H. Shirzad, A. Baradaran, and M. Rafieian-kopaei, "Antioxidant plants and diabetes mellitus," *Journal of Research in Medical Sciences*, vol. 20, no. 5, pp. 491–502, 2015.

[10] S. K. Basha, G. Sudarsanam, M. S. Mohammad, and N. Parveen, "Investigations on anti-diabetic medicinal plants used by Sugali tribal inhabitants of Yerramalais of Kurnool district, Andhra Pradesh India," *Stamford Journal of Pharmaceutical Sciences*, vol. 4, no. 2, 2012.

[11] R. B. Kasetti, M. D. Rajasekhar, V. K. Kondeti et al., "Antihyperglycemic and antihyperlipidemic activities of methanol: water (4, 1) fraction isolated from aqueous extract of *Syzygium alternifolium* seeds in streptozotocin induced diabetic rats," *Food and Chemical Toxicology*, vol. 48, no. 4, pp. 1078–1084, 2010.

[12] W. Goreja, *Black Seed: Nature's Miracle Remedy*, Amazing Herbs Press, New York, NY, USA, 2003.

[13] H. Ijaz, U. R. Tulain, J. Qureshi et al., "*Nigella sativa* (prophetic medicine): a review," *Pakistan Journal of Pharmaceutical Sciences*, vol. 30, no. 1, 2017.

[14] L. Canonica, G. Jommi, C. Scolastico, and A. Bonati, "The pharmacologically active principle in *Nigella sativa*," *Gazzetta Chimica Italiana*, vol. 93, pp. 1404–1407, 1963.

[15] J. Danladi, A. Abdusalam, J. Timbuak, A. Miriga, and A. Dahiru, "Hepatoprotective effect of black seed (*Nigella sativa*) oil on carbon tetrachloride (CCl_4) induced liver toxicity in adult Wistar rats," *IOSR Journal of Dental and Medical Sciences*, vol. 4, no. 3, pp. 56–62, 2013.

[16] M. M. Abdel-Daim and E. W. Ghazy, "Effects of *Nigella sativa* oil and ascorbic acid against oxytetracycline-induced hepatorenal toxicity in rabbits," *Iranian Journal of Basic Medical Sciences*, vol. 18, no. 3, pp. 221–227, 2015.

[17] Z. Gholamnezhad, H. Rafatpanah, H. R. Sadeghnia, and M. H. Boskabady, "Immunomodulatory and cytotoxic effects of *Nigella sativa* and thymoquinone on rat splenocytes," *Food and Chemical Toxicology*, vol. 86, Supplement C, pp. 72–80, 2015.

[18] A. M. S. Gani and S. A. John, "Effect of *Nigella sativa* L. on liver enzymes and kidney morphology on D-GalN induced toxicity in rats," *World Journal of Pharmacy and Phamaceutical Sciences*, vol. 5, no. 12, pp. 1193–1200, 2016.

[19] H. A. El Rabey, M. N. Al-Seeni, and A. S. Bakhashwain, "The antidiabetic activity of *Nigella sativa* and propolis on streptozotocin-induced diabetes and diabetic nephropathy in male rats," *Evidence-based Complementary and Alternative Medicine*, vol. 2017, Article ID 5439645, 14 pages, 2017.

[20] F. Beheshti, M. Khazaei, and M. Hosseini, "Neuropharmacological effects of *Nigella sativa*," *Avicenna Journal of Phytomedicine*, vol. 6, no. 1, pp. 104–116, 2016.

[21] A. F. Majdalawieh and M. W. Fayyad, "Recent advances on the anti-cancer properties of *Nigella sativa*, a widely used food additive," *Journal of Ayurveda and Integrative Medicine*, vol. 7, no. 3, pp. 173–180, 2016.

[22] H. Hosseinzadeh and S. Parvardeh, "Anticonvulsant effects of thymoquinone, the major constituent of *Nigella sativa* seeds, in mice," *Phytomedicine*, vol. 11, no. 1, pp. 56–64, 2004.

[23] B. Meddah, R. Ducroc, M. El Abbes Faouzi et al., "*Nigella sativa* inhibits intestinal glucose absorption and improves glucose tolerance in rats," *Journal of Ethnopharmacology*, vol. 121, no. 3, pp. 419–424, 2009.

[24] Y. K. Mahmoud, S. Y. Saleh, A. Abd El Rehim, and I. A. Ibrahim, "Biochemical efficacy of *Nigella sativa* oil and metformin on induced diabetic male rats," *American Journal of Animal and Veterinary Sciences*, vol. 9, no. 4, pp. 277–284, 2014.

[25] M. Balbaa, M. El-Zeftawy, D. Ghareeb, N. Taha, and A. W. Mandour, "*Nigella sativa* relieves the altered insulin receptor signaling in streptozotocin-induced diabetic rats fed with a high-fat diet," *Oxidative Medicine and Cellular Longevity*, vol. 2016, Article ID 2492107, 16 pages, 2016.

[26] N. W. Tietz, *Tietz Clinical Guide to Laboratory Tests*, WB Saunders Company, Philadelphia, PA, USA, 1990.

[27] H. Aebi, "Catalase in vitro," *Methods in Enzymology*, vol. 105, pp. 121–126, 1984.

[28] F. Tietze, "Enzymic method for quantitative determination of nanogram amounts of total and oxidized glutathione: applications to mammalian blood and other tissues," *Analytical Biochemistry*, vol. 27, no. 3, pp. 502–522, 1969.

[29] J. Bancroft and M. Gamble, "Hematoxylin and eosin, connective tissue and stain, carbohydrates," in *Theory and Practice in Histological Techniques*, p. pp. 121–186, Churchill-Livingstone, Edinburgh, 2008.

[30] A. G. E. Pearse, "Histochemistry," *Theoretical and Applied*, vol. 1, pp. 1–759, 1968.

[31] S. O. Adewole and J. A. O. Ojewole, "Insulin-induced immunohistochemical and morphological changes in pancreatic beta-cells of streptozotocin-treated diabetic rats," *Methods and Findings in Experimental and Clinical Pharmacology*, vol. 29, no. 7, pp. 447–455, 2007.

[32] R. A. R. Elgawish, H. G. A. Rahman, and H. M. A. Abdelrazek, "Green tea extract attenuates CCl_4-induced hepatic injury in male hamsters via inhibition of lipid peroxidation and p53-mediated apoptosis," *Toxicology Reports*, vol. 2, Supplement C, pp. 1149–1156, 2015.

[33] V. Ramakrishna and R. Jailkhani, "Evaluation of oxidative stress in insulin dependent diabetes mellitus (IDDM) patients," *Diagnostic Pathology*, vol. 2, no. 1, p. 22, 2007.

[34] T. van Bremen, D. Drömann, K. Luitjens et al., "Triggering receptor expressed on myeloid cells-1 (Trem-1) on blood neutrophils is associated with cytokine inducibility in human *E. coli* sepsis," *Diagnostic Pathology*, vol. 8, no. 1, p. 24, 2013.

[35] J. M. Forbes, M. T. Coughlan, and M. E. Cooper, "Oxidative stress as a major culprit in kidney disease in diabetes," *Diabetes*, vol. 57, no. 6, pp. 1446–1454, 2008.

[36] K. Huynh, B. C. Bernardo, J. R. McMullen, and R. H. Ritchie, "Diabetic cardiomyopathy: mechanisms and new treatment strategies targeting antioxidant signaling pathways," *Pharmacology & Therapeutics*, vol. 142, no. 3, pp. 375–415, 2014.

[37] M. Tag Hend, M. A. Abdelazek Heba, S. Mahoud Yasmen, and S. el Shenawy Nahla, "Efficacy of *Tribulus terrestris* extract and metformin on fertility indices and oxidative stress of testicular tissue in streptozotocin-induced diabetic male rats," *African Journal of Pharmacy and Pharmacology*, vol. 9, no. 48, pp. 1088–1098, 2015.

[38] N. M. Omar and G. M. Atia, "Effect of *Nigella sativa* on pancreatic β-cell damage in streptozotocin-induced diabetic rats," *The Egyptian Journal of Histology*, vol. 35, no. 1, pp. 106–116, 2012.

[39] K. K. Wong and E. S. Tzeng, "Appearance of different diabetic symptoms after streptozotocin administration: a comparison study," *Biochemistry and Molecular Biology International*, vol. 30, no. 6, pp. 1035–1041, 1993.

[40] A. Doğan and İ. Çelik, "Healing effects of sumac (*Rhus coriaria*) in streptozotocin-induced diabetic rats," *Pharmaceutical Biology*, vol. 54, no. 10, pp. 2092–2102, 2016.

[41] M. Kanter, O. Coskun, A. Korkmaz, and S. Oter, "Effects of *Nigella sativa* on oxidative stress and β-cell damage in streptozotocin-induced diabetic rats," *The Anatomical Record*, vol. 279, no. 1, pp. 685–691, 2004.

[42] M. Kaleem, D. Kirmani, M. Asif, Q. Ahmed, and B. Bano, *Biochemical Effects of Nigella sativa L Seeds in Diabetic Rats*, 2006.

[43] Z. Houcher, K. Boudiaf, M. Benboubetra, and B. Houcher, "Effects of methanolic extract and commercial oil of *Nigella sativa* L. on blood glucose and antioxidant capacity in alloxan-induced diabetic rats," *Pteridines*, vol. 18, no. 1, 2007.

[44] T. Szkudelski, "The mechanism of alloxan and streptozotocin action in B cells of the rat pancreas," *Physiological Research*, vol. 50, no. 6, pp. 537–546, 2001.

[45] K. M. Fararh, Y. Atoji, Y. Shimizu, T. Shiina, H. Nikami, and T. Takewaki, "Mechanisms of the hypoglycaemic and immunopotentiating effects of *Nigella sativa* L. oil in streptozotocin-induced diabetic hamsters," *Research in Veterinary Science*, vol. 77, no. 2, pp. 123–129, 2004.

[46] H. Rchid, H. Chevassus, R. Nmila et al., "*Nigella sativa* seed extracts enhance glucose-induced insulin release from rat-isolated Langerhans islets," *Fundamental & Clinical Pharmacology*, vol. 18, no. 5, pp. 525–529, 2004.

[47] K. M. Fararh, Y. Atoji, Y. Shimizu, and T. Takewaki, "Isulinotropic properties of *Nigella sativa* oil in streptozotocin plus nicotinamide diabetic hamster," *Research in Veterinary Science*, vol. 73, no. 3, pp. 279–282, 2002.

[48] K. M. S. Mansi, "Effects of oral administration of water extract of *Nigella sativa* on serum concentrations of insulin and testosterone in alloxan-induced diabetic rats," *Pakistan Journal of Biological Sciences*, vol. 8, no. 8, pp. 1152–1156, 2005.

[49] B. Krishnamurthy, J. Chee, G. Jhala et al., "Complete diabetes protection despite delayed thymic tolerance in NOD8.3 TCR transgenic mice due to antigen-induced extrathymic deletion of T cells," *Diabetes*, vol. 61, no. 2, pp. 425–435, 2012.

[50] K. A. Coughlan, R. J. Valentine, N. B. Ruderman, and A. K. Saha, "AMPK activation: a therapeutic target for type 2 diabetes?," *Diabetes, Metabolic Syndrome and Obesity: Targets and Therapy*, vol. 7, p. 241, 2014.

[51] D. F. Horrobin, "The roles of essential fatty acids in the development of diabetic neuropathy and other complications of diabetes mellitus," *Prostaglandins, Leukotrienes, and Essential Fatty Acids*, vol. 31, no. 3, pp. 181–197, 1988.

[52] I. J. Goldberg, "Diabetic dyslipidemia: causes and consequences," *The Journal of Clinical Endocrinology & Metabolism*, vol. 86, no. 3, pp. 965–971, 2001.

[53] Y. Kocyigit, Y. Atamer, and E. Uysal, "The effect of dietary supplementation of *Nigella sativa* L. on serum lipid profile in rats," *Saudi Medical Journal*, vol. 30, no. 7, pp. 893–896, 2009.

[54] M. Ismail, G. Al-Naqeep, and K. W. Chan, "*Nigella sativa* thymoquinone-rich fraction greatly improves plasma antioxidant capacity and expression of antioxidant genes in hypercholesterolemic rats," *Free Radical Biology and Medicine*, vol. 48, no. 5, pp. 664–672, 2010.

[55] G. Al-Naqeeb and M. Ismail, "Regulation of apolipoprotein A-1 and apolipoprotein B100 genes by thymoquinone rich fraction and thymoquinone in HEPG2 cells," *Journal of Food Lipids*, vol. 16, no. 2, pp. 245–258, 2009.

[56] S. Ahmad and Z. H. Beg, "Hypolipidemic and antioxidant activities of thymoquinone and limonene in atherogenic suspension fed rats," *Food Chemistry*, vol. 138, no. 2-3, pp. 1116–1124, 2013.

[57] J. W. Baynes, "Role of oxidative stress in development of complications in diabetes," *Diabetes*, vol. 40, no. 4, pp. 405–412, 1991.

[58] S. Tsimikas and Y. I. Miller, "Oxidative modification of lipoproteins: mechanisms, role in inflammation and potential clinical applications in cardiovascular disease," *Current Pharmaceutical Design*, vol. 17, no. 1, pp. 27–37, 2011.

[59] O. E. Kelany, H. E. Khaled, M. Amal, H. M. Abdelrazek, and M. M. Abdel-Daim, "Hepatoprotective and metabolic effects of dietary soy phytoestrogens against hyper caloric diet in cyclic female albino rats is mediated through estradiol receptors beta," *Biomedical and Pharmacology Journal*, vol. 10, no. 3, pp. 1061–1069, 2017.

[60] I. Meral, Z. Yener, T. Kahraman, and N. Mert, "Effect of *Nigella sativa* on glucose concentration, lipid peroxidation, anti-oxidant defence system and liver damage in experimentally-induced diabetic rabbits," *Journal of Veterinary Medicine Series A*, vol. 48, no. 10, pp. 593–599, 2001.

[61] S. O. Adewole, E. A. Caxton-Martins, and J. A. Ojewole, "Protective effect of quercetin on the morphology of pancreatic β-cells of streptozotocin-treated diabetic rats," *African Journal of Traditional, Complementary and Alternative Medicines*, vol. 4, no. 1, pp. 64–74, 2007.

[62] A. Gökçe, S. Oktar, A. Koc, and Z. Yonden, "Protective effects of thymoquinone against methotrexate-induced testicular injury," *Human & Experimental Toxicology*, vol. 30, no. 8, pp. 897–903, 2010.

[63] O. A. Badary, A. B. Abdel-Naim, M. H. Abdel-Wahab, and F. M. Hamada, "The influence of thymoquinone on doxorubicin-induced hyperlipidemic nephropathy in rats," *Toxicology*, vol. 143, no. 3, pp. 219–226, 2000.

[64] G. P. Widodo, R. Herowati, J. M. Perangin-Angin, and J. E. Kamlasi, "Antihyperglycemic, antioxidant, and pancreas regeneration activities of black cumin (*Nigella sativa* L.) seeds ethanol extract in alloxan-induced diabetic rats," *International Journal of Pharmacy and Pharmaceutical Sciences*, vol. 8, no. 5, pp. 37–40, 2016.

[65] R. H. Tuhin, M. M. Begum, M. S. Rahman et al., "Wound healing effect of *Euphorbia hirta* Linn. (Euphorbiaceae) in alloxan induced diabetic rats," *BMC Complementary and Alternative Medicine*, vol. 17, no. 1, p. 423, 2017.

[66] M. G. Bischof, E. Bernroider, M. Krssak et al., "Hepatic glycogen metabolism in type 1 diabetes after long-term near normoglycemia," *Diabetes*, vol. 51, no. 1, pp. 49–54, 2002.

[67] A. R. Saltiel and C. R. Kahn, "Insulin signalling and the regulation of glucose and lipid metabolism," *Nature*, vol. 414, no. 6865, pp. 799–806, 2001.

Hindawi
Oxidative Medicine and Cellular Longevity
Volume 2018, Article ID 5106469, 10 pages
https://doi.org/10.1155/2018/5106469

Research Article

Rutin Isolated from *Chrozophora tinctoria* Enhances Bone Cell Proliferation and Ossification Markers

Ashraf B. Abdel-Naim,[1,2] **Abdullah A. Alghamdi**,[3] **Mardi M. Algandaby**,[1,4] **Fahad A. Al-Abbasi**,[1,3] **Ahmed M. Al-Abd**,[2,5] **Basma G. Eid**,[2] **Hossam M. Abdallah**,[6,7] **and Ali M. El-Halawany**[7]

[1]*Medicinal Plants Research Group, Deanship of Scientific Research, King Abdulaziz University, Jeddah, Saudi Arabia*
[2]*Department of Pharmacology and Toxicology, Faculty of Pharmacy, King Abdulaziz University, Jeddah, Saudi Arabia*
[3]*Department of Biochemistry, Faculty of Science, King Abdulaziz University, Jeddah, Saudi Arabia*
[4]*Department of Biological Sciences, Faculty of Science, King Abdulaziz University, Jeddah, Saudi Arabia*
[5]*Pharmacology Department, Medical Division, National Research Centre, Giza, Egypt*
[6]*Department of Natural Products, Faculty of Pharmacy, King Abdulaziz University, Jeddah, Saudi Arabia*
[7]*Department of Pharmacognosy, Faculty of Pharmacy, Cairo University, Cairo, Egypt*

Correspondence should be addressed to Ashraf B. Abdel-Naim; abnaim@yahoo.com

Received 12 October 2017; Revised 25 November 2017; Accepted 17 December 2017; Published 13 February 2018

Academic Editor: Lotfi Aleya

Osteoporosis is a chronic disease in which the skeleton loses a weighty proportion of its mineralized mass and mechanical pliability. Currently available antiosteoporotic agents suffer adverse effects that include elevated risk of thrombosis and cancer. Phytochemicals may constitute a safer and effective option. In the current work, six flavonoids were obtained from *Chrozophora tinctoria* and identified as amentoflavone (1), apigenin-7-*O*-*β*-D-glucopyranoside (2), apigenin-7-*O*-6″-*E*-*p*-coumaroyl-*β*-D-glucopyranoside (3), acacetin-7-*O*-*β*-D-[*α*-L-rhamnosyl(1→6)]3″-*E*-*p*-coumaroyl glucopyranoside (4), apigenin-7-*O*-(6″-*Z*-*p*-coumaroyl)-*β*-D-glucopyranoside (5), and rutin (6). An extensive review of the literature as well as NMR and mass spectral techniques was employed in order to elucidate the compound structures. Proliferation was enhanced in MCF7, MG-63, and SAOS-2 cells after exposure to subcytotoxic levels of the tested flavonoids. Rutin was chosen for subsequent studies in SAOS-2 cells. Rutin was not found to cause any alteration in the index of proliferation of these cells, when examining the cell cycle distribution by DNA flowcytometric analysis. Rutin was, however, found to increase osteocyte and osteoblast-related gene expression and lower the expression of RUNX suppressor and osteoclast genes. When examining the influence of rutin on vitamin D levels and the activity of alkaline phosphatase enzyme, it was found to enhance both, while decreasing acid phosphatase which is a marker of osteoporosis. Thus, rutin enhances proliferation and ossification markers in bone cells.

1. Introduction

Osteoporosis is a chronic disease in which the skeleton loses a weighty proportion of its mineralized mass and mechanical pliability [1]. It occurs when bone resorption surpasses bone formation, causing an imbalance [2]. As a result, the bones tend to become more fragile and more susceptible to fractures [3]. Studies have shown that 50% of women and 20% of men are likely to have a fracture resulting from osteoporosis during their lifetime [4]. Such fractures impose a heavy health and economic burden worldwide [5, 6]. The risk of developing osteoporosis has been shown to be directly linked to diet. Studies have reported that people eating healthy diets with a high fruit and vegetable content tend to have lower bone resorption than their counterparts eating poor diets rich in processed foods [7]. Pharmacological management of osteoporosis involves the use of bisphosphonates and estrogen replacement therapy. However, these

medicines suffer adverse effects that may range from gastric irritation to increased thromboembolic and cancer risks [8–10]. Therefore, it is imperative that we look for safer and effective alternatives. In this regard, medicinal herbs and plant-derived molecules have gained wide acceptance by the public and scientific communities [11].

Flavonoids, which are widely found in fruit and vegetables, are bioactive polyphenols with anti-inflammatory and antioxidant properties. Bone health has been associated with the intake of flavonoids. Intake of flavonoids increases bone mass density (BMD) in the neck and spine and decreases bone resorption in perimenopausal women [12]. Moreover, catechins and flavanones were found to associate with markers of bone resorption negatively. At the hip and spine, anthocyanins were found to be strongly linked with BMD [13]. It has been postulated that the reduction of low-grade inflammation and oxidative stress by flavonoids is the hallmark of protecting bone loss. In addition, flavonoids are thought to promote the upregulation of signaling pathways that increase the activity of osteoblasts [14].

Chrozophora tinctoria (L.) A. Juss. has several other names including turnsole, Dyer's croton or giradol. It is an annual plant that belongs to the *Euphorbiaceae* family [15]. Experimentally, it exhibited antioxidant and wound healing effects [16, 17]. It exerts pronounced anti-inflammatory activities which involve inhibition of TNF-α, PGE_2, IL-1β, and IL-6 [18]. Phytochemically, this plant is rich in biflavones, such as amentoflavone in addition to many flavonoids including apigenin, rutin, quercetin, and acacetin [15, 18–20]. The current work aimed at isolating, identifying, and assessing the activity of major flavonoids isolated from *C. tinctoria* on markers of ossification and proliferation of bone cells.

2. Materials and Methods

2.1. Material for Phytochemical Studies. UV IKON 940 spectrophotometer was used to measure UV spectra. A Bruker Apex III Fourier-transform ion cyclotron resonance (FTICR) mass spectrometer (Bruker Daltonics, Billerica, USA) including an Infinity™ cell and a 7.0 Tesla superconducting magnet (Bruker, Karlsruhe, Germany) was used to perform mass spectrometric studies. A Bruker DRX-600 MHz Ultrashield spectrometer (Bruker BioSpin, Billerica, MA, USA) was utilized to measure NMR spectra. Chromatographic separation of the active compounds was performed on Silica gel 60 (70-230 mesh, Merck, Darmstadt, Germany), Silica gel 100 C_{18}-Reversed phase (0.04–0.063 mm, Merck, Darmstadt, Germany), and Sephadex LH-20 (Pharmacia Fine Chemicals Inc., Uppsala, Sweden). Monitoring of the isolation process was carried out on TLC plates with Silica gel 60 F_{254} (Merck, Darmstadt, Germany).

2.2. Plants Utilized in the Study. Chrozophora tinctoria (L.) A. Juss., Euphorbiaceae aerial parts were obtained from Al-Hadda road, Kingdom of Saudi Arabia (April 2015). These specimens were authenticated by Dr. Emad Al-Sharif, Department of Biology, King Abdulaziz University, Saudi Arabia. A specimen (reg. number CO-1080) was retained in the herbarium of the Department of Natural Products and Alternative Medicine, Saudi Arabia.

2.3. Phenolic Compound Extraction. The isolation process was performed as previously reported [18]. In brief, two kilograms of the aerial parts of *C. tinctoria* were dried and methanol was used as an extraction solvent till exhaustion to give a 150 g residue. The total extract was suspended in the least amount of water and extracted with chloroform leaving flavonoid-rich mother liquor that was separated using a Diaion HP-20 column starting with water up to 100% methanol to give three fractions (A–C). Fraction A was free from any phenolic compounds. Silica gel column chromatography was employed to separate fraction B (50×5 cm, 180 g). $CHCl_3$: MeOH was employed with gradient elution resulting in three fractions, I, II, and III. The first fraction (0.5 g) was separated on CC Sephadex LH-20 using the eluent MeOH to give compound 1 (50 mg). The second fraction (1.5 g) was subjected to chromatography with reversed phase Silica gel 100 C_{18}–column and MeOH : H_2O, 3 : 7 as an eluent to give compound 2 (40 mg). The third fraction (2 g) was repeatedly fractionated on Sephadex LH-20 using MeOH as an eluent; followed by CC on reversed phase Silica gel 100 C_{18} using a system of MeOH : water, 3 : 7; and finally purification was performed on HPLC using a Zorbax SB-C18 column (9.4×250 mm), flow rate 5 ml/min to give to compounds 3 (20 mg), 4 (35 mg), and 5 (45 mg). Fraction C was chromatographed on Sephadex LH-20 using MeOH as an eluent to give compound 6 (20 mg).

2.4. Chemical Compounds and Media. Sulfarhodamine B (SRB), RNAse-A enzyme, 17β-hydroxyestradiol, and propidium iodide (PI) were obtained from Sigma-Aldrich (St. Louis, MO, USA). Cell culture materials such as DMEM media, fetal bovine serum (FBS), McCoy's-5A media, and MEM media were obtained from Gibco™, Thermo Fisher Scientific (Waltham, MA, USA). The chemicals utilized in this study were of the highest available analytical grade.

2.5. Cell Culture. The cell lines used in this study were human breast adenocarcinoma cells (MCF-7 cell line), in addition to human osteosarcoma cell lines (SAOS-2 and MG-63). These estrogen-dependent cell lines were purchased from the VACCERA (Giza, Egypt). The cells were kept in DMEM, MEM, and McCoy's-5A media, respectively. Streptomycin (100 μg/ml), penicillin (100 units/ml), and heat-inactivated FBS (10% *v*/*v*) were added to the media. Cells were kept in at 37°C and in humid conditions 5% (*v*/*v*) CO_2 atmosphere.

2.6. Assessment of Cytotoxicity. The cytotoxic effects of the compounds obtained from *C. tincturia* were examined in MCF-7, SAOS-2, and MG-63 cells using SRB assay as described in the previous work [21]. Trypsin-EDTA (0.25% *w*/*v*) was utilized to briefly detach exponentially growing cells. Subsequently, cells were transferred to 96-well plates (10^3 cells per well). The test compounds were applied for 72 h to the cells. The cells were then fixed using TCA (10% *w*/*v*) at 4°C for 1 h. Subsequently, the cells were washed three times and SRB solution (0.4% *w*/*v*) was added in a dark room

for 10 min after which glacial acetic acid (1% *v*/*v*) was applied for a final wash. Cells were dried and the SRB-stained cells were dissolved by Tris-HCl (0.1 M). A microplate reader was utilized to record the color intensity at 540 nm.

2.7. Determination of Doubling Time Using the Proliferation Assay. SRB assay was employed to calculate the doubling time (as a measure for the proliferative effect) of MCF-7, SAOS-2, and MG-63 cells in the presence of and absence of incubation with the compounds isolated from *C. tincturia*. A subcytotoxic concentration (1 μM) of the flavonoids obtained from *C. tincturia* was shortly applied to cells growing exponentially in media free of phenol red for 96 h. SRB solution was used to stain cells in order to carry out their quantification and to calculate doubling time using the best fit linear regression analysis curve [22].

2.8. Cell Cycle Distribution Study. In order to determine the effects of rutin on the cell cycle distribution, 1 μM rutin was applied to SAOS-2 cells for 48 h and a comparison was made relative to 0.1 μM estradiol. Trypsin was used to detach and collect the cells, after which PBS was added to wash the cells twice at 4°C. The cells were then resuspended in PBS (0.5 ml). Ethanol (ice-cold 70% *v*/*v*) (2 ml) was applied while shaking. This was followed by an incubation of the cells for 1 h at 4°C to allow fixation to occur. Cells were then analyzed, washed, and resuspended in PBS (1 ml) containing 50 μg/ml of RNAase-A and 10 μg/ml of PI. The cells were kept in the dark (20°C) for 20 minutes and the DNA contents were determined. After being passed into an ACEA Novocyte™ flow cytometer (ACEA Biosciences Inc., San Diego, CA, USA), the cells were analyzed using a FL2 signal detector (λex/em 535/617 nm) for PI positive events. Phases of the cell cycle were determined by ACEA NovoExpress™ software (ACEA Biosciences Inc., San Diego, CA, USA) for every sample (12,000 events per sample) subsequent to defining cell fragment-free fluorescent gate. Cells in the supra-G_2/M phase were identified using ungated events. Total cells in S- and G_2/M phases were divided by cells in G_0/G_1 phases in order to calculate the proliferation index.

2.9. Gene Array Studies. Expression of osteogenic- and osteolytic-related genes was studied by exposing the cells (1×10^6) to either 1 μM rutin or 0.1 μM estradiol for 48 h. The latter served as a positive control. RNeasy Mini Kit® (Qiagen Inc., Valencia, CA, USA) was used for RNA extraction. cDNA was obtained by reverse transcription with a cDNA Reverse Transcription Kit (Applied Biosystems, Foster City, CA). PCR was performed in real time on the cDNA via GeneQuery™ Human Osteogenic Differentiation qPCR Array (Science Cell Research Laboratories Inc., Carlsbad, CA, USA) according to the manufacturer's instructions [23]; β-actin was selected as the housekeeping gene. The formula: $2^{-\Delta\Delta Cq}$ was employed to detect the normalized change in the gene expression of the studied genes after treatment with rutin and estradiol.

2.10. Osteoporosis Marker Assessment. The effects of rutin on ossification markers in the SAOS-2 cell line were determined by the application of 1 μM rutin or 0.1 μM estradiol to 1×10^6 cells for 48 h. The latter served as a positive control. After collecting the media, assays of vitamin D, alkaline phosphatase (ALP), osteocalcin (OC), and acid phosphatase (ACP) were performed. A direct HTS-ready colorimetric kit (Abcam, Cambridge, UK) was used to determine ALP as well as tartrate-resistant ACP [24]. Uscan® immunoassay ELISA Kit (Life Science Inc., Wuhan, China) was utilized to detect osteocalcin [25]. Human Total 25-OH Vitamin D IVD ELISA Kit (R&D Systems, Inc., Minneapolis, MN, USA) was used to detect vitamin D in its active form.

2.11. Statistical Analysis. Data are presented as mean ± SD. Analysis of variance (ANOVA) and Tukey's post hoc test were used to calculate statistical significance by SPSS® for Windows, version 17.0.0. $p < 0.05$ was regarded as being statistically significant.

3. Results and Discussion

There is an immense need for the development of novel drugs to treat osteoporosis which are devoid of potentially life-threatening side effects, namely, stroke and carcinogenesis [8, 26]. We have previously found that the phenolic compound paradol, isolated from *Aframomum meleguea* seeds, showed proliferative effects in bone cells [27]. Flavonoids have been shown by numerous studies to prevent bone loss [12, 28–31]. Since *C. tinctoria* is rich in flavonoids as apigenin, rutin, quercetin, and acacetin [18, 20], we examined the effects of these compounds on proliferation and ossification markers. Mechanistically, the plant has been shown to impede several pathologic processes leading to osteoporosis as oxidative stress and inflammation [18]. Our study focused on isolating and determining the activity of its flavonoids on bone cell proliferation and ossification markers. Six metabolites were isolated from the *C. tinctoria* after phytochemical analysis (Figure 1). Cochromatography with authentic samples was used to identify these compounds, in addition to referring to spectral data from the literature. The identified compounds were amentoflavone (1) [32, 33], apigenin-7-*O*-β-D-glucopyranoside (2) [34], apigenin-7-*O*-6″-*E*-*p*-coumaroyl-β-D-glucopyranoside (3) [35], acacetin-7-*O*- β-D-[α-L-rhamnosyl(1→6)]3″-*E*-*p*-coumaroyl glucopyranoside (4) [18], apigenin-7-*O*-(6″-*Z*-*p*-coumaroyl)-β-D-glucopyranoside (5) [18], and rutin (6) [34].

The cytotoxicity of these compounds was studied using the SRB viability assay in various estrogenic cell lines, namely, MCF-7, SAOS-2, and MG-63 cells. We have previously used these cell lines to study the effects of paradol on *A. meleguea* seeds, where we noted an accelerated proliferation [27]. In the present study, when looking at the effects on MCF-7 cells, the compounds showed a maximum of 20% alteration in the viability of cells, after being applied to the compounds for 72 h in 10 μM concentrations. Exposing the cells to a higher concentration (100 μM) of amentoflavone for 72 h (1) lead to a 78.8% viability of the control untreated cells (Table 1). As in the MCF-7 cells, exposure of SAOS-2 cells to the compounds at 10 μM concentration for 72 h showed a maximum of 20% change in viability. However, increasing the concentration of the compounds 1, 3, 5,

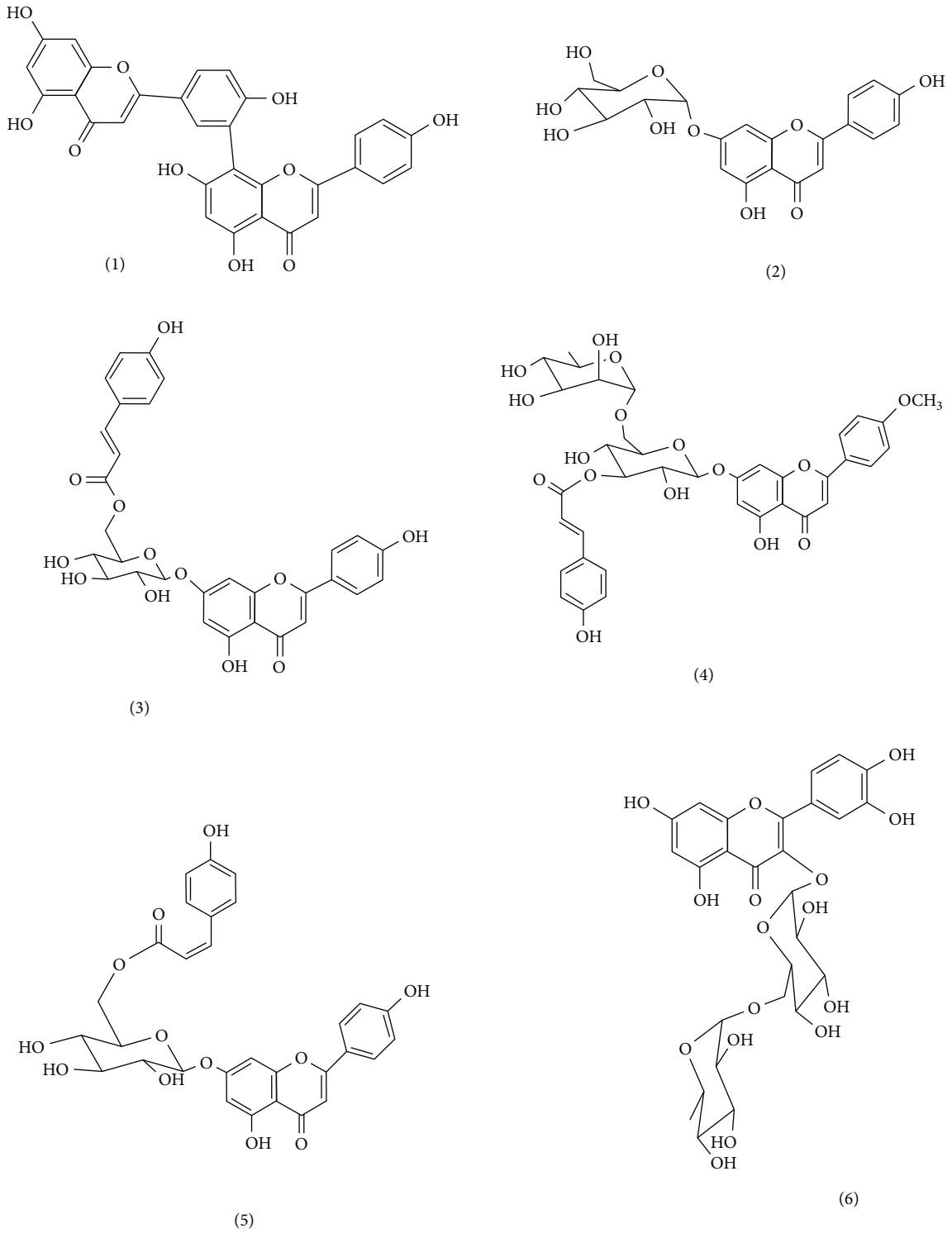

Figure 1: Isolated compounds from *Chrozophora tincturia*.

and 6 to 100 μM induced a viability drop down to 70.1%, 66.2%, 77.1%, and 76.2% of the untreated control cells, respectively (Table 1). Interestingly, MG-63 cells were the most affected by the compounds under investigation. The addition of the compounds under investigation (0.1 μM) to MG-63 cells for 72 h had no more than a 20% change in the viability of the cells. However, exposure to 1 μM of 1 and 5 reduced cell viability to 74.9% and 78.1% of the control cells, respectively. The addition of a greater concentration (10 μM) of all flavonoids under investigation induced 20–40% killing effect at 72 h of exposure. Further exposure to 100 μM of all compounds under investigation dropped cell viability of MG-63 cells to 40–70% of the control untreated cells (Table 1).

Table 1: Cytotoxicity assessment of compounds isolated from *C. tincturia*.

	Cpd	Percent viability				
		0.01 μM	0.1 μM	1 μM	10 μM	100 μM
MCF-7	1	95.8 ± 1.6	91.5 ± 3.4	88.6 ± 3.3	84.8* ± 1.6	78.8* ± 0.3
	2	99.4 ± 1.2	94.8 ± 3.3	91.1 ± 3.2	90.3 ± 2.4	85.9* ± 1.6
	3	99.1 ± 0.3	95.1 ± 3.4	94.0 ± 2.5	92.8 ± 1.7	90.5* ± 0.3
	4	99.8 ± 0.5	96.0 ± 0.5	94.5 ± 3.1	91.1 ± 2.4	87.9* ± 0.6
	5	98.3 ± 1.2	91.8 ± 2.7	88.9 ± 2.8	86.9* ± 1.7	80.2* ± 1.2
	6	97.5 ± 1.5	93.2 ± 3.8	90.4 ± 3.4	88.2* ± 2.1	80.3* ± 1.7
SAOS-2	1	98.9 ± 0.8	95.1 ± 0.9	92.1 ± 0.9	80.4* ± 0.9	70.1* ± 0.2
	2	99.2 ± 0.6	97.4 ± 2.0	94.5 ± 1.3	92.8 ± 1.6	89.3* ± 1.5
	3	97.4 ± 1.0	96.8 ± 0.9	91.9 ± 1.7	84.7 ± 3.4	66.2* ± 1.2
	4	98.4 ± 0.7	95.8 ± 0.8	92.7 ± 0.4	90.1 ± 0.9	84.7* ± 1.0
	5	97.0 ± 1.5	92.9 ± 0.8	90.9 ± 0.5	85.4* ± 0.5	77.1* ± 0.5
	6	96.6 ± 0.8	93.6 ± 0.7	92.6 ± 1.9	88.5* ± 1.2	76.2* ± 0.9
MG-63	1	88.2 ± 0.1	82.3 ± 1.2	74.9* ± 2.0	61.3* ± 0.4	40.4* ± 0.5
	2	95.9 ± 2.7	88.8 ± 2.0	81.1* ± 0.3	74.9* ± 1.4	70.9* ± 0.6
	3	96.7 ± 2.0	92.2 ± 1.6	87.4 ± 1.2	80.8* ± 0.2	64.3* ± 1.1
	4	98.1 ± 0.4	93.2 ± 1.3	87.2* ± 0.8	79.8* ± 2.0	60.2* ± 1.7
	5	93.1 ± 0.9	83.4 ± 1.2	78.1* ± 0.8	67.7* ± 1.1	54.7* ± 2.1
	6	91.1 ± 0.7	86.2 ± 0.8	82.2 ± 1.2	73.0* ± 1.2	63.4* ± 0.4

Cells were treated with test compounds for 72 h and viability was determined using SRB assay. Data are expressed as mean ± SD; $n = 6$. *Significantly different from control untreated cells ($p < 0.05$).

It has been previously reported that several flavonoids and related phytochemicals interact with estrogen receptors [36, 37]. The influence of a subcytotoxic concentration (1 μM) from all compounds under investigation on doubling times of MCF-7, SAOS-2, and MG-63 cells was tested. A concentration of 0.1 μM E_2 served as a positive control. Compounds 1, 3, and 6 caused a significant lowering of the doubling times of MCF-7 cells from 16.6 ± 1.4 h to 9.3 ± 0.2 h, 8.6 ± 0.4 h, and 7.2 ± 0.5 h, respectively. The addition of E_2 to MCF-7 cells resulted in a lowering of the doubling time to 8.5 ± 0.4 h (Table 2). When studying the cell lines derived from bone osteosarcoma, compounds 1, 3, 4, 5, and 6 caused a decrease in the doubling time of SAOS-2 cells from 49.3 ± 4.1 h to 26.6 ± 1.4 h, 14.7 ± 0.7 h, 29.0 ± 2.9 h, 29.4 ± 3.5 h, and 15.7 ± 0.2 h, respectively. In SAOS-2 cells, it was noted that E_2 decreased the doubling time to 20.1 ± 1.2 h (Table 2). In addition, compounds 1, 3, 5, and 6 lowered the MG-63 cells doubling time from 36.8 ± 2.2 h to 20.9 ± 0.3 h, 21.0 ± 0.3 h, 23.5 ± 1.1 h, and 20.8 ± 0.5 h, respectively, in comparison to 23.1 ± 0.1 h by E_2 (Table 2). It is worth mentioning that some flavonoids might be equipotent or ever more potent than E_2 which might be attributed to the higher concentrations used (more than 10-fold). When comparing all tested flavonoids, rutin (6) showed promising proliferative properties with minimal expected mutagenic influence. This is in line with reports by Hyun et al. regarding its osteoclast activating properties [38]. Additionally, the selection of SAOS-2 cells for future studies was based upon their low viability drop when treated with the flavonoids being studied.

In this study, the flavonoids obtained from *C. tinctoria* displayed clear proliferative effects in all the three studied cell lines. Although several studies have reported that estrogen along with various estrogen metabolites possesses proliferative properties, this was limited by the fact that they cause mutagenicity [22, 39]. Therefore, it was of importance to record the impact of rutin on the distribution of the phases of cell cycle in relation to the progression of the cell cycle flow cytometry to determine DNA content. Treatment of SAOS-2 cells with 1 μM rutin for 48 h was carried out. Exposing the cells to 0.1 μM E_2 served as a positive control. Interestingly, rutin produced a significant increase of cells in G_0/G_1 from 55.2 ± 2.4% to 62.6 ± 1.1% with a reciprocal decrease for cells in S-phase from 30.7 ± 2.9% to 22.5 ± 1.0%. G_2/M phase was

Table 2: Proliferative effects of compounds isolated from *C. tincturia*: doubling time assessment.

	MCF-7	SAOS2	MG-63
Control	16.6 ± 1.4	49.3 ± 4.1	36.8 ± 2.2
1	9.3* ± 0.2	26.3* ± 1.4	20.9* ± 0.3
2	14.8 + 1.7	35.7 ± 3.4	27.5 ± 2.1
3	8.6* ± 0.4	14.7* ± 0.7	21.0* ± 0.3
4	11.8 ± 3.6	29.0* ± 2.9	25.8* ± 3.5
5	13.4 ± 3.2	29.4* ± 3.5	23.5* ± 1.1
6	7.2* ± 0.5	15.7* ± 0.2	20.8* ± 0.5
E_2	8.5* ± 0.4	20.1* ± 1.2	23.1* ± 0.1

Cells were treated with test compounds (1 μM) for up to 96 h and viability was determined using SRB assay. Doubling times were calculated and compared to control untreated cells and E_2 (0.1 μM) treated cells (positive control). Data are expressed as mean ± SD; $n = 6$. *Significantly different from the corresponding untreated cells; $p < 0.05$.

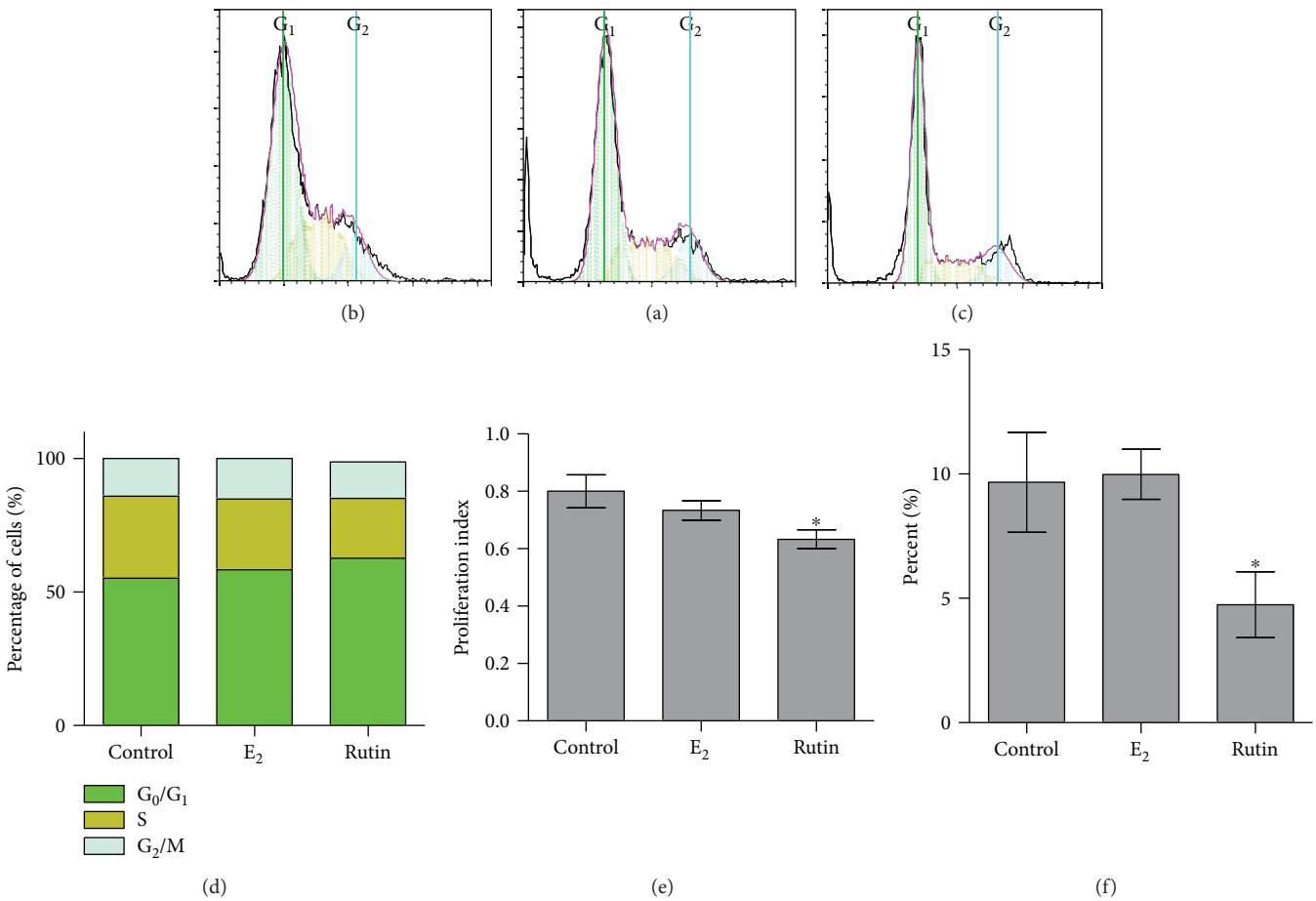

FIGURE 2: Effect of rutin on the cell cycle distribution of SAOS-2 cells. Cells were exposed to rutin (1 μM) for 48 h (b) and compared to control untreated cells (a) and E_2- (0.1 μM) treated cells (c). Cell cycle distribution was determined using DNA cytometry analysis and different cell phases were plotted (d) as percentage of total events. Proliferation index was calculated and plotted (e). Supra-G_2/M cell population was plotted as percent of total events (f). Data are presented as mean ± SD; $n = 3$. *Significantly different from the control untreated cells; $p < 0.05$.

not affected by treatment with rutin (Figures 2(a), 2(c), and 2 (d)). However, 0.1 μM E_2 produced a significant drop of cells in the S-phase (30.7 ± 2.9% to 26.5 ± 0.9%). Treating SAOS-2 cells with E_2 caused no significant changes of cells in G_0/G1 or S-phases (Figures 2(a), 2(b), and 2(d)). When studying the proliferating cell fraction balance in SAOS-2 cells, rutin significantly decreased the proliferation index; on the other hand, treatment with E_2 did not alter their proliferation index (Figure 2(e)). In a previous study in our laboratory, paradol showed no influence on the proliferation index of SAOS-2 cells [27]. Our current data are in alignment with our studies on SAOS-2 cells where 1 μM rutin was found to decrease the doubling time. Yet, we tested the nature of the rutin proliferative effect in SAOS-2; accumulation of cells in the supra-G_2 compartment (multiploidy phase) might indicate uncontrolled cell proliferation. Interestingly, after SAOS-2 exposure to rutin, cells in supra-G_2 phase were much lower than control cells (Figure 2(f)). This indicates a punctuated cell division without cell accumulation in multiploidy phase [40]. This gains support by the known chemopreventive and anticarcinogenic properties of rutin [41–43].

Several studies have reported that targeting ossification is a more fruitful approach than targeting proliferation, when looking at developing new drug targets to treat osteoporosis. [44, 45]. The effects of rutin on osteogenic marker gene expression were quantitatively studied using RT-PCR gene array battery kit that comprises various osteogenic gene families. These include osteocyte, osteoclast, and osteoblast activity markers, as well as RUNX suppressor genes. When studying the osteocyte activity markers (*BGN*, *FGF23*, *PDPN*, *HYOU1*, and *SOST*), rutin and E_2 caused an increase in expression of all the tested osteocyte activity gene markers by 1.9- to 2.9-folds and 2.7- to 3.5-folds, respectively (Figure 3(a)). The role of osteocytes in calcium and phosphate homeostasis has been previously reported. Osteocytes cloned with BGN caused acceleration of osteoblast differentiation in vitro and an increase in the area of lamellar bone-like matrices in vivo [46]. Phosphate levels are known to decline due to the presence of the FGF23 protein [47]. Dividing osteocytes are known to express PDPN, which is regarded as a marker of activity [48]. They also secrete SOST causing a negative effect on the formation of bones [49]. Also, rutin

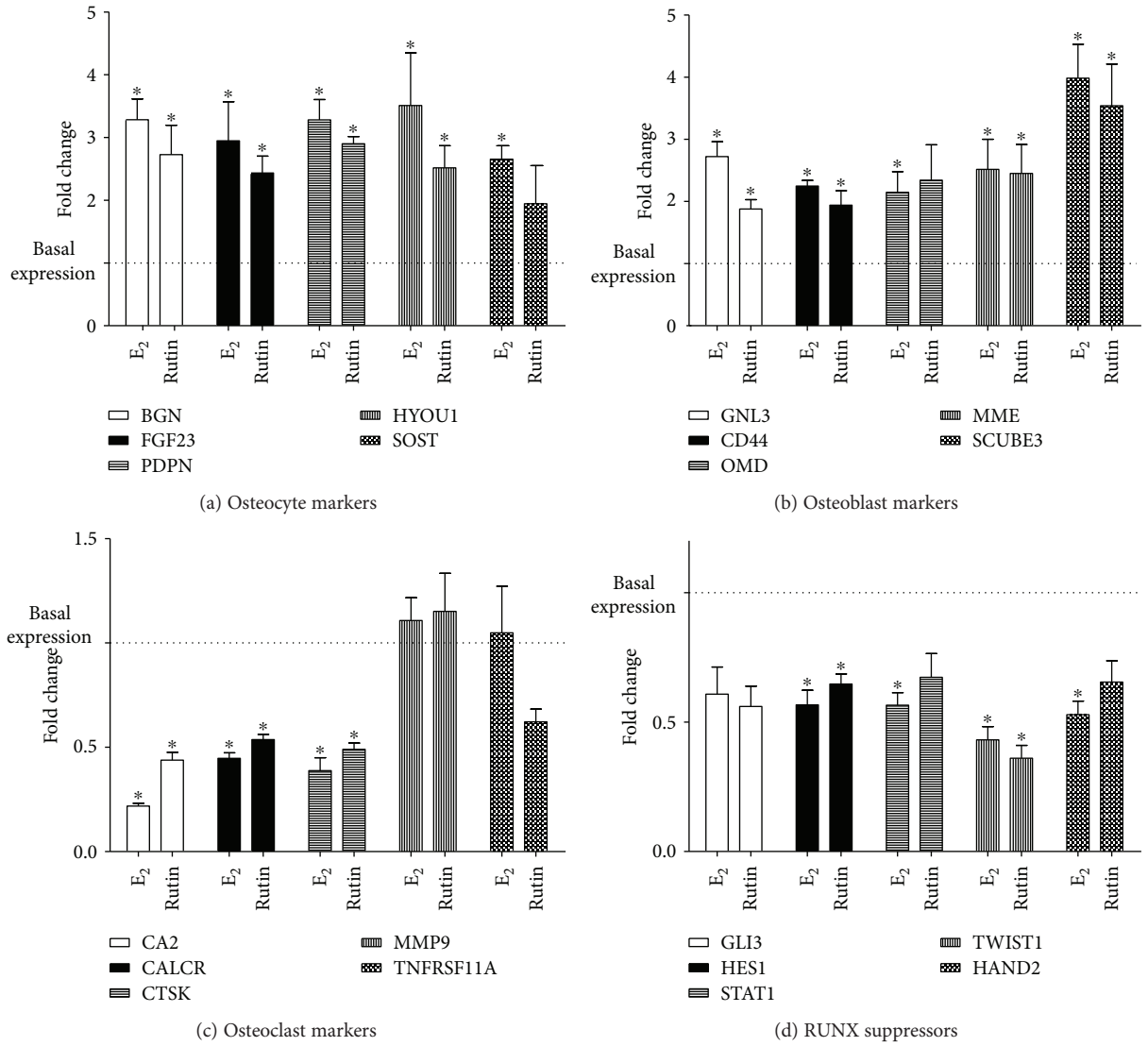

Figure 3: Effect of rutin on mRNA expression of some ossification related genes in SAOS-2 cell line. Cells were incubated with rutin (1 μM) or E_2 (0.1 μM) for 48 h. Total RNA was extracted and subjected to RT-PCR. Data were normalized to β-actin; fold changes were calculated and expressed as mean ± SD; $n = 3$. *Significantly different from the control untreated cells; $p < 0.05$.

increased the expression level of *GNL3*, *CD44*, *MME*, and *SCUBE3* osteoblast activity markers, by 1.8 ± 0.2-, 1.9 ± 0.3-, 2.5 ± 0.7-, and 3.5 ± 0.9-folds, respectively. *OMD* expression after rutin treatment was not changed. The five tested gene markers of osteoblast activity were augmented by 2.1- to 4.0-folds after the application of E_2 (Figure 3(b)). Compared to our previous work on paradol [27], rutin significantly increased HYOU1 but not SOST. Further, rutin could significantly enhance expression of the osteoblast marker CD44 while paradol failed to exert a similar effect. With respect to osteoclast activity markers, both rutin and E_2 downregulated *CA2*, *CALCR*, and *CTSK* expression to 0.4- to 0.5-folds and 0.2- to 0.4-folds, respectively. The expression of *MMP9 and TNFRSF11A* genes was unaltered after treatment with either rutin or E_2 (Figure 3(c)). These findings confirm the potential favorable effects of rutin. This is further supported by studies in the bone marrow that showed rutin inhibits osteoclastogenesis [50]. When studying the *RUNX* suppressor gene family (*GLB*, *HES1*, *STAT1*, *TWIST1*, and *HAND2*), rutin downregulated the expression of *HES1*and *TWIST1* mRNA to 0.7 ± 0.1- and 0.4 ± 0.07-folds of the control cells, respectively. On the other hand, E_2 was found to suppress *HES1*, *STAT1*, *TWIST1*, and *HAND2* gene expression to 0.4- to 0.6-folds of control (Figure 3(d)). Studies have reported that RUNX regulates RANKL leading to the maturation and differentiation of osteoblasts [51]. The lowered expression of *HES1*and *TWIST1* (RUNX suppressors) by rutin supports its osteogenic effects. All these data are in alignment with our previous publication on paradol [27]. However, rutin showed superior activities with regard to suppressing *CALCR* expression.

In the present study, we determined the effects of treating SAOS-2 cells with 1 μM rutin for 48 h on the levels of four essential osteoporosis-related markers. The results were compared with treatment of the cells with 0.1 μM E_2 as a positive control. Rutin produced a significant increase in the activity/concentrations of all ossification markers, ALP

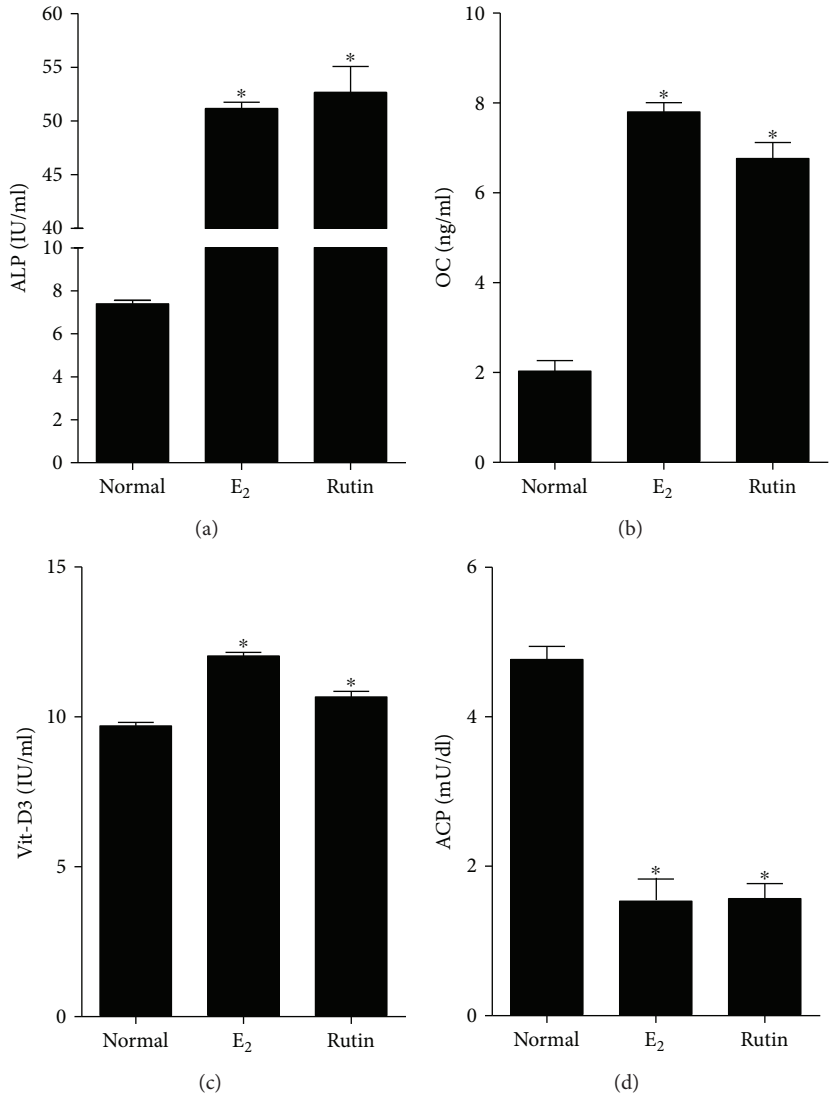

Figure 4: Biochemical assessment for antiosteoporosis effect of rutin *in vitro*. SAOS-2 cells were treated with rutin (1 μM) and E_2 (0.1 μM) for 48 h and compared to the control untreated cells. Biochemical assessment of osteoporosis was evaluated by measuring alkaline phosphatase (a), osteocalcin (b), vitamin D3 (c), and acid phosphatase (d). Data are presented as mean ± SD; $n = 3$. *Significantly different from the control untreated cells; $p < 0.05$.

enzyme, OCN hormone, and active Vit-D3 concentration, by 7.1-, 3.4-, and 1.1-folds, respectively. Similarly, E_2 increased the activity/concentrations of ALP enzyme, OCN hormone, and active Vit-D3 concentration, by 6.9-, 3.9-, and 1.2-folds, respectively (Figures 4(a)–4(c)). On the other hand, rutin produced a statistically significant drop in ACP enzyme activity (bone resorption marker) from 4.7 ± 0.4 IU/ml to 1.6 ± 0.4 IU/ml compared to 1.5 ± 0.4 IU/ml for E_2-treated cells (Figure 4(d)). The biochemical markers chosen in this study are well documented in the literature as reliable markers having antiosteoporotic properties. [52]. In conclusion, the analysis of *C. tinctoria* extract led to the isolation of various flavonoids showing antiosteoporosis influence. Rutin was especially promising as it showed ossification in bone cells as well as possessing punctuate proliferative activity with minimal influence to cell cycle distribution. In other words, rutin might be further studied as a potential antiosteoprotic agent with minimal expected mutagenic effects.

Conflicts of Interest

The authors declare no conflicts of interest.

Acknowledgments

This project was funded by the Deanship of Scientific Research (DSR), King Abdulaziz University, Jeddah, Saudi Arabia, under Grant no. (1-166-35 RG). The authors, therefore, acknowledge with thanks DSR for technical and financial support.

References

[1] R. M. Martin and P. H. S. Correa, "Bone quality and osteoporosis therapy," *Arquivos Brasileiros de Endocrinologia & Metabologia*, vol. 54, no. 2, pp. 186–199, 2010.

[2] K. Akesson, "New approaches to pharmacological treatment of osteoporosis," *Bulletin of the World Health Organization*, vol. 81, no. 9, pp. 657–664, 2003.

[3] K. E. Ensrud and C. J. Crandall, "Osteoporosis," *Annals of Internal Medicine*, vol. 167, no. 3, pp. ITC17–ITC32, 2017.

[4] T. P. van Staa, E. M. Dennison, H. G. Leufkens, and C. Cooper, "Epidemiology of fractures in England and Wales," *Bone*, vol. 29, no. 6, pp. 517–522, 2001.

[5] W. D. Leslie, C. J. Metge, M. Azimaee et al., "Direct costs of fractures in Canada and trends 1996–2006: a population-based cost-of-illness analysis," *Journal of Bone and Mineral Research*, vol. 26, no. 10, pp. 2419–2429, 2011.

[6] J. P. van den Bergh, T. A. van Geel, and P. P. Geusens, "Osteoporosis, frailty and fracture: implications for case finding and therapy," *Nature Reviews Rheumatology*, vol. 8, no. 3, pp. 163–172, 2012.

[7] A. C. Hardcastle, L. Aucott, W. D. Fraser, D. M. Reid, and H. M. Macdonald, "Dietary patterns, bone resorption and bone mineral density in early post-menopausal Scottish women," *European Journal of Clinical Nutrition*, vol. 65, no. 3, pp. 378–385, 2011.

[8] L. M. Brass, "Estrogens and stroke: use of oral contraceptives and postmenopausal use of estrogen: current recommendations," *Current Treatment Options in Neurology*, vol. 6, no. 6, pp. 459–467, 2004.

[9] W. Strampel, R. Emkey, and R. Civitelli, "Safety considerations with bisphosphonates for the treatment of osteoporosis," *Drug Safety*, vol. 30, no. 9, pp. 755–763, 2007.

[10] D. A. Yardley, "Pharmacologic management of bone-related complications and bone metastases in postmenopausal women with hormone receptor-positive breast cancer," *Breast Cancer: Targets and Therapy*, vol. 8, pp. 73–82, 2016.

[11] L. Wu, Z. Ling, X. Feng, C. Mao, and Z. Xu, "Herb medicines against osteoporosis: active compounds & relevant biological mechanisms," *Current Topics in Medicinal Chemistry*, vol. 17, no. 15, pp. 1670–1691, 2017.

[12] A. C. Hardcastle, L. Aucott, D. M. Reid, and H. M. Macdonald, "Associations between dietary flavonoid intakes and bone health in a Scottish population," *Journal of Bone and Mineral Research*, vol. 26, no. 5, pp. 941–947, 2011.

[13] A. Welch, A. MacGregor, A. Jennings, S. Fairweather-Tait, T. Spector, and A. Cassidy, "Habitual flavonoid intakes are positively associated with bone mineral density in women," *Journal of Bone and Mineral Research*, vol. 27, no. 9, pp. 1872–1878, 2012.

[14] A. A. Welch and A. C. Hardcastle, "The effects of flavonoids on bone," *Current Osteoporosis Reports*, vol. 12, no. 2, pp. 205–210, 2014.

[15] R. Gibbs, *Chemotaxonomy of Flowering Plants*, McGill-Queen's University Press, Montreal, 1974.

[16] F. Oke-Altuntas, S. Ipekcioglu, A. Sahin Yaglioglu, L. Behcet, and I. Demirtas, "Phytochemical analysis, antiproliferative and antioxidant activities of *Chrozophora tinctoria*: a natural dye plant," *Pharmaceutical Biology*, vol. 55, no. 1, pp. 966–973, 2017.

[17] H. Maurya, M. Semwal, and S. K. Dubey, "Pharmacological evaluation of *Chrozophora tinctoria* as wound healing potential in diabetic rat's model," *BioMed Research International*, vol. 2016, Article ID 7475124, 7 pages, 2016.

[18] H. M. Abdallah, F. M. Almowallad, A. Esmat, I. A. Shehata, and E. A. Abdel-Sattar, "Anti-inflammatory activity of flavonoids from *Chrozophora tinctoria*," *Phytochemistry Letters*, vol. 13, pp. 74–80, 2015.

[19] E. Hecker, "Cocarcinogenic principles from the seed oil of *Croton tiglium* and from other Euphorbiaceae," *Cancer Research*, vol. 28, no. 11, pp. 2338–2349, 1968.

[20] U. W. Hawas, "Antioxidant activity of brocchlin carboxylic acid and its methyl ester from *Chrozophora brocchiana*," *Natural Product Research*, vol. 21, no. 7, pp. 632–640, 2007.

[21] P. Skehan, R. Storeng, D. Scudiero et al., "New colorimetric cytotoxicity assay for anticancer-drug screening," *JNCI Journal of the National Cancer Institute*, vol. 82, no. 13, pp. 1107–1112, 1990.

[22] H. A. Mosli, M. F. Tolba, A. M. Al-Abd, and A. B. Abdel-Naim, "Catechol estrogens induce proliferation and malignant transformation in prostate epithelial cells," *Toxicology Letters*, vol. 220, no. 3, pp. 247–258, 2013.

[23] J. Vandesompele, K. De Preter, F. Pattyn et al., "Accurate normalization of real-time quantitative RT-PCR data by geometric averaging of multiple internal control genes," *Genome Biology*, vol. 3, article RESEARCH0034, 2002.

[24] W. Gerhardt, M. L. Nielsen, O. V. Nielsen, J. S. Olsen, and B. E. Statland, "Clinical evaluation of routine measurement of liver and bone alkaline phosphatases in human serum: differential inhibition by L-phenylalanine and carbamide (urea) on the LKB 8600 reaction rate analyzer," *Clinica Chimica Acta*, vol. 53, no. 3, pp. 291–297, 1974.

[25] J. Y. Fu and D. Muller, "Simple, rapid enzyme-linked immunosorbent assay (ELISA) for the determination of rat osteocalcin," *Calcified Tissue International*, vol. 64, no. 3, pp. 229–233, 1999.

[26] P. D. Papapetrou, "Bisphosphonate-associated adverse events," *Hormones*, vol. 8, no. 2, pp. 96–110.

[27] A. B. Abdel-Naim, A. A. Alghamdi, M. M. Algandaby et al., "Phenolics isolated from *Aframomum meleguta* enhance proliferation and ossification markers in bone cells," *Molecules*, vol. 22, no. 9, 2017.

[28] I. Fernandes, R. Pérez-Gregorio, S. Soares, N. Mateus, and V. de Freitas, "Wine flavonoids in health and disease prevention," *Molecules*, vol. 22, no. 4, p. 292, 2017.

[29] C.-L. Shen and M.-C. Chyu, "Tea flavonoids for bone health: from animals to humans," *Journal of Investigative Medicine*, vol. 64, no. 7, pp. 1151–1157, 2016.

[30] Y. Gao, F. Yang, H. Xi, W. Li, P. Zhen, and K. Chen, "Effects of icariin total flavonoids capsule on bone mineral density and bone histomorphometry in growing rats," *Zhejiang Da Xue Xue Bao. Yi Xue Ban*, vol. 45, no. 6, pp. 581–586, 2016.

[31] Y.-L. Huang, C.-C. Shen, Y.-C. Shen, W.-F. Chiou, and C.-C. Chen, "Anti-inflammatory and Antiosteoporosis flavonoids from the rhizomes of *Helminthostachys zeylanica*," *Journal of Natural Products*, vol. 80, no. 2, pp. 246–253, 2017.

[32] C. A. Carbonezi, L. Hamerski, A. A. L. Gunatilaka et al., "Bioactive flavone dimers from *Ouratea multiflora* (Ochnaceae)," *Revista Brasileira de Farmacognosia*, vol. 17, no. 3, pp. 319–324, 2007.

[33] Y.-M. Zhang, R. Zhan, Y.-G. Chen, and Z.-X. Huang, "Two new flavones from the twigs and leaves of *Cephalotaxus lanceolata*," *Phytochemistry Letters*, vol. 9, pp. 82–85, 2014.

[34] M. Shabana, M. El-Sherei, M. Moussa, A. Sleem, and H. Abdallah, "Investigation of phenolic constituents of Carduncellus eriocephalus Boiss. Var. albiflora Gauba and their biological activities," *Natural Product Communications*, vol. 2, pp. 823–828, 2007.

[35] M. Plioukas, A. Termentzi, C. Gabrieli, M. Zervou, P. Kefalas, and E. Kokkalou, "Novel acylflavones from *Sideritis syriaca* ssp. *syriaca*," *Food Chemistry*, vol. 123, no. 4, pp. 1136–1141, 2010.

[36] S. Lecomte, M. Lelong, G. Bourgine, T. Efstathiou, C. Saligaut, and F. Pakdel, "Assessment of the potential activity of major dietary compounds as selective estrogen receptor modulators in two distinct cell models for proliferation and differentiation," *Toxicology and Applied Pharmacology*, vol. 325, pp. 61–70, 2017.

[37] X. Wang, N. Zheng, J. Dong, X. Wang, L. Liu, and J. Huang, "Estrogen receptor-α36 is involved in icaritin induced growth inhibition of triple-negative breast cancer cells," *The Journal of Steroid Biochemistry and Molecular Biology*, vol. 171, pp. 318–327, 2017.

[38] H. Hyun, H. Park, J. Jeong et al., "Effects of watercress containing rutin and rutin alone on the proliferation and osteogenic differentiation of human osteoblast-like MG-63 cells," *The Korean Journal of Physiology & Pharmacology*, vol. 18, no. 4, pp. 347–352, 2014.

[39] A. M. Soto and C. Sonnenschein, "The role of estrogens on the proliferation of human breast tumor cells (MCF-7)," *Journal of Steroid Biochemistry*, vol. 23, no. 1, pp. 87–94, 1985.

[40] J. M. Mitchison and B. L. A. Carter, "Chapter 11 cell cycle analysis," *Methods in Cell Biology*, vol. 11, pp. 201–219, 1975.

[41] M. G. Hertog, P. C. Hollman, M. B. Katan, and D. Kromhout, "Intake of potentially anticarcinogenic flavonoids and their determinants in adults in The Netherlands," *Nutrition and Cancer*, vol. 20, no. 1, pp. 21–29, 1993.

[42] C. Chaumontet, M. Suschetet, E. Honikman-Leban et al., "Lack of tumor-promoting effects of flavonoids: studies on rat liver preneoplastic foci and on *in vivo* and *in vitro* gap junctional intercellular communication," *Nutrition and Cancer*, vol. 26, no. 3, pp. 251–263, 1996.

[43] S. Sharma, A. Ali, J. Ali, J. K. Sahni, and S. Baboota, "Rutin: therapeutic potential and recent advances in drug delivery," *Expert Opinion on Investigational Drugs*, vol. 22, no. 8, pp. 1063–1079, 2013.

[44] J. A. Kanis and C. C. Glüer, "An update on the diagnosis and assessment of osteoporosis with densitometry," *Osteoporosis International*, vol. 11, no. 3, pp. 192–202, 2000.

[45] T. D. Rachner, S. Khosla, and L. C. Hofbauer, "Osteoporosis: now and the future," *The Lancet*, vol. 377, no. 9773, pp. 1276–1287, 2011.

[46] D. Parisuthiman, Y. Mochida, W. R. Duarte, and M. Yamauchi, "Biglycan modulates osteoblast differentiation and matrix mineralization," *Journal of Bone and Mineral Research*, vol. 20, no. 10, pp. 1878–1886, 2005.

[47] R. Sapir-Koren and G. Livshits, "Osteocyte control of bone remodeling: is sclerostin a key molecular coordinator of the balanced bone resorption–formation cycles?," *Osteoporosis International*, vol. 25, no. 12, pp. 2685–2700, 2014.

[48] D. Dayong Guo and L. F. Bonewald, "Advancing our understanding of osteocyte cell biology," *Therapeutic Advances in Musculoskeletal Disease*, vol. 1, no. 2, pp. 87–96, 2009.

[49] X. Li, M. S. Ominsky, Q.-T. Niu et al., "Targeted deletion of the sclerostin gene in mice results in increased bone formation and bone strength," *Journal of Bone and Mineral Research*, vol. 23, no. 6, pp. 860–869, 2008.

[50] C. M. Rassi, M. Lieberherr, G. Chaumaz, A. Pointillart, and G. Cournot, "Modulation of osteoclastogenesis in porcine bone marrow cultures by quercetin and rutin," *Cell and Tissue Research*, vol. 319, no. 3, pp. 383–393, 2005.

[51] T. Komori, "Roles of runx2 in skeletal development," *Advances in Experimental Medicine and Biology*, vol. 962, pp. 83–93, 2017.

[52] H. M. Abdallah, A. M. Al-Abd, G. F. Asaad, A. B. Abdel-Naim, and A. M. El-halawany, "Isolation of antiosteoporotic compounds from seeds of *Sophora japonica*," *PLoS One*, vol. 9, no. 6, article e98559, 2014.

Hindawi
Oxidative Medicine and Cellular Longevity
Volume 2017, Article ID 6745840, 8 pages
https://doi.org/10.1155/2017/6745840

Research Article

Comparison of Selected Parameters of Redox Homeostasis in Patients with Ataxia-Telangiectasia and Nijmegen Breakage Syndrome

Barbara Pietrucha,[1] Edyta Heropolitanska-Pliszka,[1] Mateusz Maciejczyk,[2] Halina Car,[2] Jolanta Sawicka-Powierza,[3] Radosław Motkowski,[4] Joanna Karpinska,[5] Marta Hryniewicka,[5] Anna Zalewska,[6] Malgorzata Pac,[1] Beata Wolska-Kusnierz,[1] Ewa Bernatowska,[1] and Bozena Mikoluc[4]

[1]*Clinical Immunology, The Children's Memorial Health Institute, Av. Dzieci Polskich 20, 04-730 Warsaw, Poland*
[2]*Department of Experimental Pharmacology, Medical University of Bialystok, Szpitalna 37 Str., 15-295 Bialystok, Poland*
[3]*Department of Family Medicine, Medical University of Bialystok, Bialystok, Poland*
[4]*Department of Pediatrics Rheumatology, Immunology, and Metabolic Bone Diseases, Medical University of Bialystok, Waszyngtona 17 Str., 15-274 Bialystok, Poland*
[5]*Institute of Chemistry, University of Bialystok, Bialystok, Poland*
[6]*Department of Conservative Dentistry, Medical University of Bialystok, Bialystok, Poland*

Correspondence should be addressed to Bozena Mikoluc; bozenam@mp.pl

Received 25 August 2017; Revised 21 November 2017; Accepted 3 December 2017; Published 31 December 2017

Academic Editor: Mohamed M. Abdel-Daim

This study compared the antioxidant status and major lipophilic antioxidants in patients with ataxia-telangiectasia (AT) and Nijmegen breakage syndrome (NBS). Total antioxidant status (TAS), total oxidant status (TOS), oxidative stress index (OSI), and concentrations of coenzyme Q10 (CoQ10) and vitamins A and E were estimated in the plasma of 22 patients with AT, 12 children with NBS, and the healthy controls. In AT patients, TAS (median 261.7 μmol/L) was statistically lower but TOS (496.8 μmol/L) was significantly elevated in comparison with the healthy group (312.7 μmol/L and 311.2 μmol/L, resp.). Tocopherol (0.8 μg/mL) and CoQ10 (0.1 μg/mL) were reduced in AT patients versus control (1.4 μg/mL and 0.3 μg/mL, resp.). NBS patients also displayed statistically lower TAS levels (290.3 μmol/L), while TOS (404.8 μmol/L) was comparable to the controls. We found that in NBS patients retinol concentration (0.1 μg/mL) was highly elevated and CoQ10 (0.1 μg/mL) was significantly lower in comparison with those in the healthy group. Our study confirms disturbances in redox homeostasis in AT and NBS patients and indicates a need for diagnosing oxidative stress in those cases as a potential disease biomarker. Decreased CoQ10 concentration found in NBS and AT indicates a need for possible supplementation.

1. Introduction

Ataxia-telangiectasia (AT; OMIM #208900) and Nijmegen breakage syndrome (NBS; OMIM #251260) belong to a group of genetically determined primary immunodeficiency disorders (PID) whose course involves defects in DNA repair processes [1]. AT is caused by null mutations in the *ATM* (*ataxia-telangiectasia mutated*) *gene* located on chromosome 11q.26 which encodes a protein of the same name. The main role of ATM protein is the coordination of cellular response to DNA double strand breaks, oxidative stress, signal transduction, and cell-cycle control. The clinical picture of the disease is characterised by cerebellar degeneration, telangiectasia, immunodeficiency, cancer susceptibility, and radiation sensitivity. Experimental studies have provided direct evidence for the presence of mitochondrial dysfunctions in AT

cells. They have demonstrated that the structural organisation of mitochondria in AT cells is abnormal compared to wild-type cells [2, 3].

NBS, similarly to AT, belongs to a group of the XCIND syndrome. The XCIND syndrome is named after Eaton et al. who found distinct hypersensitivity to ionizing (X-ray) irradiation, cancer susceptibility, immunodeficiency, neurological abnormality, and double-strand DNA breakage in these cases [4]. Mutations causative of NBS occur in the NBS1 gene, located on human chromosome 8q21. NBS1 encodes for nibrin, the key regulatory protein of the R/M/N (RAD50/MRE11/NBS1) protein complex which senses and mediates cellular response to DNA damage caused by ionizing radiation [5, 6]. The chromosome instability in AT and NBS patients results from a defective response to DNA double-strand breaks. In addition, AT and NBS patients display a few common characteristics such as growth retardation, premature aging, and neurodegeneration. It is believed that these symptoms can be caused not only by chromosomal instability and aberrant DNA damage response but also by oxidative stress and mitochondrial abnormalities [1, 2].

Recent studies indicate new, alternative sources of ROS and oxidative stress in AT and NBS cells, including NADPH oxidase 4, oxidised low-density lipoprotein (ox-LDL), or poly (ADP-ribose) polymerases (PARP-1, PARP-2, and PARP-3) [1, 7–10]. Mitochondrial dysfunction such as aberrant structural organisation of mitochondria, excess mitochondrial ROS (mROS) production and mitochondrial injury have also been reported in AT and NBS cells [1, 3, 11]. Valentin-Vega et al. [11] showed increased mROS production in AT cells, which resulted from a decline in the activity of complex I of the electron transport chain in mitochondria. Noteworthy is a study conducted by Weyemi et al. [9] who stressed that NADPH oxidase 4 (the main source of free radicals in the cell) was highly upregulated in AT cells and correlated with higher oxidative damage and apoptosis. To date, however, little is still known about the oxidant/antioxidant abnormalities in AT and NBS patients. Therefore, the purpose of our study was to measure selected parameters of redox homeostasis in patients with AT and NBS. Both disorders are characterised by symptoms typical of the XCIND syndrome, and therefore we intended to evaluate total antioxidant status (TAS), total oxidant status (TOS), and oxidative stress index (OSI) as well as concentrations of the most common lipophilic antioxidants, CoQ10, and vitamins A and E. It appears that the thorough understanding of disturbances in the body's antioxidant defense mechanisms could lead to new therapeutic strategies in AT and NBS, similarly as in other oxidative stress-related genetic disorders.

2. Materials and Methods

2.1. Patients. The study included 12 Caucasian children with NBS (5 females, 7 males) whose average age was 12 years and 1 month with a confirmed mutation in the *NBS1 gene* and 22 patients with AT (9 females, 13 males) whose average age was 13 years and 7 months with a confirmed mutation in *ATM gene*. All study participants were under the medical care of the Department of Immunology at the Children's Memorial Health Institute in Warsaw, Poland. The patients were included in the study on the basis of their medical history and physical examination, and they were found to be in good health at the time of enrollment (normal biochemical and morphological blood parameters, negative markers of inflammation). Diagnosis was based on clinical symptoms and genetic and biochemical tests according to ESID (European Society for Immunodeficiencies) criteria. None of the patients enrolled in the study were diagnosed with cancer, diabetes, hypertension, and HIV infection. The control group consisted of, respectively, 12 and 22 healthy individuals matched for age and sex. Plasma samples of the study and the control group were collected between February 2016 and January 2017.

The study was approved by the Bioethical Committee at the Medical University, Bialystok, Poland. Parents of all respondents gave informed written consent for their children's participation in the study.

2.2. Determination of Plasma Total Antioxidant Status (TAS), Total Oxidant Status (TOS), and Oxidative Stress Index (OSI). Total antioxidant status (TAS) and total oxidant status (TOS) were determined using commercial colorimetric kits (ImAnOx (TAS/TAC) Kit, Immundiagnostik, Bensheim, Germany and PerOx (TOS/TOC) Kit, Immundiagnostik, Bensheim, Germany, resp.) in accordance with the manufacturer's instructions. The determination of TAS was based on a reaction between antioxidants contained in the sample with exogenous hydrogen peroxide, while the determination of TOS was performed by the reaction of peroxidase with total lipid peroxides in the sample. The resulting coloured products were measured colorimetrically at a wavelength of 450 nm using Mindray MR-96 Microplate Reader, China. All assays were performed in duplicate samples. To assess the redox balance disorders, we have also used the oxidative stress index (OSI), which may be considered as a gold indicator of oxidative stress in biological systems. OSI was calculated according to the formula $\mathrm{OSI} = \mathrm{TOS}/\mathrm{TAS} \times 100$ [12].

2.3. Determination of Plasma Vitamin A (All-Trans-Retinol), Vitamin E (L-Tocopherol), and Coenzyme Q10. Analyses were performed using high performance liquid chromatograph coupled with MS detector equipped with triple quadrupole (Shimadzu LCMS/MS-8040). Ionization was conducted using APCI (atmospheric pressure chemical ionization) mode. Data acquisition and processing were performed using Shimadzu LabSolutions LCMS Software.

The compounds were separated with a Kinetex XB-C18 100A analytical column (50 mm × 3.0 mm, 1.7 μm). The mobile phase consisted of an isocratic solvent A (methanol) 0.01-2 min and then isocratic solvent B (methanol-n-hexan, 72 : 28, *v*/*v*) 2.5–6 min. The flow rate was 0.4 mL/min, and the temperature of the analytical column was 400°C. The injection volumes of standard and sample solutions were 10 μL. Acquisition settings and method were optimized by the infusion of a 10 μg/mL solution of each fixed compound. The mass spectrometer was operated in the positive ion atmospheric pressure chemical ionization mode. The APCI temperature was set at 350°C and the ion current 4.5 μA.

The flow of the drying gas (N2) and the flow of the nebulizing gas were 10 L/min and 3 L/min, respectively. The desolvation line (DL) and heat block temperature was 230°C.

All analytes were detected in the MS/MS multiple reaction monitoring (MRM) with unit resolution at both Q1 and Q3. The MS conditions for generation of the positive ions are presented in Table 1. The described above chromatographic conditions were used for quantification of target analytes in plasma samples. The chromatogram of real sample is visualized in Figure 1. Plasma samples were prepared according to the procedure published previously [13].

2.4. Statistical Analysis. The examined variable distribution was assessed by means of the Kolmogoroff-Smirnow test. Due to the fact that the tested variables were inconsistent with normal distribution, the Mann–Whitney U test was used. Results are expressed as median, minimum, and maximum. The Spearman's method was applied in assessing correlations between variables. In calculations, the relevance level of $p < 0.05$ was accepted as statistically significant, authorising the rejection of individual zero hypotheses. The data were processed using the Polish version of Statistica 12.0 statistical software for PC with Windows.

3. Results

Our study demonstrated that in patients with AT plasma TAS levels were statistically lower ($p = 0.002$) and plasma TOS was statistically significantly elevated ($p = 0.001$) in comparison with the control group. Similarly to TOS, OSI was elevated in AT patients ($p = 0.001$) (Figure 2).

Tocopherol plasma concentrations were significantly reduced in AT patients as compared to the control group ($p = 0.021$). The concentrations of endogenous free radical scavenger coenzyme Q10 were statistically decreased in the plasma of AT patients versus the healthy controls ($p = 0.001$). There were no significant differences in the concentrations of plasma retinol between both groups ($p = 0.076$) (Figure 2).

Similarly to the AT group, NBS patients displayed statistically lower plasma TAS levels in comparison with the control group ($p = 0.044$). In contrast to AT, plasma TOS in NBS was not significantly different in comparison with the healthy controls ($p = 0.102$). The OSI value, similarly to AT, was higher in comparison with the controls ($p = 0.004$) (Figure 3).

We demonstrated that in patients with NBS the concentration of vitamin A precursor, beta carotene, was significantly elevated in comparison with that in the control group ($p = 0.011$). The difference in CoQ10 concentration in NBS patients and healthy controls points to a significantly lower level in NBS patients ($p = 0.001$). The concentrations of plasma vitamin E were similar in the control group and NBS patients ($p = 0.582$) (Figure 3).

It is worth noting that we did not observe statistically significant differences between the evaluated parameters in patients with AT and those with NBS (Table 2). In addition, we did not find significant correlations in the assessed markers of oxidative stress between the study groups and controls.

Table 1: The MS conditions for generation of positive ions of the analytes.

Compound	Precursor ion (m/z)	Product ions (m/z)	Collision energy [eV]
Retinol	269.10	213.20	−12
		93.10	−23
α-Tocopherol	429.30	165.10	−25
		137.05	−48
Coenzyme Q10	863.60	197.15	−45
		109.10	−47

m/z: mass-to-charge ratio.

4. Discussion

This study compared the redox balance as well as major lipophilic antioxidants in patients with AT and NBS diseases. We have shown that AT and NBS are associated with impaired redox homeostasis including disturbances in lipophilic free radical scavengers such as coenzyme Q10 and alpha-tocopherol (Figure 4).

We aimed to investigate the oxidant/antioxidant status via the measurement of plasma TAS and TOS, which could provide a systemic reflection of redox homeostasis in biological systems. Concentration of TAS was significantly reduced in AT and NBS patients, which suggests the exhaustion or inefficiency of protective antioxidant systems resulting from the overproduction or enhanced activity of reactive oxygen species (ROS). It is believed that oxidative stress plays a key role in the development of many systemic complications including growth retardation, endocrine abnormalities, neurodegeneration, and premature aging as well as immunodeficiency [14–16], which are the major phenotypic hallmarks in AT and NBS diseases [1]. Our study did not directly demonstrate oxidative stress in patients with AT and NBS, since it would have been necessary to measure oxidative modification products. Nevertheless, we showed the existence of cellular redox abnormalities in the AT (↓ TAS, ↑ OSI, and ↑ TOS) and NBS groups (↓ TAS and ↑ OSI), which can constitute the basis for the development of oxidative stress leading to DNA mutations and protein oxidation as well as lipid peroxidation. We would like to emphasise that we did not find significant differences between the researched parameters of redox balance when we compared AT with NBS. A lack of correlation may indicate a similarity of redox imbalance in AT and NBS disorders, although these changes tend to be more severe in patients with AT. However, we recorded significantly elevated TOS levels only in patients with AT and therefore, TOS may be subtle distinguishing between AT and NBS diseases.

There is a consensus in the literature regarding enhanced oxidative stress in neurodegenerative disorders such as Alzheimer's or Parkinson's disease (PD) [17, 18]. Clinical studies have confirmed increased oxidant status and comparable, decreased antioxidant status in patients with PD [19–21]. It is probable that similar changes occur in the

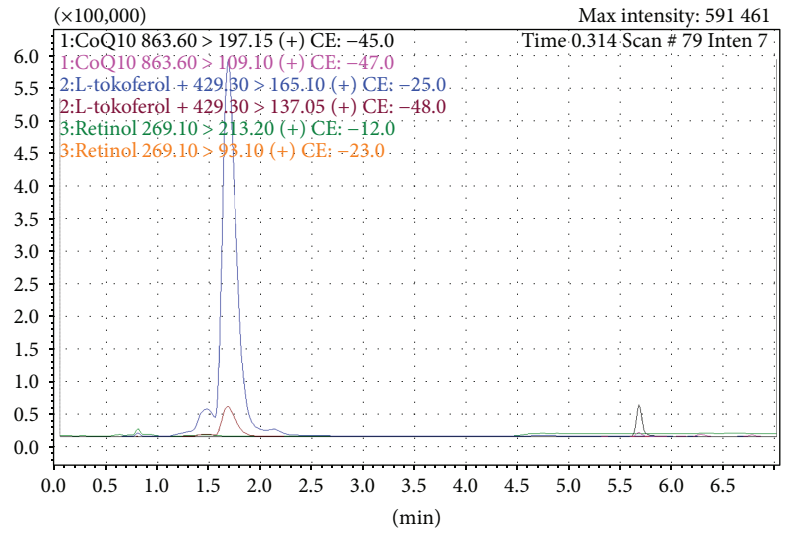

Figure 1: Chromatogram of a real sample (plasma).

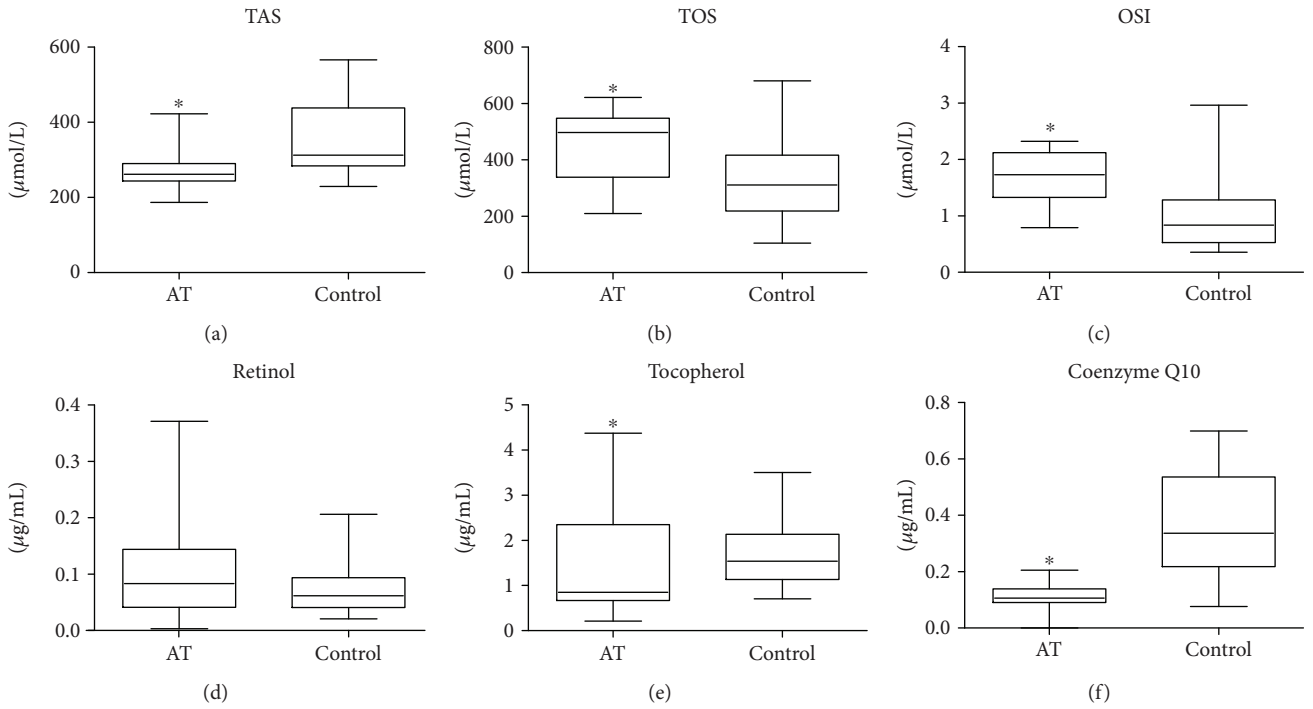

Figure 2: Lipophilic antioxidants and total antioxidant/oxidant status in patients with AT and control group. TAS: total antioxidant status; TOS: total oxidant status; OSI: oxidative stress index; $^{*}p < 0.05$.

course of AT and NBS. However, the available literature contains limited data regarding oxidative stress/redox disturbances in those cases [1]. Additionally, it should be noted that the measurement of plasma TAS and TOS provides information about antioxidant properties conditioned primarily by low molecular weight (LWMA) hydrophilic antioxidants (e.g., uric acid (UA) and ascorbic acid (AA) as well as thiol groups), but not lipophilic antioxidants [22]. Taking this into consideration, we also decided to measure levels of major lipophilic free radical scavengers (CoQ10, vitamins A and E).

Our study confirm decreased CoQ10 concentration both in AT and NBS. Coenzyme Q10 (also called ubiquinone) is a lipid soluble benzoquinone which is a key component of the mitochondrial respiratory chain for adenosine triphosphate (ATP) synthesis [23]. It has been demonstrated that most of the CoQ10 in the human body is produced endogenously; 25% of the stores are obtained from dietary intake [24]. Coenzyme Q10 deficiency results not only in abnormal respiratory chain function with inadequate cellular energy production, increased generation of free radicals, and degradation of mitochondria but also impacts on the immune

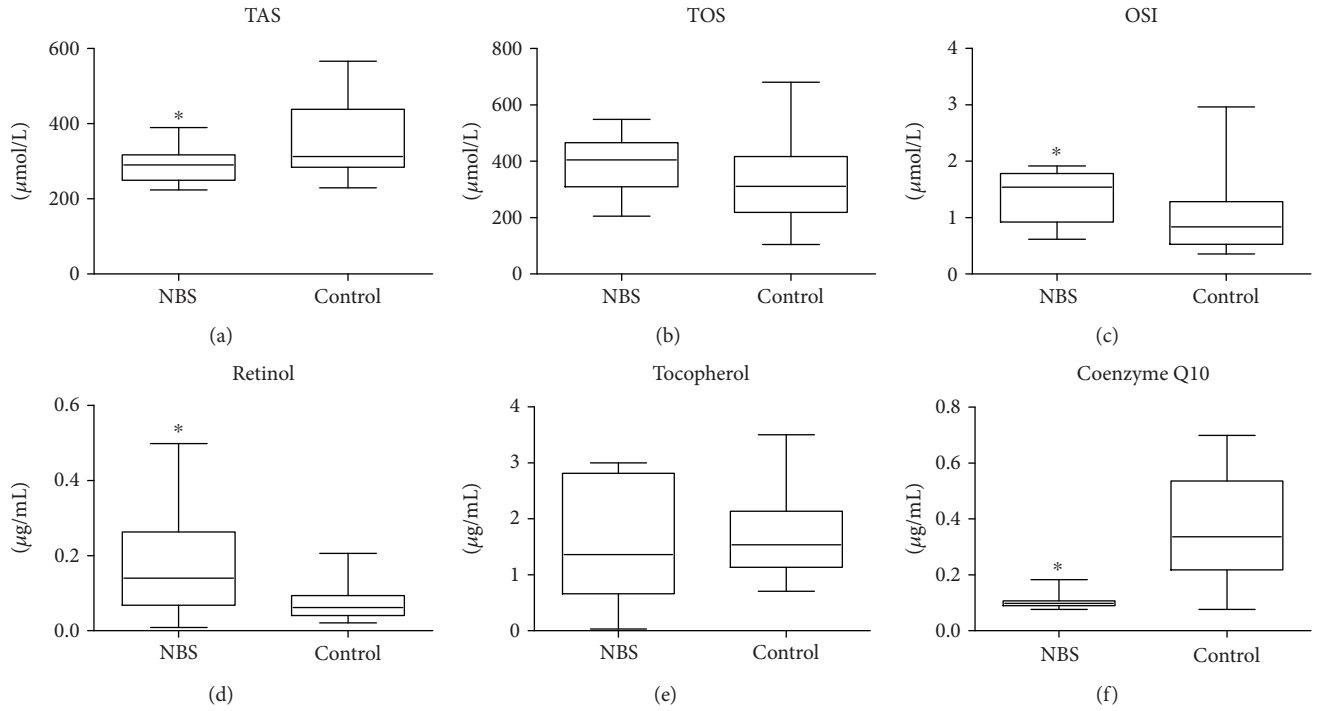

Figure 3: Lipophilic antioxidants and total antioxidant/oxidant status in patients with NBS and control group. TAS: total antioxidant status; TOS: total oxidant status; OSI: oxidative stress index; $^{*}p < 0.05$.

Table 2: Differences between lipophilic antioxidants and total antioxidant/oxidant status in patients with AT and NBS.

Parameters examined	AT group		NBS group		p
	Median	Min–max	Median	Min–max	
Retinol (μg/mL)	0.083	0.003–0.371	0.140	0.009–0.498	0.109
α-Tocopherol (μg/mL)	0.847	0.213–4.371	1.361	0.032–3.003	0.929
Coenzyme Q10 (μg/mL)	0.108	0.085–0.206	0.098	0.077–0.183	0.290
TAS (μmol/L)	261.745	186.852–422.515	290.288	223.966–389.895	0.327
TOS (μmol/L)	496.839	209.803–621.354	404.795	204.741–548.632	0.094
OSI	1.730	0.790–2.320	1.543	0.615–1.915	0.157

TAS: total antioxidant status; TOS: total oxidant status; OSI: oxidative stress index.

system [25]. Literature reports demonstrate that CoQ10 supplementation has improved CD4 T cell counts in patients with AIDS and outcomes in herpes and HPV infections. Furthermore, leukocyte activity is conditioned, inter alia, by proper CoQ10 activity [25]. CoQ10 deficiency may contribute to the abnormal function of mitochondria in the course of diseases such as AIDS, Alzheimer's disease, Parkinson's disease, and cancer [26, 27]. Similar disturbances have been observed in AT and NBS cells, which may suggest a potential involvement of CoQ10 in the pathogenesis of these disorders [1]. Considering the protective action of CoQ10 in neurodegenerative processes and its role in the immune system, decreased CoQ10 concentration in AT and NBS patients indicates a need for monitoring its concentration and potential supplementation. At this stage, we are unable to answer the question to what degree clinical symptoms observed in AT, such as cerebellar degeneration, immunodeficiency, cancer susceptibility, and radiation sensitivity, result from oxidative stress disturbances observed in our study. Are these disturbances primary or secondary? However, they undeniably confirm CoQ10 involvement in the pathomechanism of the observed changes. It should be also emphasised that rare autosomal recessive disorder, CoQ10 deficiency (mutation in CABC1; COQ2; COQ9; PDSS1; PDSS2 genes), is frequently associated with seizures, cognitive decline, pyramidal track signs, myopathy, and prominent cerebellar ataxia [28, 29]. Some of these symptoms occur in both AT and NBS. Additionally, it is very likely that, in AT and NBS patients, a decrease in CoQ10 levels may be associated with impaired DNA repair mechanisms, similarly as in other bioenergetics disorders such as xeroderma pigmentosum (XP), Cockayne Syndrome (CS), Fanconi anaemia (FA), and Hutchinson-Gilford syndrome (HGS) [1].

Deficiency in lipid soluble antioxidants has been demonstrated in various conditions such as eating disorders, nicotine addiction, chronic diseases, and aging. Antioxidant vitamins and trace elements contribute to maintaining an effective immune response [30–33]. Treatments are also

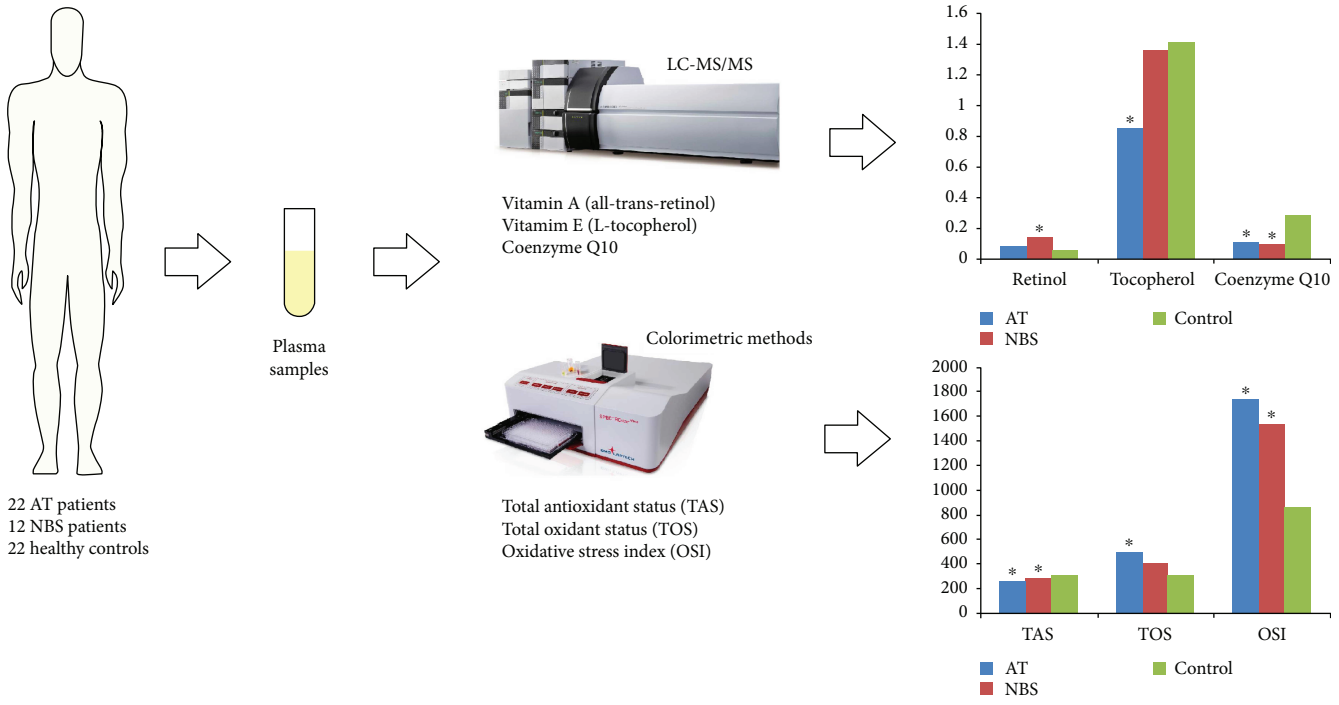

Figure 4: Graphical presentation of the study. $^{*}p < 0.05$ versus control.

available for a few autosomal recessive ataxias: vitamin E therapy for ataxia with vitamin E deficiency (AVED), chenodeoxycholic acid for cerebrotendinous xanthomatosis, CoQ10 for CoQ10 deficiency, and dietary restriction of phytanic acid for Refsum disease. Idebenone may ameliorate the cardiac and neurological manifestations of Friedreich ataxia (FRDA). No other specific treatments exist for hereditary ataxias [34]. Unfortunately, no sufficiently effective causal therapy is available for AT and NBS patients at present. Our results indicate a need for introducing CoQ10 and tocopherol into AT and NBS treatment, taking into consideration their plasma levels.

Alpha-tocopherol primarily inhibits the production of new free radicals and thus might help in preventing or delaying chronic diseases associated with reactive oxygen species molecules [35]. Decreased vitamin E concentration in AT may result in a decline in the body's antioxidant activity and anti-inflammatory as well as cell-mediated and humoral immune functions. In AT cases, we found decreased concentrations of both CoQ10 and vitamin E, which enhance disturbances in the redox balance and may increase ROS production, accumulation of damaged mitochondrial DNA (mDNA), and progressive respiratory chain dysfunction. The few experimental studies found in the available literature report that disturbances in redox processes also occur in NBS [1]. Our study of NBS cases demonstrated decreased TAS and enhanced OSI on the one hand and a reduced concentration of CoQ10 and increased concentration of vitamin A, on the other hand. Despite the fact that the interpretation of obtained results is difficult at this stage of research advancement due to a lack of comparable studies, we would like to emphasise that we did not find any differences in the tested parameters between AT and NBS.

To date, only few studies have evaluated the antioxidant defenses in AT and NBS patients [1, 36]. In one of the first reports on the subject, Reichenbach et al. showed a decrease in the levels of total antioxidant capacity, vitamin A, and vitamin E in AT patients. In contrast to our study, CoQ10 levels in AT were not significantly reduced [37]. In our study patients with AT, we found not only significantly reduced levels of CoQ10 but also of α-tocopherol. However, retinol concentration, in line with studies by Da Silva et al., was similar to the control group [38]. It is probable that the aforementioned dissimilarities result from differences in the size of study groups and research methodologies. At this point, it should be emphasized that our study is the first in which the largest group of AT and NBS patients took part.

In summary, we demonstrated a significant decrease in the level of plasma TAS in AT and NBS patients as well as an increase in the oxidative stress index. It appears that disturbances in the body's antioxidant defense mechanisms may lead to oxidative damage and altered cellular redox homeostasis and thus affect clinical manifestations of AT and NBS phenotypes. Redox imbalance in patients with AT and NBS appears to exist at a comparable level. However, a significant increase in total oxidant status (TOS) was demonstrated only in patients with AT in whom plasma TOS may be a subtle distinguishing feature of AT and NBS disorders. We are considering the theory that antioxidant supplementation with tocopherol and CoQ10 may be one of the factors enhancing treatment efficacy in AT and NBS diseases and improving patients' clinical status. Further studies regarding CoQ10 in AT and NBS are needed in order to assess its concentration not only in the blood but also in selected tissues and to evaluate the dynamics of change in relation to disease duration. The issue of a possible link between

CoQ10 deficiency and the occurrence of mutations responsible for CoQ10 deficiency remains open.

When analyzing the results of our research, one must bear in mind its limitations. We evaluated only selected parameters of redox balance in patients with AT and NBS, so determination of other markers may lead to other conclusions and clinical applications. Additionally, blood oxidative stress biomarkers cannot be mechanistically informative for some reasons. Firstly, blood and the respective tissue under study do not share common redox components and/or pathways (e.g., lack of mitochondria in erythrocytes and plasma). Secondly, both plasma and blood cells can autonomously produce significant amounts of ROS [15, 16]. However, it should be also emphasized that extremely strong point of our study is the large number of patients in the study groups compared to previously published works. Our research may also provide a new practical aspects for clinicians.

5. Conclusions

(1) Our study confirms disturbances in redox homeostasis in AT and NBS patients and indicates a need for diagnosing oxidative stress in those cases as a potential disease biomarker.

(2) The statistically significantly decreased coenzyme Q10 concentration found in NBS and AT indicates a need for possible supplementation aimed at remedying the diagnosed deficiencies in those individuals.

Abbreviations

APCI:	Atmospheric pressure chemical ionization
AT:	Ataxia-telangiectasia
ATM:	Ataxia-telangiectasia mutated
CoQ10:	Coenzyme Q10
ESID:	European Society for Immunodeficiencies
LWMA:	Low molecular weight hydrophilic antioxidants
MRM:	MS/MS multiple reaction monitoring
NBS:	Nijmegen breakage syndrome
OSI:	Oxidative stress index
PARP:	Poly (ADP-ribose) polymerase
PID:	Primary immunodeficiency disorder
ROS:	Reactive oxygen species
TAS:	Total antioxidant status
TOS:	Total oxidant status
XCIND syndrome:	Hypersensitivity to ionizing (X-ray) irradiation, cancer susceptibility, immunodeficiency, neurological abnormality, and double-strand DNA breakage.

Conflicts of Interest

The authors declare that they have no conflicts of interest.

Authors' Contributions

Barbara Pietrucha, Edyta Heropolitanska-Pliszka, and Mateusz Maciejczyk had equal participation.

Acknowledgments

The investigation was supported by Grant nos. 143-26591L and N/ST/ZB/16/001/1126 from the Medical University in Bialystok.

References

[1] M. Maciejczyk, B. Mikoluc, B. Pietrucha et al., "Oxidative stress, mitochondrial abnormalities and antioxidant defense in ataxia-telangiectasia, bloom syndrome and Nijmegen breakage syndrome," *Redox Biology*, vol. 11, pp. 375–383, 2017.

[2] F. V. Pallardó, A. Lloret, M. Lebel et al., "Mitochondrial dysfunction in some oxidative stress-related genetic diseases: ataxia-telangiectasia, down syndrome, Fanconi anaemia and Werner syndrome," *Biogerontology*, vol. 11, no. 4, pp. 401–419, 2010.

[3] M. Ambrose, J. V. Goldstine, and R. A. Gatti, "Intrinsic mitochondrial dysfunction in ATM-deficient lymphoblastoid cells," *Human Molecular Genetics*, vol. 16, no. 18, pp. 2154–2164, 2007.

[4] J. S. Eaton, Z. P. Lin, A. C. Sartorelli, N. D. Bonawitz, and G. S. Shadel, "Ataxia-telangiectasia mutated kinase regulates ribonucleotide reductase and mitochondrial homeostasis," *The Journal of Clinical Investigation*, vol. 117, no. 9, pp. 2723–2734, 2007.

[5] K. H. Chrzanowska, W. J. Kleijer, M. Krajewska-Walasek et al., "Eleven Polish patients with microcephaly, immunodeficiency, and chromosomal instability: the Nijmegen breakage syndrome," *American Journal of Medical Genetics*, vol. 57, no. 3, pp. 462–471, 1995.

[6] S. Mizutani and M. Takagi, "XCIND as a genetic disease of X-irradiation hypersensitivity and cancer susceptibility," *International Journal of Hematology*, vol. 97, no. 1, pp. 37–42, 2013.

[7] S. Squadrone, P. Brizio, C. Mancini et al., "Blood metal levels and related antioxidant enzyme activities in patients with ataxia telangiectasia," *Neurobiology of Disease*, vol. 81, pp. 162–167, 2015.

[8] M. Semlitsch, R. E. Shackelford, S. Zirkl, W. Sattler, and E. Malle, "ATM protects against oxidative stress induced by oxidized low-density lipoprotein," *DNA Repair*, vol. 10, no. 8, pp. 848–860, 2011.

[9] U. Weyemi, C. E. Redon, T. Aziz et al., "NADPH oxidase 4 is a critical mediator in ataxia telangiectasia disease," *Proceedings of the National Academy of Sciences of the United States of America*, vol. 112, no. 7, pp. 2121–2126, 2015.

[10] H. Krenzlin, I. Demuth, B. Salewsky et al., "DNA damage in Nijmegen breakage syndrome cells leads to PARP hyperactivation and increased oxidative stress," *PLoS Genetics*, vol. 8, no. 3, article e1002557, 2012.

[11] Y. A. Valentin-Vega, K. H. MacLean, J. Tait-Mulder et al., "Mitochondrial dysfunction in ataxia-telangiectasia," *Blood*, vol. 119, no. 6, pp. 1490–1500, 2012.

[12] J. Borys, M. Maciejczyk, A. J. Krętowski et al., "The redox balance in erythrocytes, plasma, and periosteum of patients

with titanium fixation of the jaw," *Frontiers in Physiology*, vol. 8, 2017.

[13] J. Karpińska, B. Mikołuć, R. Motkowski, and J. Piotrowska-Jastrzebska, "HPLC method for simultaneous determination of retinol, α-tocopherol and coenzyme Q10 in human plasma," *Journal of Pharmaceutical and Biomedical Analysis*, vol. 42, no. 2, pp. 232–236, 2006.

[14] O. I. Aruoma, "Free radicals, oxidative stress, and antioxidants in human health and disease," *Journal of the American Oil Chemists' Society*, vol. 75, no. 2, pp. 199–212, 1998.

[15] M. Valko, D. Leibfritz, J. Moncol, M. T. D. Cronin, M. Mazur, and J. Telser, "Free radicals and antioxidants in normal physiological functions and human disease," *The International Journal of Biochemistry & Cell Biology*, vol. 39, no. 1, pp. 44–84, 2007.

[16] B. Uttara, A. V. Singh, P. Zamboni, and R. T. Mahajan, "Oxidative stress and neurodegenerative diseases: a review of upstream and downstream antioxidant therapeutic options," *Current Neuropharmacology*, vol. 7, no. 1, pp. 65–74, 2009.

[17] A. Arikanoglu, E. Akil, S. Varol et al., "Relationship of cognitive performance with prolidase and oxidative stress in Alzheimer disease," *Neurological Sciences*, vol. 34, no. 12, pp. 2117–2121, 2013.

[18] A. Kirbas, S. Kirbas, M. C. Cure, and A. Tufekci, "Paraoxonase and arylesterase activity and total oxidative/anti-oxidative status in patients with idiopathic Parkinson's disease," *Journal of Clinical Neuroscience*, vol. 21, no. 3, pp. 451–455, 2014.

[19] M. Y. Sherman and A. L. Goldberg, "Cellular defenses against unfolded proteins: a cell biologist thinks about neurodegenerative diseases," *Neuron*, vol. 29, no. 1, pp. 15–32, 2001.

[20] T. B. Shea, Y. L. Zheng, D. Ortiz, and H. C. Pant, "Cyclin-dependent kinase 5 increases perikaryal neurofilament phosphorylation and inhibits neurofilament axonal transport in response to oxidative stress," *Journal of Neuroscience Research*, vol. 76, no. 6, pp. 795–800, 2004.

[21] A. K. Verma, J. Raj, V. Sharma, T. B. Singh, S. Srivastava, and R. Srivastava, "Plasma Prolidase activity and oxidative stress in patients with Parkinson's disease," *Parkinson's Disease*, vol. 2015, Article ID 598028, 6 pages, 2015.

[22] C. Rice-Evans and N. J. Miller, "Total antioxidant status in plasma and body fluids," *Methods in Enzymology*, vol. 234, pp. 279–293, 1994.

[23] L. Ernster and G. Dallner, "Biochemical, physiological and medical aspects of ubiquinone function," *Biochimica et Biophysica Acta (BBA) - Molecular Basis of Disease*, vol. 1271, no. 1, pp. 195–204, 1995.

[24] H. N. Bhagavan and R. K. Chopra, "Coenzyme Q10: absorption, tissue uptake, metabolism and pharmacokinetics," *Free Radical Research*, vol. 40, no. 5, pp. 445–453, 2006.

[25] S. Farough, A. Karaa, M. A. Walker et al., "Coenzyme Q10 and immunity: a case report and new implications for treatment of recurrent infections in metabolic diseases," *Clinical Immunology*, vol. 155, no. 2, pp. 209–212, 2014.

[26] J. Garrido-Maraver, M. D. Cordero, M. Oropesa-Ávila et al., "Coenzyme Q10 therapy," *Molecular Syndromology*, vol. 5, no. 3-4, pp. 187–197, 2014.

[27] I. P. Hargreaves, "Coenzyme Q10 as a therapy for mitochondrial disease," *The International Journal of Biochemistry & Cell Biology*, vol. 49, pp. 105–111, 2014.

[28] C. Lamperti, M. H. a Naini, D. C. De Vivo et al., "Cerebellar ataxia and coenzyme Q10 deficiency," *Neurology*, vol. 60, no. 7, pp. 1206–1208, 2003.

[29] R. Montero, M. Pineda, A. Aracil et al., "Clinical, biochemical and molecular aspects of cerebellar ataxia and coenzyme Q10 deficiency," *Cerebellum*, vol. 6, no. 2, pp. 118–122, 2007.

[30] J. A. Drisko, "The use of antioxidants in transmissible spongiform encephalopathies: a case report," *Journal of the American College of Nutrition*, vol. 21, no. 1, pp. 22–25, 2002.

[31] D. Q. Pham and R. Plakogiannis, "Vitamin E supplementation in Alzheimer's disease, Parkinson's disease, tardive dyskinesia, and cataract: part 2," *The Annals of Pharmacotherapy*, vol. 39, no. 12, pp. 2065–2072, 2005.

[32] C. Ramassamy, "Emerging role of polyphenolic compounds in the treatment of neurodegenerative diseases: a review of their intracellular targets," *European Journal of Pharmacology*, vol. 545, no. 1, pp. 51–64, 2006.

[33] D. Brambilla, C. Mancuso, M. R. Scuderi et al., "The role of antioxidant supplement in immune system, neoplastic, and neurodegenerative disorders: a point of view for an assessment of the risk/benefit profile," *Nutrition Journal*, vol. 7, no. 1, p. 29, 2008.

[34] S. Jayadev and T. D. Bird, "Hereditary ataxias: overview," *Genetics in Medicine*, vol. 15, no. 9, pp. 673–683, 2013.

[35] S. Rizvi, S. T. Raza, F. Ahmed, A. Ahmad, S. Abbas, and F. Mahdi, "The role of vitamin E in human health and some diseases," *Sultan Qaboos University Medical Journal*, vol. 14, no. 2, pp. 157–165, 2014.

[36] A. Lloret, R. Calzone, C. Dunster et al., "Different patterns of in vivo pro-oxidant states in a set of cancer- or aging-related genetic diseases," *Free Radical Biology & Medicine*, vol. 44, no. 4, pp. 495–503, 2008.

[37] J. Reichenbach, R. Schubert, C. Schwan, K. Müller, H. J. Böhles, and S. Zielen, "Anti-oxidative capacity in patients with ataxia telangiectasia," *Clinical and Experimental Immunology*, vol. 117, no. 3, pp. 535–539, 1999.

[38] R. da Silva, E. C. dos Santos-Valente, F. Burim Scomparini, R. O. Saccardo Sarni, and B. T. Costa-Carvalho, "The relationship between nutritional status, vitamin a and zinc levels and oxidative stress in patients with ataxia-telangiectasia," *Allergologia et Immunopathologia*, vol. 42, no. 4, pp. 329–335, 2014.

Hindawi
Oxidative Medicine and Cellular Longevity
Volume 2017, Article ID 3035184, 13 pages
https://doi.org/10.1155/2017/3035184

Research Article

Insulin-Like Growth Factor (IGF) Binding Protein-2, Independently of IGF-1, Induces GLUT-4 Translocation and Glucose Uptake in 3T3-L1 Adipocytes

Biruhalem Assefa,[1,2] Ayman M. Mahmoud,[1,2,3] Andreas F. H. Pfeiffer,[1,4] Andreas L. Birkenfeld,[5,6] Joachim Spranger,[1,2,7] and Ayman M. Arafat[1,2,4]

[1]*Department of Endocrinology, Diabetes and Nutrition, Charité-University Medicine Berlin, Berlin, Germany*
[2]*Department of Endocrinology, Diabetes and Nutrition at the Center for Cardiovascular Research (CCR), Charité-University Medicine Berlin, Berlin, Germany*
[3]*Division of Physiology, Department of Zoology, Faculty of Science, Beni-Suef University, Beni-Suef, Egypt*
[4]*Department of Clinical Nutrition, German Institute of Human Nutrition Potsdam-Rehbrücke, Nuthetal, Germany*
[5]*Section of Metabolic Vascular Medicine, Medical Clinic III, and Paul Langerhans Institute Dresden (PLID), Dresden University of Technology, Dresden, Germany*
[6]*Division of Diabetes & Nutritional Sciences, Faculty of Life Sciences & Medicine, King's College London, London, UK*
[7]*Department of Endocrinology, Diabetes and Nutrition at the Experimental and Clinical Research Centre (ECRC), Charité-University Medicine Berlin and Max-Delbrück Center Berlin-Buch, Berlin, Germany*

Correspondence should be addressed to Ayman M. Arafat; ayman.arafat@charite.de

Received 13 September 2017; Accepted 23 October 2017; Published 20 December 2017

Academic Editor: Mohamed M. Abdel-Daim

Insulin-like growth factor binding protein-2 (IGFBP-2) is the predominant IGF binding protein produced during adipogenesis and is known to increase the insulin-stimulated glucose uptake (GU) in myotubes. We investigated the IGFBP-2-induced changes in basal and insulin-stimulated GU in adipocytes and the underlying mechanisms. We further determined the role of insulin and IGF-1 receptors in mediating the IGFBP-2 and the impact of IGFBP-2 on the IGF-1-induced GU. Fully differentiated 3T3-L1 adipocytes were treated with IGFBP-2 in the presence and absence of insulin and IGF-1. Insulin, IGF-1, and IGFBP-2 induced a dose-dependent increase in GU. IGFBP-2 increased the insulin-induced GU after long-term incubation. The IGFBP-2-induced impact on GU was neither affected by insulin or IGF-1 receptor blockage nor by insulin receptor knockdown. IGFBP-2 significantly increased the phosphorylation of PI3K, Akt, AMPK, TBC1D1, and PKCζ/λ and induced GLUT-4 translocation. Moreover, inhibition of PI3K and AMPK significantly reduced IGFBP-2-stimulated GU. In conclusion, IGFBP-2 stimulates GU in 3T3-L1 adipocytes through activation of PI3K/Akt, AMPK/TBC1D1, and PI3K/PKCζ/λ/GLUT-4 signaling. The stimulatory effect of IGFBP-2 on GU is independent of its binding to IGF-1 and is possibly not mediated through the insulin or IGF-1 receptor. This study highlights the potential role of IGFBP-2 in glucose metabolism.

1. Introduction

Insulin-like growth factor-1 (IGF-1) bears structural homology with proinsulin [1] and plays a key role in the proliferation and differentiation of adipocytes [2]. *In vitro,* it is known to exert mitogenic effects at nanomolar concentrations [3] and to induce insulin-like metabolic effects in both muscle and adipose tissues [4]. The production and secretion of IGF-1 is affected by age, nutritional status, and other hormones [5]. Because of the ability of insulin to induce hepatic growth hormone (GH) receptor gene expression [6] and protein abundance [7], the GH-induced synthesis and

release of IGF-1 is highly dependent on the hepatic insulin sensitivity. This interplay among GH, insulin, and IGF-1 is of key importance for metabolic and growth regulation [8].

The bioavailability of IGFs is regulated by a family of seven structurally conserved binding proteins (IGFBPs) [9–11]. These IGFBPs bind IGF-1 and IGF-2 but not insulin [12]. The IGF-1 independent role of IGFBPs in growth and metabolism has also been reported at least *in vitro* [13, 14]. IGFBP-2 is the predominant binding protein produced during adipogenesis of white preadipocytes [15]. Both inhibitory and stimulatory effects of IGFBP-2 on the cellular actions of IGF-1 and IGF-2 have been reported [16, 17]. IGFBP-2 is reported to be a key regulator of metabolic diseases, such as diabetes and obesity. Low IGFBP-2 has been shown to be associated with higher fasting glucose levels and reduced insulin sensitivity suggesting it as a biomarker for identification of insulin-resistant individuals [18]. Moreover, IGFBP-2 gene expression was downregulated in visceral white adipose tissue of mice and its circulating levels were reduced in obese ob/ob, db/db, and high fat-fed mice [19]. Low levels of circulating IGFBP-2 have also been reported in obese adults [20] and children [21].

Wheatcroft and colleagues demonstrated that IGFBP-2 overexpression conferring protection against age-associated decline in insulin sensitivity in mice [22]. Moreover, the leptin-induced overexpression of IGFBP-2 has been shown to reverse diabetes in insulin-resistant obese mice and hyperinsulinemic clamp studies showed a threefold improvement in hepatic insulin sensitivity following IGFBP-2 treatment of ob/ob mice [23]. However, only few information exists to date regarding the mechanisms underlying the positive IGFBP-2-induced impact on glucose metabolism. Indeed, IGFBP-2 has been shown to increase the insulin-stimulated glucose uptake in myotubes [24] but nothing is known about its impact on glucose uptake in adipocytes with respect to the insulin or IGF-1-induced effects. We, therefore, aimed to investigate the IGFBP-2-induced changes in both basal and insulin-stimulated glucose uptake in 3T3-L1 adipocytes and the underlying mechanisms. We further investigated the role of insulin and IGF-1 receptors in mediating the IGFBP-2 and even the impact of IGFBP-2 on the IGF-1-induced improvement in glucose uptake.

2. Materials and Methods

2.1. Reagents, Hormones, and Antibodies. IGF-1 and IGF-1 Long R3 (IGF-1 LR3) were purchased from BioVision Inc. (Milpitas, CA, USA). IGFBP-2, Dulbecco's Modified Eagle Medium (DMEM), penicillin/streptomycin, and fetal bovine serum (FBS) were purchased from Biochrom AG (Berlin, Germany). Insulin, dexamethasone, LY294002, and picropodophyllin (PPP) were supplied by Sigma-Aldrich (Darmstadt, Germany). 3-Isobutyl-1-methylxanthine (IBMX), S961, wortmannin, and Compound C were purchased from Biomol GmbH (Hamburg, Germany), Phoenix Biotech (Beijing, China), Merck Chemicals (Darmstadt, Germany), and BIOZOL Diagnostica Vertrieb (Eching, Germany), respectively. RevertAid First Strand cDNA Synthesis Kit, SYBR Green master mix, Bicinchoninic Acid (BCA) protein assay kit, and ECL reagent were supplied by Thermo Fisher Scientific (Dreieich, Germany). DNA primers were purchased from Eurogentec Deutschland GmbH (Köln, Germany). All other chemicals were supplied by Sigma-Aldrich (Darmstadt, Germany).

2.2. Cell Culture. The murine fibroblast cell line 3T3-L1 (ATCC, Manassas, VA, USA) was cultured in DMEM supplemented with 4.5 g/L glucose, 10% fetal bovine serum (FBS), 4 mM glutamine, 50 U/ml penicillin, and 50 μg/ml streptomycin until confluence. The cells were incubated to differentiate into adipocytes following the method of Woody et al. [25] with slight modifications. Briefly, 2 days post-confluence, cells were treated with 0.5 mM IBMX, 1 μM dexamethasone, and 1 μM insulin supplemented DMEM for 2 days. The cells were then maintained in 1 μM insulin-supplemented growth medium for 3 days and in growth medium for 4 days prior to experiments.

2.3. Transfection of Insulin Receptor (INSR) siRNAs. Differentiated 3T3-L1 adipocytes were transfected with control or INSR specific siRNA (validated siRNA from Dharmacon) using Lipofectamine RNAiMAX (Invitrogen) for 72 h. The efficiency of transfection was assessed by using qPCR and Western blot.

2.4. Measurement of Glucose Uptake. Glucose uptake was assayed using the method described by Yamamoto et al. [26]. Briefly, differentiated 3T3-L1 adipocytes were serum starved for 4 h followed by incubation in D-glucose free DMEM for 1 h. The adipocytes were washed with PBS (pH 7.4) and then incubated for 30 min in Krebs-Ringer bicarbonate buffer (KRBP) with different concentrations of insulin, IGF-1, IGF-1 LR3 and/or IGFBP-2. IGF1 LR3 is an analogue of IGF-1 in which the glutamic acid at carbon 3 (Glu3) is replaced by arginine and contains 13 extra amino acids to the N-terminus. It has a very low affinity towards IGFBPs as compared to IGF-1 [27]. The rationale for using IGF1-LR3 was to investigate whether IGFBP-2 is able to impact the IGF-1-induced increase in glucose uptake regardless of its binding to IGF-1 itself. Had IGFBP-2 exerted additive effect on the IGF-1-induced glucose uptake, it would be imperative to scrutinize the observed effect as due to binding or other means. In some experiments, the adipocytes were incubated with 100 nM S961 (INSR blocker) for 2 h, 60 nM PPP (IGF-1 receptor blocker) for 4 h, 100 μM LY294002 (PI3K inhibitor) for 1 h, 200 nM wortmannin (PI3K inhibitor) for 30 min, or 200 μM Compound C (AMPK inhibitor) for 20 min before the treatment. The adipocytes were treated with [^{3}H] 2-Deoxy-D-glucose (0.5 μCi/ml in HEPES) for 10 min at room temperature (RT) and then washed with PBS. Thereafter, the cells were lysed in 50 mM NaOH/1% Triton X-100 for scintillation counting using a liquid scintillation counter (PerkinElmer Wallac GmbH, Freiburg, Germany). Each experiment was performed with three technical replicates and total number of experiments was three.

2.5. Quantitative Reverse Transcriptase-Polymerase Chain Reaction (qRT-PCR) Analysis. Total RNA was isolated from

3T3-L1 adipocytes using TRizol reagent and was treated with DNase I. RNA was quantified at 260 nm using a NanoDrop (Peqlab Biotechnologie, Erlangen, Germany) and samples with A260/A280 ratios < 1.8 were discarded. 1 μg RNA was reverse transcribed into cDNA using RevertAid First Strand cDNA Synthesis Kit (Thermo Fisher Scientific, Dreieich, Germany). cDNA was amplified using SYBR Green master mix (Thermo Fisher Scientific, Dreieich, Germany) with the primers set outlined in Table 1 and with the following conditions: initial denaturation step at 95°C for 10 min, followed by 40 cycles of 15 sec at 95°C, 60 sec at annealing temperature of respective primer, and 60 sec at 72°C for extension. Melting curve analysis was used to assess the quality of PCR products and the cycle threshold (CT) values were analyzed using the $2^{-\Delta\Delta Ct}$ method. Data were normalized to 36B4 and presented as % of control.

2.6. Preparation of a Plasma Membrane Fraction for Glucose Transporter (GLUT)-4 Translocation Assay. The amount of GLUT-4 in the cell membranes was determined using subcellular fractionation [28] followed by Western blotting analysis. Adipocytes were washed 3 times with ice-cold HEPES-EDTA-sucrose (HES) buffer (pH 7.4) containing proteinase inhibitors. The cell suspension was homogenized by passing through 22-gauge needles 10 times on ice. The homogenate was centrifuged at 16000g for 30 min at 4°C, and the pellet was suspended in HES buffer followed by centrifugation at 16000g for 30 min at 4°C. The pellet was resuspended in HES buffer, layered on the top of sucrose cushion (38.5% sucrose, 20 mM HEPES and 1 mM EDTA, pH 7) in 1 : 1 volume ratio, and centrifuged at 100000g for 1 h at 4°C. The plasma membrane fraction (middle layer) was carefully collected and centrifuged at 40000g for 20 min at 4°C. The pellet was used to determine the amount of GLUT-4 using Western blotting.

2.7. Western Blot Analysis. Treated 3T3-L1 adipocytes were lysed in RIPA buffer supplemented with inhibitors for proteinases and phosphatases. For the GLUT-4 translocation experiments, the samples were lysed in a specific buffer (10 mM Tris-HCl [pH 7.2], 150 mM NaCl, 5 mM EDTA, 1% Triton X-100, 1% sodium deoxycholate, and 0.1% SDS) supplemented with proteinase and phosphatase inhibitors. The protein content in the samples was measured by BCA assay kit. Proteins (30–50 μg) were denatured and resolved in 10% SDS/PAGE and transferred to nitrocellulose membranes. For GLUT-4, 8% SDS/PAGE was used. Blots were blocked for 1 h and probed with 1 : 1000 diluted primary antibodies for phosphoinositide 3-kinase (PI3K) p85, phospho-(Tyr) PI3K p85, protein kinase B (Akt), phospho-Akt (Ser473), AMP-activated protein kinase alpha (AMPKα), phospho-AMPKα (Thr172), atypical protein kinase (PKCζ), phospho-PKCζ/λ (Thr410/403), TBC1D1 (tre-2/USP6, BUB2, cdc16 domain family member 1), phospho-TBC1D1 (Ser237), and GAPDH overnight at 4°C and with GLUT-4 antibody and Na^+/K^+-ATPase for 1 h at RT. The blots were washed and incubated with 1 : 2000 diluted corresponding horseradish peroxidase- (HRP-) labeled secondary antibodies. Details of the used antibodies are listed in Table 2. After washing, the membranes were developed with an ECL reagent and visualized and densitometry analysis using Image Lab™ Software (Bio-Rad Laboratories GmbH, Munich, Germany) was used to quantify protein signal.

Table 1: Primers used for qRT-PCR.

Gene	Sequence (5′-3′)
INSR	F: GTACTGGGAGAGGCAAGCAG
	R: ACTGGCCGAGTCGTCATACT
36B4	F: TCATCCAGCAGGTGTTTGACA
	R: GGCACCGAGGCAACAGTT

2.8. Statistical Analysis. Data were analyzed for statistical significance by one-way analysis of variance (ANOVA) with Tukey's post hoc test using GraphPad Prism 5 (La Jolla, CA, USA). The results were presented as means ± standard error of the mean (SEM) with values of $P < 0.05$ were considered significant.

3. Results

3.1. Effect of IGFBP-2 on Basal as well as Insulin and IGF-1-Induced Increase in Glucose Uptake in 3T3-L1 Adipocytes. To study the effect of insulin, IGF-1, IGF-1 LR3, and IGFBP-2 on glucose uptake in 3T3-L1 adipocytes, the cells were incubated with different concentrations of all tested agents for 30 min and [^{3}H] 2-Deoxy-D-glucose uptake was assayed. Insulin and IGF-1 were able to exert statistically significant effects on glucose uptake. As represented in Figure 1(a), different concentrations of insulin (10, 20, 50, and 100 nM) were able to exert a significant ($P < 0.001$) increase in glucose uptake. IGF-1 as well produced a significant increase in glucose uptake at either 10 nM ($P < 0.05$) or higher concentrations ($P < 0.001$) as depicted in Figure 1(b).

Treatment of the cells with the lengthened analogue of IGF-1, IGF-1 LR3, induced significant increase in glucose uptake first at higher concentrations (20, 50, and 100 nM) (Figure 1(c)). Similarly, IGFBP-2 was able to significantly ($P < 0.01$) increase glucose uptake in adipocytes first at a concentration of 100 nM as compared to control cells (Figure 1(d)).

Next, we determined both the short- and long-term impact of IGFBP-2 on insulin, IGF-1, and IGF-1 LR3-induced glucose uptake in adipocytes.

Short-term incubation of the cells with 1 : 1 stoichiometric ratio of IGFBP-2 and either insulin, IGF-1, or IGF-1 LR3 for 30 min resulted in no additive increase in glucose uptake when compared to insulin, IGF-1, or IGF-1 LR3 alone (Figure 1(e)).

Long-term incubation (24 h) of the cells with IGFBP-2 significantly ($P < 0.05$) increased basal glucose uptake and exerted an additive effect ($P < 0.01$) on insulin-stimulated glucose uptake. However, adipocytes treated with IGFBP-2 for 24 h showed nonsignificant changes in either IGF-1 or IGF-1 LR3-induced glucose uptake (Figure 1(f)).

Table 2: List of antibodies used.

Antibody	Species	Supplier	Catalog number
Anti-Phospho-AMPKα (Thr172)	Rabbit	Cell Signaling Technology	2535
Anti-AMPKα	Rabbit	Cell Signaling Technology	2532
Anti-Phospho-Akt (Ser473)	Rabbit	Cell Signaling Technology	9271
Anti-Akt	Rabbit	Cell Signaling Technology	9272
Anti-Phospho-(Tyr) p85 PI3K	Rabbit	Cell Signaling Technology	3821
Anti-PI3K p85	Rabbit	Cell Signaling Technology	4292
Anti-Phospho-TBC1D1 (Ser237)	Rabbit	Millipore	07–2268
Anti-TBC1D1	Rabbit	Cell Signaling Technology	5929
Anti-Phospho-PKCζ/λ (Thr410/403)	Rabbit	Cell Signaling Technology	9378
Anti-PKCζ	Mouse	Santa Cruz Biotechnology	SC-17781
Anti-GLUT-4	Rabbit	Sigma	G4173
Anti-Na^+, K^+-ATPase	Rabbit	Cell Signaling Technology	3010
Anti-GAPDH	Rabbit	Cell Signaling Technology	2118
Goat anti-rabbit IgG HRP-linked	Goat	Cell Signaling Technology	4074
Horse anti-mouse IgG HRP-linked	Horse	Cell Signaling Technology	4076

3.2. The IGFBP-2-Induced Impact on Glucose Uptake Is Not Mediated through the Activation of Insulin or IGF-1 Receptor. To investigate whether the stimulatory effect of IGFBP-2 on glucose uptake is mediated through its binding to insulin or IGF-1 receptors, we incubated 3T3-L1 adipocytes with either insulin receptor blocker (S961) or IGF-1 receptor blocker (PPP).

3T3-L1 adipocytes incubated for 2 h with S961 showed a significant ($P < 0.05$) decrease in basal glucose uptake when compared with the control cells (Figure 2(a)). The insulin receptor blocker S961 significantly reduced insulin ($P < 0.001$), IGF-1 ($P < 0.001$), and IGF-1 LR3 ($P < 0.01$) and stimulated glucose uptake, whereas no impact ($P > 0.05$) of such treatment on IGFBP-2-stimulated glucose uptake was seen.

When compared with S961, the IGF-1 receptor blocker PPP was not able to induce any significant ($P > 0.05$) effect on glucose uptake in adipocytes neither under basal conditions nor following stimulation with IGF-1, IGF-1 LR3, or IGFBP-2 (Figure 2(b)).

In 3T3-L1 adipocytes transfected with control or INSR-specific siRNA (Figures 2(c) and 2(d)), insulin (Figure 2(e)) and IGF-1-stimulated glucose uptake (Figure 2(f)) were significantly ($P < 0.05$) reduced, whereas INSR knockdown potentiated the effect of IGFBP-2 on glucose uptake when compared with the control cells ($P < 0.01$) (Figure 2(g)).

3.3. IGFBP-2 Stimulates Glucose Uptake in a PI3K-Dependent Manner. Adipocytes treated with insulin and IGF-1 for 30 min exhibited significant ($P < 0.001$) increase in PI3K phosphorylation when compared with the control cells. Similarly, IGFBP-2 induced a significant increase in PI3K phosphorylation in 3T3-L1 adipocytes treated for either 30 min ($P < 0.01$) or 24 hr ($P < 0.001$) (Figure 3(a)).

The effect of PI3K inhibitors (LY294002 and wortmannin) on glucose uptake was investigated to further determine the role of PI3K in mediating the IGFBP-2-stimulated glucose uptake in 3T3-L1 adipocytes. Treatment of the adipocytes with either LY294002 (Figure 3(b)) or wortmannin (Figure 3(c)) induced a significant decline in basal as well as insulin-, IGF-1-, and IGFBP-2-stimulated glucose uptake ($P < 0.001$).

3.4. IGFBP-2 Induces Akt and AMPK Phosphorylation and the Subsequent Increase in GLUT-4 Translocation in a PI3K-Dependent Manner. We further investigated the impact of IGFBP-2 on Akt and AMPK phosphorylation as well as on GLUT-4 translocation. As expected, insulin and IGF-1 significantly ($P < 0.001$) upregulated Akt phosphorylation in treated 3T3-L1 adipocytes. Similarly, IGFBP-2 induced a noticeable increase in Akt phosphorylation in 3T3-L1 adipocytes treated for either 30 min ($P < 0.05$) or 24 h ($P < 0.01$) (Figure 4(a)).

IGF-1 significantly ($P < 0.001$) increased, whereas insulin failed to induce ($P > 0.05$) AMPK phosphorylation in 3T3-L1 adipocytes (Figure 4(b)). Similarly, treatment of adipocytes with IGFBP-2 for either 30 min or 24 h induced a significant ($P < 0.001$) increase in AMPK phosphorylation.

To further confirm the involvement of AMPK phosphorylation in IGFBP-2-stimulated glucose uptake, adipocytes were treated with IGFBP-2 with or without previous incubation with the AMPK inhibitor Compound C. Treatment of the 3T3-L1 adipocytes with IGFBP-2 significantly ($P < 0.01$) increased glucose uptake, an effect that was significantly ($P < 0.001$) abolished by Compound C (Figure 3(c)).

Insulin and IGF-1 stimulation increased TBC1D1 phosphorylation significantly ($P < 0.05$) when compared with the control adipocytes (Figure 4(d)). Similarly, treatment of the 3T3-L1 adipocytes with IGFBP-2 for either 30 min or 24 h induced a significant ($P < 0.05$) increase in TBC1D1 phosphorylation (Figure 4(d)).

GLUT-4 translocation was assessed by subcellular fractionation followed by Western blotting. Treatment of

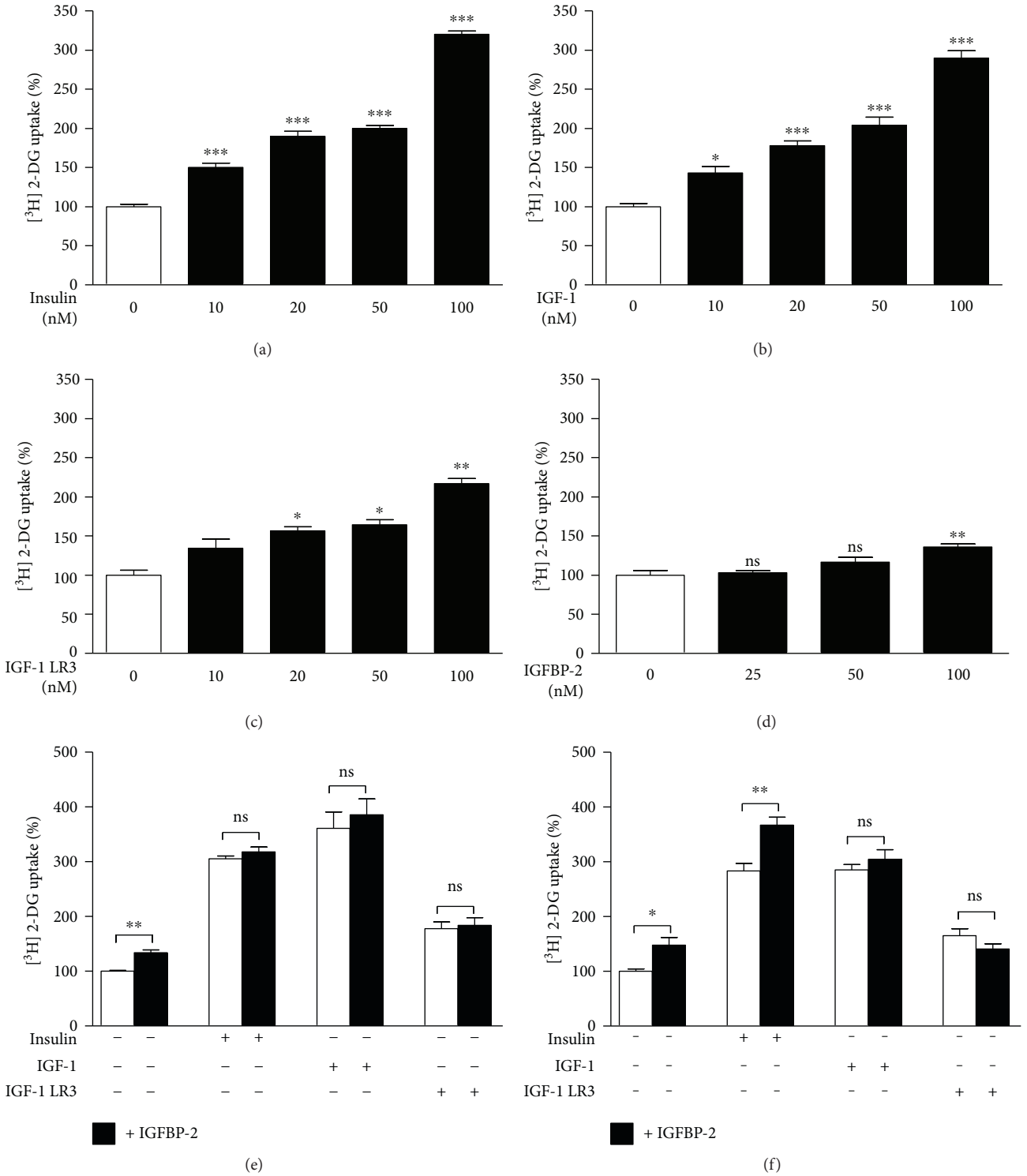

Figure 1: Effects of IGFBP-2 on insulin and IGF-1-stimulated glucose uptake in 3T3-L1 adipocytes. (a–d) Dose-dependent effects of insulin, IGF-1, IGF-1 LR3, and IGFBP-2 on glucose uptake in 3T3-L1 adipocytes. $^{*}P < 0.05$, $^{**}P < 0.01$, and $^{***}P < 0.001$ versus control. (e and f) Effect of IGFBP-2 (100 nM) (black bars) on basal and insulin (20 nM), IGF-1 (20 nM), and IGF-1 LR3 (20 nM)-induced glucose uptake (white bars) after short- and long-term incubations. $^{*}P < 0.05$ and $^{**}P < 0.01$. Each experiment was performed with three technical replicates and total number of experiments was three. The glucose uptake values are percentage of the controls. The results are presented as mean ± SEM.

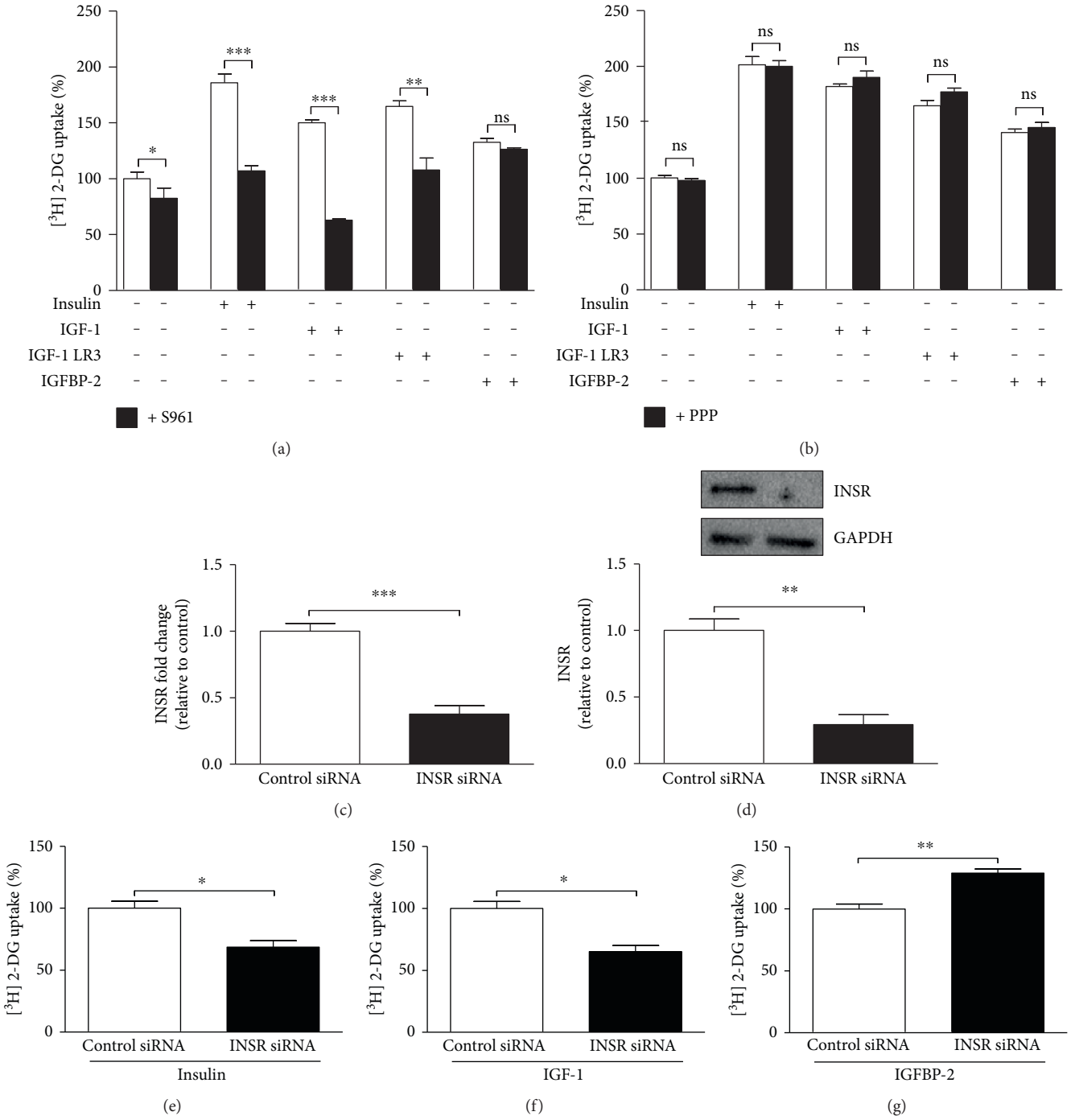

Figure 2: IGFBP-2 stimulates glucose uptake in insulin receptor and IGF-1 receptor-independent mechanism. (a) Effect of the insulin receptor (INSR) blocker S961 (black bars) on basal and insulin, IGF-1, IGF-1 LR3, and IGFBP-2-induced glucose uptake (white bars). (b) Effect of the IGF-1 receptor blocker PPP (black bars) on basal and insulin, IGF-1, IGF-1 LR3, and IGFBP-2 induced glucose uptake (white bars). Differentiated 3T3-L1 adipocytes were incubated with 100 nM S961 for 2 h or 60 nM PPP for 4 h before treatment with insulin, IGF-1, IGF-1 LR3, or IGFBP-2 for 30 min. (c and d) Relative mRNA expression, normalized to 36B4, and Western blot analysis of INSR following siRNA transfection, respectively. (e, f, and g) Effect of 30 min treatment with insulin, IGF-1, and IGFBP-2 on glucose uptake in control siRNA and INSR siRNA transfected 3T3-L1 adipocytes. Each experiment was performed with three technical replicates and total number of experiments was three. The glucose uptake values are percentage of the controls. The results are presented as mean ± SEM. $^{*}P < 0.05$, $^{**}P < 0.01$, and $^{***}P < 0.001$.

the adipocytes with insulin significantly ($P < 0.01$) stimulated GLUT-4 translocation from the cytoplasm to the plasma membrane. IGF-1 was also able to significantly ($P < 0.05$) stimulate GLUT-4 translocation. Similarly, IGFBP-2 induced a significant ($P < 0.05$) increase in GLUT-4 translocation in treated 3T3-L1 adipocytes (Figure 4(e)).

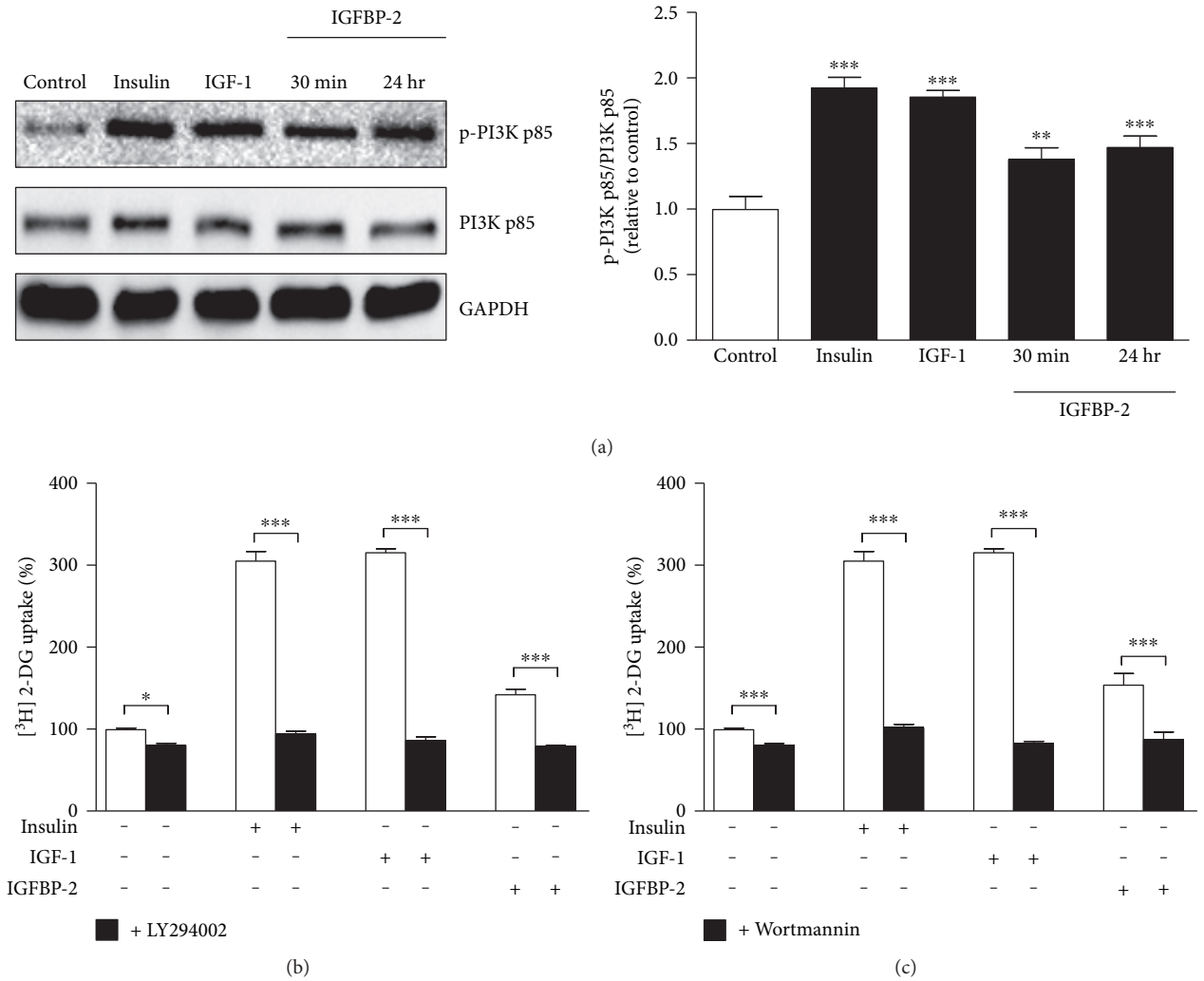

Figure 3: IGFBP-2 stimulates glucose uptake in a PI3K-dependent manner. (a) Insulin, IGF-1, and IGFBP-2 increase the phosphorylation of PI3K. 3T3-L1 cells were cultured and differentiated in 24-well plates for glucose uptake assay and in 6-well plates for Western blotting analysis. The results are presented as mean ± SEM. $^{*}P < 0.05$, $^{**}P < 0.01$, and $^{***}P < 0.001$ versus control. (b and c) The PI3K inhibitors, LY294002 and wortmannin (black bars), significantly reduce basal as well as insulin, IGF-1, and IGFBP-2-induced glucose uptake (white bars). Differentiated 3T3-L1 adipocytes were incubated with 100 μM LY294002 for 1 h or 200 nM wortmannin for 30 min before treatment with insulin, IGF-1, or IGFBP-2 for 30 min. The results are presented as mean ± SEM. $^{***}P < 0.001$. Each experiment was performed with three technical replicates and total number of experiments was three.

3.5. IGFBP-2 Stimulates PKCζ/λ Thr410/403 Phosphorylation in 3T3-L1 Adipocytes. A significant increase in the phosphorylated levels of the PKCζ/λ isoform was seen after stimulation with insulin ($P < 0.05$) or IGF-1 ($P < 0.01$) (Figure 5). Similarly, treatment of the cells with IGFBP-2 induced a significant increase in PKCζ/λ phosphorylation after either 30 min ($P < 0.01$) or 24 h ($P < 0.001$) (Figure 5).

4. Discussion

Previous studies have indicated the role of IGFBP-2 in adipogenesis and lipogenesis, but its effects on basal glucose uptake and the underlying mechanistic pathways have not yet been addressed. We, herein, provide the first evidence for insulin and IGF-1 independent positive impact of IGFBP-2 on glucose uptake in adipocytes. We further show that the effect of IGFBP-2 on glucose uptake is mediated through the activation of PI3K/Akt and AMPK pathways. Finally, we show that the IGF-1 receptor is neither involved in the IGF-1-induced nor in the IGFBP-2-induced increase in glucose uptake.

Insulin and IGF-1 exerted significant dose-dependent effects on glucose uptake in 3T3-L1 adipocytes. These findings are in agreement with the reports from different previous studies [29–33]. Multiple *in vivo* studies reported the role of IGF-1 in enhancing insulin sensitivity and glucose metabolism. A low-serum level of IGF-1 has been associated with insulin resistance, and treatment with recombinant IGF-1 has been shown to improve insulin sensitivity and glucose metabolism [34, 35]. A study by Arafat et al. [36] revealed that long-term treatment of GH-deficient patients with low-dose GH results in improved insulin sensitivity

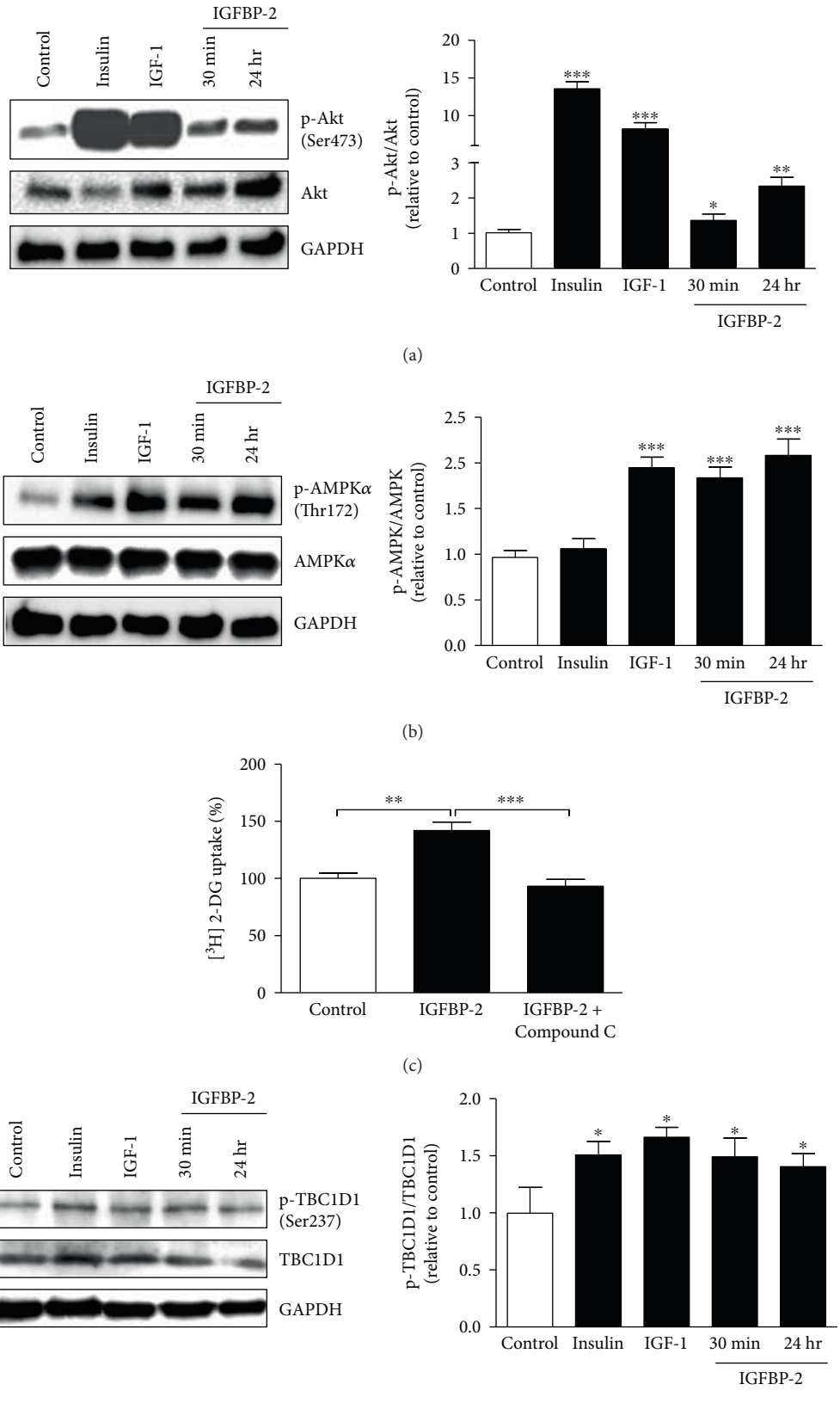

Figure 4: Continued.

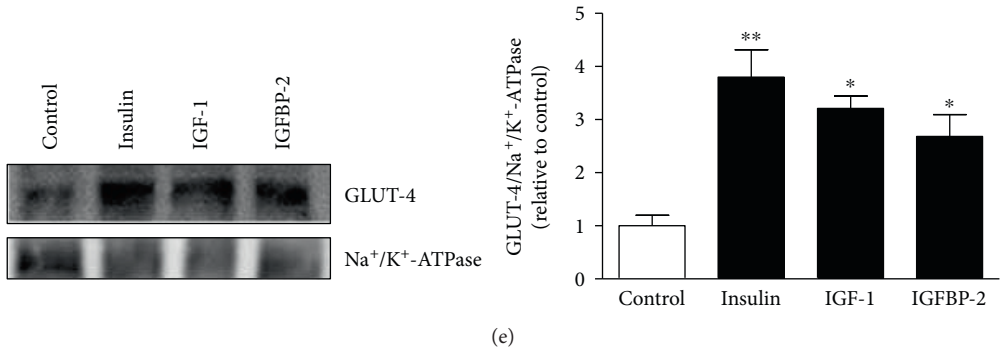

Figure 4: IGFBP-2 stimulates Akt and AMPK activation and thus increased GLUT-4 translocation. (a) Insulin, IGF-1, and IGFBP-2 significantly increase Akt Ser473 phosphorylation. (b) IGF-1 and IGFBP-2 but not insulin increase AMPK Thr172 phosphorylation. $^{*}P < 0.05$, $^{**}P < 0.01$, and $^{***}P < 0.001$ versus control. (c) The AMPK inhibitor, Compound C, abolishes IGFBP-2-induced glucose uptake in 3T3-L1 adipocytes. Differentiated 3T3-L1 adipocytes were incubated with 200 μM Compound C for 20 min before treatment with IGFBP-2 for 30 min. $^{*}P < 0.05$ and $^{***}P < 0.001$. Insulin, IGF-1, and IGFBP-2 significantly increase TBC1D1 Ser237 phosphorylation (d) and GLUT-4 translocation (e). $^{*}P < 0.05$, $^{**}P < 0.01$, and $^{***}P < 0.001$ versus control. Each experiment was performed with three technical replicates and total number of experiments was three. The glucose uptake values are percentage of the controls. The results are presented as mean ± SEM.

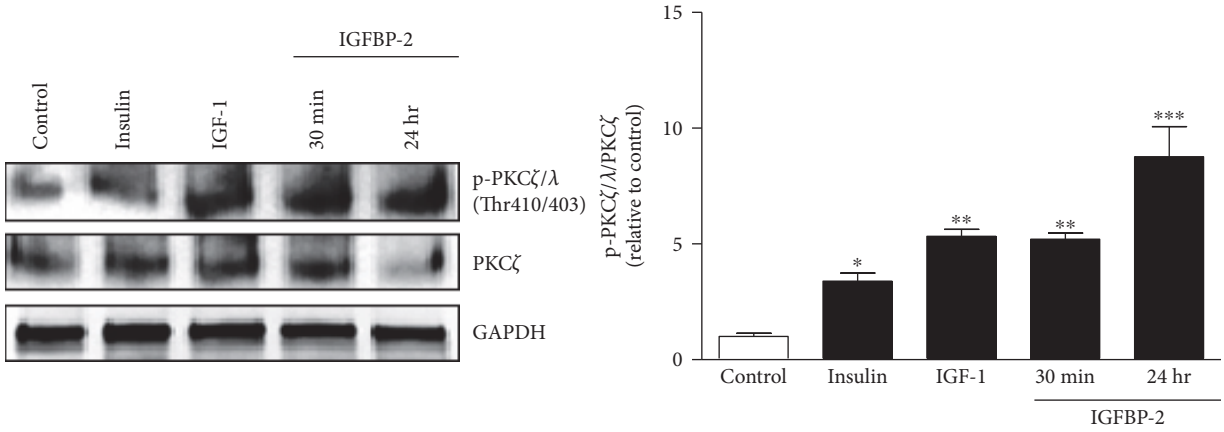

Figure 5: IGFBP-2 stimulates PKCζ/λ Thr410/403 phosphorylation in 3T3-L1 adipocytes. Insulin, IGF-1, and IGFBP-2 increase the phosphorylation of PKCζ/λ. Each experiment was performed with three technical replicates and total number of experiments was three. The results are presented as mean ± SEM. $^{*}P < 0.05$, $^{**}P < 0.01$, and $^{***}P < 0.001$ versus control.

and enhanced glucose metabolism. This improvement in insulin sensitivity is believed to be mediated by IGF-1, which is secreted as a result of GH stimulation. In another clinical study, IGF-1 combined with IGFBP-3 has been shown to improve insulin sensitivity and to reduce complications associated with insulin resistance in HIV/AIDS patients on antiretroviral therapy [37]. Blocking the insulin receptor with S961 or knocking down the INSR using siRNA significantly reduced basal and insulin-stimulated glucose uptake. The mechanisms behind the effect of S961 on basal glucose uptake in 3T3-L1 are not known so far. However, our results were concordant with previously reported impact of S961 on insulin-stimulated glucose uptake in 3T3-L1 adipocytes [38, 39]. Despite the fact that insulin and IGF-1 have different affinities to INSR and IGF-1R, they are able to stimulate both receptors [40]. However, blocking the IGF-1 receptor using PPP [41] in our present study did not affect the impact of IGF-1 on glucose uptake, whereas blocking or even knocking down the INSR did, pointing to the role of INSR in mediating these IGF-1 effects. In the study of Girnita et al. [41], PPP efficiently blocked IGF-1R activity and reduced phosphorylation of Akt and extracellular signal-regulated kinase 1 and 2 (Erk1/2) in cultured IGF-1R-positive tumor cells. In an *in vitro* kinase assay, PPP did not affect the INSR or compete with ATP [41]. Our findings are also supported by various reports that demonstrated a dramatic increase in INSR and a decrease in IGF-1R during the transition from preadipocytes to adipocytes in the 3T3-L1 cell line [42–45].

IGF-1-dependent and independent effects of IGFBPs on metabolism represent a rapidly growing field of research. IGFBP-1 was reported to inhibit IGF-1-stimulated glucose uptake but not insulin-stimulated glucose uptake in 3T3-L1 adipocytes [31]. IGFBP-3 can lead to insulin resistance in 3T3-L1 adipocytes as reported by Chan et al. [46]. There is increasing evidence for the role of IGFBP-2 in regulating normal metabolism [47]. Low-serum levels of IGFBP-2 are

correlated with obesity [22], metabolic syndrome [18], and type 2 diabetes [48], whereas overexpression of IGFBP-2 protects against diabetes and obesity [22, 23]. Roles of IGFBP-2 on metabolism such as inhibition of adipogenesis and lipogenesis [49], enhancing insulin-stimulated glucose uptake in skeletal myotubes [50], and inhibition of preadipocyte differentiation *in vitro* [14] have been reported. However, the effects of IGFBP-2 on basal glucose uptake and the mechanisms underlying its IGF-1-independent role on glucose uptake are not well studied. Here, we reported significantly increased glucose uptake in 3T3-L1 adipocytes treated with 100 nM IGFBP-2. To our knowledge, this is the first report to show the stimulatory effects of IGFBP-2 on basal glucose uptake in adipocytes. In addition, our data showed a nonsignificant effect for short- and long-term treatment with IGFBP-2 on IGF-1 and IGF-1 LR3-stimulated glucose uptake. Adipocytes treated with IGFBP-2 for 24 h followed by 30 min stimulation with IGF-1 showed a trend increase in glucose uptake. Increased basal glucose uptake in control cells incubated with IGFBP-2 for 24 h may explain this increase. However, incubation with IGFBP-2 for 24 h exerted a significant additive effect on the insulin-stimulated glucose uptake which coincides with the study of Yau et al. [50] who reported similar effect for IGFBP-2 in human skeletal muscle cells *in vitro*. It can be postulated that the additive increase in the acute insulin-induced stimulation of glucose uptake after long-term treatment with IGFBP-2 is due to the impact of IGFBP-2 on basal glucose uptake that is likely also mediated through different signaling pathways other than the PI3K/Akt pathway. Moreover, these findings provide a notion that IGFBP-2 binding to IGF-1 does not inhibit IGF-1 from exerting its biological role, at least on glucose uptake *in vitro*.

In addition to its ability to bind and modulate the activity of IGFs, IGFBP-2 can bind to proteoglycans [51] through two heparin-binding domains (HBDs) as well as to integrins through its integrin-binding motif, Gly-Arg-Asp (RGD) [51, 52]. This may explain, at least in part, the IGFR-independent IGFBP-2 activities [49].

Interestingly, neither S961 nor PPP blocked the stimulatory effect of IGFBP-2 on glucose uptake. Moreover, INSR knockdown even increased IGFBP-2-induced increase in glucose uptake. These findings indicate the involvement of other receptors or pathways in IGFBP-2-stimulated glucose uptake in 3T3-L1 adipocytes. This is concordant with the findings of Xi et al. [53], who reported that IGFBP-2 stimulates AMPK via its own receptor.

Signaling via INSR and IGF-1R shares many common signaling pathways at target cells. One of the common pathways in mediating glucose uptake and metabolism is the PI3K pathway [40, 54]. Insulin and IGF-1 are known to stimulate the activity of PI3K by triggering its phosphorylation at specific tyrosine residues by upstream components of the INSR and IGF-1R signaling pathways [55]. In the present study, the PI3K inhibitors, LY294002 and wortmannin, reduced basal and insulin, IGF-1, and even IGFBP-2-stimulated glucose uptake in adipocytes, pointing to the role of PI3K pathway in mediating the IGFBP-2 effect on glucose uptake. We, therefore, investigated the impact of short- and long-term treatment with IGFBP-2 on PI3K phosphorylation in 3T3-L1 adipocytes, using insulin and IGF-1 as controls. As expected, treatment of the adipocytes with either insulin or IGF-1 significantly increased PI3K phosphorylation. Similarly, IGFBP-2 induced marked increase in PI3K phosphorylation after both short- and long-term treatment, confirming the involvement of PI3K activation in mediating IGFBP-2 effects.

Given that IGFBP-2 activates PI3K, we tested its effect on the downstream signaling molecules Akt and AMPK and GLUT-4 translocation. As a result of PI3K activation, insulin and IGF-1 stimulated the phosphorylation of Akt. These findings are in agreement with the studies of Karlsson et al. [56] and Zhang et al. [57]. Moreover, IGF-1 significantly increased AMPK phosphorylation. IGF-1 has been previously shown to stimulate the phosphorylation of AMPK at its alpha subunit [58]. On the other hand, insulin did not affect the level of p-AMPK indicating that insulin mainly uses the PI3K pathway to exert its effects on glucose metabolism. Our findings are in agreement with Shen et al. [59] who clearly showed that insulin does not stimulate AMPK. In the same context, pharmacological activation of AMPK increases glucose uptake in skeletal muscles of subjects with type 2 diabetes [60] by an insulin-independent mechanism [61].

Similarly, IGFBP-2 produced a significant increase in Akt phosphorylation which is attributed to its stimulatory effect on PI3K. Concordant data were reported by Yau et al. [50] in human skeletal muscle cells. The surface proteoglycan receptor-type protein tyrosine phosphatase β (RPTPβ) has been identified as a functionally active cell surface receptor that links IGFBP-2 and the activation of Akt [62]. IGFBP-2 binds RPTPβ through its HBD, resulting in inhibition of RPTPβ phosphatase activity and subsequently phosphatase and tensin homolog (PTEN) suppression [62]. PTEN is known to prevent Akt activation by dephosphorylating phosphatidylinositol-3,4,5-triphosphate (PIP3). The study of Shen et al. [62] showed that IGFBP-2$^{-/-}$ mice had increased RPTPβ activity and impaired Akt activation, changes that were reversed by administration of IGFBP-2.

In addition, both short- and long-term treatment of the adipocytes with IGFBP-2 induced a significant increase in AMPK phosphorylation. IGFBP-2 and IGF-1 have been recently reported by Xi et al. [53] to induce stimulatory effects on AMPK in osteoblasts. Our results were further confirmed through testing the effect of AMPK inhibitor, Compound C, on IGFBP-2-stimulated glucose uptake. Incubation of the adipocytes with Compound C significantly abolished IGFBP-2-induced glucose uptake. Taken together, AMPK activation plays a potential role in mediating IGFBP-2-stimulated glucose uptake in 3T3-L1 adipocytes.

One of the major metabolic changes elicited by AMPK activation is the promotion of glucose uptake [63]. AMPK induces glucose uptake either acutely through GLUT-4 translocation or in the longer term via upregulation of GLUT-4 expression [63]. Here, we show that treatment of the 3T3-L1 adipocytes with IGFBP-2 for 30 min stimulates GLUT-4 translocation to the plasma membrane. This effect is attributed to the ability of IGFBP-2 to activate AMPK. In

addition, we show a significant increase in the phosphorylation of the Rab-GAP protein TBC1D1 by IGFBP-2. Therefore, the mechanism underlying the IGFBP-2 impact on GLUT-4 translocation and the subsequent promotion of glucose uptake involves the phosphorylation of TBC1D1 at least partly through AMPK-pathway activation. This effect is similar to the complementary regulation of TBC1D1 by insulin and AMPK activators [64, 65]. Increased TBC1D1 phosphorylation and GLUT-4 translocation by IGFBP-2 could also be directly mediated by Akt activation. In the skeletal muscle of rodents, Akt phosphorylates TBC1D1 [66] which promotes the hydrolysis of guanosine-5′-triphosphate on GLUT-4-containing vesicles [67].

The atypical protein kinase PKCζ/λ/GLUT-4 is another signaling pathway we thought to have a role in mediating the positive effect of IGFBP-2 on glucose uptake in adipocytes. In our study, insulin, IGF-1, and IGFBP-2 induced a significant increase in PKCζ/λ phosphorylation. Since, PKCζ/λ is dependent on PI3K activation [29, 68], it was expected to be activated in adipocytes treated with insulin, IGF-1, and IGFBP-2 because of their ability to activate PI3K. Following activation, PI3K signaling diverges into Akt-dependent and PKCζ/λ-mediated pathways [69]. PKCζ/λ is known to play little or no role in mediating insulin effects on glucose uptake in 3T3-L1 adipocytes [70], which may explain the IGFBP-2-induced additive increase in the insulin-induced glucose uptake after long-term treatment in our present study. However, further studies using inhibitors or gene silencing are needed to explore the precise involvement of PKCζ/λ in mediating the IGFBP-2-induced increase in glucose uptake and GLUT-4 translocation. One of the limitations of our study was the IGFBP-2 concentrations used to elicit a significant impact on glucose uptake. IGFBP-2 increased glucose uptake at concentrations 7–10-fold higher than those described in humans. Therefore, further *in vivo* studies are needed to explore the precise impact of physiological concentrations of IGFBP-2 on glucose utilization in humans.

In summary, this study shows that IGFBP-2 stimulates glucose uptake in 3T3-L1 adipocytes and that synergistic activation of Akt and AMPK mediates the modulatory effect of IGFBP-2. The PI3K/PKCζ/λ/GLUT-4 signaling is here shown to mediate the IGFBP-2-induced increase in glucose uptake. Furthermore, we showed that IGFBP-2-induced glucose uptake is independent of its binding to IGF-1, INSR, and IGF-1R. Our findings highly strengthen the potential and novel role for IGFBP-2 in glucose metabolism.

Conflicts of Interest

The authors have declared that no competing interests exist.

Authors' Contributions

Ayman M. Arafat conceived the study and acquired funding for the experiment. Biruhalem Assefa and Ayman M. Mahmoud performed the experiments and analyzed the results. Biruhalem Assefa, Ayman M. Mahmoud, and Ayman M. Arafat wrote the manuscript. Andreas F. H. Pfeiffer, Andreas L. Birkenfeld, and Joachim Spranger revised and commented on the manuscript. All authors read and approved the final manuscript.

Acknowledgments

The authors would like to thank Dr. Michael Laue and Lars Möller from the Robert Koch Institute (Berlin) for their technical support during subcellular fractionation procedures. Biruhalem Assefa and Ayman M. Arafat were funded by the graduate school Grant no. 1208/2 from the German Research Foundation (DFG). Ayman M. Mahmoud is funded by a postdoctoral fellowship (ID 1158232) from the Alexander Von Humboldt Foundation.

References

[1] E. Rinderknecht and R. E. Humbel, "The amino acid sequence of human insulin-like growth factor I and its structural homology with proinsulin," *Journal of Biological Chemistry*, vol. 253, no. 8, pp. 2769–2776, 1978.

[2] P. J. Smith, L. S. Wise, R. Berkowitz, C. Wan, and C. S. Rubin, "Insulin-like growth factor-I is an essential regulator of the differentiation of 3T3-L1 adipocytes," *Journal of Biological Chemistry*, vol. 263, no. 19, pp. 9402–9408, 1988.

[3] S. D. O'Dell and I. N. M. Day, "Insulin-like growth factor II (IGF-II)," *International Journal of Biochemistry & Cell Biology*, vol. 30, no. 7, pp. 767–771, 1998.

[4] R. Monzavi and P. Cohen, "IGFs and IGFBPs: role in health and disease," *Best Practice & Research Clinical Endocrinology & Metabolism*, vol. 16, no. 3, pp. 433–447, 2002.

[5] A. Skottner, "Biosynthesis of growth hormone and insulin-like growth factor-I and the regulation of their secretion," *The Open Endocrinology Journal*, vol. 6, no. 1, pp. 3–12, 2012.

[6] S. T. Butler, A. L. Marr, S. H. Pelton, R. P. Radcliff, M. C. Lucy, and W. R. Butler, "Insulin restores GH responsiveness during lactation-induced negative energy balance in dairy cattle: effects on expression of IGF-I and GH receptor 1A," *Journal of Endocrinology*, vol. 176, no. 2, pp. 205–217, 2003.

[7] R. P. Rhoads, J. W. Kim, B. J. Leury et al., "Insulin increases the abundance of the growth hormone receptor in liver and adipose tissue of periparturient dairy cows," *The Journal of Nutrition*, vol. 134, no. 5, pp. 1020–1027, 2004.

[8] D. R. Clemmons, "The relative roles of growth hormone and IGF-1 in controlling insulin sensitivity," *The Journal of Clinical Investigation*, vol. 113, no. 1, pp. 25–27, 2004.

[9] L. A. Bach, S. J. Headey, and R. S. Norton, "IGF-binding proteins – the pieces are falling into place," *Trends in Endocrinology & Metabolism*, vol. 16, no. 5, pp. 228–234, 2005.

[10] M. Kutsukake, R. Ishihara, K. Momose et al., "Circulating IGF-binding protein 7 (IGFBP7) levels are elevated in patients with endometriosis or undergoing diabetic hemodialysis," *Reproductive Biology and Endocrinology*, vol. 6, p. 54, 2008.

[11] D. R. Clemmons, "Role of IGF binding proteins in regulating metabolism," *Trends in Endocrinology & Metabolism*, vol. 27, no. 6, pp. 375–391, 2016.

[12] V. C. Russo, P. D. Gluckman, E. L. Feldman, and G. A. Werther, "The insulin-like growth factor system and its pleiotropic functions in brain," *Endocrine Reviews*, vol. 26, no. 7, pp. 916–943, 2005.

[13] S. Mohan and D. J. Baylink, "IGF-binding proteins are multifunctional and act via IGF-dependent and -independent mechanisms," *Journal of Endocrinology*, vol. 175, no. 1, pp. 19–31, 2002.

[14] S. B. Wheatcroft and M. T. Kearney, "IGF-dependent and IGF-independent actions of IGF-binding protein-1 and -2: implications for metabolic homeostasis," *Trends in Endocrinology & Metabolism*, vol. 20, no. 4, pp. 153–162, 2009.

[15] C. M. Boney, B. M. Moats-Staats, A. D. Stiles, and A. J. D'Ercole, "Expression of insulin-like growth factor-I (IGF-I) and IGF-binding proteins during adipogenesis," *Endocrinology*, vol. 135, no. 5, pp. 1863–1868, 1994.

[16] A. Hoeflich, R. Reisinger, H. Lahm et al., "Insulin-like growth factor-binding protein 2 in tumorigenesis: protector or promoter?," *Cancer Research*, vol. 61, no. 24, pp. 8601–8610, 2001.

[17] T. Fukushima and H. Kataoka, "Roles of insulin-like growth factor binding protein-2 (IGFBP-2) in glioblastoma," *Anticancer Research*, vol. 27, no. 6A, pp. 3685–3692, 2007.

[18] A. H. Heald, K. Kaushal, K. W. Siddals, A. S. Rudenski, S. G. Anderson, and J. M. Gibson, "Insulin-like growth factor binding protein-2 (IGFBP-2) is a marker for the metabolic syndrome," *Experimental and Clinical Endocrinology & Diabetes*, vol. 114, no. 07, pp. 371–376, 2006.

[19] Z. Li and F. Picard, "Modulation of IGFBP2 mRNA expression in white adipose tissue upon aging and obesity," *Hormone and Metabolic Research*, vol. 42, no. 11, pp. 787–791, 2010.

[20] S. Y. Nam, E. J. Lee, K. R. Kim et al., "Effect of obesity on total and free insulin-like growth factor (IGF)-1, and their relationship to IGF-binding protein (BP)-1, IGFBP-2, IGFBP-3, insulin, and growth hormone," *International Journal of Obesity*, vol. 21, no. 5, pp. 355–359, 1997.

[21] M. Claudio, F. Benjamim, B. Riccardo, C. Massimiliano, B. Francesco, and C. Luciano, "Adipocytes IGFBP-2 expression in prepubertal obese children," *Obesity*, vol. 18, no. 10, pp. 2055–2057, 2010.

[22] S. B. Wheatcroft, M. T. Kearney, A. M. Shah et al., "IGF-binding protein-2 protects against the development of obesity and insulin resistance," *Diabetes*, vol. 56, no. 2, pp. 285–294, 2007.

[23] K. Hedbacker, K. Birsoy, R. W. Wysocki et al., "Antidiabetic effects of IGFBP2, a leptin-regulated gene," *Cell Metabolism*, vol. 11, no. 1, pp. 11–22, 2010.

[24] S. W. Yau, V. C. Russo, I. J. Clarke, G. A. Werther, and M. A. Sabin, "IGFBP-2 enhances insulin signalling and glucose uptake in human skeletal myotubes," *Obesity Research & Clinical Practice*, vol. 7, pp. e44–e45, 2013.

[25] S. Woody, R. Stall, J. Ramos, and Y. M. Patel, "Regulation of myosin light chain kinase during insulin-stimulated glucose uptake in 3T3-L1 adipocytes," *PLoS One*, vol. 8, no. 10, article e77248, 2013.

[26] N. Yamamoto, M. Ueda, T. Sato et al., "Measurement of glucose uptake in cultured cells," *Current Protocols in Pharmacology*, vol. 12, pp. 12.14 11–12.14.22, 2011.

[27] L. G. Laajoki, G. L. Francis, J. C. Wallace, J. A. Carver, and M. A. Keniry, "Solution structure and backbone dynamics of long-[Arg^3]insulin-like growth factor-I," *Journal of Biological Chemistry*, vol. 275, no. 14, pp. 10009–10015, 2000.

[28] T. Ramlal, V. Sarabia, P. J. Bilan, and A. Klip, "Insulin-mediated translocation of glucose transporters from intracellular membranes to plasma membranes: sole mechanism of stimulation of glucose transport in L6 muscle cells," *Biochemical and Biophysical Research Communications*, vol. 157, no. 3, pp. 1329–1335, 1988.

[29] K. Kotani, W. Ogawa, M. Matsumoto et al., "Requirement of atypical protein kinase Cλ for insulin stimulation of glucose uptake but not for Akt activation in 3T3-L1 adipocytes," *Molecular and Cellular Biology*, vol. 18, no. 12, pp. 6971–6982, 1998.

[30] K. M. Rice and C. W. Garner, "IGF-I regulates IRS-1 expression in 3T3-L1 adipocytes," *Biochemical and Biophysical Research Communications*, vol. 255, no. 3, pp. 614–617, 1999.

[31] K. W. Siddals, M. Westwood, J. M. Gibson, and A. White, "IGF-binding protein-1 inhibits IGF effects on adipocyte function: implications for insulin-like actions at the adipocyte," *Journal of Endocrinology*, vol. 174, no. 2, pp. 289–297, 2002.

[32] M. Takahashi, Y. Takahashi, K. Takahashi et al., "Chemerin enhances insulin signaling and potentiates insulin-stimulated glucose uptake in 3T3-L1 adipocytes," *FEBS Letters*, vol. 582, no. 5, pp. 573–578, 2008.

[33] M. Berenguer, J. Zhang, M. C. Bruce et al., "Dimethyl sulfoxide enhances GLUT4 translocation through a reduction in GLUT4 endocytosis in insulin-stimulated 3T3-L1 adipocytes," *Biochimie*, vol. 93, no. 4, pp. 697–709, 2011.

[34] K. C. Yuen and D. B. Dunger, "Impact of treatment with recombinant human GH and IGF-I on visceral adipose tissue and glucose homeostasis in adults," *Growth Hormone & IGF Research*, vol. 16, Supplement A, pp. S55–S61, 2006.

[35] K. C. Yuen and D. B. Dunger, "Therapeutic aspects of growth hormone and insulin-like growth factor-I treatment on visceral fat and insulin sensitivity in adults," *Diabetes, Obesity and Metabolism*, vol. 9, no. 1, pp. 11–22, 2007.

[36] A. M. Arafat, M. Möhlig, M. O. Weickert, C. Schöfl, J. Spranger, and A. F. Pfeiffer, "Improved insulin sensitivity, preserved beta cell function and improved whole-body glucose metabolism after low-dose growth hormone replacement therapy in adults with severe growth hormone deficiency: a pilot study," *Diabetologia*, vol. 53, no. 7, pp. 1304–1313, 2010.

[37] M. N. Rao, K. Mulligan, V. Tai et al., "Effects of insulin-like growth factor (IGF)-I/IGF-binding protein-3 treatment on glucose metabolism and fat distribution in human immunodeficiency virus-infected patients with abdominal obesity and insulin resistance," *The Journal of Clinical Endocrinology & Metabolism*, vol. 95, no. 9, pp. 4361–4366, 2010.

[38] L. Schäffer, C. L. Brand, B. F. Hansen et al., "A novel high-affinity peptide antagonist to the insulin receptor," *Biochemical and Biophysical Research Communications*, vol. 376, no. 2, pp. 380–383, 2008.

[39] L. Knudsen, B. F. Hansen, P. Jensen et al., "Agonism and antagonism at the insulin receptor," *PLoS One*, vol. 7, no. 12, article e51972, 2012.

[40] K. Siddle, "Molecular basis of signaling specificity of insulin and IGF receptors: neglected corners and recent advances," *Frontiers in Endocrinology*, vol. 3, p. 34, 2012.

[41] A. Girnita, L. Girnita, F. del Prete, A. Bartolazzi, O. Larsson, and M. Axelson, "Cyclolignans as inhibitors of the insulin-like growth factor-1 receptor and malignant cell growth," *Cancer Research*, vol. 64, no. 1, pp. 236–242, 2004.

[42] B. C. Reed, S. H. Kaufmann, J. C. Mackall, A. K. Student, and M. D. Lane, "Alterations in insulin binding accompanying differentiation of 3T3-L1 preadipocytes," *Proceedings of the National Academy of Sciences of the United States of America*, vol. 74, no. 11, pp. 4876–4880, 1977.

[43] C. M. Boney, R. M. Smith, and P. A. Gruppuso, "Modulation of insulin-like growth factor I mitogenic signaling in 3T3-L1 preadipocyte differentiation," *Endocrinology*, vol. 139, no. 4, pp. 1638–1644, 1998.

[44] S. Hong, H. Huo, J. Xu, and K. Liao, "Insulin-like growth factor-1 receptor signaling in 3T3-L1 adipocyte differentiation requires lipid rafts but not caveolae," *Cell Death and Differentiation*, vol. 11, no. 7, pp. 714–723, 2004.

[45] J. Boucher, Y. H. Tseng, and C. R. Kahn, "Insulin and insulin-like growth factor-1 receptors act as ligand-specific amplitude modulators of a common pathway regulating gene transcription," *Journal of Biological Chemistry*, vol. 285, no. 22, pp. 17235–17245, 2010.

[46] S. S. Chan, S. M. Twigg, S. M. Firth, and R. C. Baxter, "Insulin-like growth factor binding protein-3 leads to insulin resistance in adipocytes," *The Journal of Clinical Endocrinology & Metabolism*, vol. 90, no. 12, pp. 6588–6595, 2005.

[47] M. A. Sabin, V. C. Russo, W. J. Azar, S. W. Yau, W. Kiess, and G. A. Werther, "IGFBP-2 at the interface of growth and metabolism–implications for childhood obesity," *Pediatric Endocrinology Reviews*, vol. 8, no. 4, pp. 382–393, 2011.

[48] J. Frystyk, C. Skjaerbaek, E. Vestbo, S. Fisker, and H. Orskov, "Circulating levels of free insulin-like growth factors in obese subjects: the impact of type 2 diabetes," *Diabetes/Metabolism Research and Reviews*, vol. 15, no. 5, pp. 314–322, 1999.

[49] S. W. Yau, V. C. Russo, I. J. Clarke, F. R. Dunshea, G. A. Werther, and M. A. Sabin, "IGFBP-2 inhibits adipogenesis and lipogenesis in human visceral, but not subcutaneous, adipocytes," *International Journal of Obesity*, vol. 39, no. 5, pp. 770–781, 2015.

[50] S. W. Yau, V. C. Russo, G. A. Werther, and M. A. Sabin, "IGFBP-2 enhances insulin signalling pathways in human skeletal muscle by cell surface binding – an IGF-independent process?," in *Endocrine Society's 96th Annual Meeting and Expo*, Endocrine Society, Chicago, IL, USA, 2014, SAT-1072.

[51] V. C. Russo, B. S. Schütt, E. Andaloro et al., "Insulin-like growth factor binding protein-2 binding to extracellular matrix plays a critical role in neuroblastoma cell proliferation, migration, and invasion," *Endocrinology*, vol. 146, no. 10, pp. 4445–4455, 2005.

[52] B. S. Schutt, M. Langkamp, U. Rauschnabel, M. B. Ranke, and M. W. Elmlinger, "Integrin-mediated action of insulin-like growth factor binding protein-2 in tumor cells," *Journal of Molecular Endocrinology*, vol. 32, no. 3, pp. 859–868, 2004.

[53] G. Xi, C. J. Rosen, and D. R. Clemmons, "IGF-I and IGFBP-2 stimulate AMPK activation and autophagy, which are required for osteoblast differentiation," *Endocrinology*, vol. 157, no. 1, pp. 268–281, 2016.

[54] K. Siddle, "Signalling by insulin and IGF receptors: supporting acts and new players," *Journal of Molecular Endocrinology*, vol. 47, no. 1, pp. R1–R10, 2011.

[55] J. Dupont and D. LeRoith, "Insulin and insulin-like growth factor I receptors: similarities and differences in signal transduction," *Hormone Research in Pædiatrics*, vol. 55, Supplement 2, pp. 22–26, 2001.

[56] H. K. Karlsson, J. R. Zierath, S. Kane, A. Krook, G. E. Lienhard, and H. Wallberg-Henriksson, "Insulin-stimulated phosphorylation of the Akt substrate AS160 is impaired in skeletal muscle of type 2 diabetic subjects," *Diabetes*, vol. 54, no. 6, pp. 1692–1697, 2005.

[57] Y. Zhang, Y. Liu, X. Li et al., "Effects of insulin and IGF-I on growth hormone- induced STAT5 activation in 3T3-F442A adipocytes," *Lipids in Health and Disease*, vol. 12, p. 56, 2013.

[58] A. Suzuki, G. Kusakai, A. Kishimoto et al., "IGF-1 phosphorylates AMPK-α subunit in ATM-dependent and LKB1-independent manner," *Biochemical and Biophysical Research Communications*, vol. 324, no. 3, pp. 986–992, 2004.

[59] Y. Shen, N. Honma, K. Kobayashi et al., "Cinnamon extract enhances glucose uptake in 3T3-L1 adipocytes and C2C12 myocytes by inducing LKB1-AMP-activated protein kinase signaling," *PLoS One*, vol. 9, no. 2, article e87894, 2014.

[60] H. A. Koistinen, D. Galuska, A. V. Chibalin et al., "5-amino-imidazole carboxamide riboside increases glucose transport and cell-surface GLUT4 content in skeletal muscle from subjects with type 2 diabetes," *Diabetes*, vol. 52, no. 5, pp. 1066–1072, 2003.

[61] T. Hayashi, M. F. Hirshman, E. J. Kurth, W. W. Winder, and L. J. Goodyear, "Evidence for 5′ AMP-activated protein kinase mediation of the effect of muscle contraction on glucose transport," *Diabetes*, vol. 47, no. 8, pp. 1369–1373, 1998.

[62] X. Shen, G. Xi, L. A. Maile, C. Wai, C. J. Rosen, and D. R. Clemmons, "Insulin-like growth factor (IGF) binding protein 2 functions coordinately with receptor protein tyrosine phosphatase β and the IGF-I receptor to regulate IGF-I-stimulated signaling," *Molecular and Cellular Biology*, vol. 32, no. 20, pp. 4116–4130, 2012.

[63] S. L. McGee, B. J. van Denderen, K. F. Howlett et al., "AMP-activated protein kinase regulates GLUT4 transcription by phosphorylating histone deacetylase 5," *Diabetes*, vol. 57, no. 4, pp. 860–867, 2008.

[64] S. Chen, J. Murphy, R. Toth, D. G. Campbell, N. A. Morrice, and C. Mackintosh, "Complementary regulation of TBC1D1 and AS160 by growth factors, insulin and AMPK activators," *Biochemical Journal*, vol. 409, no. 2, pp. 449–459, 2008.

[65] C. Pehmoller, J. T. Treebak, J. B. Birk et al., "Genetic disruption of AMPK signaling abolishes both contraction- and insulin-stimulated TBC1D1 phosphorylation and 14-3-3 binding in mouse skeletal muscle," *American Journal of Physiology - Endocrinology and Metabolism*, vol. 297, no. 3, pp. E665–E675, 2009.

[66] E. B. Taylor, D. An, H. F. Kramer et al., "Discovery of TBC1D1 as an insulin-, AICAR-, and contraction-stimulated signaling nexus in mouse skeletal muscle," *Journal of Biological Chemistry*, vol. 283, no. 15, pp. 9787–9796, 2008.

[67] H. Sano, S. Kane, E. Sano et al., "Insulin-stimulated phosphorylation of a Rab GTPase-activating protein regulates GLUT4 translocation," *Journal of Biological Chemistry*, vol. 278, no. 17, pp. 14599–14602, 2003.

[68] M. Ishiki and A. Klip, "Minireview: recent developments in the regulation of glucose transporter-4 traffic: new signals, locations, and partners," *Endocrinology*, vol. 146, no. 12, pp. 5071–5078, 2005.

[69] G. Bandyopadhyay, M. L. Standaert, M. P. Sajan et al., "Dependence of insulin-stimulated glucose transporter 4 translocation on 3-phosphoinositide-dependent protein kinase-1 and its target threonine-410 in the activation loop of protein kinase C-ζ," *Molecular Endocrinology*, vol. 13, no. 10, pp. 1766–1772, 1999.

[70] M. Tsuru, H. Katagiri, T. Asano et al., "Role of PKC isoforms in glucose transport in 3T3-L1 adipocytes: insignificance of atypical PKC," *American Journal of Physiology - Endocrinology and Metabolism*, vol. 283, no. 2, pp. E338–E345, 2002.

Hindawi
Oxidative Medicine and Cellular Longevity
Volume 2017, Article ID 8235069, 11 pages
https://doi.org/10.1155/2017/8235069

Research Article

Modulatory Effect of Fermented Papaya Extracts on Mammary Gland Hyperplasia Induced by Estrogen and Progestin in Female Rats

Zhenqiang You,[1] Junying Sun,[2] Feng Xie,[1] Zhiqin Chen,[1] Sheng Zhang,[1] Hao Chen,[1] Fang Liu,[1] Lili Li,[3] Guocan Chen,[1] Yisheng Song,[1] Yaoxian Xuan,[1] Gaoli Zheng,[1] and Yanfei Xin[1]

[1]*State Key Laboratory of Safety Evaluation for New Drugs, Zhejiang Academy of Medical Sciences, Hangzhou, Zhejiang, China*
[2]*Institute of Animal Health, Guangdong Academy of Agricultural Sciences, Guangzhou, Guangdong, China*
[3]*Collaborative Innovation Center of Yangtze River Delta Region Green Pharmaceuticals, Zhejiang University of Technology, Hangzhou, Zhejiang, China*

Correspondence should be addressed to Yanfei Xin; xinyanfei@gmail.com

Received 21 June 2017; Revised 24 August 2017; Accepted 25 September 2017; Published 20 November 2017

Academic Editor: Nadia I. Zakhary

Fermented papaya extracts (FPEs) are obtained by fermentation of papaya by *Aspergillus oryzae* and yeasts. In this study, we investigated the protective effects of FPEs on mammary gland hyperplasia induced by estrogen and progestogen. Rats were randomly divided into 6 groups, including a control group, an FPE-alone group, a model group, and three FPE treatment groups (each receiving 30, 15, or 5 ml/kg FPEs). Severe mammary gland hyperplasia was induced upon estradiol benzoate and progestin administration. FPEs could improve the pathological features of the animal model and reduce estrogen levels in the serum. Analysis of oxidant indices revealed that FPEs could increase superoxide dismutase (SOD) and glutathione peroxidase (GSH-Px) activities, decrease malondialdehyde (MDA) level in the mammary glands and serum of the animal models, and decrease the proportion of cells positive for the oxidative DNA damage marker 8-oxo-dG in the mammary glands. Additionally, estradiol benzoate and progestin altered the levels of serum biochemical compounds such as aspartate transaminase (AST), total bilirubin (TBIL), and alanine transaminase (ALT), as well as hepatic oxidant indices such as SOD, GSH-Px, MDA, and 8-oxo-2′-deoxyguanosine (8-oxo-dG). These indices reverted to normal levels upon oral administration of a high dose of FPEs. Taken together, our results indicate that FPEs can protect the mammary glands and other visceral organs from oxidative damage.

1. Introduction

Fermented fruit and vegetable juices are popular functional foods in China. They contain large amounts of probiotics, amino acids, carbohydrates, and functional enzymes, which can be easily digested. In addition, fermented fruit and vegetable juice exhibits antioxidant, antitumor, antidiabetic, and anti-inflammatory activities [1, 2]. Papaya is used in traditional medicine because of its antioxidant, antitumor, and immune regulatory effects [3–6]; these effects could be due to the high content of α-tocopherol, flavonoid, benzyl isothiocyanate, lycopene, and papain in papaya [7–10]. Fermented papaya is used in medical treatment and has been developed as a commercial functional food in Japan, United States, and several European countries [11]. Studies have shown that fermented papaya products (FPP) protect hemocytes from oxidative damage, prevent complications of aging, and cure Alzheimer's disease (AD) [12–14]. Due to its antioxidant activity, FPP exhibits potential for tumor treatment, immune regulation, and wound healing in diabetics [4, 6, 15]. Fermented papaya extracts (FPEs) are the fermentation liquor extracted from papaya through long-term fermentation by *Aspergillus* and yeast; they are commercially available in the form of tablets and powder. Clinically, FPEs are applied

as functional food to regulate endocrine disorders and antioxidant activity, as well as to improve immune and anti-inflammatory responses.

Mammary gland hyperplasia is a common noninflammatory and nontumor disease that occurs in women of child-bearing age. This condition accounts for 75% of all breast diseases [16, 17]. Women suffering from mammary gland hyperplasia exhibits two to three times higher risk of breast cancer than the general population. The risk is five to eight times higher among patients with atypical hyperplasia [18, 19]. The occurrence of mammary gland hyperplasia is directly related to endocrine disorders, which are mainly caused by imbalance of estrogen and progestin [20]. Hyperplasia of mammary epithelial cells can also be induced by cholesterol and its oxidative product cholesterol epoxide [21, 22]. In the present study, animal models of mammary gland hyperplasia were established using estradiol benzoate and progestin based on the underlying mechanism of mammary gland hyperplasia. Using these models, the protective effect, functions, and mechanism of FPEs in estrogen-induced mammary gland hyperplasia were investigated.

2. Materials and Methods

2.1. FPEs and Drugs. Immature papaya (half a month from maturity) were peeled and cut into 2 mm slices after removing the seeds. The prepared papaya was fermented for 3 months through *Aspergillus oryzae* (isolated from millet catsup and stored at our laboratory), and then fermented for 3 months using yeasts (*Saccharomyces cerevisiae*, provided by Desheng Biotechnology Co. Ltd., Zhejiang, China) with 5% glucose at 24–28°C. The FPEs were obtained by squeezing and filtering after fermentation. Total flavonoids, one of the important functional constituents in FPEs, were nearly 11.65 mg/ml detected by UV method. Estradiol (2 mg/ml) and progestin (10 mg/ml) were purchased from Hangzhou Animal Pharmaceutical Factory, China.

2.2. Animals and Treatments. Thirty-six female SPF Sprague-Dawley (SD) rats (180–200 g, 7-8 weeks old, and at sexual maturity) were purchased from the Shanghai Slack Laboratory Animal Co. Ltd. All animals were groomed in the barrier system with a clean environment at 20°C–25°C under 50–60% humidity and with a 12 h light and 12 h dark cycle. Animal experiments were conducted in laboratories that passed the AAALAC (Association for Assessment and Accreditation of Laboratory Animal Care International) authentication. The rats were randomly divided into six groups, with each group containing six rats.

Group 1, the blank control group, received daily intramuscular injection of 0.5 ml/kg saline and were orally administered 30 ml distilled water/kg weight. Group 2, the FPE control group, was orally administered 30 ml of FPEs/kg weight at the beginning of the experiment. Group 3, the model group, received intramuscular injection of 0.5 mg (0.5 ml)/kg estradiol benzoate from day 1 to day 25 and 4 mg (0.5 ml)/kg progestin from day 26 to day 30. As treatment groups, group 4, group 5, and group 6 received estradiol benzoate and progestin the same as the model group and were orally treated with FPEs from day 1 to day 30. Group 4, treatment group I, was administered an oral dose of 30 ml of FPEs/kg. Group 5, treatment group II, was administered an oral dose of 15 ml of FPEs plus 15 ml of distilled water/kg. Group 6, treatment group III, was administered an oral dose of 5 ml of FPEs plus 25 ml of distilled water/kg.

2.3. Nipple Measurement. On the 31st day, the third nipple on the right side of the rats in each group was shaved. The diameter and height of the shaved nipple were measured using a Vernier caliper.

2.4. Sample Collection. On the 31st day, all experimental rats were anesthetized with 2.5% pentobarbital solution and killed humanely. Blood and tissue samples were collected from the mammary glands, heart, liver, spleen, lung, kidney, ovary, and uterus. To avoid interference from blood cells, the blood in the liver was cleared by injecting saline through the portal vein. Once blood clotted at room temperature, the serum was separated within 10 min by centrifugation at 3000 ×g. A portion of the serum was immediately used for biochemical detection, and the remainder was stored at −70°C for analysis of hormones and oxidant indices. Half of the collected tissue samples were stored in 10% formaldehyde for pathological and immunohistochemical (IHC) tests, and the remaining half was stored at −70°C for testing oxidant indices and 8-oxo-2′-deoxyguanosine (8-oxo-dG).

2.5. Sex Hormone Concentrations. The concentration of each sex hormone in the serum was tested as per standard specifications using estradiol (E2), progesterone (P), luteinizing hormone (LH), and follicle-stimulating hormone (FSH) detection kits (Beijing Kemei Biological Technology Co. Ltd.).

2.6. Oxidative Index Detection. Malondialdehyde (MDA) level, superoxide dismutase (SOD), and glutathione peroxidase (GSH-Px) activities in the serum, mammary glands, and livers were detected using commercially available detection kits following the manufacturer's instructions (Sigma-Aldrich).

2.7. Blood Biochemistry. Serum biochemical parameters including aspartate transaminase (AST), alanine transaminase (ALT), total bilirubin (TBIL), alkaline phosphatase (ALP), creatine kinase (CK), blood urea nitrogen (BUN), creatinine (Crea), total protein (TP), albumin (ALB), glucose (GLU), total cholesterol (T-CHO), triglyceride (TG), potassium (K^+), serum sodium (Na^+), chloride (Cl^-), and total calcium (TCa) were analyzed using a Hitachi 7020 automatic biochemical analyzer.

2.8. Detection of 8-Oxo-2′-deoxyguanosine (8-oxo-dG) through Enzyme-Linked Immunosorbent Assay (ELISA) and IHC. The biomarker 8-oxo-dG was detected in the mammary glands and liver tissues through ELISA and IHC analyses. For ELISA, 50 mg of the tissues was collected. Total DNA was extracted using a genome extraction kit (Sigma-Aldrich) and quantified by colorimetric method. Approximately 300 ng of DNA was extracted from each sample. The content of 8-oxo-dG in the total DNA was determined using the EpiQuik™ 8-OHdG

Table 1: Effect of FPEs on the nipple and sex hormones in rats.

Groups	Nipple (mm)		Sex hormones			
	Height	Diameter	E2 (pg/ml)	P (pg/ml)	LH (pg/ml)	FSH (pg/ml)
Control	1.22 ± 0.14^{b}	1.27 ± 0.10^{b}	33.56 ± 12.43^{b}	70.44 ± 13.34^{b}	4.63 ± 0.69^{b}	5.17 ± 0.83^{b}
SPE control	1.27 ± 0.11^{b}	1.29 ± 0.14^{b}	38.24 ± 8.31^{b}	79.25 ± 16.08^{b}	5.27 ± 1.08^{b}	4.63 ± 1.32^{b}
EB + PR	1.86 ± 0.17^{a}	1.78 ± 0.12^{a}	166.55 ± 46.51^{a}	151.22 ± 26.25^{a}	9.16 ± 2.71^{a}	18.46 ± 3.15^{a}
EB + PR+ 30 ml SPE/kg	1.45 ± 0.23^{b}	1.41 ± 0.21^{b}	$62.55 \pm 42.63^{a,b}$	$125.53 \pm 19.23^{a,b}$	5.77 ± 1.54^{b}	8.64 ± 3.24^{b}
EB + PR+ 15 ml SPE/kg	1.64 ± 0.24^{a}	1.46 ± 0.18^{ab}	98.24 ± 31.31^{ab}	142.65 ± 7.19^{a}	7.15 ± 2.26^{ab}	10.52 ± 2.54^{ab}
EB + PR+ 5 ml SPE/kg	1.76 ± 0.09^{a}	1.72 ± 0.16^{a}	135.62 ± 36.89^{ab}	138.97 ± 16.52^{a}	8.23 ± 1.84^{a}	16.63 ± 2.11^{ab}

SPE: fermented papaya extract; EB: estradiol benzoate; PR: progestin; E2: estradiol; P: progesterone; LH: luteinizing hormone; FSH: follicle-stimulating hormone. Statistical differences are within the individuals at the same column. $^{a}p < 0.05$ compared with control group; $^{b}p < 0.05$ compared with EB + PR group.

DNA Damage Quantification Direct Kit (Colorimetric) (EpiGentek). The results are presented as the ratio of 8-oxo-dG-positive cells.

For IHC, mammary glands were fixed in 10% formaldehyde for at least 24 h and sliced into 4 μm sections after embedding in wax. After dewaxing, hydration, antigen retrieval, DNA hybridization, and sealing treatment, the slices were incubated overnight in anti-8-oxo-dG monoclonal antibody (1 : 250, Trevigen) at 4°C. Next, the slices were incubated in DyLight 594-labled goat anti-mouse IgG (1 : 250, Jackson) for 30 min. After washing, the slices were evaluated using a fluorescence microscope.

2.9. Pathological Mechanism Detection. Each major visceral organ was fixed in 10% formaldehyde for at least 24 h, sliced into 4 μm sections after embedding with wax, and dyed with standard HE dyeing procedures. The pathological state of each visceral organ was observed by optical microscopy. Signs of pathological damage, such as lobule increase, acinar increase, mammary duct and lumen ectasia, and mammary duct and lumen secretion, were analyzed.

2.10. Statistical Analysis. Results are reported as mean ± SEM (standard error of mean) and were analyzed using SPSS 22.0. One-way ANOVA was conducted to compare data among more than two groups. $p < 0.05$ was considered statistically significant.

3. Results

3.1. Protective Effect of FPEs on Serum Sex Hormone Index of Rats. The regulatory effect of FPEs on sex hormone concentration in the model rats was determined by detecting serum E2, P, LH, and FSH levels. After administering the model rats with estradiol benzoate and progestin, the serum levels of these hormones increased (compared with those in the control group, $p < 0.05$). After treatment with FPEs, the levels of E2 and FSH were found to be evidently decreased (compared with those in the model group, $p < 0.05$) and dose-dependent. In addition, the level of P was significantly decreased in the larger-dose (30 ml of FPEs/kg) group, and the level of LH was obviously reduced both in the larger-dose group and the middle-dose (15 ml of FPEs/kg) group (compared with those in the model group, $p < 0.05$) (Table 1).

3.2. Effect of FPEs on Nipple Size of Rats. The diameter and height of the nipples of rats increased upon estradiol benzoate and progestin administration (compared with those in the control group, $p < 0.05$). However, upon treatment with FPEs, the diameter and height of their nipples improved. In the larger-dose group, the diameter and height of their nipples were significantly attenuated (compared with those in the model group, $p < 0.05$). Additionally, the middle-dose group apparently alleviated the diameter of nipples. However, the smaller-dose (5 ml of FPEs/kg) group did not show an evident modulatory role in the diameter and height of nipples (Table 1).

3.3. Protective Effect of FPEs on Mammary Gland Pathology in Model Animals. In this study, mammary gland hyperplasia was induced by administering estradiol benzoate and progestin and treated with FPEs. Histopathological analysis showed that the lobules and acinars in the control group and group administered with FPEs alone showed no apparent hyperplasia, with few acinars and no clear secretion in the mammary ducts and lumens. By contrast, severe pathological changes, including mammary gland hyperplasia, lobule increase, acinar increase, mammary duct and lumen ectasia, and mammary duct and lumen secretion increase, were observed in the model group. Table 2 shows the statistics for several pathological features related to mammary gland hyperplasia across the study groups. The pathology of the mammary glands in the model rats given with the larger dose and middle dose of FPEs improved, with significant changes observed in lobule number, acinar number, and mammary duct and lumen secretion. Mammary duct and lumen secretion in the treatment group administered a high dose of FPEs almost returned to the normal level. In addition, pathological improvements of mammary gland hyperplasia were found to be positively correlated with FPE dosage (Figure 1).

3.4. FPEs Improve Mammary Gland Hyperplasia in Model Rats via Its Antioxidant Effects. Mammary gland hyperplasia induced by estradiol benzoate and progestin resulted in oxidative damage. Oxidant indices such as SOD and GSH-Px activities and MDA level in the serum and mammary glands were detected the day after mammary gland hyperplasia was induced. Therefore, we sought to evaluate the protective effect of FPEs against oxidative damage in the mammary glands. As shown in Figure 2, SOD and GSH-Px activities

Table 2: Effect of SM on estradiol benzoate and progestin induced mammary gland changes on histopathology.

Groups	Mammary gland hyperplasia	Lobule increase	Acinar increase	Mammary duct and lumen ectasia	Mammary duct and lumen secretion
Control	–	–	–	–	–
FPEs control	–	–	–	–	–
EB + PR	+++	+++	+++	+++	+++
EB + PR+ 30 ml FPEs/kg	+	+	+	++	+/–
EB + PR+ 15 ml FPEs/kg	++	++	++	+++	+
EB + PR+ 5 ml FPEs/kg	+++	+++	+++	+++	++

FPEs: fermented papaya extracts; EB: estradiol benzoate; PR: progestin. The histopathology changes were determined at the end of experiment. –: none; +/–: some have and some not; +: mild; ++: moderate; +++: severe.

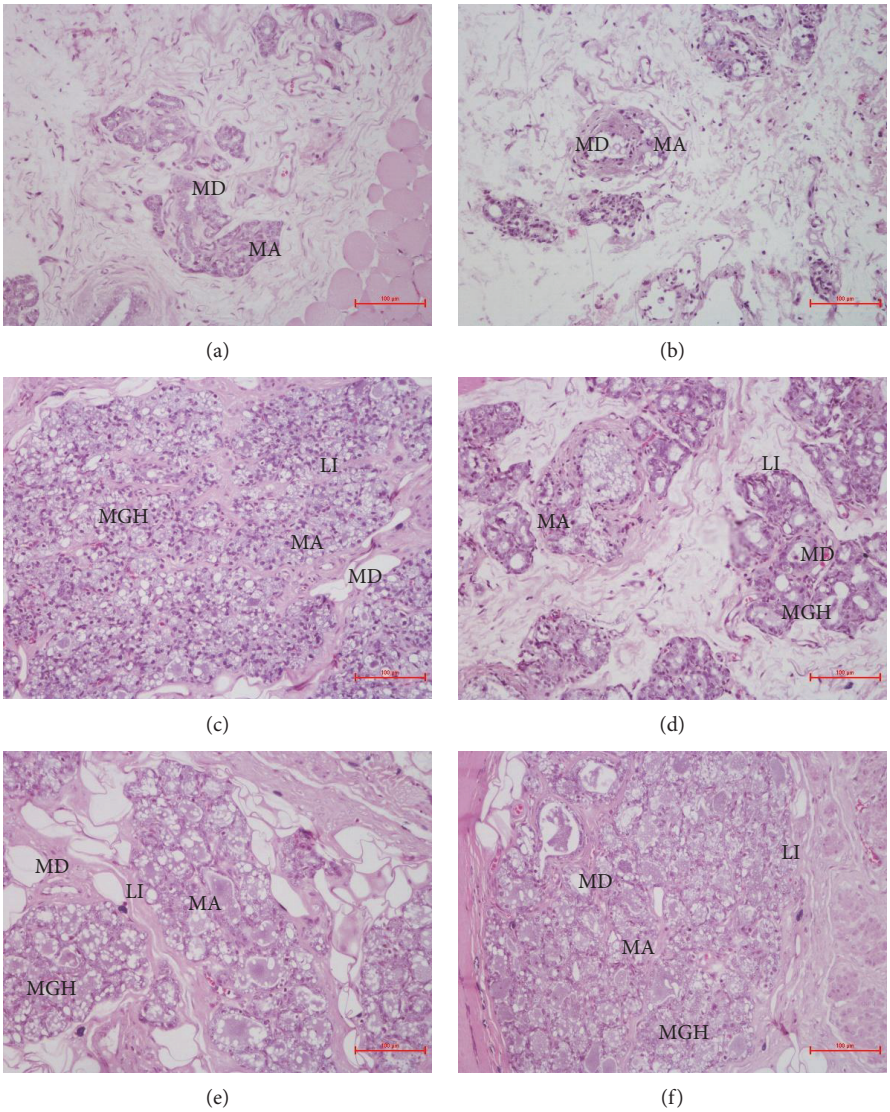

Figure 1: Photomicrographs showing mammary gland of rats in the control and treatment groups (200x). There was no apparent hyperplasia and no clear secretion in the mammary ducts and lumens in the control group (a) and the FPE-treatment-alone group (b). However, severe mammary gland hyperplasia (MGH), lobule increase (LI), acinar (MA) increase, mammary duct (MD) and lumen ectasia, and mammary duct and lumen secretion were observed in the estradiol benzoate and progestin treatment group (c). The pathology of the mammary glands of the model rats improved upon treatment with FPEs at 30 ml/kg (d), 15 ml/kg (e) and 5 ml/kg (f). Scale bar, 100 μm.

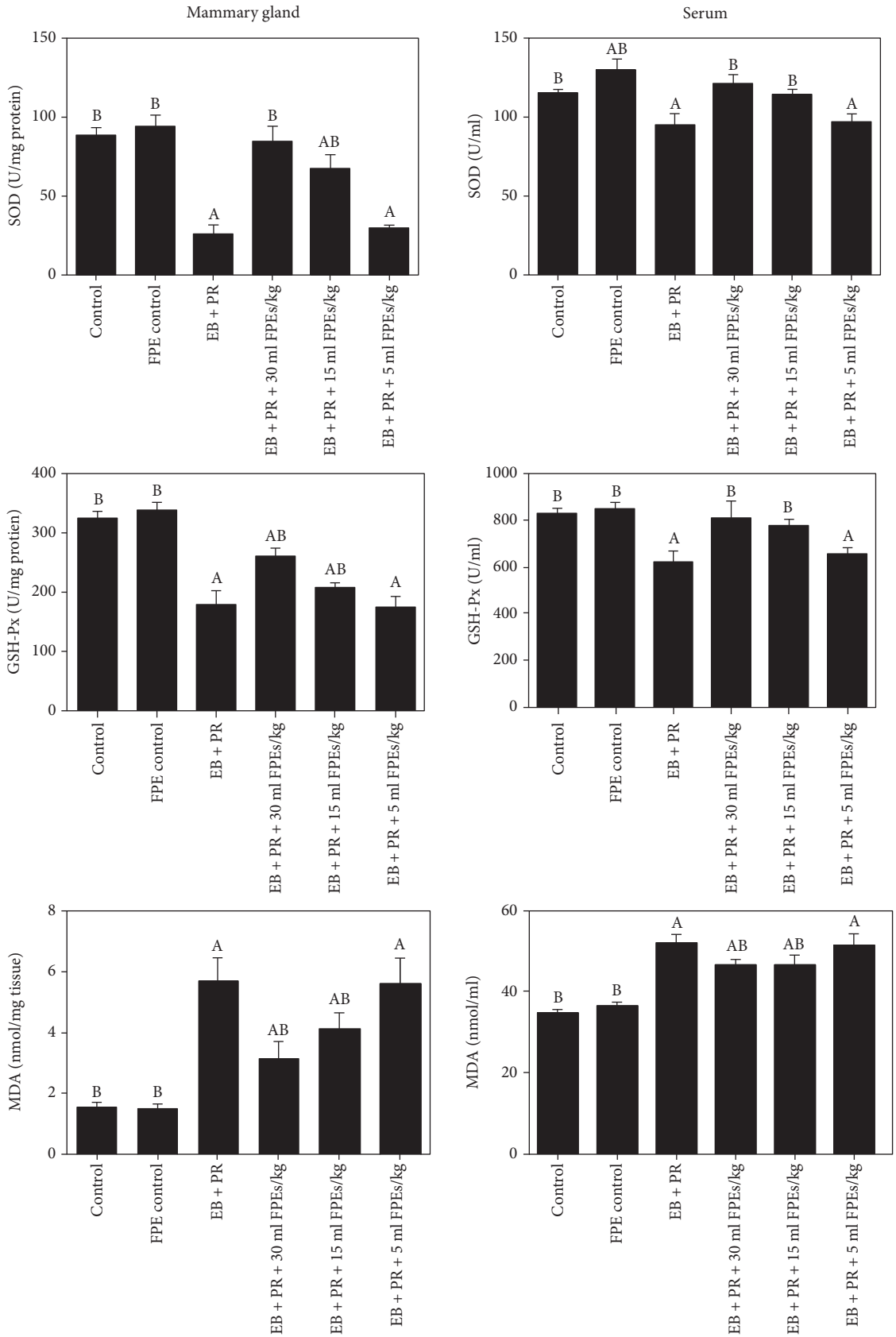

Figure 2: Effect of FPEs on SOD and GSH-Px activities and MDA level in the serum and mammary glands, which had changed upon treatment with estradiol benzoate and progestin. Data are presented as mean ± SEM. $^{A}p < 0.05$ compared with the control group; $^{B}p < 0.05$ compared with the EB + PR group.

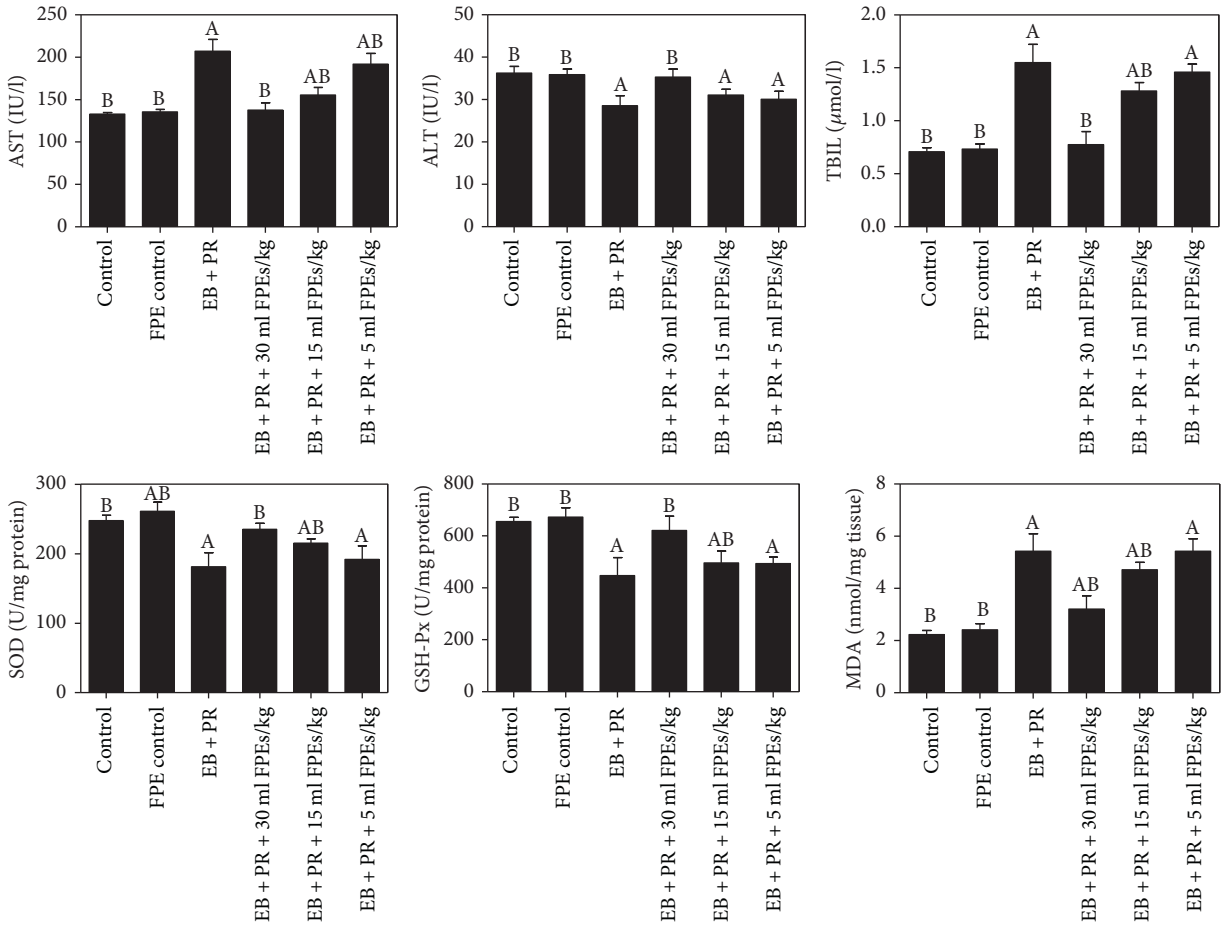

Figure 3: Effect of FPEs on AST, ALT, and TBIL biochemistry indices and SOD, GSH-Px, and MDA oxidative indices in the livers, which changed upon treatment with estradiol benzoate and progestin administration. Data are presented as mean ± SEM. $^{A}p < 0.05$ compared with the control group; $^{B}p < 0.05$ compared with the EB + PR group.

and MDA level in the mammary glands and serum of the model rats obviously changed compared with that in the control group ($p < 0.05$). These oxidative indices in the mammary glands and serum of the model rats also significantly improved after treatment with FPEs both in the larger-dose group and the middle-dose group (compared with those in the model group, $p < 0.05$). SOD and GSH-Px activities in the serum of model rats treated with high doses of FPEs recovered to levels observed in the control group. Moreover, SOD activity in the serum of rats treated with FPEs alone (group 2) was higher than that in the control group ($p < 0.05$). Although the smaller-dose group did not show an apparent antioxidant effect, these results indicate that FPEs can increase the antioxidant levels and inhibit the hyperplasia of mammary glands by antioxidants.

3.5. Blood Biochemistry. Each serum biochemical index was determined to investigate the damage induced by estradiol benzoate and progestin in the body and the protective effect of FPEs. The AST and TBIL indices in the model rats obviously increased, and the ALT index obviously decreased in the model rats (compared with those in the control group, $p < 0.05$). Compared with those in the model group, the AST, TBIL, and ALT indices in the larger-dose FPE treatment group were obviously improved and recovered to the levels of the control group ($p < 0.05$). Furthermore, FPEs showed a dose-dependent effect on AST index. The TBIL index was also evidently reduced in the middle-dose group. However, the TBIL and ALT indices in the smaller-dose group were not significantly changed (compared with those in the model group, $p > 0.05$) (Figure 3).

3.6. FPEs Inhibit Liver Damage in Model Rats via Their Antioxidant Effects. Estradiol benzoate and progestin can induce mammary gland hyperplasia and change AST, TBIL, and ALT, which suggested that estradiol benzoate and progestin could induce damage to other visceral organs. Pathological examination of the major visceral organs did not reveal any obvious pathological change in the visceral organs, except for the liver, which underwent inflammatory infiltration. Mammary gland hyperplasia is inhibited by FPEs mainly via antioxidants. The SOD and GSH-Px activities and MDA levels in the liver were examined to determine whether liver damage induced by estradiol benzoate and progestin was caused by oxidative stress and whether the liver was protected by FPEs via antioxidants. The liver was completely cleaned with saline to avoid interference from blood. Results showed that SOD and GSH-Px activities were obviously

decreased, and the MDA level was increased in the model group (compared with those in the control group, $p < 0.05$). These oxidative indices in the liver tissues of the model rats treated with FPEs were obviously restored both in the larger-dose group and the middle-dose group. The SOD and GSH-Px activities in the larger-dose group were increased to the same level as the control group (compared with those in the model group, $p < 0.05$, and compared with those in the control group, $p > 0.05$). However, the smaller-dose group did not show a significant protective effect. In addition, the SOD activity in rats orally administered FPEs alone was higher than that in the control group ($p < 0.05$). Thus, our results demonstrated that FPEs also prevented liver damage via their antioxidant properties (Figure 3).

3.7. Treatment with FPEs Reduced the Oxidative Stress Marker 8-oxo-dG. A part of mammary gland hyperplasia is the early pathological changes of breast cancer. Oxidative stress plays a crucial role in breast cancer induced by estrogen. The biomarker of 8-oxo-dG is one of the predominant forms of free radical-induced oxidative lesions and has therefore been widely used in the evaluation of oxidative DNA damage and carcinogenesis [23].

Results of IHC and ELISA analyses showed that the number of cells expressing 8-oxo-dG in mammary gland tissues was increased by estradiol benzoate and progestin. By contrast, the number of 8-oxo-dG-positive cells was remarkably reduced in the larger-dose and the middle-dose FPE treatments (compared with that in the model group, $p < 0.05$) (Figure 4).

ELISA was conducted to detect 8-oxo-dG content in liver tissues. Similarly, the content of 8-oxo-dG in liver tissues of the animal models was reduced in the larger-dose and the middle-dose FPE treatments (compared with that in the model group, $p < 0.05$). The 8-oxo-dG contents in livers of rats administered with these two doses of FPEs had recovered to the level in the control group (Figure 5).

4. Discussion

The pathogenesis of mammary gland hyperplasia remains unclear, and studies suggest that this condition could be attributed to endocrine dyscrasia [24]. Increase in estrogen level in the body is known to promote multiplication of mammary gland cells, and long-term high-estrogen stimulation destroys the balance of mammary gland tissue hyperplasia and recovery during menstrual cycles. These phenomena result in gland duct expansion, adenomatosis, and acinus increase and further cause pathological mammary gland hyperplasia [20]. A large amount of reactive oxygen species (ROS) was found to be produced by long-term high-estrogen stimulation, which in turn caused oxidative stress injury in mammary gland tissues [25–27]. Given the aforementioned mechanism of mammary gland hyperplasia, estrogen and progestin can be utilized to induce mammary gland hyperplasia in model rats [18, 28]. In the present study, model rats with mammary gland hyperplasia induced by estradiol benzoate and progestin exhibited obvious elevation of estrogen level in the serum. Concomitant with this rise in estrogen level, severe pathological changes were observed. Oxidative stress is also a crucial factor in mammary gland hyperplasia. After mammary gland hyperplasia was induced by estrogen and progestin, SOD and GSH-Px activities, which are the major antioxidant enzymes that capture harmful active oxygen, in the serum and mammary glands of rats, were found to be obviously decreased.

FPPs are widely applied as functional food in the treatment and remission of various diseases [29, 30]. Although the mechanism underlying their therapeutic effects still remains unclear, antioxidant activity is one of its major functions [12, 31]. Antioxidant activity has been shown to be effective in the treatment and remission of complications related to age [32], erythrocyte oxidative damage [13], wound healing in diabetics [11, 33, 34], and AD [14]. In this study, FPEs can not only improve oxidative indices in the animal models, but can also increase SOD activity in the normal animals. This indicates that FPEs exhibit strong antioxidant activity, and their protective effect on mammary gland hyperplasia is likely related to this property.

Estrogen can induce cell multiplication and inhibit DNA repair [35, 36]. Previous studies showed that breast tumor is induced by estrogen through oxidative DNA damage [25, 37, 38]. The biomarker 8-oxo-dG is a product of ROS that induces oxidative DNA damage, which is regarded as a cell marker of oxidative stress and oxidative DNA damage, and is the most common product of oxidative stress damage induced by estrogen [39, 40]. After long-term estrogen inducement, 8-oxo-dG-positive cells in the mammary gland obviously increased, but improved when the animal models were given with FPEs. This finding indicates that, in addition to its antioxidant activity, FPEs also have the ability to inhibit oxidative DNA damage. This is consistent with a previous report that FPP can reduce oxidative DNA damage and improve cytokine balance [41].

In this study, a panel of blood biochemical markers in the experimental animals were detected. The AST, ALT, and TBIL indices in the serum of the animals with mammary gland hyperplasia induced by estrogen were remarkably increased. Meanwhile, these biochemical indices in the animal models treated with FPEs had recovered to the level of the control group. This result indicates that estrogen can cause mammary gland hyperplasia and damage other visceral organs. However, FPEs can protect these organs from being injured. AST and ALT are markers of heart and liver damage, whereas TBIL is a marker of liver damage. After pathological detection of the major visceral organs, no obvious pathological changes to the heart, spleen, lung, kidney, ovary, and uterus were observed. However, pathological changes in the liver, which mainly consisted of inflammatory cell infiltration, were still induced. However, high-dose FPEs completely protected the liver from being injured. Oxidant indices and oxidative DNA damage markers indicate that FPE acts as an antioxidant to protect the liver from damage. Previous studies showed that FPP can protect liver activity and inhibit liver cancer, which is mainly achieved via its antioxidant activity [42, 43]. Oxidative stress plays an important role in mediating hepatotoxicity associated with many diseases [44, 45]. FPEs improve and protect the organs, and

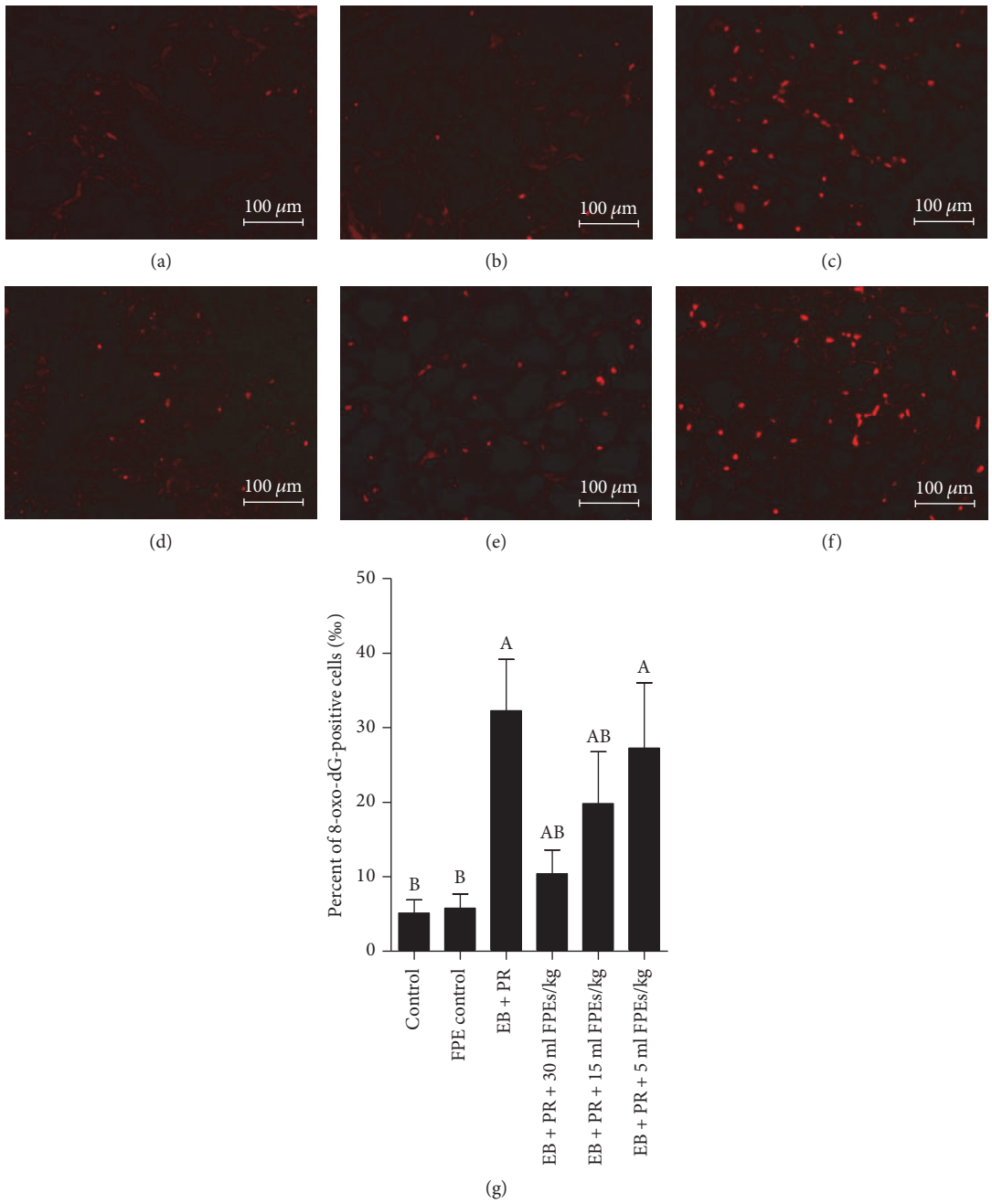

Figure 4: Effect of SPE supplementation on oxidative stress in mammary gland hyperplasia of rats induced by estradiol benzoate and progestin administration. (a–f) Representative images of 8-oxo-dG immunostaining in the mammary glands (200x). No apparent 8-oxo-dG-positive cells were observed in the control group (a) and the FPE-treatment-alone group (b). A high percentage of 8-oxo-dG-positive cells were observed in the estradiol benzoate and progestin treatment group (c). Scale bar, 100 μm. However, the percentage of 8-oxo-dG-positive cells decreased upon treatment with FPEs at 30 ml/kg (d), 15 ml/kg (e) and 5 ml/kg (f). (g) Quantification of 8-oxo-dG-positive cells in the mammary glands by ELISA. Data are presented as mean ± SEM. $^{A}p < 0.05$ compared with the control group; $^{B}p < 0.05$ compared with the EB + PR group.

in turn improve blood biochemical indexes, through their antioxidative effects.

FPP is available in the market in powdered form after papaya fermentation with edible fungi. FPEs, the extracting solution fermented by papaya through the collaboration of *A. oryzae* and yeasts for six months, can be easily prepared and consumed. Clinically, FPEs are mainly used for improving digestion and immune regulation, endocrine dyscrasia improvement, and weight reduction. In this study, three FPE treatment groups (each receiving 30, 15, or 5 ml/kg FPEs) was used for evaluating the protective effect on mammary gland hyperplasia. The results provide convincing evidence that FPEs with higher and middle doses could obviously improve hormone levels, clinical

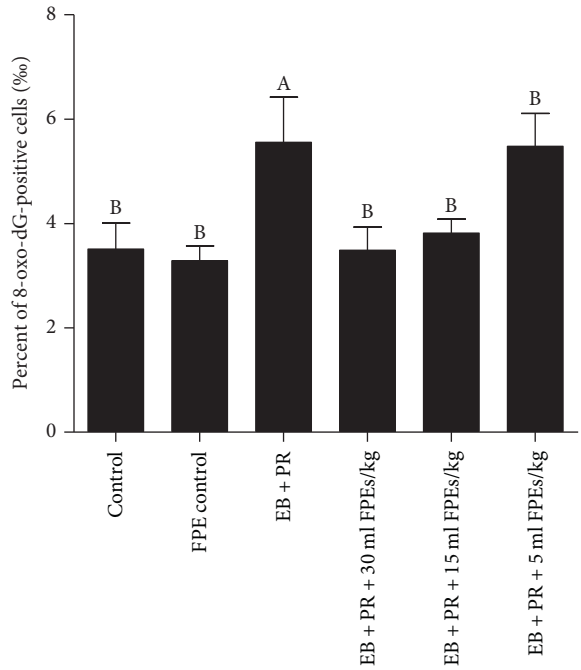

Figure 5: Quantification of 8-oxo-dG-positive cells in the liver by ELISA. Data are presented as mean ± SEM. $^{A}p < 0.05$ compared with the control group; $^{B}p < 0.05$ compared with the EB + PR group.

signs, oxidative indices, biochemical index, and pathological changes in model animals of mammary gland hyperplasia, and with smaller dose had no significant modulatory role. Moreover, the higher dose is the optimal dose, which was converted into an adult dose 70 ml/kg approximately according to body surface area. In general, the clinical dose of adult women is 100 ml/d. A 1-month safety evaluation of FPEs for SD rats was conducted. The results showed that blood biochemistry, hematology, histopathology, ingestion, and water intake of the rats administered the recommended clinical dose of FPEs four times did not obviously change. However, an obvious decrease in body weight was documented, which is also a possible reason for the observed change in body shape.

Studies have shown that mammary gland hyperplasia induced by estrogen can be effectively inhibited by FPEs via their antioxidant effects. In addition, FPEs can also improve and repair oxidative damage in the liver. FPEs contain abundant nutrients, such as alpha-tocopherol [8], flavonoid [9], glutamic acid, cystine, cytosine, nicotinic acid, pipecolic acid, homoserine, quinic acid, and glucuronic acid, which possess antioxidant and antitumor functions. In recent years, liquor obtained via fruit fermentation has become popular in China and is commonly sold as commercial food. Each active element in FPEs should be further analyzed. Future studies should focus on the functions and mechanism of FPEs in various diseases and in developing FPEs as functional food.

Conflicts of Interest

The authors declare that there is no conflict of interest regarding the publication of this article.

Acknowledgments

The project was supported by the Science and Technology Department of Zhejiang Province (2016F30009) and the Natural Science Foundation of Zhejiang Province (LQY18H160001, LY17H310009).

References

[1] M. Lu, Y. Toshima, X. Wu, X. Zhang, and Y. Q. Cai, "Inhibitory effects of vegetable and fruit ferment liquid on tumor growth in Hepatoma-22 inoculation model," *Asia Pacific Journal of Clinical Nutrition*, vol. 16, no. S1, pp. 443–446, 2007.

[2] H. Y. Huang, M. Korivi, C. H. Tsai, J. H. Yang, and Y. C. Tsai, "Supplementation of lactobacillus plantarum K68 and fruit-vegetable ferment along with high fat-fructose diet attenuates metabolic syndrome in rats with insulin resistance," *Evidence-based Complementary and Alternative Medicine*, vol. 2013, Article ID 943020, 12 pages, 2013.

[3] S. Mehdipour, N. Yasa, G. Dehghan et al., "Antioxidant potentials of Iranian *Carica papaya* juice *in vitro* and *in vivo* are comparable to α-tocopherol," *Phytotherapy Research*, vol. 20, no. 7, pp. 591–594, 2006.

[4] K. M. Sadek, "Antioxidant and immunostimulant effect of *Carica papaya* Linn. aqueous extract in acrylamide intoxicated rats," *Acta Informatica Medica*, vol. 20, no. 3, pp. 180–185, 2012.

[5] J. A. Osato, L. A. Santiago, G. M. Remo, M. S. Cuadra, and A. Mori, "Antimicrobial and antioxidant activities of unripe papaya," *Life Sciences*, vol. 53, no. 17, pp. 1383–1389, 1993.

[6] N. Otsuki, N. H. Dang, E. Kumagai, A. Kondo, S. Iwata, and C. Morimoto, "Aqueous extract of *Carica papaya* leaves exhibits anti-tumor activity and immunomodulatory effects," *Journal of Ethnopharmacology*, vol. 127, no. 3, pp. 760–767, 2010.

[7] A. Basu and S. Haldar, "Dietary isothiocyanate mediated apoptosis of human cancer cells is associated with Bcl-xL phosphorylation," *International Journal of Oncology*, vol. 33, no. 4, pp. 657–663, 2008.

[8] L. S. Ching and S. Mohamed, "Alpha-tocopherol content in 62 edible tropical plants," *Journal of Agricultural and Food Chemistry*, vol. 49, no. 6, pp. 3101–3105, 2001.

[9] K. H. Miean and S. Mohamed, "Flavonoid (myricetin, quercetin, kaempferol, luteolin, and apigenin) content of edible tropical plants," *Journal of Agricultural and Food Chemistry*, vol. 49, no. 6, pp. 3106–3112, 2001.

[10] D. Telgenhoff, K. Lam, S. Ramsay et al., "Influence of papain urea copper chlorophyllin on wound matrix remodeling," *Wound Repair and Regeneration*, vol. 15, no. 5, pp. 727–735, 2007.

[11] E. Collard and S. Roy, "Improved function of diabetic wound-site macrophages and accelerated wound closure in response to oral supplementation of a fermented papaya preparation," *Antioxidants and Redox Signaling*, vol. 13, no. 5, pp. 599–606, 2010.

[12] O. I. Aruoma, R. Colognato, I. Fontana et al., "Molecular effects of fermented papaya preparation on oxidative damage, MAP kinase activation and modulation of the benzo [a] pyrene mediated genotoxicity," *BioFactors*, vol. 26, no. 2, pp. 147–159, 2006.

[13] F. Marotta, M. Weksler, Y. Naito, C. Yoshida, M. Yoshioka, and P. Marandola, "Nutraceutical supplementation: effect of a fermented papaya preparation on redox status and DNA

damage in healthy elderly individuals and relationship with GSTM1 genotype," *Annals of the New York Academy of Sciences*, vol. 1067, no. 1, pp. 400–407, 2006.

[14] M. Barbagallo, F. Marotta, and L. J. Dominguez, "Oxidative stress in patients with Alzheimer's disease: effect of extracts of fermented papaya powder," *Mediators of Inflammation*, vol. 2015, Article ID 624801, 6 pages, 2015.

[15] B. S. Nayak, R. Ramdeen, A. Adogwa, A. Ramsubhag, and J. R. Marshall, "Wound-healing potential of an ethanol extract of *Carica papaya* (Caricaceae) seeds," *International Wound Journal*, vol. 9, no. 6, pp. 650–655, 2012.

[16] K. H. Allison, P. R. Eby, J. Kohr, W. B. DeMartini, and C. D. Lehman, "Atypical ductal hyperplasia on vacuum-assisted breast biopsy: suspicion for ductal carcinoma in situ can stratify patients at high risk for upgrade," *Human Pathology*, vol. 42, no. 1, pp. 41–50, 2011.

[17] D. J. Marchant, "Benign breast disease," *Obstetrics and Gynecology Clinics of North America*, vol. 29, no. 1, pp. 1–20, 2002.

[18] L. Wang, D. Zhao, L. Di et al., "The anti-hyperplasia of mammary gland effect of *Thladiantha dubia* root ethanol extract in rats reduced by estrogen and progestogen," *Journal of Ethnopharmacology*, vol. 134, no. 1, pp. 136–140, 2011.

[19] D. Medina, "Biological and molecular characteristics of the premalignant mouse mammary gland," *Biochimica et Biophysica Acta (BBA)-Reviews on Cancer*, vol. 1603, no. 1, pp. 1–9, 2002.

[20] J. L. Yang, Y. Ren, L. Wang et al., "PTEN mutation spectrum in breast cancers and breast hyperplasia," *Journal of Cancer Research and Clinical Oncology*, vol. 136, no. 9, pp. 1303–1311, 2010.

[21] E. C. Ontsouka and C. Albrecht, "Cholesterol transport and regulation in the mammary gland," *Journal of Mammary Gland Biology and Neoplasia*, vol. 19, no. 1, pp. 43–58, 2014.

[22] C. E. Ontsouka, X. Huang, E. Aliyev, and C. Albrecht, "In vitro characterization and endocrine regulation of cholesterol and phospholipid transport in the mammary gland," *Molecular and Cellular Endocrinology*, vol. 5, no. 439, pp. 35–45, 2017.

[23] A. Valavanidis, T. Vlachogianni, and C. Fiotakis, "8-hydroxy-2′ -deoxyguanosine (8-OHdG): a critical biomarker of oxidative stress and carcinogenesis," *Journal of Environmental Science and Health, Part C: Environmental Carcinogenesis & Ecotoxicology Reviews*, vol. 27, no. 2, pp. 120–139, 2009.

[24] N. L. Henry, "Endocrine therapy toxicity: management options," *American Society of Clinical Oncology Educational Book*, vol. 34, pp. e25–e30, 2014.

[25] S. D. Gupta, J. Y. So, J. Wahler et al., "Tocopherols inhibit oxidative and nitrosative stress in estrogen-induced early mammary hyperplasia in ACI rats," *Molecular Carcinogenesis*, vol. 54, no. 9, pp. 916–925, 2015.

[26] L. Marinelli, G. Gabai, J. Wolfswinkel, and J. A. Mol, "Mammary steroid metabolizing enzymes in relation to hyperplasia and tumorigenesis in the dog," *The Journal of Steroid Biochemistry and Molecular Biology*, vol. 92, no. 3, pp. 167–173, 2004.

[27] S. M. Mense, F. Remotti, A. Bhan et al., "Estrogen-induced breast cancer: alterations in breast morphology and oxidative stress as a function of estrogen exposure," *Toxicology and Applied Pharmacology*, vol. 232, no. 1, pp. 78–85, 2008.

[28] T. Chen, J. Li, J. Chen, H. Song, and C. Yang, "Anti-hyperplasia effects of Rosa rugosa polyphenols in rats with hyperplasia of mammary gland," *Environmental Toxicology and Pharmacology*, vol. 39, no. 2, pp. 990–996, 2015.

[29] S. Murakami, S. Eikawa, S. Kaya, M. Imao, and T. Aji, "Antitumor and immunoregulatory effects of fermented papaya preparation (FPP: SAIDO-PS501)," *Asian Pacific Journal of Cancer Prevention*, vol. 17, no. 7, pp. 3077–3084, 2016.

[30] Z. F. Kharaeva, L. R. Zhanimova, M. S. Mustafaev et al., "Effects of standardised fermented papaya gel on clinical symptoms, inflammatory cytokines, and nitric oxide metabolites in patients with chronic periodontitis: an open randomised clinical study," *Mediators of Inflammation*, vol. 2016, Article ID 9379840, 12 pages, 2016.

[31] I. Calzuola, G. L. Gianfranceschi, and V. Marsili, "Comparative activity of antioxidants from wheat sprouts, *Morinda citrifolia*, fermented papaya and white tea," *International Journal of Food Sciences and Nutrition*, vol. 57, no. 3-4, pp. 168–177, 2006.

[32] F. Marotta, K. Pavasuthipaisit, C. Yoshida, F. Albergati, and P. Marandola, "Relationship between aging and susceptibility of erythrocytes to oxidative damage: in view of nutraceutical interventions," *Rejuvenation Research*, vol. 9, no. 2, pp. 227–230, 2006.

[33] R. Dickerson, B. Deshpande, U. Gnyawali et al., "Correction of aberrant NADPH oxidase activity in blood-derived mononuclear cells from type II diabetes mellitus patients by a naturally fermented papaya preparation," *Antioxidants and Redox Signaling*, vol. 17, no. 3, pp. 485–491, 2012.

[34] S. Gurung and N. Skalko-Basnet, "Wound healing properties of Carica papaya latex: in vivo evaluation in mice burn model," *Journal of Ethnopharmacology*, vol. 121, no. 2, pp. 338–341, 2009.

[35] S. J. Weroha, S. A. Li, O. Tawfik, and J. J. Li, "Overexpression of cyclins D1 and D3 during estrogen-induced breast oncogenesis in female ACI rats," *Carcinogenesis*, vol. 27, no. 3, pp. 491–498, 2006.

[36] K. P. Singh, J. Treas, T. Tyagi, and W. Gao, "DNA demethylation by 5-aza-2-deoxycytidine treatment abrogates 17 beta-estradiol-induced cell growth and restores expression of DNA repair genes in human breast cancer cells," *Cancer Letters*, vol. 316, no. 1, pp. 62–69, 2012.

[37] B. Singh, A. Chatterjee, A. M. Ronghe, N. K. Bhat, and H. K. Bhat, "Antioxidant-mediated up-regulation of OGG1 via NRF2 induction is associated with inhibition of oxidative DNA damage in estrogen-induced breast cancer," *BMC Cancer*, vol. 13, no. 1, p. 253, 2013.

[38] S. M. Mense, B. Singh, F. Remotti, X. Liu, and H. K. Bhat, "Vitamin C and α-naphthoflavone prevent estrogen-induced mammary tumors and decrease oxidative stress in female ACI rats," *Carcinogenesis*, vol. 30, no. 7, pp. 1202–1208, 2009.

[39] M. M. Montano, L. J. Chaplin, H. Deng et al., "Protective roles of quinone reductase and tamoxifen against estrogen-induced mammary tumorigenesis," *Oncogene*, vol. 26, no. 24, pp. 3587–3590, 2007.

[40] B. Singh, N. K. Bhat, and H. K. Bhat, "Induction of NAD (P) H-quinone oxidoreductase 1 by antioxidants in female ACI rats is associated with decrease in oxidative DNA damage and inhibition of estrogen-induced breast cancer," *Carcinogenesis*, vol. 33, no. 1, pp. 156–163, 2012.

[41] F. Marotta, C. Yoshida, R. Barreto, Y. Naito, and L. Packer, "Oxidative-inflammatory damage in cirrhosis: effect of vitamin E and a fermented papaya preparation," *Journal of*

Gastroenterology and Hepatology, vol. 22, no. 5, pp. 697–703, 2007.

[42] J. Somanah, S. Ramsaha, S. Verma et al., "Fermented papaya preparation modulates the progression of N-methyl-N-nitrosourea induced hepatocellular carcinoma in Balb/c mice," *Life Sciences*, vol. 151, pp. 330–338, 2016.

[43] B. Rajkapoor, B. Jayakar, S. Kavimani, and N. Murugesh, "Effect of dried fruits of *Carica papaya* Linn on hepatotoxicity," *Biological and Pharmaceutical Bulletin*, vol. 25, no. 12, pp. 1645-1646, 2002.

[44] N. Houstis, E. D. Rosen, and E. S. Lander, "Reactive oxygen species have a causal role in multiple forms of insulin resistance," *Nature*, vol. 440, no. 7086, pp. 944–948, 2006.

[45] S. C. Gupta, D. Hevia, S. Patchva, B. Park, W. Koh, and B. B. Aggarwal, "Upsides and downsides of reactive oxygen species for cancer: the roles of reactive oxygen species in tumorigenesis, prevention, and therapy," *Antioxidants Redox Signaling*, vol. 16, no. 11, pp. 1295–1322, 2012.

Hindawi
Oxidative Medicine and Cellular Longevity
Volume 2017, Article ID 4824371, 10 pages
https://doi.org/10.1155/2017/4824371

Research Article

Protective Effects and Possible Mechanisms of Ergothioneine and Hispidin against Methylglyoxal-Induced Injuries in Rat Pheochromocytoma Cells

Tuzz-Ying Song,[1] Nae-Cherng Yang,[2] Chien-Lin Chen,[1] and Thuy Lan Vo Thi[1]

[1]*Department of Bioindustry Technology, Da-Yeh University, Dacun, Taiwan*
[2]*Department of Nutrition, Chung Shan Medical University Hospital, Taichung, Taiwan*

Correspondence should be addressed to Tuzz-Ying Song; song77@mail.dyu.edu.tw

Received 6 June 2017; Revised 8 August 2017; Accepted 23 August 2017; Published 17 October 2017

Academic Editor: Mohamed M. Abdel-Daim

Diabetic encephalopathy (DE) is often a complication in patients with Alzheimer's disease due to high blood sugar induced by diabetic mellitus. Ergothioneine (EGT) and hispidin (HIP) are antioxidants present in *Phellinus linteus*. Methylglyoxal (MGO), a toxic precursor of advanced glycated end products (AGEs), is responsible for protein glycation. We investigated whether a combination EGT and HIP (EGT + HIP) protects against MGO-induced neuronal cell damage. Rat pheochromocytoma (PC12) cells were preincubated with EGT (2 μM), HIP (2 μM), or EGT + HIP, then challenged with MGO under high-glucose condition (30 μM MGO + 30 mM glucose; GLU + MGO) for 24–96 h. GLU + MGO markedly increased protein carbonyls and reactive oxygen species in PC12 cells; both of these levels were strongly reduced by EGT or HIP with effects comparable to those of 100 nM aminoguanidine (an AGE inhibitor) but stronger than those of 10 μM epalrestat (an aldose reductase inhibitor). GLU + MGO significantly increased the levels of AGE and AGE receptor (RAGE) protein expression of nuclear factor kappa-B (NF-κB) in the cytosol, but treatment with EGT, HIP, or EGT + HIP significantly attenuated these levels. These results suggest that EGT and HIP protect against hyperglycemic damage in PC12 cells by inhibiting the NF-κB transcription pathway through antioxidant activities.

1. Introduction

In general, there is a higher prevalence of diabetes among patients suffering from various neurodegenerative disorders, such as Alzheimer's disease (AD) [1]. Recently, several reports revealed an epidemiological association between diabetes mellitus (DM) and cognitive impairment known as diabetic encephalopathy (DE), which has been recognized as an important CNS complication of diabetes [2]. Accumulating data indicate that DE results from neuronal cell apoptosis in the hippocampal region due to brain insulin deficiency [3], impaired brain insulin signaling [4], and hyperglycemia-induced oxidative stress in the brain [5].

Glucose and other reducing sugars are important glycating agents; however, the most reactive and physiologically relevant glycating agents are the dicarbonyls, in particular methylglyoxal (MGO). Excessive glucose causes the accumulation of MGO and advanced glycation end products (AGE). MGO can react with amino acids to induce protein glycation and consequently form AGE [6]. Many studies have revealed an association between MGO and AGEs in the pathogenesis of cognitive disorders such as DE and AD [7, 8]. In addition, the importance of the receptor for advanced glycation end products (RAGE), which function as signal-transducing cell surface accepters for AGE in DE and for β-amyloid in AD, was recently highlighted [9]. MGO is more toxic and reactive than glucose and forms adducts with proteins, phospholipids, and nucleic acids. MGO exposure itself, without hyperglycemia, can induce diabetes-like complications [10]. Hyperglycemic condition is known to activate both oxidative stress and inflammatory pathways. The interaction of these two pathways complicates

the hyperglycemia-mediated neuronal damage. Oxidative stress-mediated inflammation is known to execute NF-κB, activator protein-1 (AP-1), and MAPK pathways [11].

Ergothioneine (2-mercaptohistidine trimethylbetaine; EGT), which is formed in some bacteria and fungi but not in animals [12], is known to be present in the mammalian brain at 0.2–1.0 mg per 100 g tissue [13]. In humans, EGT is derived from a plant-based diet, primarily from edible mushrooms. In vitro studies have shown that EGT possesses antioxidant, antiradiation, and anti-inflammatory activities [14, 15], and sufficient evidence suggests that EGT functions as a physiological antioxidant [15]. EGT also protects neurons from cytotoxicity induced by various neurotoxins, including N-methyl-D-aspartate, β-amyloid, and cisplatin [16–18]. In our previous study, we demonstrated that EGT protects against learning and memory deficits in aging mice treated with Aβ [19] or D-galactose [20] by improving parameters related to oxidative stress. However, little is known about the effects of EGT on MGO-induced injuries in neurons.

Hispidin (HIP), 6-(3,4-dihydroxystyryl)-4-hydroxy-2-pyrone, is a phenolic compound first purified from *Inonotus hispidus* [21]. Later, it was found in medicinal mushrooms, particularly the genus *Phellinus* (a traditional medicinal mushroom used in Asian countries for the treatment of various diseases). HIP has garnered significant attention due to its antioxidant [22], anti-inflammatory [23], antiproliferative, and antimetastatic effects [24]. HIP also protects against peroxynitrite-mediated DNA damage and prevents hydroxyl radical generation [25, 26]. In addition, HIP possesses potent aldose reductase and protein glycation inhibitory activity [27, 28] and acts as an antidiabetic agent by preventing beta cells from the damage by reactive oxygen species (ROS) in diabetes [29, 30]. Importantly, protein kinase Cβ (PKCβ) expression in humans is activated during high blood sugar or diabetic conditions, whereas HIP can inhibit PKC expression and prevent diabetic complications [26].

Liu et al. [31] used high-glucose concentration (35 mM) rather than normal-glucose concentration (5.5 mM) to induce AGE formation. Miller et al. [32] indicated that a high-glucose environment (30 mM D-glucose) alone does not induce apoptosis within 7 days of incubation and that a combination of high glucose with glyoxalase I (an MGO-metabolizing enzyme) inhibitor can maintain cells under hyperglycemic conditions. To reduce reaction time, we use MGO and high-glucose concentration as a high-sugar concentration. Few studies have explored the ameliorative effects of EGT, HIP, or a combination EGT and HIP on MGO-induced injuries in neuronal cells. In this study, we therefore employed rat pheochromocytoma (PC12) cells to investigate the cytoprotective effect and possible mechanistic actions of HIP, EGT, and their combination against neurotoxicity induced by MGO and a high-glucose concentration.

2. Materials and Methods

2.1. Chemical Reagents. PC12 cells (BCRC 60048) were purchased from the Food Industry Research & Development Institute (Hsinchu, Taiwan). EGT, HIP, L-glutamine, sodium bicarbonate ($NaHCO_3$), horse serum (HS), fetal bovine serum (FBS), penicillin, streptomycin, MTT: (3-(4,5-dimethylthiazol-2-yl)-2,5-diphenyltetrazolium bromide) tetrazolium, and all other reagents were purchased from Sigma Chemical Company (St. Louis, MO, USA). 2′,7′-Dichlorofluorescein diacetate (H_2DCFDA) was purchased from Molecular Probes Inc. (Eugene, OR, USA). Well plates were bought from FALCON (Becton Dickinson, NJ, USA).

2.2. Preparation of PC12 Culture. Rat pheochromocytoma (PC12 cells (BCRC 60048)) was obtained from the Food Industry Research & Development Institute (Hsinchu, Taiwan) and maintained in 5% FBS, 10% HS, 84% RPMI, 1% NEAA with 2 mM L-glutamine containing 1.5 g/L sodium bicarbonate, and antibiotics (100 U/mL penicillin and 100 μg/mL streptomycin) at 37°C in a humidified atmosphere with 5% CO_2. The medium was replaced every 2 days. Cells were seeded at a density of 1×10^5 cells/well onto a 24-well plate for 24 h before sample treatment.

2.3. Cell Viability Assay. Cells were seeded at a density of 1×10^5 cells/well onto a 24-well plate (FALCON, Becton Dickinson, NJ, USA) 24 h before the treatment. The cells were divided in eight groups: (A) control (CON), (B) hyperglycemic conditions (30 μM MGO + 30 mM D-glucose (GLU + MGO group)), (C) 30 mM mannitol group (excluding the impact of glucose osmosis), (D) epalrestat (EPA, 10 μM, aldose reductase inhibitor), (E) 100 nM aminoguanidine (AMG, AGE inhibitor), (F) 2 μM EGT, (G) 2 μM HIP, and (H) EGT + HIP (2 μM + 2 μM). Groups B and C were only treated with GLU + MGO or mannitol for 24–96 h. PC12 cells were added to groups D, E, F, G, and H and allowed to stand for 2 h. Then, GLU + MGO was added to the five groups and the cells were incubated for 24–96 h. Using 0.4% trypan blue dye, cell viability was calculated with a hemocytometer in an inverted microscope (BestScope International Limited, Beijing, China) at 100x magnification. The percentage of cell viability was calculated as follows: cell viability on treatment/cell viability in control × 100%. All tests were performed at least in triplicate, and graphs were plotted using an average of three measurements.

2.4. Measurement of Intracellular ROS. Intracellular ROS levels were measured using the fluorogenic probe 2′,7′-dichlorodihydrofluorescein diacetate (H_2DCFDA) to detect H_2O_2 levels, as previously described [33]. Cells were seeded at 1×10^6 cells/mL in a 10 cm dish and incubated for 24 h. Cells in the D, E, F, G, and H groups were incubated for 2 h, then GLU + MGO was added and incubated for 24, 48, and 72 h. Then, H_2DCFDA (5 μM) was added at 37°C for 30 min, and the cells were centrifuged at 4°C, 900 g for 5 min. The cell pellet was collected, and 1 mL of 1 × PBS was added and mixed before being transferred to a flow cytometer tube for measurement of ROS level using flow cytometry.

2.5. Measurement of Protein Carbonyl. Protein carbonyl content was measured as described by Reznick and Packer [34] with minor modifications. Cells (2×10^6 cells/mL) were seeded in a 6-well plate and incubated for 24 h. Groups D,

E, F, G, and H were pretreated with GLU + MGO for 2 h and incubated with GLU + MGO for 24, 48, and 72 h. Then, the cells were centrifuged at 1500 rpm for 5 min, collected, and mixed to 1.5-fold with Triton X-100 (0.5%/PBS). These cells were frozen in liquid nitrogen for 1 min and placed in a water bath at 37°C for 5 min. Next, the cells were centrifuged at 4°C, 12,000 ×g for 10 min. To collect protein, 100 μL of supernatant and 0.5 mL of 10 mM DNPH/2N HCl were mixed in the dark at room temperature and kept for 1 h with shaking every 15 min. The protein was precipitated by adding 0.6 mL of 20% TCA and centrifugation at 10000 rpm for 10 min. The supernatant was removed, and the precipitate was washed thrice with ethanol/ethyl acetate (1 : 1, *v*/*v*) to remove residual DNPH. The precipitate was dissolved using 1 mL of 6 M guanidine-HCl (pH 2.3) and incubated at 37°C for 1 h. Then, the sample was centrifuged at 12000 rpm for 15 min. The absorption of protein carbonyl was measured at 370 nm using a spectrophotometer ($E370 = 2.2 \times 10^3\,M^{-1}\,cm^{-1}$ terms of protein carbonyl).

2.6. Determination of AGE and RAGE. The levels of AGE and RAGE were assessed using ELISA kit (Cell Biolabs Inc. CA, USA) according to the manufacturer's instructions. We detected AGE content by carboxymethyllysine (CML). CML, also known as N(epsilon)-(carboxymethyl) lysine, is an advanced glycation end product (AGE) found on proteins and lipids as a result of oxidative stress and chemical glycation. The quantity of AGE adduct in protein samples is determined by comparing its absorbance (450 nm) with that of a known AGE-BSA standard curve. The minimum detectable concentration was 0.39 μg/mL for AGEs and 0.41 ng/mL for RAGE.

2.7. Measurement of Protein Expression of NF-κB with Western Blotting. After incubation with GLU + MGO, cells were collected and resuspended in radio immunoprecipitation assay (RIPA) buffer (Millipore, Bedford, MA, USA) containing inhibitor cocktail (protease and phosphatase inhibitor) to obtain whole cell lysates. Cytoplasmic and nuclear lysates were isolated by NE-PER nuclear and cytoplasmic extraction reagents (Thermo Scientific, Rockford, IL, USA) according to manufacturer's protocol. Total protein contents of whole cell lysates or cytoplasmic and nuclear extracts were assayed using Bradford's reagent (Bio-Rad Hercules, CA, USA). Then, a portion of the protein (50 μg) was subjected to 10% SDS-PAGE and transferred onto the PVDF membranes. After blocking with 5% skimmed milk for 2 h at 37°C, the membranes were incubated with primary antibodies (IκBα (Santa Cruz Biotechnology) at 1 : 500 dilution, nuclear factor-kappa B (NF-κB) p65 (Santa Cruz Biotechnology) at 1 : 200 dilution, and β-actin (Santa Cruz Biotechnology) at 1 : 500 dilution). After being washed with Tris-buffered saline with Tween 20 (TBS-T), the membranes were then incubated with goat anti-rabbit horseradish peroxidase-conjugated secondary antibodies (Sigma, St. Louis, MO) for 1 h at 1 : 2000 dilution at room temperature. The immunoreactive bands were visualized using an enhanced chemiluminescence kits (Amersham; ECL kits) and quantified with densitometry analysis—Amersham Imager 600 (GE, USA). β-Actin was used as a loading control.

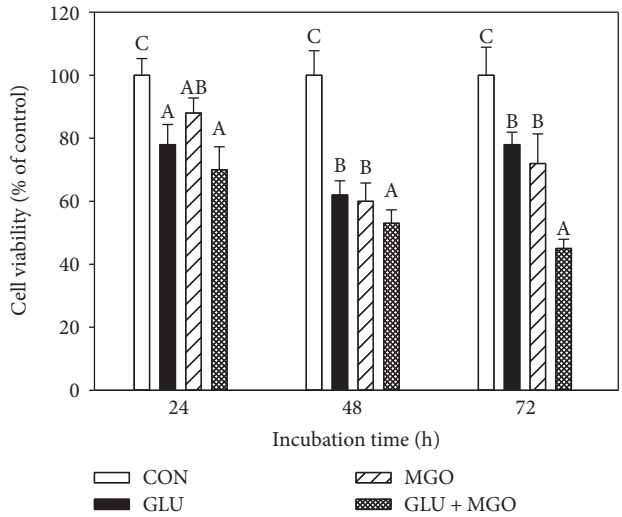

Figure 1: Effects of glucose (GLU), methylglyoxal (MGO), and GLU + MGO on viability of PC12 cells. Cell viability was estimated by trypan blue dye exclusion method. Values (means ± SD of triplicate tests) without a superscript letter are significantly different ($P < 0.05$).

2.8. Statistical Analysis. Data are expressed as means ± SD and analyzed using one-way ANOVA followed by Fisher's protected LSD test for multiple comparisons of group means. All statistical analyses were performed using SPSS for Windows, version 10 (SPSS, Inc.); a P value < 0.05 is considered statistically significant [35].

3. Results

3.1. Effects of High-Glucose Concentration on PC12 Cell Viability. As shown in Figure 1, after treatment with GLU + MGO for 24, 48, and 72 h, the viability of PC12 cells significantly decreased with time compared with treatment with GLU or MGO only ($P < 0.05$). After treatment of PC12 cells with GLU + MGO for 72 h, the cell viability decreased to about 45%, which was lower than that after treatment with GLU (78%) or MGO (75%). Therefore, we chose 30 mM GLU and 30 μM MGO for the hyperglycemic condition for PC12 cells.

3.2. Effects of EGT, HIP, and EGT + HIP on PC12 Cell Viability at High-Glucose Concentration. Figure 2 shows that the viability of cells treated with GLU + MGO was significantly decreased with increasing culture time (70%, 50%, and 45% at 24, 48, and 72 h, resp.). On the contrary, the cell viability of the group treated with mannitol to induce high osmotic pressure was above 80% even after 72 h of incubation, indicating that GLU + MGO decreases cell viability by other actions such as glycation besides high osmotic pressure. However, both EGT (2 μM) and HIP (2 μM) alone significantly attenuated cytotoxicity induced by GLU + MGO.

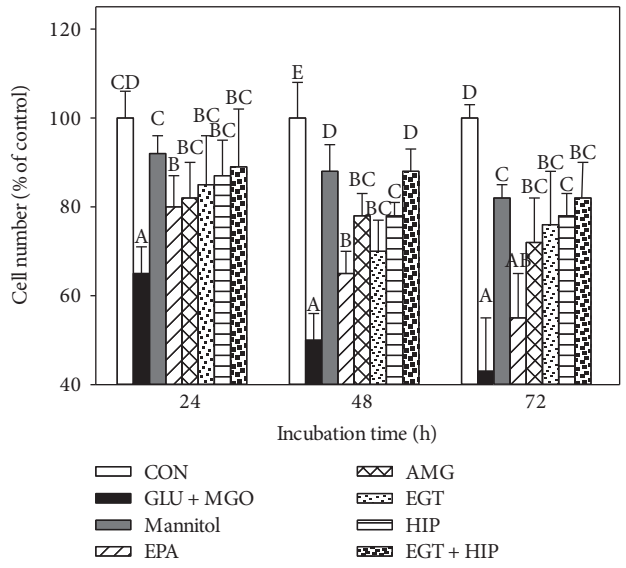

Figure 2: Effects of ergothioneine (EGT), hispidin (HIP), and EGT + HIP on viability of PC12 cells treated with 30 mM glucose and 30 μM methylglyoxal (GLU + MGO). PC12 cells were pretreated with epalrestat (EPA), aminoguanidine (AMG), ETG, HIP, and EGT + HIP for 2 h and incubated with GLU + MGO or mannitol for 24, 48, and 72 h. Cell viability was estimated by the trypan blue dye exclusion method. Values (means ± SD of triplicate tests) without a superscript letter are significantly different ($P < 0.05$).

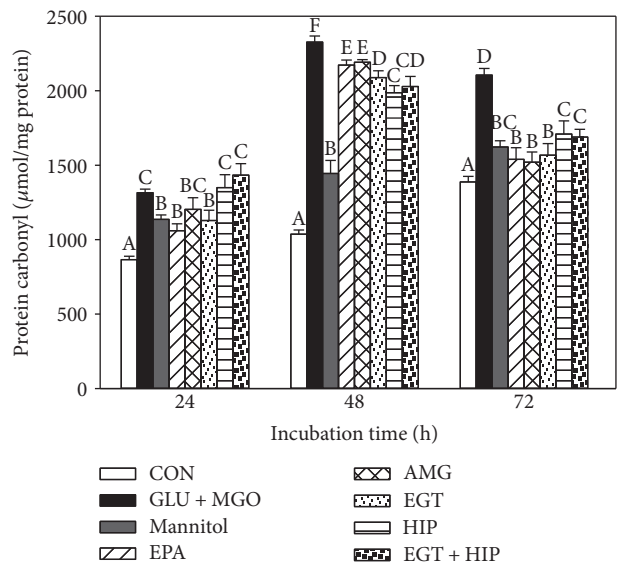

Figure 3: Effects of ergothioneine (EGT), hispidin (HIP), and EGT+HIP on protein carbonyl levels in PC12 cells treated with 30 mM glucose and 30 μM methylglyoxal (GLU + MGO). PC12 cells were pretreated with epalrestat (EPA), aminoguanidine (AMG), ETG, HIP, and EGT + HIP for 2 h and incubated with GLU + MGO or mannitol for 24, 48, and 72 h. Values (means ± SD of triplicate tests) without a superscript letter are significantly different ($P < 0.05$).

EGT and HIP were significantly more effective than 10 μM EPA and 100 nM AMG (55% and 72% at 72 h of incubation) ($P < 0.05$). The cell viability of the EGT + HIP group increased to 82–90% after 24, 48, and 72 h of incubation, and the viability was not significantly different ($P > 0.05$) from that in the EGT or HIP group.

3.3. Effects of EGT, HIP, and EGT + HIP on Protein Carbonyl Levels in PC12 Cells under Hyperglycemic Condition. As shown in Figure 3, treatment with GLU + MGO significantly increased protein carbonyl levels in PC12 cells at each incubation time (24, 48, and 72 h), and the highest level was detected at 48 h of incubation. Treatment with EGT alone significantly decreased protein carbonyl, and the effect of EGT was roughly comparable to those of 10 μM EPA and 100 nM AMG. HIP alone significantly decreased protein carbonyls at 48 and 72 h, but not at 24 h, of incubation, and EGT + HIP produced no synergistic inhibition on protein carbonyls, as compared with the GLU + MGO group.

3.4. Effects of EGT, HIP, and EGT + HIP on ROS in PC12 Cells under Hyperglycemic Condition. As shown in Figure 4(a), after 48 and 72 h of incubation, the ROS levels in PC12 cells induced by GLU + MGO (36% and 43.6%) were significantly increased, as compared with that in the control group (12.7% and 15.3%, at 48 and 72 h, resp.). In the mannitol group, the ROS levels (12.1% at 48 h and 18.5% at 72 h) were not significantly different from those of the control. The result revealed that the intracellular ROS production induced by GLU + MGO was not due to the osmotic effect. In addition, intracellular ROS levels in the EGT, HIP, and EGT + HIP groups were significantly decreased (to 28.1%, 25.2%, and 23.4% after 72 h of incubation, resp.), as compared with that in the GLU + MGO group (Figure 4(b)). Treatment with EGT, HIP, or EGT + HIP inhibited ROS by 54.8%, 65.0%, and 71.4%, respectively, but no synergistic effect of EGT and HIP was observed. The inhibitory effect of EGT + HIP on ROS (71.4% at 72 h) in PC12 cells under high-glucose concentration was stronger than that of EPA (21.6%) and AMG (61.1%).

3.5. Effects of EGT, HIP, and EGT + HIP on AGE and RAGE Levels in PC12 Cells under Hyperglycemic Condition. Table 1 shows that the AGE and RAGE levels were significantly increased in the GLU + MGO group, as compared with those in the control group ($P < 0.05$) during incubation of PC12 cells for 72 and 96 h. AGE levels were significantly higher (at 72 h) in cells treated with EGT, HIP, or EGT + HIP than in their absence (control), because after adding the EGT, HIP, or EGT + HIP for 2 h, the cells were added with GLU + MGO. After PC12 cells were treated with GLU + MGO for 72 h, AGE levels in cells treated with EGT, HIP, or EGT + HIP were significantly lower (at 72 h) than those of the GLU + MGO-treated group but were significantly higher than those of the control group. AGE and RAGE levels in the group treated with mannitol (to induce high osmotic pressure) were significantly higher than those in the control group ($P < 0.05$) but were significantly lower than those in the GLU + MGO group after 72 h of incubation ($P < 0.05$). AGE level of the mannitol-treated group was not

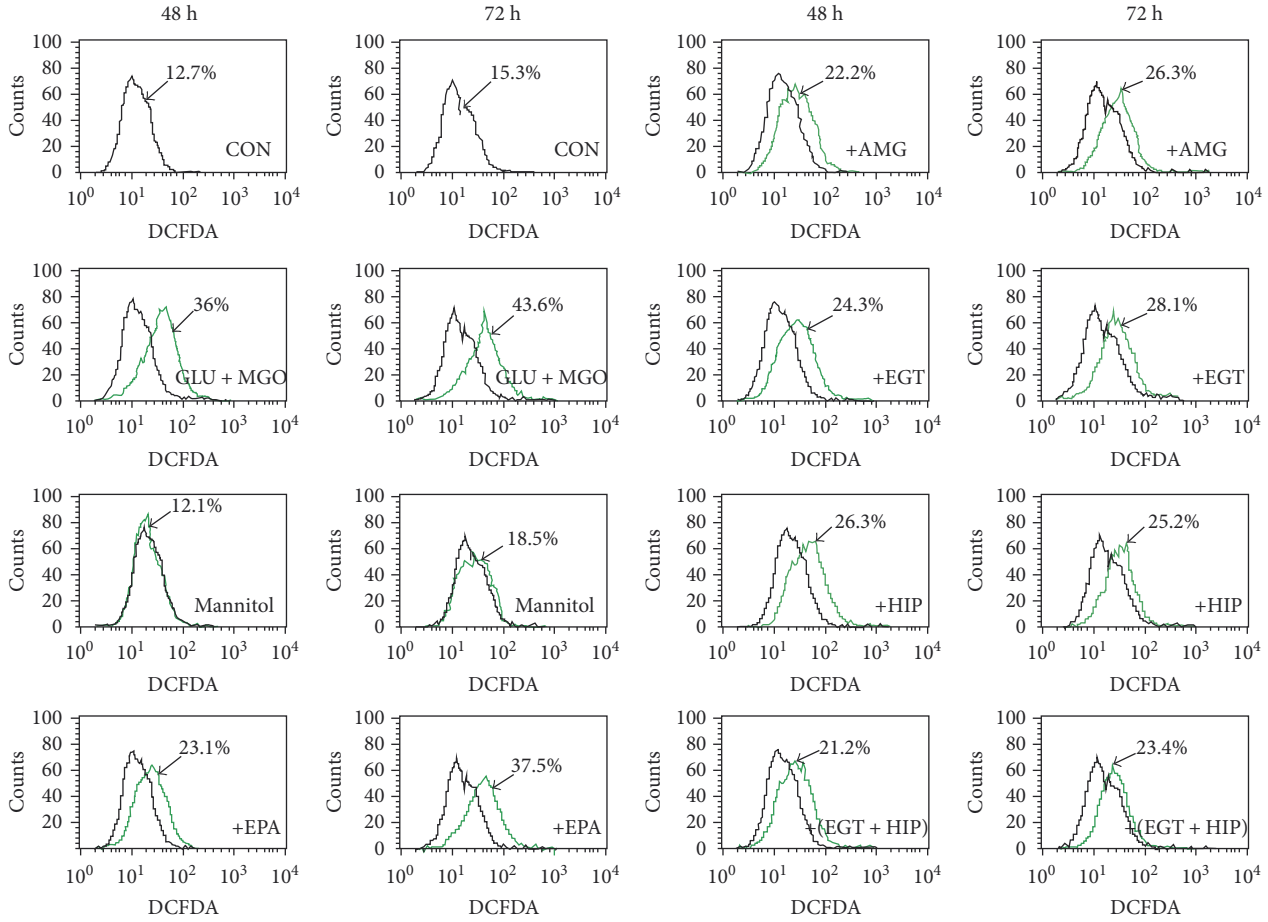

Figure 4: Effects of ergothioneine (EGT), hispidin (HIP), and EGT + HIP on ROS production in PC12 cells treated with 30 mM glucose and 30 μM methylglyoxal (GLU + MGO). PC12 cells were pretreated with epalrestat (EPA), aminoguanidine (AMG), ETG, HIP, and EGT + HIP for 2 h and incubated with GLU + MGO or mannitol for 48 h and 72 h. (a) Cells were collected and incubated with 5 μmol/L DCFH-DA at 37°C for 30 min, washed with PBS, and evaluated by flow cytometry. (b) Quantitative analysis indicated ROS levels in PC12 cells. Values (means ± SD of triplicate tests) without a superscript letter are significantly different ($P < 0.05$).

Table 1: Effects of ergothioneine, hispidin, and ergothioneine + hispidin on production of advanced glycated end products and receptor for advanced glycated end products in PC12 cells induced by glucose + methylglyoxal.

Treatments	AGE (ng/mL)				RAGE (ng/mL)			
	72 h	IP %[3]	96 h	IP %	72 h	IP %	96 h	IP %
CON	191 ± 10^{a4}		302 ± 13^{bc}		2.8 ± 0.5^{a}		11.4 ± 1.0^{a}	
Mannitol	230 ± 6^{bc}		308 ± 10^{bc}		24.9 ± 1.2^{b}		24.1 ± 0.5^{c}	
GLU + MGO[1]	294 ± 18^{d}		411 ± 11^{d}		32.0 ± 1.6^{c}		43.0 ± 1.1^{e}	
+EPA	235 ± 11^{bc}	20.07	299 ± 9^{bc}	27.25	32.6 ± 1.3^{c}	−1.88	25.1 ± 0.6^{c}	41.63
+AMG	202 ± 9^{a}	31.29	269 ± 8^{b}	34.55	29.9 ± 1.0^{c}	6.56	20.7 ± 1.7^{b}	51.86
+EGT	264 ± 14^{c}	10.20	275 ± 8^{b}	33.09	26.9 ± 1.2^{b}	15.94	20.3 ± 0.7^{b}	52.79
+HIP	296 ± 14^{d}	−0.68	296 ± 10^{bc}	27.98	31.7 ± 2.4^{c}	0.94	28.6 ± 0.9^{d}	33.49
+(EGT + HIP)	231 ± 10^{bc}	21.43	233 ± 14^{a}	43.31	24.5 ± 2.6^{b}	23.44	22.9 ± 1.5^{bc}	46.74

[1]GLU + MGO: 30 mM glucose (GLU) and 30 μM methylglyoxal (MGO); EPA: epalrestat; AMG: aminoguanidine. [2]PC12 cells were pretreated with EPA, AMG, ETG, HIP, and EGT + HIP for 2 h and incubated with GLU + MGO for 72 h and 96 h. [3]IP% = [1 − (sample/(GLU + MGO))] × 100. [4]Values (means ± SD of triplicate tests) without a superscript letter are significantly different ($P < 0.05$).

significantly different from that of the control group after 96 h incubation ($P > 0.05$), and RAGE level did not increase after 72–96 h of incubation. These results indicate that GLU + MGO increases AGE and RAGE levels by glycation besides high osmotic pressure.

Treatment of EGT alone significantly decreased AGE and RAGE levels, as compared with that of GLU + MGO, and the effect was comparable to that of EPA and AMG treatment alone. However, treatment of HIP alone only significantly decreased AGE or RAGE levels at 96 h (but not at 72 h) of incubation, as compared with that of GLU + MGO. EGT + HIP significantly inhibited AGE and RAGE levels induced by GLU + MGO, but the combined treatment only significantly decreased AGE levels at 96 h of incubation, as compared with the EGT treatment alone. The combined treatment did not significantly decrease RAGE levels, as compared with that of EGT alone at either 72 or 96 h of incubation.

3.6. Effects of EGT, HIP, and EGT + HIP on NF-κB-Associated Pathways in PC12 Cells under Hyperglycemic Condition. As shown in Figure 5, after exposure of PC12 cells to GLU + MGO for 72 h, the cytoplasmic NF-κB was significantly decreased ($P < 0.05$) and the nuclear NF-κB was significantly increased ($P < 0.05$). However, no difference in cytoplasmic IκB was observed between the GLU + MGO and control groups ($P > 0.05$). In contrast, when PC12 cells were pretreated with EPA, AMG, HIP, or EGT, nuclear NF-κB activation induced by GLU + MGO was markedly inhibited ($P < 0.05$). We also found that EGT + HIP increases the regulation of cytoplasmic NF-κB expression and decrease nuclear NF-κB expression compared with EGT or HIP alone. The expression of cyt-IκB in cells treated with EGT + HIP was somewhat decreased, but not significantly decreased, as compared with that of the control. The quantified results of cytoplasmic IκB and NF-κB and nuclear NF-κB protein levels are presented in Figures 5(b), 5(c), and 5(d), respectively. These results suggest that EGT, HIP, and EGT + HIP inhibit GLU + MGO-mediated inflammatory responses through NF-κB cleavage from IκB.

4. Discussion

The aim of this study was to evaluate the neuroprotective effect of EGT, HIP, and EGT + HIP on hyperglycemic condition-mediated cytotoxicity and the possible pathways in PC12 cells for gaining insights to prevent cognitive impairment induced by DM. In Figure 1, we provide the evidence that GLU + MGO more strongly decreased the cell viability in PC12 cells than did GLU or MGO alone. Thus, GLU + MGO was used as a glycemic-inducing agent in the following experiment. In our study, we found that cytotoxicity, protein carbonyl levels, and ROS levels were significantly increased under hyperglycemic condition. Both EGT and HIP alone can increase cell viability, ameliorate the antioxidant status, and reduce glycation levels in PC12 cells. Though EGT + HIP demonstrated higher cell viability, ROS production, and cytoplasmic NF-κB expression than EGT or HIP alone, no synergistic effect was observed.

Numerous studies have reported the role of EGT in diseases and its physiological antioxidant activities under experimental conditions involving oxidative stress [15]. Cheah et al. [36] demonstrated that declining EGT levels in elderly subjects are associated with age and incidence of mild cognitive impairment. EGT ameliorates the response to acetylcholine in the arteries of rats with streptozotocin-induced diabetes and reduces diabetic embryopathy in pregnant rats with diabetes, probably through the modulation of hyperglycemia-mediated oxidative stress [37]. Servillo et al. [38] indicated that the antioxidant mechanisms of EGT may provide new perspectives in targeted therapies against the production of ROS in diabetes. Our results also revealed that EGT significantly decreased ROS and protein carbonyl levels induced by GLU + MGO in PC12 cells. In addition, EGT supplementation decreased the secretion of AGE and RAGE in PC12 cells and inhibited the expression of the NF-κB transcription factor in the nucleus. These results demonstrate that EGT, through its antioxidant activities, can mitigate the damage caused by DE.

HIP, a PKC inhibitor, possesses strong antioxidant, anticancer, and antidiabetic activities [26, 29, 39]. HIP exhibits

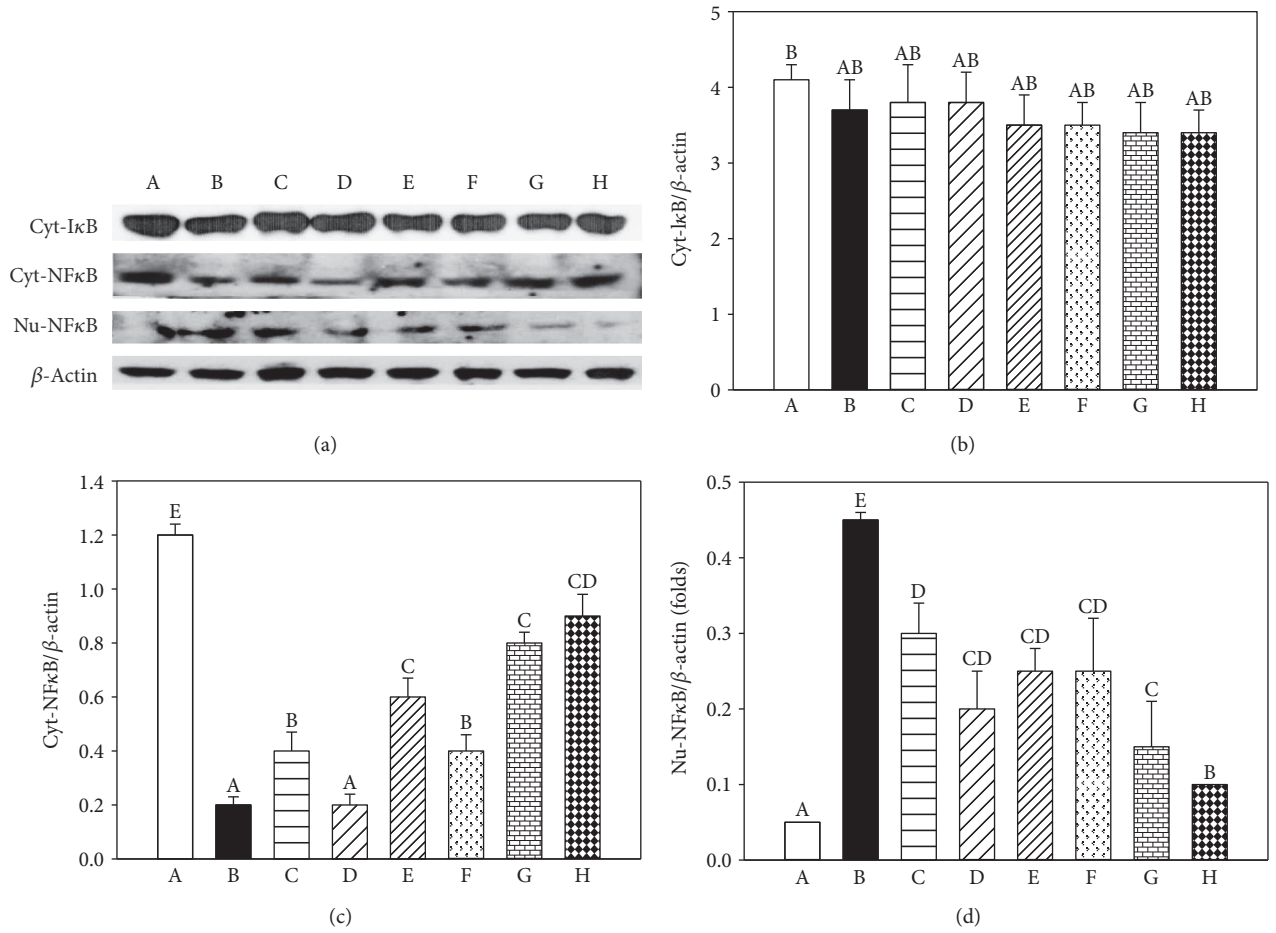

Figure 5: Effects of ergothioneine (EGT), hispidin (HIP), and EGT + HIP on cytoplasm IκB (Cyt-IκB), cytoplasm NF-κB (Cyt-NF-κB), and nuclear NF-κB (Nu-NFκB) protein expression in PC12 cells treated with 30 mM glucose and 30 μM methylglyoxal GLU + MGO) or 30 mM mannitol (to exclude the impact of glucose osmosis). β-Actin serves as an internal control. PC12 cells were pretreated with epalrestat (EPA), aminoguanidine (AMG), ETG, HIP, and EGT + HIP for 2 h and incubated with GLU + MGO for 72 h. A: control; B: GLU + MGO; C: 30 mM mannitol; D: 10 μM EPA; E: 100 nM AMG; F: 2 μM EGT; G: 2 μM HIP; H: 2 μM EGT + 2 μM HIP. (b–d) Quantitative data for Cyt-IκB, Cyt-NF-κB, and Nu-NF-κB expression. A portion of the protein (50 μg) was loaded to 10% SDS-PAGE. Values (means ± SD of triplicate tests) without a superscript letter are significantly different ($P < 0.05$).

potent α-glucosidase inhibitor activity, with IC_{50} value of 297 μg/mL, and aldose reductase inhibitor activity, with IC_{50} value of 48 μg/mL [39]. These findings suggest that HIP may be an effective antidiabetic agent. However, to the best of our knowledge, no study has examined the action of HIP against oxidative stress or the detailed molecular mechanism underlying its preventive effect against DE. Our present results indicated that HIP significantly decreased AGE and RAGE levels induced by GLU + MGO at 96 h of incubation. In addition, HIP inhibited the levels of ROS and protein carbonyl as well as the activation of NF-κB transcription factor to obstruct mitochondria-associated apoptosis pathways, leading to an increase in cell viability. Epalrestat is an aldose reductase inhibitor that is used for the improvement of subjective neuropathy symptoms [40]. Recently, hispidin was shown to exhibit potent aldose reductase inhibitory activity. Thus, we used epalrestat as a positive control to understand whether hispidin has protective effects on PC12 cells in addition to aldose reductase inhibitory effect.

NF-κB is a pleiotropic regulator of many cellular signaling pathways, providing a mechanism for the cells in response to various stimuli associated with inflammation and oxidative stress. IκB degradation triggers NF-κB release, and the nuclear-translocated heterodimer (or homodimer) can associate with the κB sites of promoter to regulate the gene transcription [41]. NF-κB can regulate the transcription of genes such as chemokines, cytokines, proinflammatory enzymes, adhesion molecules, and other factors to modulate the neuronal survival [41]. Both high glucose and ROS activate signal transduction cascade (PKC, mitogen-activated protein kinases, and janus kinase/signal transducers and activators of transcription) and transcription factors (NF-κB, activated protein-1, and specificity protein 1) further promote the formation of AGEs [42]. Morgan and Liu [43] pointed out that ROS interacts with NF-κB signaling pathways in many ways. The transcription of NF-κB-dependent genes influences the levels of ROS in the cell, and in turn, the levels of NF-κB activity are regulated by the levels of ROS.

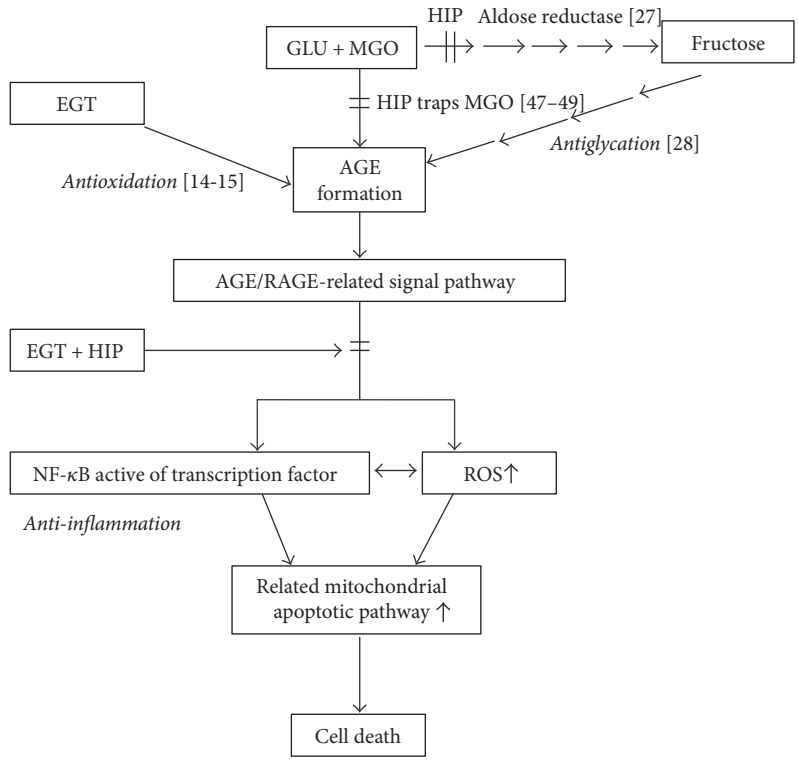

Figure 6: Proposed protective pathways of ergothioneine and hispidin against glycation induced by glucose + methylglyoxal in PC12 cells.

It is true that blots of cyt-NFκB had higher density than those of Nu-NFκB, but this only occurred in the control group. In contrast, in GLU + MGO-treated PC12 cells, Nu-NFκB expression was significantly increased, and cyt-NFκB expression was decreased. Besides, ROS, protein carbonyl, and AGE levels were significantly induced by GLU + MGO. Thus, our data suggested that GLU + MGO increased NF-κB translocation. The present study showed that EGT and HIP protect PC12 cell damage under high-glucose condition by inhibiting NF-κB transcription cascade to inhibit ROS production and AGE formation.

A previous study reported that the binding of AGE to RAGE induces pathophysiological cascades linked to the downstream activation of NF-κB, which in turn leads to ROS generation [11] and inflammatory processes [44]. Haslbeck et al. [45] reported that the AGE/RAGE/NF-κB pathway may contribute to the pathogenesis of polyneuropathy in impaired glucose tolerance. NF-κB is a transcription factor that upregulates the gene expression of proinflammatory cytokines and also is responsible for the induction of neuronal apoptosis. Activation of NF-κB also suppresses the expression of antioxidant genes by downregulating the Nrf-2 pathway and thus indirectly weakening the innate antioxidant defense [46]. Several natural inhibitors of NF-κB such as curcumin, resveratrol, and melatonin have been used in experimental diabetic animals. The use of NF-κB inhibitors can prevent the AGE-mediated proinflammatory cytokine production and thus halts the events associated with neuroinflammation [11].

Our results showed that the AGE/RAGE/NF-κB system was significantly activated in the GLU + MGO-treated cells but was markedly inhibited by EGT + HIP. These results suggest that EGT + HIP protects PC12 cells against GLU + MGO-induced cytotoxicity by inhibiting the AGE/RAGE/NF-κB pathway. We hypothesize that EGT + HIP involved two quite different pathways in synergistic effects of glycation; one was the inhibition of aldose reductase activity (HIP) [39], and the other was the inhibition of the production of reactive oxygen species in the AGE/RAGE/NF-κB pathway (EGT) [38]. Thus, we speculate that EGT, HIP, and EGT + HIP have the potential to improve DE induced by DM and that their effects are comparable to those of AMG (an AGE inhibitor) added at 100 nM and better than those of EPA (an aldose reductase inhibitor) added at 10 μM.

Combination of EGT and HIP had the ability of the synergistic effects of inhibition of the formation of AGE to inhibit the AGE/RAGE/NF-κB pathway; however, EGT and HIP did not exhibit a synergistic effect in increasing cell viability and decreasing protein carbonyl and ROS levels. However, EGT and HIP did not exhibit a synergistic effect in increasing cell viability and decreasing protein carbonyl and ROS levels. Intriguingly, our results displayed that the treatment with EGT in combination with HIP (EGT + HIP) was more effective than that with EGT or HIP alone in inhibiting the AGE/RAGE/NF-κB pathway induced by GLU + MGO in PC12 cells. Thus, we speculated that EGT + HIP plays synergistic role in antiglycation activity, but not antioxidant activity.

Evidence shows that tea polyphenols have strong MGO-trapping abilities to form mono- and di-MGO adducts under physiological conditions (pH 7.4, 37°C) [47, 48]. Shao et al.

[49] also reported that apple polyphenol-phloretin traps more than 80% MGO within 10 min, and phloridzin traps more than 70% MGO within 24 h under physiological conditions. Thus, HIP could trap MGO and lead to decreased AGE formation. In addition, S-cysteinyl compounds could react with polyphenol (catechin, chlorogenic acid, dihydrocaffeic acid, hydroxytyrosol, nordihydroguaiaretic acid, and rosmarinic acid) to form S-cysteinyl polyphenols under peroxidase-catalyzed oxidation [50]. Thus, we speculated that EGT could react with HIP to decrease the MGO-trapping ability of HIP. Therefore, this may explain why no synergistic effect in antioxidant activity of EGT + HIP in protecting PC12 cells.

5. Conclusion

In conclusion, the present study shows that HIP inhibits aldose reductase activity and reduces AGE/RAGE levels (i.e., the antiglycation pathway). HIP may also trap MGO directly [47–49]. HIP + EGT further reduces the activation of NF-κB leading to reduced inflammation and oxidative response in PC12 cells (Figure 6). In contrast, EGT can reduce AGE formation primarily through its antioxidant capacity. EGT and HIP do not show a synergistic protective effect in PC12 cells, possibly because EGT may react with HIP *in vitro*. *In vivo* studies are required to elucidate whether EGT and HIP exert a synergistic effect on protection against DE.

Conflicts of Interest

The authors declare that there are no conflicts of interest.

Acknowledgments

This study was supported by a grant from the National Science Council, ROC. (NSC 100-2313-B-235-001-MY3).

References

[1] M. Ristow, "Neurodegenerative disorders associated with diabetes mellitus," *Journal of Molecular Medicine*, vol. 82, pp. 510–529, 2004.

[2] Z. Arvanitakis, R. S. Wilson, J. L. Bienias, D. A. Evans, and D. A. Bennett, "Diabetes mellitus and risk of Alzheimer disease and decline in cognitive function," *Archives of Neurology*, vol. 61, pp. 661–666, 2004.

[3] Z. G. Li, W. Zhang, G. Grunberger, and A. A. Sima, "Hippocampal neuronal apoptosis in type 1 diabetes," *Brain Research*, vol. 946, pp. 221–231, 2002.

[4] A. A. Sima and Z. G. Li, "The effect of C-peptide on cognitive dysfunction and hippocampal apoptosis in type 1 diabetic rats," *Diabetes*, vol. 54, pp. 1497–1505, 2005.

[5] C. A. Grillo, G. G. Piroli, D. R. Rosell, E. K. Hoskin, B. S. McEwen, and L. P. Reagan, "Region specific increases in oxidative stress and superoxide dismutase in the hippocampus of diabetic rats subjected to stress," *Neuroscience*, vol. 121, pp. 133–140, 2003.

[6] T. H. Fleming, P. M. Humpert, P. P. Nawroth, and A. Bierhaus, "Reactive metabolites and AGE/RAGE-mediated cellular dysfunction affect the aging process - a mini-review," *Gerontology*, vol. 57, pp. 435–443, 2011.

[7] C. Toth, J. Martinez, and D. W. Zochodne, "RAGE, diabetes, and the nervous system," *Current Molecular Medicine*, vol. 7, pp. 766–776, 2007.

[8] S. Di Loreto, V. Zimmitti, P. Sebastiani, C. Cervelli, S. Falone, and F. Amicarelli, "Methylglyoxal causes strong weakening of detoxifying capacity and apoptotic cell death in rat hippocampal neurons," *The International Journal of Biochemistry and Cell Biology*, vol. 40, pp. 245–257, 2008.

[9] O. Arancio, H. P. Zhang, X. Chen et al., "RAGE potentiates Aβ-induced perturbation of neuronal function in transgenic mice," *The EMBO Journal*, vol. 23, pp. 4096–4105, 2004.

[10] J. Berlanga, D. Cibrian, I. Guillen et al., "Methylglyoxal administration induces diabetes-like microvascular changes and perturbs the healing process of cutaneous wounds," *Clinical Science*, vol. 109, pp. 83–95, 2005.

[11] R. Sandireddy, V. G. Yerra, A. Areti, P. Komirishetty, and A. Kumar, "Neuroinflammation and oxidative stress in diabetic neuropathy: futuristic strategies based on these targets," *International Journal of Endocrinology*, vol. 2014, Article ID 674987, 10 pages, 2014.

[12] D. B. Melville, W. H. Horner, C. C. Otken, and M. L. Ludwig, "Studies on the origin of ergothioneine in animals," *The Journal of Biological Chemistry*, vol. 213, pp. 61–68, 1955.

[13] N. Nakamichi, T. Taguchi, H. Hosotani et al., "Functional expression of carnitine/organic cation transporter OCTN1 in mouse brain neurons: possible involvement in neuronal differentiation," *Neurochemistry International*, vol. 61, pp. 1121–1132, 2012.

[14] O. I. Aruoma, M. Whiteman, T. G. England, and B. Halliwell, "Antioxidant action of ergothioneine: assessment of its ability to scavenge peroxynitrite," *Biochemical and Biophysical Research Communications*, vol. 231, pp. 389–391, 1997.

[15] I. K. Cheah and B. Halliwell, "Ergothioneine; antioxidant potential, physiological function and role in disease," *Biochimica et Biophysica Acta (BBA) - Molecular Basis of Disease*, vol. 1822, pp. 784–793, 2012.

[16] J. A. Moncaster, D. T. Walsh, S. M. Gentleman, L. S. Jen, and O. I. Aruoma, "Ergothioneine treatment protects neurons against *N*-methyl-D-aspartate excitotoxicity in an in vivo rat retinal model," *Neuroscience Letters*, vol. 328, pp. 55–59, 2002.

[17] J. H. Jang, O. I. Aruoma, L. S. Jen, H. Y. Chung, and Y. J. Surh, "Ergothioneine rescues PC12 cells from β-amyloid-induced apoptotic death," *Free Radical Biology and Medicine*, vol. 36, pp. 288–299, 2004.

[18] T. Y. Song, C. L. Chen, J. W. Liao, O. HC, and M. S. Tsai, "Ergothioneine protects against neuronal injury induced by cisplatin both in vitro and in vivo," *Food and Chemical Toxicology*, vol. 48, pp. 3492–3499, 2010.

[19] N. C. Yang, H. C. Lin, W. JH et al., "Ergothioneine protects against neuronal injury induced by β-amyloid in mice," *Food and Chemical Toxicology*, vol. 50, pp. 3902–3911, 2012.

[20] T. Y. Song, H. C. Lin, C. L. Chen, W. JH, J. W. Liao, and M. L. Hu, "Ergothioneine and melatonin attenuate oxidative stress and protect against learning and memory deficits in C57BL/6J mice treated with D-galactose," *Free Radical Research*, vol. 48, pp. 1049–1060, 2014.

[21] N. A. Ali, J. Lüdtke, H. Pilgrim, and U. Lindequist, "Inhibition of chemiluminescence response of human mononuclear cells

and suppression of mitogen-induced proliferation of spleen lymphocytes of mice by hispolon and hispidin," *Pharmazie*, vol. 51, pp. 667–670, 1996.

[22] I. H. Park, S. K. Chung, K. B. Lee et al., "An antioxidant hispidin from the mycelial cultures of *Phellinus linteus*," *Archives of Pharmacal Research*, vol. 27, pp. 615–618, 2004.

[23] H. G. Kim, D. H. Yoon, W. H. Lee et al., "*Phellinus linteus* inhibits inflammatory mediators by suppressing redox-based NF-κB and MAPKs activation in lipopolysaccharide-induced RAW 264.7 macrophage," *Journal of Ethnopharmacology*, vol. 114, pp. 307–315, 2007.

[24] T. Y. Song, H. G. Lin, N. C. Yang, and M. L. Hu, "Antiproliferative and antimetastatic effects of the ethanolic extract of *Phellinus igniarius* (Linnearus: Fries) Quelet," *Journal of Ethnopharmacology*, vol. 115, pp. 50–56, 2008.

[25] W. Chen, L. Feng, Z. Huang, and H. Su, "Hispidin produced from *Phellinus linteus* protects against peroxynitrite- mediated DNA damage and hydroxyl radical generation," *Chemico-Biological Interactions*, vol. 199, pp. 137–142, 2012.

[26] C. Gonindard, C. Bergonzi, C. Denier et al., "Synthetic hispidin, a PKC inhibitor, is more cytotoxic toward cancer cells than normal cells in vitro," *Cell Biology and Toxicology*, vol. 13, pp. 141–153, 1997.

[27] Y. S. Lee, Y. H. Kang, J. Y. Jung et al., "Inhibitory constituents of aldose reductase in the fruiting body of *Phellinus linteus*," *Biological and Pharmaceutical Bulletin*, vol. 31, pp. 765–768, 2008.

[28] Y. S. Lee, Y. H. Kang, J. Y. Jung et al., "Protein glycation inhibitors from the fruiting body of *Phellinus linteus*," *Biological and Pharmaceutical Bulletin*, vol. 31, pp. 1968–1972, 2008.

[29] J. S. Jang, J. S. Lee, J. H. Lee et al., "Hispidin produced from *Phellinus linteus* protects pancreatic β-cells from damage by hydrogen peroxide," *Archives of Pharmacal Research*, vol. 33, pp. 853–861, 2010.

[30] J. H. Lee, J. S. Lee, Y. R. Kim et al., "Hispidin isolated from *Phellinus linteus* protects against hydrogen peroxide-induced oxidative stress in pancreatic MIN6N β-cells," *Journal of Medicinal Food*, vol. 14, pp. 1431–1438, 2011.

[31] J. Liu, J. Mao, Y. Jiang et al., "AGEs induce apoptosis in rat osteoblast cells by activating the caspase-3 signaling pathway under a high-glucose environment in vitro," *Applied Biochemistry and Biotechnology*, vol. 178, pp. 1015–1027, 2016.

[32] A. G. Miller, D. G. Smith, M. Bhat, and R. H. Nagaraj, "Glyoxalase I is critical for human retinal capillary pericyte survival under hyperglycemic conditions," *The Journal of Biological Chemistry*, vol. 281, pp. 11864–11871, 2006.

[33] C. S. Yang, H. M. Lee, J. Y. Lee et al., "Reactive oxygen species and p47phox activation are essential for the *Mycobacterium tuberculosis*-induced pro-inflammatory response in murine microglia," *Journal of Neuroinflammation*, vol. 4, p. 27, 2007.

[34] A. Z. Reznick and L. Packer, "Oxidative damage to proteins: spectrophotometric method for carbonyl assay," *Methods in Enzymology*, vol. 233, pp. 357–363, 1994.

[35] M. A. Seaman, J. R. Levin, and R. C. Serlin, "New developments in pairwise multiple comparisons: some powerful and practicable procedures," *Psychological Bulletin*, vol. 110, pp. 577–586, 1991.

[36] I. K. Cheah, L. Feng, R. M. Tang, K. H. Lim, and B. Halliwell, "Ergothioneine levels in an elderly population decrease with age and incidence of cognitive decline; a risk factor for neurodegeneration?," *Biochemical and Biophysical Research Communications*, vol. 478, pp. 162–167, 2016.

[37] R. W. Li, C. Yang, A. S. Sit et al., "Uptake and protective effects of ergothioneine in human endothelial cells," *The Journal of Pharmacology and Experimental Therapeutics*, vol. 350, pp. 691–700, 2014.

[38] L. Servillo, N. D'Onofrio, R. Casale et al., "Ergothioneine products derived by superoxide oxidation in endothelial cells exposed to high-glucose," *Free Radical Biology and Medicine*, vol. 108, pp. 8–18, 2017.

[39] G. J. Huang, W. T. Hsieh, H. Y. Chang, S. S. Huang, Y. C. Lin, and Y. H. Kuo, "α-Glucosidase and aldose reductase inhibitory activities from the fruiting body of *Phellinus merrillii*," *Journal of Agricultural and Food Chemistry*, vol. 59, pp. 5702–5706, 2011.

[40] M. A. Ramirez and N. L. Borja, "Epalrestat: an aldose reductase inhibitor for the treatment of diabetic neuropathy," *Pharmacotherapy*, vol. 28, pp. 646–655, 2008.

[41] R. H. Shih, C. Y. Wang, and C. M. Yang, "NF-kappaB signaling pathways in neurological inflammation: a mini review," *Frontiers in Molecular Neuroscience*, vol. 8, p. 77, 2015.

[42] H. B. Lee, M. R. Yu, Y. Yang, Z. Jiang, and H. Ha, "Reactive oxygen species-regulated signaling pathways in diabetic nephropathy," *Journal of the American Society of Nephrology*, vol. 14, no. 8, Supplement 3, pp. S241–S245, 2003.

[43] M. J. Morgan and Z. G. Liu, "Crosstalk of reactive oxygen species and NF-κB signaling," *Cell Research*, vol. 21, pp. 103–115, 2011.

[44] S. D. Yan, A. M. Schmidt, G. M. Anderson et al., "Enhanced cellular oxidant stress by the interaction of advanced glycation end products with their receptors/binding proteins," *The Journal of Biological Chemistry*, vol. 269, pp. 9889–9897, 1994.

[45] K. M. Haslbeck, E. Schleicher, A. Bierhaus et al., "The AGE/RAGE/NF-κB pathway may contribute to the pathogenesis of polyneuropathy in impaired glucose tolerance (IGT)," *Experimental and Clinical Endocrinology and Diabetes*, vol. 113, pp. 288–291, 2005.

[46] V. Ganesh Yerra, G. Negi, S. S. Sharma, and A. Kumar, "Potential therapeutic effects of the simultaneous targeting of the Nrf2 and NF-κB pathways in diabetic neuropathy," *Redox Biology*, vol. 1, pp. 394–397, 2013.

[47] S. Sang, X. Shao, N. Bai, C. Y. Lo, C. S. Yang, and C. T. Ho, "Tea polyphenol (−)-epigallocatechin-3-gallate: a new trapping agent of reactive dicarbonyl species," *Chemical Research in Toxicology*, vol. 20, pp. 1862–1870, 2007.

[48] D. Tan, Y. Wang, C. Y. Lo, and C. T. Ho, "Methylglyoxal: its presence and potential scavengers," *Asia Pacific Journal of Clinical Nutrition*, vol. 17, Supplement 1, pp. 261–264, 2008.

[49] X. Shao, N. Bai, K. He, C. T. Ho, C. S. Yang, and S. Sang, "Apple polyphenols, phloretin and phloridzin: new trapping agents of reactive dicarbonyl species," *Chemical Research in Toxicology*, vol. 21, pp. 2042–2050, 2008.

[50] S. Honda, Y. Miura, T. Masuda, and A. Masuda, "Effective conversion of metmyoglobin to oxymyoglobin by cysteine-substituted polyphenols," *Journal of Agricultural and Food Chemistry*, vol. 64, pp. 806–811, 2016.

Hindawi
Oxidative Medicine and Cellular Longevity
Volume 2017, Article ID 3269379, 21 pages
https://doi.org/10.1155/2017/3269379

Research Article

MicroRNA-34a: A Key Regulator in the Hallmarks of Renal Cell Carcinoma

Eman A. Toraih,[1] Afaf T. Ibrahiem,[2] Manal S. Fawzy,[3,4] Mohammad H. Hussein,[5] Saeed Awad M. Al-Qahtani,[6] and Aly A. M. Shaalan[7,8]

[1]*Faculty of Medicine, Genetics Unit, Department of Histology and Cell Biology, Suez Canal University, P.O. 41522, Ismailia, Egypt*
[2]*Faculty of Medicine, Department of Pathology, Mansoura University, Mansoura, Egypt*
[3]*Faculty of Medicine, Department of Medical Biochemistry, Suez Canal University, P.O. 41522, Ismailia, Egypt*
[4]*Faculty of Medicine, Department of Medical Biochemistry, Northern Border University, Arar, Saudi Arabia*
[5]*Ministry of Health, Cairo, Egypt*
[6]*Faculty of Medicine, Department of Physiology, Jazan University, Jazan, Saudi Arabia*
[7]*Faculty of Medicine, Department of Histology and Cell Biology, Suez Canal University, Ismailia, Egypt*
[8]*Faculty of Medicine, Department of Anatomy and Histology, Jazan University, Jazan, Saudi Arabia*

Correspondence should be addressed to Eman A. Toraih; emantoraih@gmail.com
and Manal S. Fawzy; manal2_khashana@ymail.com

Received 29 April 2017; Revised 7 August 2017; Accepted 20 August 2017; Published 20 September 2017

Academic Editor: Simona G. Bungău

Renal cell carcinoma (RCC) incidence has increased over the past two decades. Recent studies reported microRNAs as promising biomarkers for early cancer detection, accurate prognosis, and molecular targets for future treatment. This study aimed to evaluate the expression levels of miR-34a and 11 of its bioinformatically selected target genes and proteins to test their potential dysregulation in RCC. Quantitative real-time PCR for miR-34a and its targets; *MET* oncogene; gene-regulating apoptosis (*TP53INP2* and *DFFA*); cell proliferation (*E2F3*); and cell differentiation (*SOX2* and *TGFB3*) as well as immunohistochemical assay for VEGFA, TP53, Bcl2, TGFB1, and Ki67 protein expression have been performed in 85 FFPE RCC tumor specimens. Clinicopathological parameter correlation and in silico network analysis have also implicated. We found RCC tissues displayed significantly higher miR-34a expression level than their corresponding noncancerous tissues, particularly in chromophobic subtype. *MET* and *E2F3* were significantly upregulated, while *TP53INP2* and *SOX2* were downregulated. ROC analysis showed high diagnostic performance of miR-34a (AUC = 0.854), *MET* (AUC = 0.765), and *E2F3* (AUC = 0.761). The advanced pathological grade was associated with strong TGFB1, VEGFA, and Ki67 protein expression and absent Tp53 staining. These findings indicate miR-34a along with its putative target genes could play a role in RCC tumorigenesis and progression.

1. Introduction

Renal cell carcinoma (RCC) accounts for approximately 3% of human malignancies, and its incidence appears to be increasing globally [1]. RCC is not a single disease; although it is derived from cells of the renal tubular epithelium, it has several histological subtypes which differ in their clinical outcome and biological features. It is classified into clear cell RCC accounting for (75%) of cases, papillary RCC (10–15%), chromophobe RCC (5%), collecting duct RCC (<1%), and unclassified subtype [2]. For the refinement of RCC therapeutic strategies, a better realization of the RCC-underlying molecular mechanisms will be mandatory [3].

Over the past few years, emerging numerous bioinformatic tools have been developed to identify candidate disease-causing genes [4], including microRNA (miRNA) genes. This class of noncoding RNAs is small, single stranded, and 19–25 nucleotide long that act as negative regulators involved in posttranscriptional silencing of the gene expression [5]. An aberrant miRNA expression could

contribute to cancer development and progression [6, 7] and could affect their target genes that are involved in many biological processes, such as cell differentiation, proliferation, apoptosis, metabolism, and development [8]. Recently, the potential therapeutic use of miRNAs has been evaluated due to their dynamic and reversible properties. This may include oncomir (oncogenic miRNA) inhibition, or tumor suppressor-miRNA replacement therapies [6, 9].

MicroRNA-34a gene (MIR-34A) that is located on chromosome 1p36 belongs to one of evolutionary-conserved miRNA families (MIR-34 family) that consists of three members: MIR-34A, MIR-34B, and MIR-34C [10]. MIR-34A has its own transcript and is expressed at higher levels than MIR-34B/C in most tissues, and this expression could be dysregulated in multiple diseases, especially in cancers [11]. It is involved in p53 pathways and is implicated in cell death/survival signaling, the cell cycle, and differentiation, thereby playing a regulatory role in carcinogenesis [12]. Previous studies have reported that several key molecules were identified as targets of miR-34a, including *Bcl-2* (B-cell lymphoma 2) [13], *TGFB* (transforming growth factor-beta) [14], the transcription inducer of cell cycle progression E2F3a [15], *MET* oncogene [16, 17], and vascular endothelial growth factor (*VEGF*) [18]. In addition, our bioinformatic analysis that has been discussed in details in Materials and Methods section of the current work has revealed other miRNA-34a-predicted target genes that could be involved in cancer-related biology, including genes for apoptosis [*TP53INP* (tumor protein p53 inducible nuclear protein), *Tp53*, and *DFFA* (DNA fragmentation factor subunit alpha)], cell proliferation (*Ki67*), and cell differentiation *SOX2* (sex-determining region Y-box 2). As miR-34a has many different targets in regulating different kinds of human cancer, Yu et al. [18] suggested the role of miR-34a is possibly tumor-specific and highly dependent on its targets in different cancer cells.

Whether miR-34a or any one of its selected aforementioned 11 putative target genes or proteins could be related to RCC pathogenesis and/or progression in our population still lacks of solid evidence. Therefore, we aimed to investigate the expression level of miR-34a and a panel of selected putative targets in an attempt to better understand the molecular mechanisms that underlie the tumorigenesis and progression of RCC. This could represent potential future therapeutic targets in renal cell carcinoma.

2. Materials and Methods

2.1. Study Population. Eighty-five archived formalin-fixed paraffin-embedded (FFPE) renal samples that have been taken from patients who underwent radical nephrectomy for a primary RCC and dating back for 3 years were collected from Pathology laboratory of Mansoura Oncology Center, Mansoura and Pathology laboratory of the Suez Canal University Hospital, Ismailia, Egypt. None of the patients received any neoadjuvant chemotherapy or radiotherapy. Complete clinicopathological data, including (patients' age, sex, and tumor's site and size), were obtained from patient medical records. Sections of cancer-free tissues adjacent to the tumor were cut, examined, and collected to serve as controls during the genetic profiling. Samples that were not homogeneous, histologically well-characterized primary renal cancer, nor had cancer-free adjacent tissues determined by an experienced pathologist have been excluded. The study was conducted in accordance with the guidelines in the Declaration of Helsinki and approved by the Medical Research Ethics Committee of Faculty of Medicine, Suez Canal University. Written informed consent was obtained from all participants before providing the archived tissue samples as part of their routine register in our University Teaching Hospitals.

2.2. Bioinformatic Selection of miRNA-34a and the Study Molecular Targets. Predicted and experimentally validated miRNAs that significantly target renal cell carcinoma KEGG pathway (hsa05211) were identified by DIANA-mirPath v3.0 web server via Reverse Search module and TarBase v7.0 pipeline [19]. The most top and highly significant miRNA involved in this pathway was hsa-miR-34a-5p ($p = 1.275767 e - 88$) with 28 target genes, including *MET* oncogene and three angiogenesis-related genes (*VEGFA*, *TGFB1*, *TGFB3*). Assessment of miR-34a regulatory roles in cancer biology was performed by DIANA-mirPath v3.0 online software (Figure 1).

The list of all experimentally validated target genes for miR-34a-5p was retrieved from miRTarBase v20 (http://mirtarbase.mbc.nctu.edu.tw/) [20] and DIANA-TarBase v7.0 (http://diana.imis.athena-innovation.gr/) [21]. A panel of other targets involved in cancer-related biology was chosen. It included genes for apoptosis (*Tp53*, *TP53INP2*, and *DFFA*), antiapoptosis (*BCL2*), cell proliferation (*E2F3* and *Ki67*), and cell differentiation (*SOX2*) (Figure 2). Structural analysis of MIR-34A gene and transcripts were retrieved from http://Ensembl.org. Gene expression of MIR-34A across normal human tissues was obtained from http://BioGPS.org and Expression Atlas. Complementary base pairing of miR-34a-5p seed region with the selected mRNA targets was confirmed by both http://microRNA.org resource [22] and miRTarBase v20. Prior publications demonstrating functional experimental validation of miRNA-target interactions by different methods (as luciferase reporter assay, western blot, microarray, qRT-PCR, and immunocytochemistry) are listed in Supplementary Table S1 available online at https://doi.org/10.1155/2017/3269379. A functional interaction network of selected target proteins was implemented using STRING v10 program (http://string-db.org), inferring protein-protein associations from coexpression data [23].

2.3. MicroRNA-34a and Gene Expression Analysis. Total RNA, including the small RNAs, was isolated from FFPE tissue sections (5 to 8 μm thick) using miRNeasy FFPE Kit (Qiagen, 217504) following the protocol supplied by the manufacturer. Briefly, after the removal of paraffin by xylene and washing the sample with ethanol several times, proteins were degraded by incubation with proteinase K solution at 45°C for a few hours and later incubation with DNAses for DNA digestion. Total RNA quantity and quality were measured by Nanodrop ND-1000 (NanoDrop Technologies, Wilmington, DE). Samples with a 260/280 nm absorbance

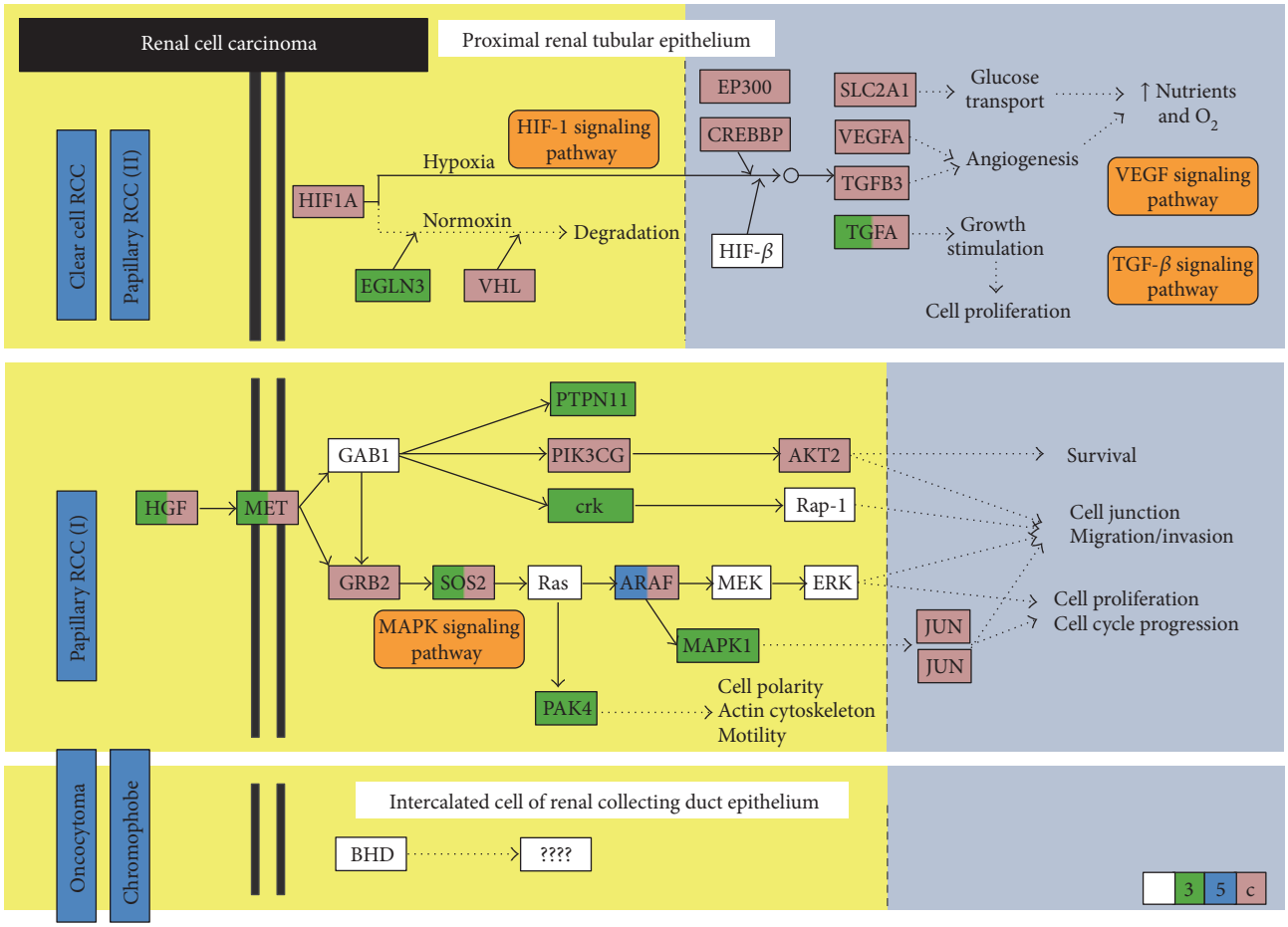

Figure 1: Predicted target genes of miRNA-34a in renal cell carcinoma pathway [KEGG hsa05211]. Disease pathways for each pathological subtype are shown. Hsa-miR-34a-5p can target several genes in RCC pathway. They have complementary regions at their 3′UTR, 5′UTR, or coding sequence (CDS): HIF-1, VEGF, and TGF-β signaling pathways in clear cell and papillary type II RCC (eosinophilic), as well as MAPK signaling pathway in papillary RCC type I (basophilic). However, candidate genes and the role of miR-34a in oncocytoma and chromophobic RCC pathways are still undetermined. Colored box: miRNA-34a target gene; green color: target on 3′UTR sequence; blue color: target on 5′UTR sequence; pink color: target on CDS; white box: not predicted target.

ratio less than 1.8 were discarded, and new sections of the corresponding tissue block were cut and purified, if possible. Subsequent reverse transcription (RT) and amplification of cDNA by real-time PCR using StepOne™ Real-Time PCR System (Applied Biosystems) were done as described in details previously [8, 24]. As the quantitation cycle (Cq) values of RNU6B small RNA and GAPDH were uniformly and stably expressed with no significant difference between cancer and noncancer tissues, they have been run for normalization of miRNA-34a and target gene mRNA expression analysis, respectively. All the PCR reactions were carried out in accordance with the Minimum Information for Publication of Quantitative Real-Time PCR Experiments guidelines [25]. Ten percent randomly selected study samples were reevaluated in separate runs for the study gene expressions to test the reproducibility of the qPCR which showed very close Cq value results and low standard deviations.

2.4. Histopathological Examination. Sections of 4 μm thickness have been cut from FFPE blocks of RCC tissues for routine H&E examination, and other sections were prepared on charged slides for immunohistochemistry. Examination of three tumor slides from each specimen was done with an Olympus CX31 light microscope. Photos were obtained by a PC-driven digital camera (Olympus E-620). Cases were reviewed to determine the histological type according to the International Society of Urological Pathology (ISUP) Vancouver Modification of WHO (2004) Histologic Classification of Kidney Tumors [26]. Nuclear grade is assessed according to Fuhrman et al. [27]. Tumors were staged according to the International Union Against Cancer [28].

2.5. Immunohistochemistry Examination and Analysis. Immunohistochemical analysis for p53 protein, Bcl2 protein, Ki67, TGFb, and VEGF with a labelled streptavidin-biotin-peroxidase complex technique was performed on tumor sections. The primary antibodies were mouse monoclonal antibodies against p53 (clone BP-53-12, monoclonal mouse anti-human p53, c-Kit, Genemed, California, USA, diluted 1 : 50), Bcl2 (code 226M98, monoclonal mouse anti-human

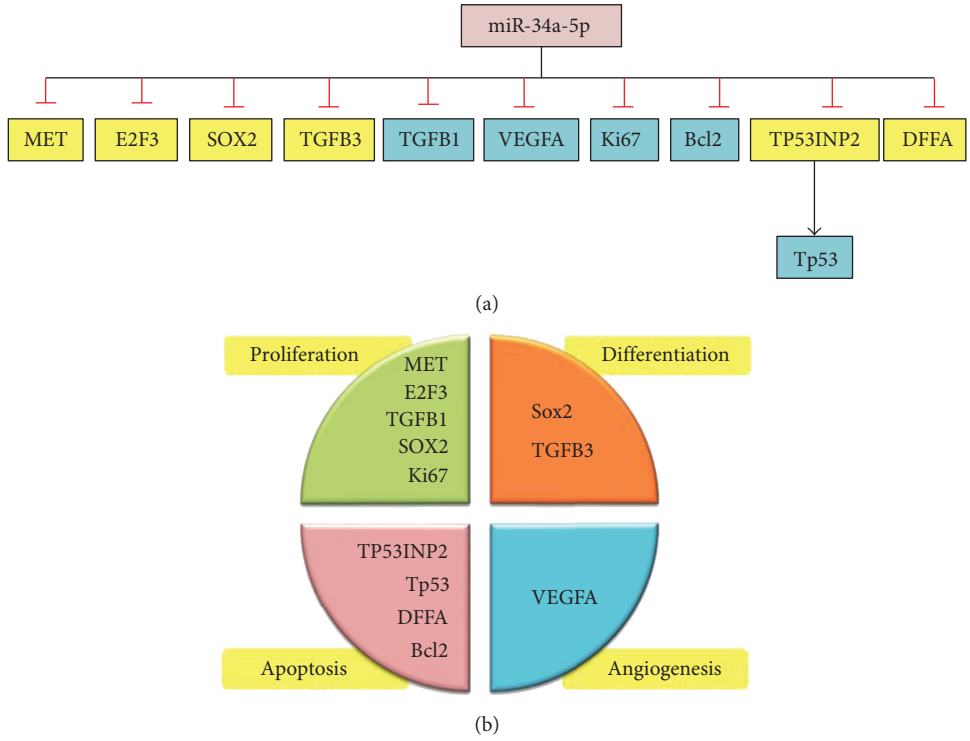

Figure 2: miR-34a target genes regulating the hallmarks of cancer. Eleven targets were investigated in the study. (a) List of targets analyzed by either immunohistochemistry (blue box) or quantitative real-time PCR (yellow box). (b) Classification of the miR-34a target genes and proteins according to their major role in cancer-related biology. They are enrolled in cellular differentiation, proliferation, apoptosis, and angiogenesis.

Bcl2, cell marque, prediluted), Ki67 (code number 1633, monoclonal mouse anti-human MIB1, DAKO corporation Carpinteria CA, USA, prediluted), TFGFB (ab9248, monoclonal mouse anti-TFGFB, abcam, USA, diluted 1 : 50), and VEGF (clone, GTX102643, monoclonal mouse anti-VEGFA, GeneTex, USA, diluted 1 : 50). A high sensitive kit has been used as a detection kit (DakoCytomation EnVision and dual link system peroxidase code K4061) using DAB as a chromogene. Antigen retrieval required pretreatment with 1 mM EDTA (at pH 8.0) for 20 minutes (p53, Bcl2, and VEGF) and 60 minutes (Ki67, and TGFb) in microwave oven. Proper positive and negative controls were performed. As a positive control, breast carcinoma has been run for p53, tonsils for Ki67, lymph node for Bcl2, and cells of proximal and distal convoluted tubules of nearby tumor-free kidney for TGFb. In addition, placental tissue was stained for VEGF as a positive control for VEGF antibody. As a negative control, sections were stained without the addition of a primary antibody.

For the immunohistochemistry assessment, examination of all prepared slides from each specimen was done with an Olympus CX31 light microscope. Photos were obtained from a PC-driven digital camera (Olympus E-620) and analyzed by Olympus Soft Imaging. Slides were scanned by ×40 magnification. Ten cellular areas were selected (i.e., the so-called hot spots) and evaluated at ×400 magnification. Positive p53 protein staining was defined as nuclear staining, and cytoplasmic staining was considered nonspecific and ignored. The percentage of tumor cell nuclei with positive staining was evaluated in relation to the total number of neoplastic nuclei in at least 10 fields observed at magnification ×400. Scoring of immunostained was categorized as mentioned in previous literature as follows: 3+ = high level (91–100% of positive cells), 2+ = medium level (11–90% of positive cells), 1+ = low level (up to 10% of positive cells), − = negative cells (0% of positive cells) [29].

Ki-67 antigen labeling was localized to the nucleus with a fine, strong, and homogenous brown granularity. Staining was considered positive if any nuclear staining was seen. Ki67 labeling index was done by calculating the ratio of positive nuclei in relation to the total number of neoplastic nuclei in 10 HPFs. Ki67 was considered to be abnormal when >10% tissue positivity was observed. The labeling index (number of positive tumor cells/total number of tumor cells expressed as a percentage) was calculated in every specimen. The Ki67 proliferation index was considered low if 0–30% of tumor cells was positive, moderate PI if 31–69% was positive, and high if ≥70% was positive. Unequivocal nuclear reactivity was considered positive [30, 31].

The BCL2 positivity was determined by cytoplasmic staining (brown) of neoplastic cells which are deep colored. The percentage of positive cells at the whole section after exclusion of the areas of reactive T cells was determined. It was scored negative if 5% or less of neoplastic cells was stained. The value of BCL2 was considered weak positive if 6% to less than 50% was brown stained, and strong positive if ≥50% of tumor cells was brown stained [32].

TGFB immunohistochemistry specimens were classified based on the intensity of staining as follows: weak or absent staining (< 10% of cells), intermediate (10–25%), focally

strong (25–50%), and strong (> 50% of cells) [33]. VEGF sections were considered positive for VEGF if the membranes or cytoplasm of more than 10% of tumor cells was stained [34].

2.6. Statistical Analysis. Data were managed using the R package (version 3.3.2). Categorical variables were compared using the chi-square (χ^2) or Fisher's exact tests where appropriate, while Mann–Whitney *U* (MW) and Kruskal-Wallis (KW) tests were used to compare continuous variables. The correlation between miR-34a level and mRNAs and protein expression was calculated by Spearman's rank correlation analysis. A two-tailed p value of < 0.05 was considered statistically significant. The receiver operating characteristic (ROC) curves were performed to get the best cutoff values of either miR-34a or mRNAs for discriminating RCC from noncancer tissues. The fold change of miRNA and mRNA expressions in each patient cancer tissue relative to the corresponding cancer-free tissue was calculated via Livak method based on the quantitative cycle (Cq) values with the following equation: relative quantity $= 2^{-\Delta\Delta Cq}$, where $\Delta\Delta C_q = (C_q \text{ miRNA}–C_q \text{ NBU6})_{RCC} – (C_q \text{ miRNA}–C_q \text{ NBU6})_{NAT}$ in case of miR-34a analysis and where $\Delta\Delta C_q = (C_q \text{ mRNA}–C_q \text{ GAPDH})_{RCC} – (C_q \text{ mRNA}–C_q \text{ GAPDH})_{NAT}$ in case of study gene target analysis [35].

3. Results

3.1. Baseline Characteristics of the Study Population. In the current study, 85 patients (32 females and 53 males) were enrolled in the study. Their age ranged from 20 to 79 years old with mean ± SD of 52.23 ± 11.12. Renal cancer samples were compared to normal tissues. There was no significant difference in age and gender between FFPE tumor samples and normal renal tissues ($p = 0.087$ and $p = 0.214$, resp.). The clinicopathological characteristics of renal cell carcinoma patients are demonstrated in Table 1. According to the 2004 WHO classification, several histological RCC subtypes were recognized in the study population. The most frequent histological subtypes included clear cell renal cell carcinomas (ccRCC), papillary renal cell carcinomas (pRCC), and chromophobe renal cell carcinomas (crRCC). Most cancer specimens were moderately or poorly differentiated; nevertheless, low proportions of tumors had high tumor size (T3), positive lymph node involvement, capsular and pelvic infiltration, and vascular invasion.

Table 1: Clinicopathological characteristics of renal cell carcinoma patients ($n = 85$).

Variables	*N*	%
Age		
20 y	5	5.9
40 y	47	55.3
60 y	33	38.8
Gender		
Females	34	40.0
Males	51	60.0
Affected side		
Right	47	44.7
Left	38	55.3
Histological type		
Clear cell RCC	47	55.3
Papillary RCC	15	17.6
Chromophobic RCC	13	15.3
Unclassified	10	11.8
Pathological grade		
Grade 1	11	12.9
Grade 2	51	60.0
Grade 3	23	27.1
Tumor size		
T1	25	29.4
T2	42	49.4
T3	18	21.2
LN involvement		
Negative	77	90.6
Positive	8	9.4
Capsular infiltration		
Negative	60	70.6
Positive	25	29.4
Vascular infiltration		
Negative	71	83.5
Positive	14	16.5
Renal pelvis infiltration		
Negative	79	92.9
Positive	6	7.1

Data are presented as *N* (number) and % (percentage); RCC: renal cell carcinoma; T: tumor size; LN: lymph node.

3.2. Gene and Protein Expression Analysis. Using qRT-PCR technology and immunohistochemistry, gene and protein expression analyses were used to identify differential molecular changes between tumor and normal renal tissues. Gene expression profiling revealed a significant overexpression of miR-34a in almost all RCC patients (91.7%) with an overall median and quartile values of 7.97 (2.37–29.54). In addition, among the 6 genes that have been predicted to be targeted by miR-34a via the in silico computational tools, two genes were significantly upregulated (*MET* and *E2F3*) in 87.1% of FFPE samples, while two others were downregulated (*TP53INP2* and *SOX2*) in almost all RCC patients compared to noncancer tissues (Figure 3). However, correlation analysis revealed no significant relationship of miR-34a with the tested target genes (Supplementary Table S2 and Figure S1).

Immunohistochemistry of renal tissue samples demonstrated variable staining patterns (Figure 4). Ki-67 expression, a cell proliferation marker, was detected in all cases of RCC but with variable level of expression. Low level of expression (<10%) was detected in 28 cases (70%), while high expression (≥10%) was noted in 12 cases (30%). Similarly, the angiogenesis-mediated protein (VEGFA) and the antiapoptotic marker (Bcl2) were expressed in all cancer tissues. Eighty percent of patients had high expression of VEGFA, while only 20% demonstrated weak staining. Antihuman

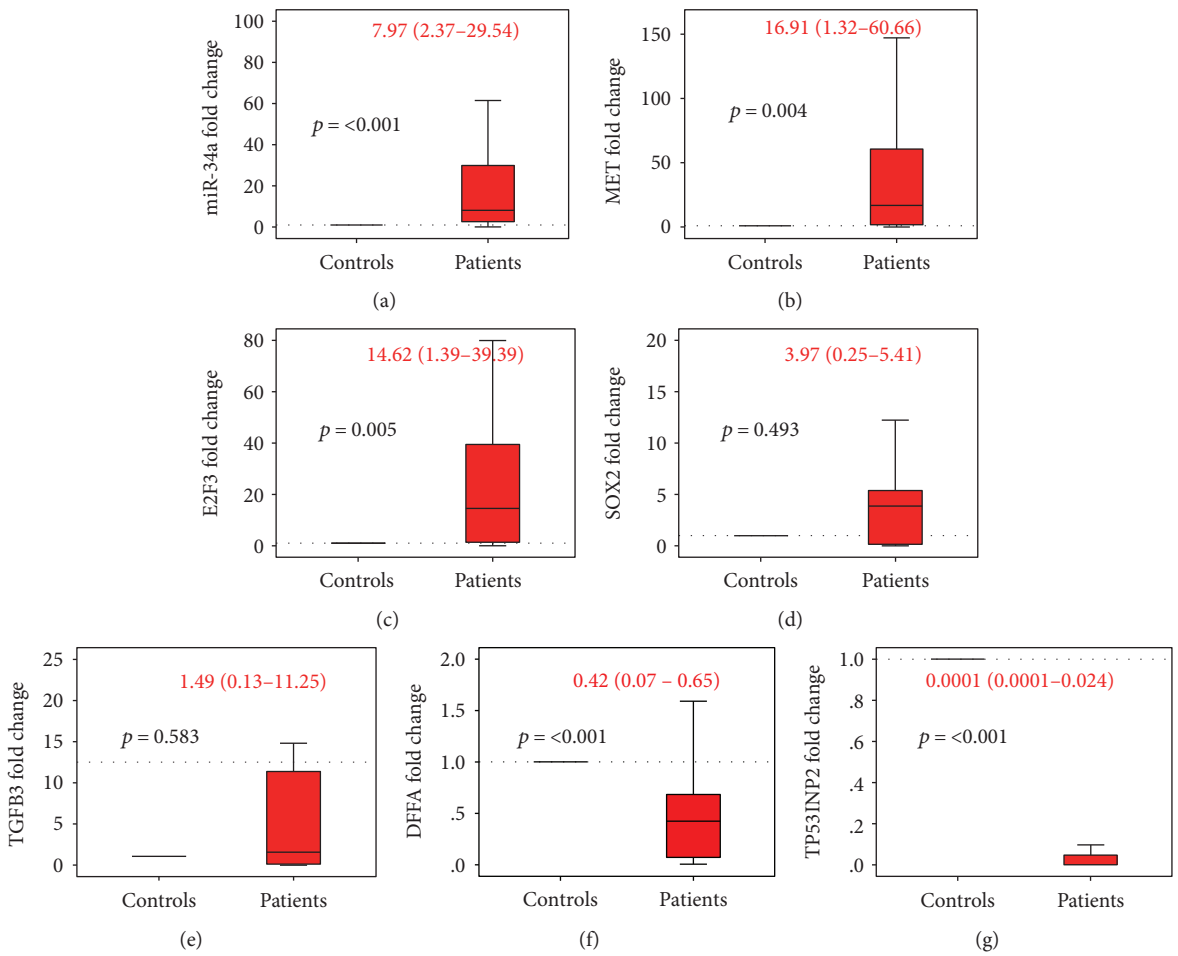

Figure 3: Gene expression profiling in cancer and normal renal tissues. Data are represented as medians. The box defines upper and lower quartiles (25% and 75%, resp.), and the error bars indicate upper and lower adjacent limits. Expression levels of miR-34a and targets in cancer and normal tissues were normalized to RNU6B and GAPDH, respectively. Fold change was calculated using the delta-delta CT method ($2^{-\Delta\Delta CT}$) in comparison to normal renal tissues. The gray dash line represents the expression level of normal renal tissues (equivalent to 1.0). p values < 0.05 were considered statistical significant. Mann–Whitney U test was used for comparison. Median and quartile values of patients are noted in red.

Bcl2 antibody was widely distributed all over the renal cancer tissues. Strong expression was noted in 75% of samples. For TGFB1 protein, most of cancer tissue attained moderate to strong expression in the cytoplasm, but the protein was less intense in approximately one-fifth of patients and absent in three samples only. In contrast, expression of the tumor suppressor protein (Tp53) was not detected by immunohistochemistry in less than half of tumor specimens. Unlike tumor cells, which had nuclear staining, lining cells of the proximal tubules stained the cytoplasm only.

ROC curve analysis of all genes and proteins showed significant high diagnostic performance of miR-34a (AUC = 0.854), *MET* (AUC = 0.765), and *E2F3* (AUC = 0.761) in differentiating between cancer specimens and noncancer tissues (Table 2).

3.3. Association of Gene and Protein Signature with Clinicopathological Features. The expression of miR-34a was markedly higher in RCC samples with chromophobic renal cell carcinoma and lower in clear cell type ($p = 0.039$) (Figure 5(a)). In addition, its level was inversely correlated with the tumor pathological grade ($r = -0.301$, $p = 0.037$). Among the target genes, lower levels of three genes *E2F3*, *SOX2*, and *DFFA* were significantly associated with capsular, pelvic, and vascular invasion, respectively (Figures 5(b), 5(c), and 5(d)). These findings were consistent with Spearman's correlation analysis (Supplementary Table S3).

Immunohistochemistry photos of the target proteins in renal tissues in relation with pathological parameters are illustrated in Figure 6. The advanced pathological grade was significantly associated with strong expression of Ki67 ($p = 0.001$), TGFB1 ($p = 0.034$), VEGFA proteins ($p = 0.001$), and absent Tp53 staining ($p = 0.029$) (Figures 7(a), 7(b), 7(c), and 7(d)). Larger tumor size and capsular infiltration also showed higher Ki67 expression ($p = 0.027$ and $p = 0.014$, resp.) (Figures 7(e) and 7(f)). Additionally, there was differential expression of TGFB1 and Tp53 proteins according to the specimen histopathological diagnosis, with stronger staining in chromophobic renal cell carcinoma type (Figures 7(g) and 7(h)). Similarly, correlation analysis

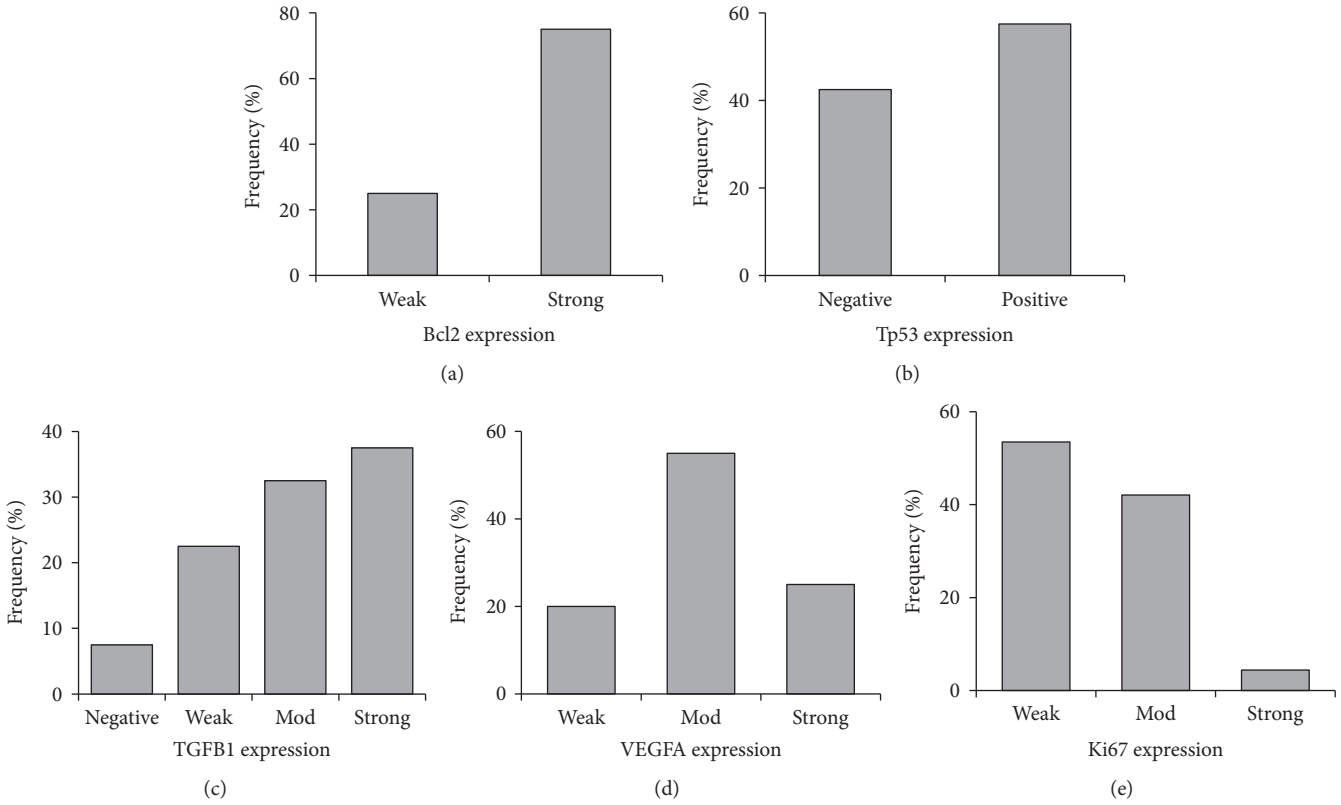

Figure 4: Frequency of Immunohistochemistry markers of miR-34a putative target proteins in RCC specimens. Five protein markers were examined, Bcl2, Tp53, TGFB1, VEGFA, and Ki67.

Table 2: ROC curve of miRNA-34a and target genes in renal cancer and normal tissues.

Variable(s)	Area	Standard error	p value	95% confidence interval	
				Lower bound	Upper bound
miR-34a	**0.854**	0.051	<0.001	0.754	0.954
MET	**0.765**	0.059	0.005	0.648	0.881
E2F3	**0.761**	0.063	0.006	0.638	0.884
SOX2	0.571	0.094	0.479	0.388	0.755
TGFB3	0.553	0.081	0.586	0.395	0.711
DFFA	0.118	0.053	0.068	0.014	0.222
TP53INP2	0.587	0.062	0.173	0.466	0.709
Combined first three markers	**0.793**	0.034	<0.001	0.727	0.859
All combined markers	**0.589**	0.030	0.014	0.530	0.648

Bold values are statistically significant at $p < 0.05$.

between proteins and clinicopathological characteristics demonstrated moderate correlation of Ki67 with histopathological diagnosis ($r = -0.419$, $p = 0.007$), grade ($r = 0.690$, $p < 0.001$), tumor size ($r = 0.389$, $p \leq 0.001$), LN invasion ($r = 0.351$, $p = 0.026$), and capsular infiltration ($r = 0.431$, $p = 0.006$). TGFB1 protein showed moderate correlation with histopathological diagnosis ($r = 0.427$, $p = 0.006$) and tumor grade ($r = 0.441$, $p = 0.004$). VEGFA protein also showed a significant positive correlation with pathological grade ($r = 0.563$, $p < 0.001$). In contrast, there was a negative correlation between Tp53 and grade ($r = -0.403$, $p = 0.010$) (Supplementary Table S3).

3.4. In Silico Data Analysis. Hsa-miR-34a is encoded by MIR-34A gene (ENSG00000284357), mapped at 1p36.22. The gene has a single exon which contains a p53-binding site within a CpG island about 30 kb upstream of the mature MIR-34A sequence and encodes for a transcript of 110 bp in length. The precursor miRNA stem-loop is processed in the cytoplasm of the cell, with the predominant miR-34a

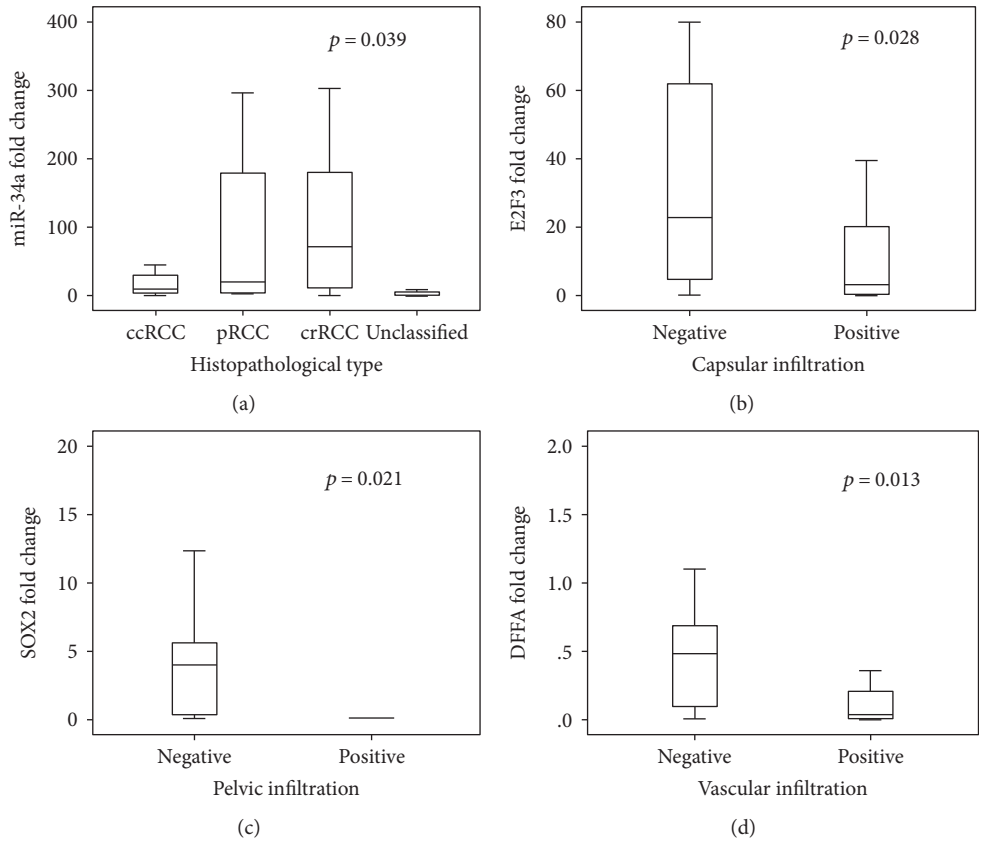

Figure 5: Association of miR-34a and target genes with the clinicopathological features in RCC patients. (a) Higher expression of miR-34a was significantly associated with chromophobic RCC subtype. (b) Lower levels of *E2F3* were associated with capsular infiltration. (c) Lower levels of *SOX2* had higher frequency of pelvic infiltration in RCC tumor tissues. (d) *DFFA* downregulation was associated with vascular infiltration.

mature sequence excised from the 5′ arm of the hairpin. Secondary structure of hsa-miR-34a stem-loop predicted by computational programs is illustrated in Figure 8(a). Functional characterization of miR-34a based on differential expression experiments revealed its control on numerous cancer-related molecular pathways and cellular processes. It can control up to 115 genes involved in pathways in cancer (hsa05200), in addition to dozens of genes in particular tumor types (Figure 8(b)). As shown in the heat map, the most top five significant pathways targeted by miR-34a were microRNAs in cancer, fatty acid biosynthesis, proteoglycans in cancer, adherence junction, and cell cycle (Figure 8(b) and Supplementary Table S4).

Interaction of mature miR-34a-5p with complementary sites of selected experimentally validated targets is shown in Supplementary Figure S2. Protein-protein interaction between the targets is shown in Supplementary Figure S3. Enrichment analysis of the target panel elucidated their functional impact on numerous biological processes and cancer KEGG pathways (Supplementary Table S5 and S6).

4. Discussion

A key goal in clinical oncology is the development of therapeutic strategies that impede specific deregulated biological pathways in cancer. Understanding these pathways which involve candidate disease-causing genes will provide new therapeutic modalities for renal cancer.

In the current study, upregulation of miR-34a was observed in more than 90% of RCC patients, with median fold change of 7.97 in RCC FFPE tissues compared to noncancer tissues. ROC analysis revealed a high diagnostic performance of miR-34a in discriminating between cancer and noncancer tissues. However, higher levels showed a better prognosis (i.e., it was moderately correlated with well differentiated tumors). In addition, expression profiles in chromophobic RCC samples were markedly greater than that of clear cell and papillary subtypes.

According to a survey across diverse normal human tissues, miR-34a was downregulated in most human normal tissues, including renal cortex and medulla (data source: U133plus2 Affymetrix microarray from http://BioGPS.org). Consistent with our findings in renal cancer tissues, miRNA-34a has been reported to support cell proliferation in oxidative stress-induced renal carcinogenesis rat model [36] and it has been found to be overexpressed in various types of human cancer [37–40]. As one of the upregulated miRNAs in RCC, it has been speculated to function by downregulating tumor suppressor genes including secreted frizzled-related protein 1 (SFRP1) [41]. In addition, miR-

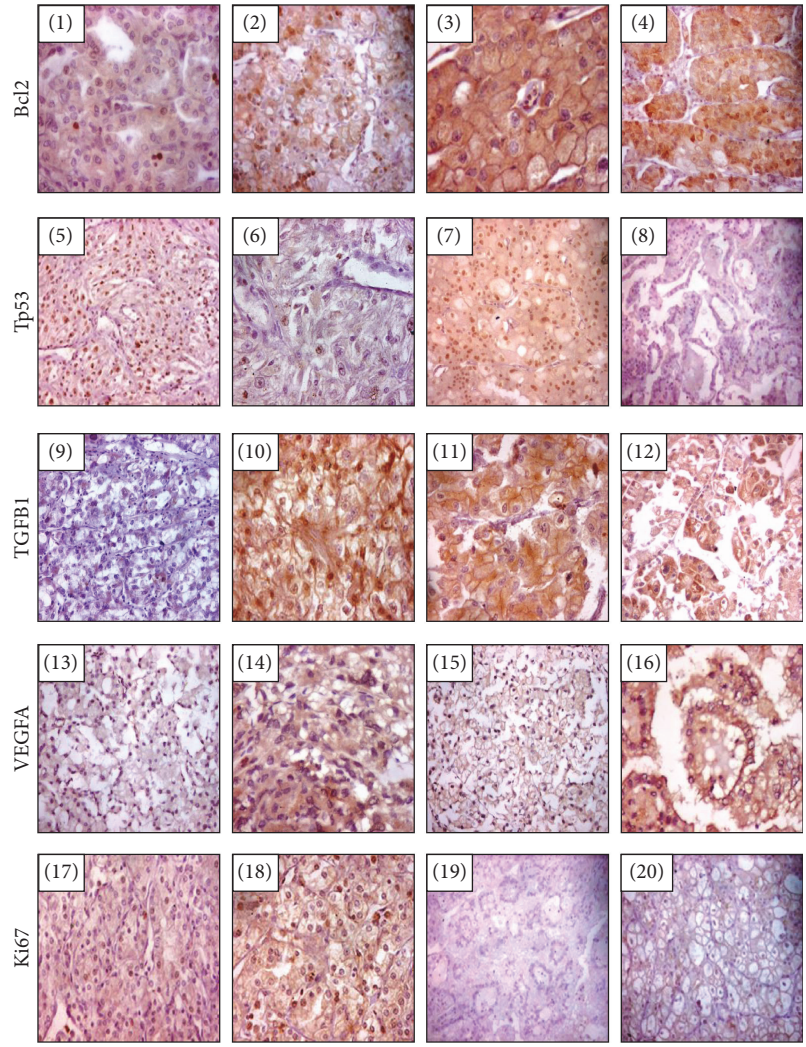

Figure 6: Immunohistochemistry images according to type and grade of RCC. Clear cell RCC (Ng1) weakly expresses bcl2 (x100), (photo 1), clear cell RCC (Ng2) with focal strong cytoplasmic bcl2 (x100) (photo 2), chromophobe RCC (Ng2) with diffuse moderate expression of bcl2 (x400) (photo 3), and papillary RCC (Ng2) with diffuse strong expression of bcl2 (x200) (photo 4). Clear cell RCC (Ng1/2) with diffuse strong nuclear expression of P53 (x100) (photo 5), clear cell RCC clear cell RCC (Ng3) showed scarce cell nuclei express P53 (X200) (photo 6), chromophobe RCC (Ng2) diffusely and strongly express P53 (X100) (photo 7), and papillary RCC do not express p53 (x100) (photo 8). Clear cell RCC (Ng2) with weak expression of TGFB1 (x100) (photo 9), RCC (Ng3) with strong expression of TGFB1 (x200) (photo 10), chromophobe RCC with focal strong expression of TGFB1 (X200) (photo 11), and papillary with focal strong expression of TGFB1 (X200) (photo 12). Clear cell RCC (Ng1) with diffuse weak expression of VEGFR (X100) (photo 13), clear RCC (Ng3) with diffuse moderate expression of VEGFR (X200) (photo 14), chromophobe RCC with weak expression of VEGF (X100) (photo 15), papillary RCC with intermediate expression of VEGFR (X200) (photo 16). RCC (Ng2) with low expression of Ki67 (X100) (photo 17), RCC (Ng3) with high expression of Ki67 (X200) (photo 18), and papillary RCC does not express Ki 67 (x100) (photo 19), and chromophobe RCC do not express Ki67 (x200) (photo 20).

34a was identified to be a direct target of the tumor suppressor Tp53 protein in human and mouse cells and mediates some of its proapoptotic biological functions [42, 43]. Similarly, He et al. found that deregulation of miR-34a on response to DNA damage and oncogenic stress depends on p53 *in vitro* and *in vivo* [13].

In vitro, miR-34a was coexpressed with Tp53 at high levels in colorectal cancer cell lines and in irradiated mice but was not expressed in Tp53-knockout mice [44]. These findings could explain the good prognosis that is implied by higher levels of miR-34a in the current samples with low pathological grade and in chromophobic RCC subtype. It has been found that miR-34a expression could suppress the cell proliferation [38, 44], promote apoptosis through the induction of caspase-dependent apoptotic pathways [42, 45] in several cancer cell lines [46–48], and cause dramatic reprogramming of gene targets that regulate apoptosis, DNA repair, cell cycle progression, epithelial-mesenchymal transition, and angiogenesis [42, 49]. In addition, miR-34a restoration in cancer cells was shown to induce cell cycle arrest at G1 and G2/M phases and sensitized the cells to chemo- and radiotherapy [16, 50]. However, low expression

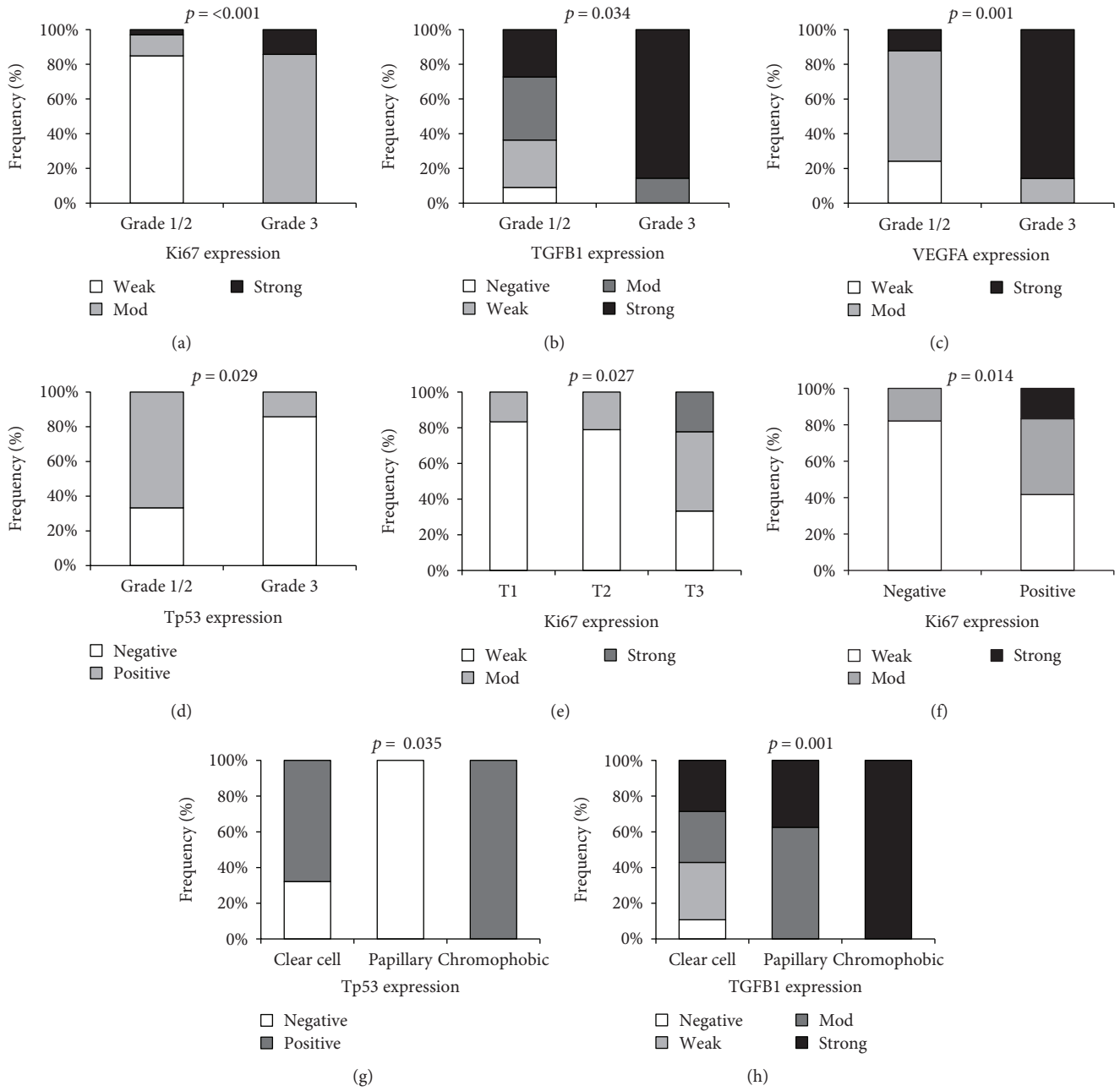

Figure 7: Association of immunohistochemistry markers with the clinicopathological features in RCC patients. The figures illustrated higher intensity of Ki67, TGFB1, VEGFA, and Tp53 in RCC tumors with advanced pathological grade (a–d), extensive staining of Ki67 antibodies in T3 samples and capsular infiltration (e-f), and differential expression of Tp53 and TGFB1 in various histopathological subtypes (g-h).

of miR-34a was noted in other types of cancer [46, 51–54], in glioblastoma and glioma with mutant Tp53 [55], in chronic lymphocytic lymphoma with Tp53 deletion [56], and in metastatic hepatocellular carcinoma [57], reflecting that miRNA-34a can work in a cell type-specific manner with a differential p53 pathway inactivation [36].

Taken our results with the findings of prior studies, we could support the hypothesis that miR-34a overexpression in the current study is a secondary consequence in cancer cells elucidated to compete the DNA damage and uncontrolled growth proliferation. Accumulation of further mutations in higher pathological grade tumors, especially those related to Tp53 gene activity or 1p36 locus itself, could account for the fall of miR-34a expression profile in those patients. Further functional studies are recommended to unravel the molecular mechanisms underlying the chromophobic RCC which has the best prognosis among all other subtypes in our cases [58–60].

In silico analysis of miR-34a targets in databases revealed numerous candidate gene targets. Functional annotation and enrichment analysis showed high linkage of miR-34a with cancer-related pathways. It can influence several pathways involved in all cancer hallmarks acquired during the multistep development of human tumors, by

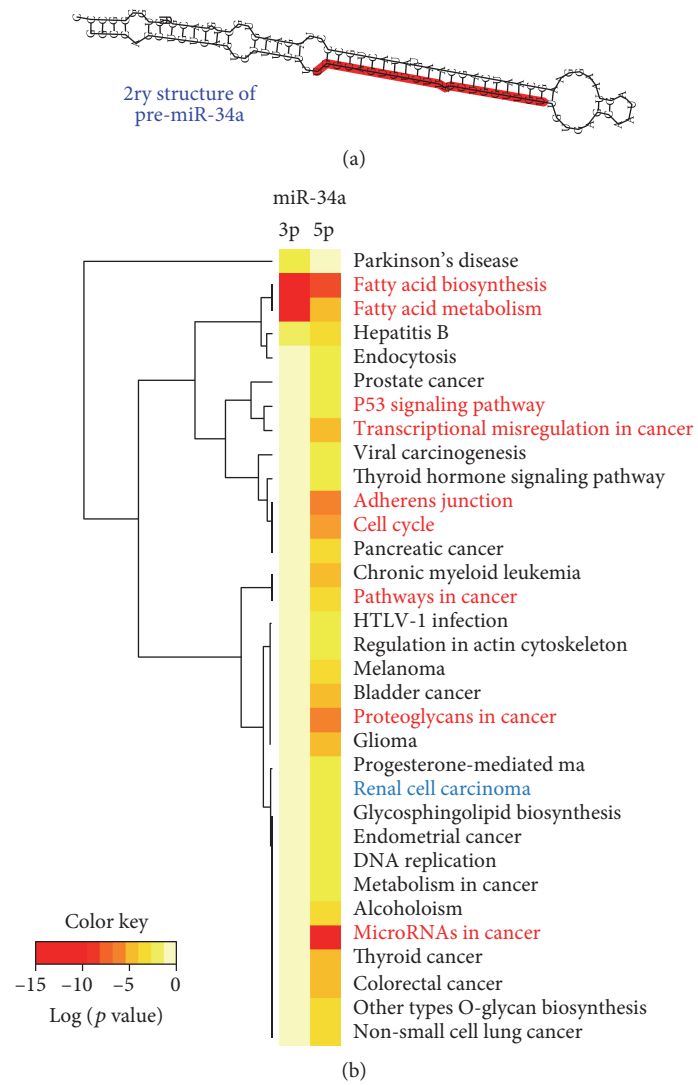

Figure 8: Structural analysis of MIR-34A gene locus and transcripts. (a) *Homo sapiens* hairpin secondary structure of pre-miR-34a stem-loop. Mature miR-34a-5p highlighted in red [data source: miRTarBase v20]. (b) Enrichment pathway analysis for miR-34a. Heat map showing targeted pathways, diseases, and cancers for both hsa-miR-34a-5p and hsa-miR-34a-3p with p values < 0.05 and microT-CDS threshold 0.4. A total of 33 pathways have target genes (in CDS or 3′ UTR regions) for miR-34a. The enrichment results of validated target genes showed that most pathways were related to cancer and cancer-related pathways. KEGG pathway annotations related specifically to current RCC work had been labeled (red). Degree of color is based on the significant p values of the predicted algorithm by DIANA tools; the red has the top significance estimated by false discovery rate (data source: DIANA-miRPath v2.0 web server).

sustaining proliferative cell signaling, evading growth suppressors, resisting apoptosis, inducing angiogenesis, and activating invasion and metastasis. In the current study, we identified predicted putative miR-34a binding sites within the 3′ UTR, 5′UTR, or coding regions of eleven mRNAs. These selected genes were functionally validated in prior experiments listed in Supplementary Table S1. Nevertheless, our data did not reveal inverse correlations of these targets with miR-34a. This could be explained by the fact that their gene expressions result from several integrated cell responses and cross talk between signaling pathways. Additionally, according to miRNA databases, there are multiple-to-multiple relationships between microRNAs and target genes; one miRNA may regulate transcription of many genes, and a single gene could be targeted by multiple miRNAs simultaneously, thus forming complex genetic circuits in human cancer [61, 62]. Liu et al., in addition, speculated the identified putative targets of miRNA could be regulated by translation inhibition rather than degradation. Subsequently, this would leave mRNA levels unaffected but reduce the protein levels. This speculation warrants the need of protein level measurement in tumor/normal samples along with the miRNA and mRNA levels for the same gene to identify such type of regulation [41].

Of the deregulated target genes expressed significantly in the current renal cancer specimens, *MET* and *E2F3* were significantly upregulated in RCC compared to non-cancer tissues with high diagnostic performance. The *Met* protooncogene, mapped at 7q31.2, has two alternative spliced isoforms (http://genecards.org). We identified two

putative miR-34a binding sites within the 3′ UTR and 5′ UTR of the human c-Met mRNA. Similarly, Li et al. [16] and Hu et al. [17] reported that c-Met is directly targeted by miR-34a. The *MET* gene encodes a receptor tyrosine kinase that is activated by hepatocyte growth factor (HGF) [16]. Ligand binding at the cell surface induces autophosphorylation of carboxyl terminus of MET on its intracellular domain that generates docking sites for second messengers, which activate several signaling pathways involving RAS-ERK, mitogen-activated protein kinase (MAPK), phosphatidylinositol 3-kinase- (PI3K-) AKT, signal transducer and activator of transcription (STAT), and phospholipase C [63]. Such downstream signaling pathways evoke a variety of pleiotropic physiological processes, including survival, morphogenesis, differentiation, epithelial-mesenchymal transition, and regulation of cell migration [64]. However, improper activation of c-MET may confer proliferative and invasive/metastatic abilities of cancer cells [65]. Similar to our findings in RCC patients, MET overexpression was associated with multiple human cancers [63, 66–71]. Its aberrant expression by different mechanisms, including point mutations [72], gene amplification [73], and oncogenic deletion [74, 75, 76], may lead to a more aggressive cancer phenotype and may be a prognostic indicator of poor overall survival and resistance to therapy [74–76].

The second upregulated gene in most of the current RCC samples was the transcription factor *E2F3*. ROC analysis showed its high discrimination accuracy in RCC diagnosis. In addition, its expression profile was associated with capsular infiltration. *E2F3* gene lies on chromosome 6p22.3 and has 3 transcript variants encoding 3 proteins of 465, 334, and 128 amino acids long. In contrast to full-length E2F3 protein, which is expressed only at the G1/S boundary, truncated isoforms are expressed throughout the cell cycle [77, 78]. E2F3 recognizes a specific sequence motif in DNA and interacts directly with the tumor suppressor retinoblastoma protein (pRB) to regulate the expression of genes involved in the G1/S boundary of the cell cycle and DNA replication; hence, E2F3 has a critical role in the control of cellular proliferation [79]. Acute loss of E2F3 activity affected the expression of genes encoding DNA replication and mitotic activities [80]. *In vitro* and *in vivo* studies showed a failure of division and proliferation in E2F3-null retinal progenitor cells [81] and early embryonic death in E2F3-null mice [82, 83]. Dysregulation of *E2F3* and altered copy number and activity of this gene have been observed in a number of malignant tumors [84–92] and correlated with several pathological features of cancer like the pathological grade and tumor cell proliferation rate [91], as well as tumor aggressiveness and poor overall survival [91, 92]. However, transgenic mice expressing inducible *E2F3* resulted in hyperplasia, but not tumor development [93], supporting its role in tumor progression rather than initiation.

As an excellent marker to determine the growth fraction of a given cell population, the expression of proliferation-related Ki67 antigen was investigated in the current study. The fraction of Ki67 positive cells is often correlated with the clinical course of the tumors. Currently, this marker of proliferation was detected in all cases of RCC, but with variable levels of expression. High expression of Ki67 was associated with advanced pathological grade, large tumor size, lymphatic invasion, and capsular infiltration. In addition, strong staining was correlated with chromophobic RCC subtype. Antigen Ki67 is a nuclear protein, encoded by *MKI67* gene that is mapped at 10q26.2. It has five splice variants; only two of them are translated to synthesize a long form (3256 aa/ 395 kDa) and a short form (2896 aa/345 kDa) proteins that differ only by the presence or absence of exon 7 [94]. Antigen Ki67 is associated with cellular proliferation [95]. During interphase, the Ki67 protein can be exclusively detected within the cell nucleus, whereas in mitosis, most of the protein is relocated to the surface of the chromosomes [96]. Ki67 protein is present during all active phases of the cell cycle (G1, S, G2, and mitosis) but is absent from resting cells (G0) [95, 97]. GO annotation identified the gene to play vital roles in chromosomal segregation regulation and organization, nuclear division, cell cycle, organ regeneration, and stress response (http://genecards.org). It is also associated with ribosomal RNA transcription and synthesis [98, 99]. Several lines of evidence have implicated the importance of Ki67 index in multiple cancers [100–106] and reported its prognostic value for survival and tumor recurrence [107–114].

Regarding the TGFB superfamily proteins, they were known to be implicated in cell growth and differentiation. These growth factors bind various TGF-beta receptors, leading to recruitment and activation of SMAD family transcription factors which regulate the expression of the downstream genes, including interferon gamma and tumor necrosis factor alpha [115]. We examined the expression profile of TGFB1 protein and *TGFB3* gene. In RCC samples, *TGFB3* mRNA did not show differential expression compared to noncancer tissues. However, TGFB1 protein showed moderate to strong cytoplasmic staining in most samples. Higher protein level expression was associated with poor tumor differentiation and chromophobic subtype. This protein is involved in embryogenesis and cell differentiation and may play an important role in apoptosis, immune defense, inflammation, and tissue repair [115, 116]. Overexpression or alterations of its active protein induced by gene somatic mutations were frequently observed in several tumor cells [117–121] and were correlated with tumor aggressiveness, invasion, angiogenesis, metastasis, immune surveillance inhibition [122], and epithelial-mesenchymal transformation [117].

SOX2 is a critical transcription factor for self-renewal and maintenance of undifferentiated embryonic stem cells [123]. *SOX2* gene is mapped at 3q26.33, consisting of a single exon that encodes a protein of 318 amino acid residues (http://genecards.org). It was reported to be involved in embryonic development regulation and in the cell fate determination, and its over expression can induce reprogramming of somatic cells to acquire pluripotency characteristics [124, 125]. SOX2 was identified as an oncogenic factor and was reported to be overexpressed in certain types of cancer [123, 126–129]. Knockdown of *SOX2* could inhibit cell viability and tumorigenesis *in vitro* and *in vivo* [123, 126] by potentiating cell cycle arrest associated with decreased levels

of CCND1 and phosphorylated Rb and/or by upregulating of p27Kip1 level [130]. In our samples, no differential expression was observed between cancer and noncancer tissues; nevertheless, lower expression of *SOX2* mRNA was correlated with cancer infiltration of renal pelvic tissues.

In the current study, one antiapoptotic and three proapoptotic miR-34a targets regulating essential cancer-related pathways were examined. The apoptotic regulator *BCL2* gene, mapped at 18q21.33, has 2 alternative transcripts and encodes an integral outer mitochondrial membrane protein [131]. It has two protein isoforms, Bcl2a (5.5-Kb mRNA/239 aa) and Bcl2b (3.5-Kb/205 aa), which are identical except for the C-terminal portion. The former contains a hydrophobic tail for membrane anchorage which seems to be necessary for antiapoptotic ability [132]. Bcl2 is found on the outer membrane of mitochondria. It functions as an apoptosis inhibitor by forming complexes with caspase-9 and APAF1, thus prevent them to initiate the protease cascade and apoptosis through caspase-3 cytochrome C-dependent activation [133]. In 2002, Marsden et al. [134] discovered that Bcl2 can also function independently via other pathways. Bcl2 constitutively blocks p53-induced apoptosis and enables the survival of colorectal cancer cells [135]. Overexpression of Bcl2 blocks TNF-related apoptosis-inducing ligand-(TRAIL-) induced apoptosis in human lung cancer cells [136]. In addition to the antiapoptotic function, Bcl2 is known to regulate mitochondrial fusion and fission dynamics [137]. Bcl2 acts as a potent regulator of cell survival in neurons both during development and throughout adult life [138]. In cancer, overexpression of the antiapoptotic Bcl2 can result in a distinct cellular growth advantage due to lack of cell death, a hallmark of cancer. In the present study, Bcl2 protein was expressed in all cancer tissues. Similarly, in previous studies, Bcl2 upregulation has been reported in many types of cancer [139–142]. Moreover, it has also been associated with poor clinical outcome and shorter overall survival in cancer patients [143]. It can confer resistance to chemotherapy and radiotherapy in some types of cancer [144, 145]. In addition, targeting Bcl2 by miR-125a, miR-206, and miR-34a was reported to inhibit the cell proliferation and induce apoptosis in multiple cancer cells [146–148].

The tumor suppressor protein Tp53, the guardian of the genome, is essential for the carcinogenesis prevention. In the current study, it was not detected by immunohistochemistry in less than one half of the specimens. Absent staining of Tp53 protein in tumor cell nuclei was significantly associated with advanced pathological grade, while positive staining was observed in the chromophobic RCC, known to have the best prognosis. The transcription factor Tp53 is encoded by *TP53* gene mapped at 17p13.1. This gene has a complex transcriptional expression pattern encoding 28 different mRNA variants through the use of an internal promoter in intron 4 and alternative splicing machinery. All variants could be detected in all tissues, and only 5 is exclusively transcribed in tissue-specific manner [149]; each isoform has distinct biological activity and subcellular localizations [150]. Normally, Tp53 is expressed at low levels and kept inactive through the action of MDM2 (mouse double minute 2 homolog) which promotes its degradation [150]. However, during cellular stresses or DNA damage, activated Tp53 induces cell cycle arrest for DNA repair or force apoptosis. It binds to DNA and regulates transcription of target genes that induce cell cycle arrest, apoptosis, and DNA repair [150–152]. It can trigger cell death independently of its transcriptional activity through subcellular translocation and activation of proapoptotic Bcl-2 family members [153]. Attenuation of Tp53 activity would render the cells more susceptible to further genetic damage and therefore to neoplastic transformation and tumor progression.

Another apoptotic gene, *Tp53INP2*, is located at 20q11.22 with 4 transcripts and encodes for 3 putative protein variants of 220, 88, and 77 amino acid long. It is thought to be a scaffold protein that is normally expressed upon induction by the Tp53 protein [154]. The protein encoded by this gene has two distinct functions depending on its cellular localization [155]. It is essential for proper autophagy, a self-degradative process that occurs at critical times in development to recycle unnecessary intracellular components and damaged organelles [156]. Tp53INP2 protein shuttles between the nucleus and the cytoplasm, depending on cellular stress conditions, and relocates in the autophagosomes during autophagy activation. It recruits Atg8-like proteins to the autophagosome membrane by interacting with the transmembrane protein VMP1 (vacuole membrane protein 1) [154]. Failure of autophagy is thought to be one of the main reasons for the accumulation of cell damage and aging [157]. In addition to its role in autophagy, it serves as a transcriptional coactivator for several nuclear receptors, such as the glucocorticoid receptor, vitamin D receptor (VDR), and peroxisome proliferator-activated receptor gamma [155], thus possess a tumor suppressor-like functionality similar to Tp53 [158, 159]. Dysregulation of *Tp53INP2* expression was found differently in several types of cancer tissues [160–164]. Therefore, our results along with previous data highlight its putative role in cancer development and progression.

Low levels of the apoptotic gene, *DFFA*, were observed in almost all RCC samples. Lower expression was associated with vascular infiltration. *DFFA* gene is located in the same region of miR-34a at 1p36.22 which is commonly deleted in human tumors. DFFA plays an essential role in apoptosis. When cleaved by caspase-3, it induces the release of its partner DFFB, which in turn triggers DNA fragmentation by its nuclease activity [165]. Hence, absence of this protein could result in aberrant apoptosis, invasive growth, and metastasis [166]. Similar to our findings, downregulated DFFA expression was observed during the exponential phase of growth in several human colonic cancer cell lines [167]. DFFA (−/−) mice exerted severe genomic instability and tumor progression in colon epithelial cells [168]. Moreover, low DFFA expression was associated with poor prognosis in esophageal cancer [169] and neuroblastoma tumors [170].

As angiogenesis is of central importance in the growth and metastasis of tumors [171], we investigated the expression of the angiogenesis-mediated protein, VEGFA in RCC compared to noncancer tissues. VEGFA protein expression was detected in all RCC tissues, with 80% of samples showing strong staining. Elevated levels were

associated with advanced tumor grade. VEGFA protein is encoded by the *VEGFA* gene, mapped at 6p21.1, a highly polymorphic region that showed association with cancer susceptibility, aggressiveness, and therapeutic response in various tumor types [172, 173]. Alternative exon splicing can generate up to 29 transcript variants with different isoforms (http://Ensembl.org). There was also evidence for alternative translation initiation codons resulting in additional isoforms. VEGFA promotes proliferation and migration of vascular endothelial cells both *in vitro* and *in vivo* and is essential for both physiological and pathological angiogenesis [172]. This prosurvival effect is mediated via PI3-kinase/Akt signal transduction pathway [174]. In addition, it induces permeabilization of blood vessels, thus known as a vascular permeability factor [175]. It induces endothelial fenestration in vascular beds [176] and enhances vasodilatation *in vitro* in a dose-dependent manner [177]. In addition, VEGFA promotes apoptosis and induces expression of the antiapoptotic protein Bcl-2 [178]. *In vivo*, VEGFA inhibition results in abnormal embryonic blood vessel formation and extensive apoptotic changes in the vasculature of neonatal mice [179, 180]. Within tumors, cancer cells and cancer-associated stroma are the major source of VEGFA [173]. It influences the newly formed blood vessels, but not the established ones. In agreement with our findings, VEGFA was reported to be overexpressed in several different tumor types [171, 181–183]. Anti-VEGF antibodies were implicated as potent inhibitory effectors [184, 185]. Furthermore, VEGFA expression is correlated with tumor stage and progression. It was found to be associated with high pathological grade, tumor size, lymph node metastasis, poor prognosis, resistance to chemotherapy, and poor overall survival and outcomes in several types of cancer [171, 172, 186–189].

5. Conclusions

The current study does confirm the association of miR-34a overexpression with RCC in our population, suggesting its potential role in pathogenesis and progression of this type of cancer. Furthermore, chromophobic RCC subtype has been postulated to attain different transcriptomics and proteomics characteristics compared to other subtypes. It has been found to have higher *MIR-34A*, *Tp53*, Ki67, and TGFB expressions. Hence, the molecular mechanism and genes involved in this particular type need to be validated in large scale multicenter study for better disease outcome and response to treatment predictions. In addition, the exact molecular interplay between the potential miR-34a target genes is still unclear and will warrant further detailed studies. One of the limitations that need to be considered is that the protein levels of the selected target genes in tumor/normal samples were not measured along with the mRNA levels. Hence, we could not suggest if the selected potential targets could be affected by translation inhibition rather than degradation in light of absence of miRNA34a-selected targets anticorrelation. Another limitation is the lack of the functional analysis either on tumor cell lines or on RCC rat models to validate the current findings and explore the detailed biological mechanisms and the potential therapeutic roles of miR-34a in RCC. This will be considered the logic next step in our ongoing research.

Abbreviations

AUC: Area under curve
Bcl-2: B-cell lymphoma 2
CDKN1A: Cyclin dependent kinase inhibitor 1A
crRCC: Chromophobe renal cell carcinomas
ccRCC: Clear cell renal cell carcinomas
DFFA: DNA fragmentation factor subunit alpha
FFPE: Formalin-fixed paraffin embedded
HGF: Hepatocyte growth factor
ISUP: International society of urological pathology
KEGG: Kyoto encyclopedia of genes and genomes
MDM2: Mouse double minute 2 homolog
miR-34a: MicroRNA-34a
miRNAs: MicroRNAs
Ng: Nuclear grade
NSCLC: Non-small-cell lung cancer
pRCC: Papillary renal cell carcinomas
PI3K: Phosphatidylinositol 3-kinase
qPCR: Quantitative polymerase chain reaction
Cq: Quantitative cycle
ROC: Receiver operating characteristic
RCC: Renal cell carcinoma
pRB: Retinoblastoma protein
RT: Reverse transcription
SFRP1: Secreted frizzled-related protein 1
STAT: Signal transducer and activator of transcription
SOX2: Sex-determining region Y-box 2
TGFB: Transforming growth factor-beta
TP53INP: Tumor protein p53 inducible nuclear protein
UTR: Untranslated region
VEGF: Vascular endothelial growth factor
VDR: Vitamin D receptor
VMP1: Vacuole membrane protein 1.

Conflicts of Interest

The authors declare that they have no competing interests.

Acknowledgments

The authors thank the Oncology Diagnostic Unit and the Center of Excellence in Molecular and Cellular Medicine, Suez Canal University, Ismailia, Egypt for providing the facilities for performing the research work.

References

[1] K. Tang and H. Xu, "Prognostic value of meta-signature miRNAs in renal cell carcinoma: an integrated miRNA expression profiling analysis," *Scientific Reports*, vol. 5, article 10272, 2015.

[2] P. Cairns, "Renal Cell Carcinoma," *Cancer Biomarkers*, vol. 9, pp. 461–473, 2011.

[3] D. L. Lim, R. Ko, and S. E. Pautler, "Current understanding of the molecular mechanisms of kidney cancer: a primer for

urologists," *Canadian Urological Association Journal*, vol. 1, pp. S13–S20, 2007.

[4] Y. Moreau and L. C. Tranchevent, "Computational tools for prioritizing candidate genes: boosting disease gene discovery," *Nature Reviews. Genetics*, vol. 13, pp. 523–536, 2012.

[5] A. Valinezhad Orang, R. Safaralizadeh, and M. Kazemzadeh-Bavili, "Mechanisms of mirna-mediated gene regulation from common downregulation to mRNA-specific upregulation," *International Journal of Genomics*, vol. 2014, Article ID 970607, 15 pages, 2014.

[6] C. Baer, R. Claus, and C. Plass, "Genome-wide epigenetic regulation of miRNAs in cancer," *Cancer Research*, vol. 73, pp. 473–477, 2013.

[7] E. A. Toraih, M. S. Fawz, M. G. Elgazzaz, M. H. Hussein, R. H. Shehata, and H. G. Daoud, "Combined genotype analyses of precursor miRNA196a2 and 499a variants with hepatic and renal cancer susceptibility a preliminary study," *Asian Pacific Journal of Cancer Prevention*, vol. 17, pp. 3369–3375, 2016.

[8] E. A. Toraih, M. S. Fawzy, E. A. Mohammed, M. H. Hussein, and M. M. El-Labban, "MicroRNA-196a2 biomarker and targetome network analysis in solid tumors," *Molecular Diagnosis & Therapy*, vol. 20, pp. 559–577, 2016.

[9] C. Grange, F. Collino, M. Tapparo, and G. Camussi, "Oncogenic micro-RNAs and renal cell carcinoma," *Frontiers in Oncology*, vol. 4, p. 49, 2014.

[10] H. Hermeking, "The miR-34 family in cancer and apoptosis," *Cell Death and Differentiation*, vol. 17, pp. 193–199, 2010.

[11] L. Li, "Regulatory mechanisms and clinical perspectives of miR-34a in cancer," *Journal of Cancer Research and Therapeutics*, vol. 10, pp. 805–810, 2014.

[12] M. Ghandadi and A. Sahebkar, "MicroRNA-34a and its target genes: key factors in cancer multidrug resistance," *Current Pharmaceutical Design*, vol. 22, pp. 933–939, 2016.

[13] L. He, X. He, L. P. Lim et al., "A microRNA component of the p53 tumour suppressor network," *Nature*, vol. 447, pp. 1130–1134, 2007.

[14] G. Genovese, A. Ergun, S. A. Shukla et al., "microRNA regulatory network inference identifies miR-34a as a novel regulator of TGF-β signaling in glioblastoma," *Cancer Discovery*, vol. 2, pp. 736–749, 2012.

[15] D. Reimer, M. Hubalek, H. Kiefel et al., "Regulation of transcription factor E2F3a and its clinical relevance in ovarian cancer," *Oncogene*, vol. 30, pp. 4038–4049, 2011.

[16] N. Li, H. Fu, Y. Tie et al., "miR-34a inhibits migration and invasion by down-regulation of c-Met expression in human hepatocellular carcinoma cells," *Cancer Letters*, vol. 275, pp. 44–53, 2009.

[17] Y. Hu, A. M. Correa, A. Hoque et al., "Prognostic significance of differentially expressed miRNAs in esophageal cancer," *International Journal of Cancer*, vol. 128, pp. 132–143, 2011.

[18] G. Yu, W. Yao, W. Xiao, H. Li, H. Xu, and B. Lang, "MicroRNA-34a functions as an anti-metastatic microRNA and suppresses angiogenesis in bladder cancer by directly targeting CD44," *Journal of Experimental & Clinical Cancer Research*, vol. 33, p. 779, 2014.

[19] I. S. Vlachos, K. Zagganas, M. D. Paraskevopoulou et al., "DIANA-miRPath v3.0: deciphering microRNA function with experimental support," *Nucleic Acids Research*, vol. 43, pp. W460–W466, 2015.

[20] C. H. Chou, N. W. Chang, S. Shrestha et al., "miRTarBase 2016: updates to the experimentally validated miRNA-target interactions database," *Nucleic Acids Research*, vol. 44, pp. D239–D247, 2016.

[21] I. S. Vlachos, M. D. Paraskevopoulou, D. Karagkouni et al., "DIANA-TarBase v7.0: indexing more than half a million experimentally supported miRNA:mRNA interactions," *Nucleic Acids Research*, vol. 43, pp. D153–D159, 2015.

[22] D. Betel, M. Wilson, A. Gabow, D. S. Marks, and C. Sander, "The microRNA.org resource: targets and expression," *Nucleic Acids Research*, vol. 36, pp. D149–D153, 2008.

[23] D. Szklarczyk, A. Franceschini, S. Wyder et al., "STRING v10: protein-protein interaction networks, integrated over the tree of life," *Nucleic Acids Research*, vol. 43, pp. D447–D452, 2015.

[24] E. M. Wagner, "Monitoring gene expression: quantitative real-time RT–PCR," *Methods in Molecular Biology*, vol. 1027, pp. 19–45, 2013.

[25] S. A. Bustin, V. Benes, J. A. Garson et al., "The MIQE guidelines: minimum information for publication of quantitative real-time PCR experiments," *Clinical Chemistry*, vol. 55, pp. 611–622, 2009.

[26] J. Srigley, B. Delahunt, J. Eble et al., "The International Society of Urological Pathology (ISUP) Vancouver classification of renal neoplasia," *The American Journal of Surgical Pathology*, vol. 37, pp. 1469–1489, 2013.

[27] S. Fuhrman, L. C. Lasky, and L. Limas, "Prognostic significance of morphologic parameters in renal cell carcinoma," *The American Journal of Surgical Pathology*, vol. 6, pp. 655–663, 1982.

[28] L. H. Sobin, C. Wittekind, and International Union Against Cancer (UICC), *TNM Classification of Malignant Tumors*, New York, 1997.

[29] D. L. Uhlman, P. L. Nguyen, J. C. Manivel et al., "Association of immunohistochemical staining for p53 with metastatic progression and poor survival in patients with renal cell carcinoma," *Journal of the National Cancer Institute*, vol. 86, pp. 1470–1475, 1994.

[30] A. F. Olumi, N. Weidner, and J. C. Presti, "P53 immunoreactivity correlates with Ki-67 and bcl-2 expression in renal cell carcinoma," *Urologic Oncology*, vol. 6, pp. 63–67, 2001.

[31] A. Bishoy, B. Gayed, R. Youssef et al., "Ki67 is an independent predictor of oncological outcomes in patients with localized clear-cell renal cell carcinoma," *BJU International*, vol. 113, pp. 668–673, 2014.

[32] J. P. Kallio, P. Hirvikoski, H. Helin et al., "Renal cell carcinoma MIB-1, Bax and Bcl-2 expression and prognosis," *The Journal of Urology*, vol. 172, pp. 2158–2161, 2004.

[33] D. Mitropoulos, A. Kiroudi, E. Christelli et al., "Expression of transforming growth factor β in renal cell carcinoma and matched non-involved renal tissue," *Urological Research*, vol. 32, pp. 317–322, 2004.

[34] S. Ambs, W. P. Bennett, W. G. Merriam et al., "Vascular endothelial growth factor and nitric oxide synthase expression in human lung cancer and the relation to p53," *British Journal of Cancer*, vol. 78, pp. 233–239, 1998.

[35] K. J. Livak and T. D. Schmittgen, "Analysis of relative gene expression data using real-time quantitative PCR and the $2_{\mathrm{T}}^{-\Delta\Delta\mathrm{C}}$ method," *Methods*, vol. 25, pp. 402–408, 2001.

[36] K. K. Dutta, Y. Zhong, Y. T. Liu et al., "Association of microRNA-34a overexpression with proliferation is cell

type-dependent," *Cancer Science*, vol. 98, pp. 1845–1852, 2007.

[37] H. He, K. Jazdzewski, W. Li et al., "The role of microRNA genes in papillary thyroid carcinoma," *Proceedings of the National Academy of Sciences of the United States of America*, vol. 102, pp. 19075–19080, 2005.

[38] H. Tazawa, N. Tsuchiya, M. Izumiya, and H. Nakagama, "Tumor-suppressive miR-34a induces senescence-like growth arrest through modulation of the E2F pathway in human colon cancer cells," *Proceedings of the National Academy of Sciences of the United States of America*, vol. 104, pp. 15472–15477, 2007.

[39] E. E. Marsh, Z. Lin, P. Yin, M. Milad, D. Chakravarti, and S. E. Bulun, "Differential expression of microRNA species in human uterine leiomyoma versus normal myometrium," *Fertility and Sterility*, vol. 89, pp. 1771–1776, 2008.

[40] D. Asslaber, J. D. Pión, I. Seyfried et al., "microRNA-34a expression correlates with MDM2 SNP309 polymorphism and treatment-free survival in chronic lymphocytic leukemia," *Blood*, vol. 115, pp. 4191–4197, 2010.

[41] H. Liu, A. R. Brannon, A. R. Reddy et al., "Identifying mRNA targets of microRNA dysregulated in cancer: with application to clear cell renal cell carcinoma," *BMC Systems Biology*, vol. 4, p. 51, 2010.

[42] T.-C. Chang, E. A. Wentzel, O. A. Kent et al., "Transactivation of miR-34a by p53 broadly influences gene expression and promotes apoptosis," *Molecular Cell*, vol. 26, pp. 745–752, 2007.

[43] V. Tarasov, P. Jung, B. Verdoodt et al., "Differential regulation of microRNAs by p53 revealed by massively parallel sequencing: miR-34a is a p53 target that induces apoptosis and G1-arrest," *Cell Cycle*, vol. 6, pp. 86–1593, 2007.

[44] C. Welch, Y. Chen, and R. L. Stallings, "MicroRNA-34a functions as a potential tumor suppressor by inducing apoptosis in neuroblastoma cells," *Oncogene*, vol. 26, pp. 5017–5022, 2007.

[45] N. Raver-Shapira, E. Marciano, E. Meiri et al., "Transcriptional activation of miR-34a contributes to p53-mediated apoptosis," *Molecular Cell*, vol. 26, pp. 731–743, 2007.

[46] C. L. Dalgard, M. Gonzalez, J. E. Deniro, and J. M. O'Brien, "Differential microRNA-34a expression and tumor suppressor function in retinoblastoma cells," *Investigative Ophthalmology & Visual Science*, vol. 50, pp. 4542–4551, 2009.

[47] Z. L. Ma, P. P. Hou, Y. L. Li et al., "MicroRNA-34a inhibits the proliferation and promotes the apoptosis of non-small cell lung cancer H1299 cell line by targeting TGFβR2," *Tumour Biology*, vol. 36, pp. 2481–2490, 2015.

[48] Y. Fujita, K. Kojima, N. Hamada et al., "Effects of miR-34a on cell growth and chemoresistance in prostate cancer PC3 cells," *Biochemical and Biophysical Research Communications*, vol. 377, pp. 114–119, 2008.

[49] Q. Ji, X. Hao, M. Zhang et al., "MicroRNA miR-34 inhibits human pancreatic cancer tumor-initiating cells," *PLoS One*, vol. 4, no. 8, article e6816, 2009.

[50] V. P. Tryndyak, S. A. Ross, F. A. Beland, and I. P. Pogribny, "Down-regulation of the microRNAs miR-34a, miR-127, and miR-200b in rat liver during hepatocarcinogenesis induced by a methyl-deficient diet," *Molecular Carcinogenesis*, vol. 48, pp. 479–487, 2008.

[51] M. Guled, L. Lahti, P. M. Lindholm et al., "CDKN2A, NF2, and JUN are dysregulated among other genes by miRNAs in malignant mesothelioma—a miRNA microarray analysis," *Genes, Chromosomes & Cancer*, vol. 48, pp. 615–623, 2009.

[52] D. Yan, X. Zhou, X. Chen et al., "MicroRNA-34a inhibits uveal melanoma cell proliferation and migration through downregulation of c-Met," *Investigative Ophthalmology & Visual Science*, vol. 50, pp. 1559–1565, 2009.

[53] I. Satzger, A. Mattern, U. Kuettler et al., "MicroRNA-15b represents an independent prognostic parameter and is correlated with tumor cell proliferation and apoptosis in malignant melanoma," *International Journal of Cancer*, vol. 126, pp. 2553–2562, 2010.

[54] K. Kozaki, I. Imoto, S. Mogi, K. Omura, and J. Inazawa, "Exploration of tumor-suppressive microRNAs silenced by DNA hypermethylation in oral cancer," *Cancer Research*, vol. 68, pp. 2094–2105, 2008.

[55] Y. Li, F. Guessous, Y. Zhang et al., "MicroRNA-34a inhibits glioblastoma growth by targeting multiple oncogenes," *Cancer Research*, vol. 69, pp. 7569–7576, 2009.

[56] M. K. Dijkstra, K. Lomvan, D. Tielemans et al., "17p13/TP53 deletion in B-CLL patients is associated with microRNA-34a downregulation," *Leukemia*, vol. 23, pp. 625–627, 2009.

[57] A. Budhu, H. L. Jia, M. Forgues et al., "Identification of metastasis-related microRNAs in hepatocellular carcinoma," *Hepatology*, vol. 47, pp. 897–907, 2008.

[58] M. W. Kattan, V. Reuter, R. J. Motzer, J. Katz, and P. Russo, "A postoperative prognostic nomogram for renal cell carcinoma," *The Journal of Urology*, vol. 166, pp. 63–67, 2001.

[59] M. F. Dall'Oglio, A. A. Antunes, A. C. Pompeo, A. Mosconi, K. R. Leite, and M. Srougi, "Prognostic relevance of the histological subtype of renal cell carcinoma," *International Braz J Urol*, vol. 34, pp. 3–8, 2008.

[60] V. F. Muglia and A. Prando, "Renal cell carcinoma: histological classification and correlation with imaging findings," *Radiologia Brasileira*, vol. 48, pp. 166–174, 2015.

[61] Y. Hashimoto, Y. Akiyama, and Y. Yuasa, "Multiple-to-multiple relationships between microRNAs and target genes in gastric cancer," *PLoS One*, vol. 8, article e62589, 2013.

[62] T. Kunej, I. Godnic, S. Horvat, M. Zorc, and G. A. Calin, "Cross talk between microRNA and coding cancer genes," *Cancer Journal (Sudbury Mass)*, vol. 18, pp. 223–231, 2012.

[63] J. R. Sierra and M.-S. Tsao, "c-MET as a potential therapeutic target and biomarker in cancer," *Therapeutic Advances in Medical Oncology*, vol. 3, pp. S21–S35, 2011.

[64] J. R. Sierra, S. Corso, L. Caione et al., "Tumor angiogenesis and progression are enhanced by Sema4D produced by tumor-associated macrophages," *The Journal of Experimental Medicine*, vol. 205, pp. 1673–1685, 2008.

[65] S. Benvenuti and P. M. Comoglio, "The MET receptor tyrosine kinase in invasion and metastasis," *Journal of Cellular Physiology*, vol. 213, pp. 316–325, 2007.

[66] M. Tokunou, T. Niki, K. Eguchi et al., "c-MET expression in myofibroblasts: role in autocrine activation and prognostic significance in lung adenocarcinoma," *The American Journal of Pathology*, vol. 158, pp. 1451–1463, 2001.

[67] E. Lengyel, D. Prechtel, J. H. Resau et al., "C-Met overexpression in node-positive breast cancer identifies patients with

poor clinical outcome independent of Her2/neu," *International Journal of Cancer*, vol. 113, pp. 678–682, 2005.

[68] S. Koochekpour, M. Jeffers, S. Rulong et al., "Met and hepatocyte growth factor/scatter factor expression in human gliomas," *Cancer Research*, vol. 57, pp. 5391–5398, 1997.

[69] C. Liu, M. Park, and M. S. Tsao, "Overexpression of c-met proto-oncogene but not epidermal growth factor receptor or c-erbB-2 in primary human colorectal carcinomas," *Oncogene*, vol. 7, pp. 181–185, 1992.

[70] T. Furukawa, W. P. Duguid, M. Kobari, S. Matsuno, and M. S. Tsao, "Hepatocyte growth factor and Met receptor expression in human pancreatic carcinogenesis," *The American Journal of Pathology*, vol. 147, pp. 889–895, 1995.

[71] R. Ramirez, D. Hsu, A. Patel et al., "Over-expression of hepatocyte growth factor/scatter factor (HGF/SF) and the HGF/SF receptor (cMET) are associated with a high risk of metastasis and recurrence for children and young adults with papillary thyroid carcinoma," *Clinical Endocrinology*, vol. 53, pp. 635–644, 2000.

[72] M. Olivero, G. Valente, A. Bardelli et al., "Novel mutation in the ATP-binding site of the MET oncogene tyrosine kinase in a HPRCC family," *International Journal of Cancer*, vol. 82, pp. 640–643, 1999.

[73] Y. Kwak, S.-I. Kim, C.-K. Park, S. H. Paek, S.-T. Lee, and S.-H. Park, "C-MET overexpression and amplification in gliomas," *International Journal of Clinical and Experimental Pathology*, vol. 8, pp. 14932–14938, 2015.

[74] F. BaccoDe, P. Luraghi, E. Medico et al., "Induction of MET by ionizing radiation and its role in radioresistance and invasive growth of cancer," *Journal of the National Cancer Institute*, vol. 103, pp. 645–661, 2011.

[75] E. C. Smyth, F. Sclafani, and D. Cunningham, "Emerging molecular targets in oncology: clinical potential of MET/hepatocyte growth-factor inhibitors," *OncoTargets and Therapy*, vol. 7, pp. 1001–1014, 2014.

[76] Z. S. Zeng, M. R. Weiser, E. Kuntz et al., "c-Met gene amplification is associated with advanced stage colorectal cancer and liver metastases," *Cancer Letters*, vol. 265, pp. 258–269, 2008.

[77] M. R. Adams, R. Sears, F. Nuckolls, G. Leone, and J. R. Nevins, "Complex transcriptional regulatory mechanisms control expression of the E2F3 locus," *Molecular and Cellular Biology*, vol. 20, pp. 3633–3639, 2000.

[78] Y. He, M. K. Armanious, M. J. Thomas, and W. D. Cress, "Identification of E2F-3B, an alternative form of E2F-3 lacking a conserved N-terminal region," *Oncogene*, vol. 19, pp. 3422–3433, 2000.

[79] G. Leone, J. DeGregori, Z. Yan et al., "E2F3 activity is regulated during the cell cycle and is required for the induction of S phase," *Genes & Development*, vol. 12, pp. 2120–2130, 1998.

[80] L. J. Kong, J. T. Chang, A. H. Bild, and J. R. Nevins, "Compensation and specificity of function within the E2F family," *Oncogene*, vol. 26, pp. 321–327, 2007.

[81] D. Chen, M. Pacal, P. Wenzel, P. S. Knoepfler, G. Leone, and R. Bremner, "Division and apoptosis of E2f-deficient retinal progenitors," *Nature*, vol. 462, pp. 925–929, 2009.

[82] L. Wu, C. Timmers, B. Maiti et al., "The E2F1-3 transcription factors are essential for cellular proliferation," *Nature*, vol. 414, pp. 457–462, 2001.

[83] S.-Y. Tsai, R. Opavsky, N. Sharma et al., "Mouse development with a single E2F activator," *Nature*, vol. 454, pp. 1137–1141, 2008.

[84] M. Y. Lee, C. S. Moreno, and H. Saavedra, "E2F activators signal and maintain centrosome amplification in breast cancer cells," *Molecular and Cellular Biology*, vol. 34, pp. 2581–2599, 2014.

[85] Q. An, Y. Wang, R. An et al., "Association of E2F3 expression with clinicopathological features of Wilms' tumors," *Journal of Pediatric Surgery*, vol. 48, pp. 2187–2193, 2013.

[86] C. S. Cooper, A. G. Nicholson, C. Foster et al., "Nuclear overexpression of the E2F3 transcription factor in human lung cancer," *Lung Cancer*, vol. 54, pp. 155–162, 2006.

[87] X. Zeng, F. Yin, X. Liu et al., "Upregulation of E2F transcription factor 3 is associated with poor prognosis in hepatocellular carcinoma," *Oncology Reports*, vol. 31, pp. 1139–1146, 2014.

[88] L. Huang, J. Luo, Q. Cai et al., "MicroRNA-125b suppresses the development of bladder cancer by targeting E2F3," *International Journal of Cancer*, vol. 128, pp. 1758–1769, 2011.

[89] M. Oeggerli, P. Schraml, C. Ruiz et al., "E2F3 is the main target gene of the 6p22 amplicon with high specificity for human bladder cancer," *Oncogene*, vol. 25, pp. 6538–6543, 2006.

[90] A. Feber, J. Clark, G. Goodwin et al., "Amplification and overexpression of E2F3 in human bladder cancer," *Oncogene*, vol. 23, pp. 1627–1630, 2004.

[91] A. Y. Olsson, A. Feber, S. R. Edwards et al., "Role of E2F3 expression in modulating cellular proliferation rate in human bladder and prostate cancer cells," *Oncogene*, vol. 26, pp. 1028–1037, 2007.

[92] C. S. Foster, A. Falconer, A. R. Dodson et al., "Transcription factor E2F3 overexpressed in prostate cancer independently predicts clinical outcome," *Oncogene*, vol. 23, pp. 5871–5879, 2004.

[93] E. Lazzerini Denchi, C. Attwooll, D. Pasini, and K. Helin, "Deregulated E2F activity induces hyperplasia and senescence-like features in the mouse pituitary gland," *Molecular and Cellular Biology*, vol. 25, pp. 2660–2672, 2005.

[94] C. Schluter, M. Duchrow, C. Wohlenberg et al., "The cell proliferation-associated antigen of antibody Ki-67: a very large, ubiquitous nuclear protein with numerous repeated elements, representing a new kind of cell cycle-maintaining proteins," *The Journal of Cell Biology*, vol. 123, pp. 513–522, 1993.

[95] T. Scholzen and J. Gerdes, "The Ki-67 protein: from the known and the unknown," *Journal of Cellular Physiology*, vol. 182, pp. 311–322, 2000.

[96] J. Gerdes, U. Schwab, H. Lemke, and H. Stein, "Production of a mouse monoclonal antibody reactive with a human nuclear antigen associated with cell proliferation," *International Journal of Cancer*, vol. 31, pp. 13–20, 1983.

[97] J. Gerdes, H. Lemke, H. Baisch, H. H. Wacker, U. Schwab, and H. Stein, "Cell cycle analysis of a cell proliferation-associated human nuclear antigen defined by the monoclonal antibody Ki-67," *Journal of Immunology*, vol. 133, no. 4, pp. 1710–1715, 1984.

[98] J. Bullwinkel, B. Baron-Lühr, A. Lüdemann, C. Wohlenberg, J. Gerdes, and T. Scholzen, "Ki-67 protein is associated with ribosomal RNA transcription in quiescent and

proliferating cells," *Journal of Cellular Physiology*, vol. 206, pp. 624–635, 2006.

[99] R. Rahmanzadeh, G. Hüttmann, J. Gerdes, and T. Scholzen, "Chromophore-assisted light inactivation of pKi-67 leads to inhibition of ribosomal RNA synthesis," *Cell Proliferation*, vol. 40, pp. 422–430, 2007.

[100] R. J. Bryant, P. M. Banks, and D. P. O'Malley, "Ki67 staining pattern as a diagnostic tool in the evaluation of lymphoproliferative disorders," *Histopathology*, vol. 48, pp. 505–515, 2006.

[101] Y. L. Ma, J. Y. Peng, P. Zhang, W. J. Liu, L. Huang, and H. L. Qin, "Immunohistochemical analysis revealed CD34 and Ki67 protein expression as significant prognostic factors in colorectal cancer," *Medical Oncology*, vol. 27, pp. 304–309, 2010.

[102] R. N. Das, U. Chatterjee, S. K. Sinha, A. K. Ray, K. Saha, and S. Banerjee, "Study of histopathological features and proliferation markers in cases of Wilms' tumor," *Indian Journal of Medical and Paediatric Oncology: Official Journal of Indian Society of Medical & Paediatric Oncology*, vol. 33, pp. 102–106, 2012.

[103] G. Fisher, Z. H. Yang, S. Kudahetti et al., "Prognostic value of Ki-67 for prostate cancer death in a conservatively managed cohort," *British Journal of Cancer*, vol. 108, pp. 271–277, 2013.

[104] N. V. Shivaprasad, S. Satish, S. Ravishankar, and M. G. Vimalambike, "Ki-67 immunostaining in astrocytomas: association with histopathological grade - a South Indian study," *Journal of Neurosciences in Rural Practice*, vol. 7, pp. 510–514, 2016.

[105] I. Markova, M. Duskova, M. Lubusky et al., "Selected immunohistochemical prognostic factors in endometrial cancer," *International Journal of Gynecological Cancer*, vol. 20, pp. 576–582, 2010.

[106] K. Kontzoglou, V. Palla, G. Karaolanis et al., "Correlation between Ki67 and breast cancer prognosis," *Oncology*, vol. 84, pp. 219–225, 2013.

[107] E. C. Inwald, M. Klinkhammer-Schalke, F. Hofstadter et al., "Ki-67 is a prognostic parameter in breast cancer patients: results of a large population-based cohort of a cancer registry," *Breast Cancer Research and Treatment*, vol. 139, pp. 539–552, 2013.

[108] M. Ishihara, H. Mukai, S. Nagai et al., "Retrospective analysis of risk factors for central nervous system metastases in operable breast cancer: effects of biologic subtype and Ki67 overexpression on survival," *Oncology*, vol. 84, pp. 135–140, 2013.

[109] U. Kucuk, U. Bayol, E. E. Pala, and S. Cumurcu, "Importance of P53, Ki-67 expression in the differential diagnosis of benign/malignant phyllodes tumors of the breast," *Indian Journal of Pathology & Microbiology*, vol. 56, pp. 129–134, 2013.

[110] S. C. Stoian, C. Simionescu, C. Margaritescu, A. Stepan, and M. Nurciu, "Endometrial carcinomas: correlation between ER, PR, Ki67 status and histopathological prognostic parameters," *Romanian Journal of Morphology and Embryology*, vol. 52, pp. 631–636, 2011.

[111] A. Mourtzikou, K. Kosmas, A. Marouga, M. Stamouli, A. Pouliakis, and P. Karakitsos, "The use of an immunocytochemical double-labeling staining can display the distribution of Bcl-2/Ki-67 cells in endometrial adenocarcinomas as well as in normal endometrium," *Clinical Laboratory*, vol. 58, pp. 133–144, 2012.

[112] U. Kucukgoz Gulec, D. Gumurdulu, A. B. Guzel et al., "Prognostic importance of survivin, Ki-67, and topoisomerase IIα in ovarian carcinoma," *Archives of Gynecology and Obstetrics*, vol. 289, pp. 393–398, 2014.

[113] B. Belev, I. Brcic, J. Prejac et al., "Role of Ki-67 as a prognostic factor in gastrointestinal stromal tumors," *World Journal of Gastroenterology*, vol. 19, pp. 523–527, 2013.

[114] M. Preusser, R. Hoeftberger, A. Woehrer et al., "Prognostic value of Ki67 index in anaplastic oligodendroglial tumours - a translational study of the European Organization for Research and Treatment of Cancer Brain Tumor Group," *Histopathology*, vol. 60, pp. 885–894, 2012.

[115] K. A. Harradine and R. J. Akhurst, "Mutations of TGFβ signaling molecules in human disease," *Annals of Medicine*, vol. 38, pp. 403–414, 2006.

[116] A. B. Roberts, "Molecular and cell biology of TGF-β," *Mineral and Electrolyte Metabolism*, vol. 24, pp. 111–119, 1998.

[117] J. Seoane, "Escaping from the TGFβ anti-proliferative control," *Carcinogenesis*, vol. 27, pp. 2148–2156, 2006.

[118] H. G. Kang, M. H. Chae, J. M. Park et al., "Polymorphisms in TGF-β1 gene and the risk of lung cancer," *Lung Cancer*, vol. 52, pp. 1–7, 2006.

[119] A. Helmy, O. A. Hammam, T. R. LithyEl, and M. M. Deen WishahiEl, "The role of TGF-beta-1 protein and TGF-beta-R-1 receptor in immune escape mechanism in bladder cancer," *MedGenMed*, vol. 9, p. 34, 2007.

[120] V. Ivanovic, M. Demajo, K. Krtolica et al., "Elevated plasma TGF-β_1 levels correlate with decreased survival of metastatic breast cancer patients," *Clinica Chimica Acta*, vol. 371, pp. 191–193, 2006.

[121] X. Sun, S. A. Robertson, and W. V. Ingman, "Regulation of epithelial cell turnover and macrophage phenotype by epithelial cell-derived transforming growth factor beta1 in the mammary gland," *Cytokine*, vol. 61, pp. 377–388, 2013.

[122] W. Wick, M. Platten, and M. Weller, "Glioma cell invasion: regulation of metalloproteinase activity by TGF-β," *Journal of Neuro-Oncology*, vol. 53, pp. 177–185, 2001.

[123] C. Ren, T. Ren, K. Yang et al., "Inhibition of SOX2 induces cell apoptosis and G1/S arrest in Ewing's sarcoma through the PI3K/Akt pathway," *Journal of Experimental & Clinical Cancer Research*, vol. 35, p. 44, 2016.

[124] K. Takahashi, K. Tanabe, M. Ohnuki et al., "Induction of pluripotent stem cells from adult human fibroblasts by defined factors," *Cell*, vol. 131, pp. 861–872, 2007.

[125] J. Yu, M. A. Vodyanik, K. Smuga-Otto et al., "Induced pluripotent stem cell lines derived from human somatic cells," *Science*, vol. 318, pp. 1917–1920, 2007.

[126] Y. Chen, L. Shi, L. Zhang et al., "The molecular mechanism governing the oncogenic potential of SOX2 in breast cancer," *The Journal of Biological Chemistry*, vol. 283, pp. 17969–17978, 2008.

[127] X. Fang, W. Yu, L. Li et al., "ChIP-seq and functional analysis of the SOX2 gene in colorectal cancers," *OMICS*, vol. 14, pp. 369–384, 2010.

[128] E. A. Toraih, M. S. Fawzy, A. I. El-Falouji et al., "Stemness-related transcriptional factors and homing gene expression profiles in hepatic differentiation and cancer," *Molecular Medicine*, vol. 22, pp. 653–663, 2016.

[129] L. Annovazzi, M. Mellai, V. Caldera, G. Valente, and D. Schiffer, "SOX2 expression and amplification in gliomas

and glioma cell lines," *Cancer Genomics & Proteomics*, vol. 8, pp. 139–147, 2011.

[130] T. Otsubo, Y. Akiyama, K. Yanagihara, and Y. Yuasa, "SOX2 is frequently downregulated in gastric cancers and inhibits cell growth through cell-cycle arrest and apoptosis," *British Journal of Cancer*, vol. 98, pp. 824–831, 2008.

[131] D. Hockenbery, G. Nunez, C. Milliman, R. D. Schreiber, and S. J. Korsmeyer, "Bcl-2 is an inner mitochondrial membrane protein that blocks programmed cell death," *Nature*, vol. 348, pp. 334–336, 1990.

[132] Y. Tsujimoto and C. M. Croce, "Analysis of the structure, transcripts, and protein products of bcl-2, the gene involved in human follicular lymphoma," *Proceedings of the National Academy of Sciences of the United States of America*, vol. 83, pp. 5214–5218, 1986.

[133] A. M. Kabel, A. A. Adwas, A. A. Elkhoely, M. N. Abdel-Rahman, and A. A. Eissa, "Apoptosis: insights into pathways and role of p53, Bcl-2 and sphingosine kinases," *Journal of Cancer Research and Treatment*, vol. 4, pp. 69–72, 2016.

[134] V. S. Marsden, L. O'Connor, L. A. O'Reilly et al., "Apoptosis initiated by Bcl-2-regulated caspase activation independently of the cytochrome c/Apaf-1/caspase-9 apoptosome," *Nature*, vol. 419, pp. 634–637, 2002.

[135] M. Jiang and J. Milner, "Bcl-2 constitutively suppresses p53-dependent apoptosis in colorectal cancer cells," *Genes & Development*, vol. 17, pp. 832–837, 2003.

[136] S. Y. Sun, P. Yue, J. Y. Zhou et al., "Overexpression of BCL2 blocks TNF-related apoptosis-inducing ligand (TRAIL)-induced apoptosis in human lung cancer cells," *Biochemical and Biophysical Research Communications*, vol. 280, pp. 788–797, 2001.

[137] A. Autret and S. J. Martin, "Bcl-2 family proteins and mitochondrial fission/fusion dynamics," *Cellular and Molecular Life Sciences*, vol. 67, pp. 1599–1606, 2010.

[138] J. Chen, J. G. Flannery, M. M. LaVail, R. H. Steinberg, J. Xu, and M. I. Simon, "Bcl-2 overexpression reduces apoptotic photoreceptor cell death in three different retinal degenerations," *Proceedings of the National Academy of Sciences of the United States of America*, vol. 93, pp. 7042–7047, 1996.

[139] A. Majid, O. Tsoulakis, R. Walewska et al., "BCL2 expression in chronic lymphocytic leukemia: lack of association with the BCL2 938A>C promoter single nucleotide polymorphism," *Blood*, vol. 111, pp. 874–877, 2008.

[140] J. Iqbal, V. T. Neppalli, G. Wright et al., "BCL2 expression is a prognostic marker for the activated B-cell-like type of diffuse large B-cell lymphoma," *Journal of Clinical Oncology*, vol. 24, pp. 961–968, 2006.

[141] I. Skirnisdottir, T. Seidal, E. Gerdin, and B. Sorbe, "The prognostic importance of p53, bcl-2, and bax in early stage epithelial ovarian carcinoma treated with adjuvant chemotherapy," *International Journal of Gynecological Cancer*, vol. 12, pp. 265–276, 2002.

[142] C. Wei, Q. Luo, X. Sun et al., "microRNA-497 induces cell apoptosis by negatively regulating Bcl-2 protein expression at the posttranscriptional level in human breast cancer," *International Journal of Clinical and Experimental Pathology*, vol. 8, pp. 7729–7739, 2015.

[143] D. F. Mühlbeier, V. A. Saddi, É. C. Paulade et al., "Prognostic significance of apoptosis-related markers in patients with soft-tissue sarcomas of extremities," *Applied Immunohistochemistry & Molecular Morphology*, vol. 24, pp. 268–274, 2016.

[144] M. Abou El Hassan, D. C. J. Mastenbroek, W. R. Gerritsen, G. Giaccone, and F. A. E. Kruyt, "Overexpression of Bcl2 abrogates chemo- and radiotherapy-induced sensitisation of NCI-H460 non-small-cell lung cancer cells to adenovirus-mediated expression of full-length TRAIL," *British Journal of Cancer*, vol. 91, pp. 171–177, 2004.

[145] S. H. Kim, J. N. Ho, H. Jin et al., "Upregulated expression of BCL2, MCM7, and CCNE1 indicate cisplatin-resistance in the set of two human bladder cancer cell lines: T24 cisplatin sensitive and T24R2 cisplatin resistant bladder cancer cell lines," *Investigative and Clinical Urology*, vol. 57, pp. 63–72, 2016.

[146] Z. Tong, N. Liu, L. Lin, X. Guo, D. Yang, and Q. Zhang, "miR-125a-5p inhibits cell proliferation and induces apoptosis in colon cancer via targeting BCL2, BCL2L12 and MCL1," *Biomedicine & Pharmacotherapy*, vol. 75, pp. 129–136, 2015.

[147] C. Sun, Z. Liu, S. Li et al., "Down-regulation of c-Met and Bcl2 by microRNA-206, activates apoptosis, and inhibits tumor cell proliferation, migration and colony formation," *Oncotarget*, vol. 6, pp. 25533–25574, 2015.

[148] L. Li, L. Yuan, J. Luo, J. Gao, J. Guo, and X. Xie, "MiR-34a inhibits proliferation and migration of breast cancer through down-regulation of Bcl-2 and SIRT1," *Clinical and Experimental Medicine*, vol. 13, pp. 109–117, 2013.

[149] J.-C. Bourdon, K. Fernandes, F. Murray-Zmijewski et al., "p53 isoforms can regulate p53 transcriptional activity," *Genes & Development*, vol. 19, pp. 2122–2137, 2005.

[150] J.-C. Bourdon, "p53 and its isoforms in cancer," *British Journal of Cancer*, vol. 97, pp. 277–282, 2007.

[151] J. E. Chipuk and D. R. Green, "Dissecting p53-dependent apoptosis," *Cell Death and Differentiation*, vol. 13, pp. 994–1002, 2006.

[152] K. H. Vousden and D. P. Lane, "p53 in health and disease," *Nature Reviews. Molecular Cell Biology*, vol. 8, pp. 275–283, 2007.

[153] U. M. Moll, S. Wolff, D. Speidel, and W. Deppert, "Transcription-independent pro-apoptotic functions of p53," *Current Opinion in Cell Biology*, vol. 17, pp. 631–636, 2005.

[154] J. Nowak and J. L. Iovanna, "TP53INP2 is the new guest at the table of self-eating," *Autophagy*, vol. 5, pp. 383-384, 2009.

[155] D. Sala and A. Zorzano, "Is TP53INP2 a critical regulator of muscle mass?," *Current Opinion in Clinical Nutrition and Metabolic Care*, vol. 18, pp. 234–239, 2015.

[156] J. Nowak, C. Archange, J. Tardivel-Lacombe et al., "The TP53INP2 protein is required for autophagy in mammalian cells," *Molecular Biology of the Cell*, vol. 20, pp. 870–881, 2009.

[157] A. M. Cuervo, E. Bergamini, U. T. Brunk, W. Dröge, M. Ffrench, and A. Terman, "Autophagy and aging: the importance of maintaining "clean" cells," *Autophagy*, vol. 1, pp. 131–140, 2005.

[158] R. Mirzayans, B. Andrais, A. Scott, and D. Murray, "New insights into p53 signaling and cancer cell response to DNA damage: implications for cancer therapy," *Journal of Biomedicine and Biotechnology*, vol. 2012, Article ID 170325, 16 pages, 2012.

[159] T. A. Haj-Ahmad, M. A. Abdalla, and Y. Haj-Ahmad, "Potential urinary protein biomarker candidates for the

accurate detection of prostate cancer among benign prostatic hyperplasia patients," *Journal of Cancer*, vol. 5, pp. 103–114, 2014.

[160] M. He, Y. Zhao, H. Yi, H. Sun, X. Liu, and S. Ma, "The combination of TP53INP1, TP53INP2 and AXIN2: potential biomarkers in papillary thyroid carcinoma," *Endocrine*, vol. 48, pp. 712–717, 2015.

[161] T. Schlomm, E. Näkel, A. Lübke et al., "Marked gene transcript level alterations occur early during radical prostatectomy," *European Urology*, vol. 53, pp. 333–344, 2008.

[162] E. Staub, J. Gröne, D. Mennerich et al., "A genome-wide map of aberrantly expressed chromosomal islands in colorectal cancer," *Molecular Cancer*, vol. 5, p. 37, 2006.

[163] A. Nordgren, M. Corcoran, A. Sääf et al., "Characterisation of hairy cell leukaemia by tiling resolution array-based comparative genome hybridisation: a series of 13 cases and review of the literature," *European Journal of Haematology*, vol. 84, pp. 17–25, 2010.

[164] K. Moran-Jones, J. Grindlay, M. Jones, R. Smith, and J. C. Norman, "hnRNP A2 regulates alternative mRNA splicing of TP53INP2 to control invasive cell migration," *Cancer Research*, vol. 69, pp. 9219–9227, 2009.

[165] S. S. Boon and S. P. Sim, "Inhibitor of caspase-activated DNase expression enhances caspase-activated DNase expression and inhibits oxidative stress-induced chromosome breaks at the mixed lineage leukaemia gene in nasopharyngeal carcinoma cells," *Cancer Cell International*, vol. 15, p. 54, 2015.

[166] J. Zhang, H. Guo, G. Qian et al., "MiR-145, a new regulator of the DNA fragmentation factor-45 (DFF45)-mediated apoptotic network," *Molecular Cancer*, vol. 9, p. 211, 2010.

[167] L. Charrier, A. Jarry, C. Toquet et al., "Growth phase-dependent expression of ICADL/DFF45 modulates the pattern of apoptosis in human colonic cancer cells," *Cancer Research*, vol. 62, pp. 2169–2174, 2002.

[168] Y. Errami, H. Brim, K. Oumouna-Benachour et al., "ICAD deficiency in human colon cancer and predisposition to colon tumorigenesis: linkage to apoptosis resistance and genomic instability," *PLoS One*, vol. 8, article e57871, 2013.

[169] S. Konishi, H. Ishiguro, Y. Shibata et al., "Decreased expression of DFF45/ICAD is correlated with a poor prognosis in patients with esophageal carcinoma," *Cancer*, vol. 95, pp. 2473–2478, 2002.

[170] F. Abel, R. M. Sjöberg, C. Krona, S. Nilsson, and T. Martinsson, "Mutations in the N-terminal domain of DFF45 in a primary germ cell tumor and in neuroblastoma tumors," *International Journal of Oncology*, vol. 25, pp. 1297–1302, 2004.

[171] H. Linardou, K. T. Kalogeras, R. Kronenwett et al., "The prognostic and predictive value of mRNA expression of vascular endothelial growth factor family members in breast cancer: a study in primary tumors of high-risk early breast cancer patients participating in a randomized Hellenic Cooperative Oncology Group trial," *Breast Cancer Research*, vol. 14, article R145, 2012.

[172] D. Sa-Nguanraksa and P. O-Charoenrat, "The role of vascular endothelial growth factor a polymorphisms in breast cancer," *International Journal of Molecular Sciences*, vol. 13, pp. 14845–14864, 2012.

[173] D. Della-Morte, S. Riondino, P. Ferroni et al., "Impact of VEGF gene polymorphisms in elderly cancer patients: clinical outcome and toxicity," *Pharmacogenomics*, vol. 16, pp. 61–78, 2015.

[174] H. P. Gerber, A. McMurtrey, J. Kowalski et al., "Vascular endothelial growth factor regulates endothelial cell survival through the phosphatidylinositol 3′-kinase/Akt signal transduction pathway. Requirement for Flk-1/KDR activation," *The Journal of Biological Chemistry*, vol. 273, pp. 30336–30343, 1998.

[175] H. F. Dvorak, "Vascular permeability factor/vascular endothelial growth factor: a critical cytokine in tumor angiogenesis and a potential target for diagnosis and therapy," *Journal of Clinical Oncology*, vol. 20, pp. 4368–4380, 2002.

[176] W. G. Roberts and G. E. Palade, "Increased microvascular permeability and endothelial fenestration induced by vascular endothelial growth factor," *Journal of Cell Science*, vol. 108, pp. 2369–2379, 1995.

[177] K. DD, J. K. Zaleski, S. Liu, and T. A. Brock, "Vascular endothelial growth factor induces EDRF-dependent relaxation in coronary arteries," *The American Journal of Physiology*, vol. 265, pp. H586–H592, 1993.

[178] H. P. Gerber, V. Dixit, and N. Ferrara, "Vascular endothelial growth factor induces expression of the antiapoptotic proteins Bcl-2 and A1 in vascular endothelial cells," *The Journal of Biological Chemistry*, vol. 273, pp. 13313–13316, 1998.

[179] L. E. Benjamin, D. Golijanin, A. Itin, D. Pode, and E. Keshet, "Selective ablation of immature blood vessels in established human tumors follows vascular endothelial growth factor withdrawal," *The Journal of Clinical Investigation*, vol. 103, pp. 159–165, 1999.

[180] H. P. Gerber, K. J. Hillan, A. M. Ryan et al., "VEGF is required for growth and survival in neonatal mice," *Development*, vol. 126, pp. 1149–1159, 1999.

[181] P. Delmotte, B. Martin, M. Paesmans et al., "VEGF and survival of patients with lung cancer: a systematic literature review and meta-analysis," *Revue des Maladies Respiratoires*, vol. 19, pp. 577–584, 2002.

[182] P. A. Kyzas, I. W. Cunha, and J. P. Ioannidis, "Prognostic significance of vascular endothelial growth factor immunohistochemical expression in head and neck squamous cell carcinoma: a meta-analysis," *Clinical Cancer Research*, vol. 11, pp. 1434–1434, 2005.

[183] G. Des Guetz, B. Uzzan, P. Nicolas et al., "Microvessel density and VEGF expression are prognostic factors in colorectal cancer. Meta-analysis of the literature," *British Journal of Cancer*, vol. 94, pp. 1823–1832, 2006.

[184] P. Borgström, M. A. Bourdon, K. J. Hillan, P. Sriramarao, and N. Ferrara, "Neutralizing anti-vascular endothelial growth factor antibody completely inhibits angiogenesis and growth of human prostate carcinoma micro tumors in vivo," *The Prostate*, vol. 1, no. 35, pp. 1–10, 1998.

[185] K. J. Kim, B. Li, J. Winer et al., "Inhibition of vascular endothelial growth factor-induced angiogenesis suppresses tumour growth in vivo," *Nature*, vol. 362, pp. 841–844, 1993.

[186] S. P. Balasubramanian, A. Cox, S. S. Cross, S. E. Higham, N. J. Brown, and M. W. Reed, "Influence of VEGF-A gene variation and protein levels in breast cancer susceptibility and severity," *International Journal of Cancer*, vol. 121, pp. 1009–1016, 2007.

[187] L. Rydén, M. Stendahl, H. Jonsson, S. Emdin, N. O. Bengtsson, and G. Landberg, "Tumor-specific VEGF-A and VEGFR2 in postmenopausal breast cancer patients with

long-term follow-up. Implication of a link between VEGF pathway and tamoxifen response," *Breast Cancer Research and Treatment*, vol. 89, pp. 135–143, 2005.

[188] H. Han, J. F. Silverman, T. S. Santucci et al., "Vascular endothelial growth factor expression in stage I non-small cell lung cancer correlates with neoangiogenesis and a poor prognosis," *Annals of Surgical Oncology*, vol. 8, pp. 72–79, 2001.

[189] G. Cao, X. Li, C. Qin, and J. Li, "Prognostic value of VEGF in hepatocellular carcinoma patients treated with sorafenib: a meta-analysis," *Medical Science Monitor*, vol. 21, pp. 3144–3151, 2015.

Hindawi
Oxidative Medicine and Cellular Longevity
Volume 2017, Article ID 1092015, 13 pages
https://doi.org/10.1155/2017/1092015

Research Article

Simvastatin Ameliorates Diabetic Cardiomyopathy by Attenuating Oxidative Stress and Inflammation in Rats

Nawal M. Al-Rasheed,[1,2] Nouf M. Al-Rasheed,[1] Iman H. Hasan,[1] Maha A. Al-Amin,[1] Hanaa N. Al-Ajmi,[1] Raeesa A. Mohamad,[3] and Ayman M. Mahmoud[4,5,6]

[1]*Department of Pharmacology and Toxicology, College of Pharmacy, King Saud University, Riyadh, Saudi Arabia*
[2]*Department of Pharmaceutical Sciences, College of Pharmacy, Princess Nourah bint Abdulrahman University, Riyadh, Saudi Arabia*
[3]*Department of Anatomy, College of Medicine, King Saud University, Riyadh, Saudi Arabia*
[4]*Physiology Division, Department of Zoology, Faculty of Science, Beni-Suef University, Beni Suef, Egypt*
[5]*Department of Endocrinology, Diabetes and Nutrition, Charité-University Medicine Berlin, Berlin, Germany*
[6]*Department of Endocrinology, Diabetes and Nutrition at the Center for Cardiovascular Research (CCR), Charité-University Medicine Berlin, Berlin, Germany*

Correspondence should be addressed to Ayman M. Mahmoud; ayman.mahmoud@science.bsu.edu.eg

Received 19 June 2017; Accepted 6 August 2017; Published 12 September 2017

Academic Editor: Simona G. Bungău

Simvastatin is a lipid-lowering agent used to treat hypercholesterolemia and to reduce the risk of heart disease. This study scrutinized the beneficial effects of simvastatin on experimental diabetic cardiomyopathy (DCM), pointing to the role of hyperglycemia-induced oxidative stress and inflammation. Diabetes was induced by intraperitoneal injection of streptozotocin and both control and diabetic rats received simvastatin for 90 days. Diabetic rats showed significant cardiac hypertrophy, body weight loss, hyperglycemia, and hyperlipidemia. Serum creatine kinase MB (CK-MB) and troponin I showed a significant increase in diabetic rats. Simvastatin significantly improved body weight, attenuated hyperglycemia and hyperlipidemia, and ameliorated CK-MB and troponin I. Simvastatin prevented histological alterations and deposition of collagen in the heart of diabetic animals. Lipid peroxidation and nitric oxide were increased in the heart of diabetic rats whereas antioxidant defenses were decreased. These alterations were significantly reversed by simvastatin. In addition, simvastatin decreased serum inflammatory mediators and expression of NF-κB in the diabetic heart. Cardiac caspase-3 was increased in the diabetic heart and decreased following treatment with simvastatin. In conclusion, our results suggest that simvastatin alleviates DCM by attenuating hyperglycemia/hyperlipidemia-induced oxidative stress, inflammation, and apoptosis.

1. Introduction

Cardiovascular disease (CVD) is the leading cause of morbidity and mortality in the world. Diabetes mellitus (DM) is a major contributing factor to CVD and heart failure [1]. A causative relationship between myocardial abnormalities and diabetes has been well demonstrated [2]. Diabetic cardiomyopathy (DCM) is the clinical condition associated with cardiac abnormalities provoked by diabetes [2]. It has been estimated that DCM affects approximately 12% of the diabetic patients and may lead to heart failure and death [3]. Cardiac hypertrophy, oxidative stress, inflammation, apoptosis, and myocardial interstitial fibrosis are the major features of DCM [4].

Persistent hyperglycemia in diabetes provokes excessive production of reactive oxygen species (ROS) and inflammation which play a key role in DCM [5, 6]. Hyperglycemia induces glucose auto-oxidation and surplus generation of ROS. Hyperlipidemia can also increase ROS production through stimulating nicotinamide adenine dinucleotide phosphate (NADPH) oxidases and inducing leakage of the mitochondrial electron transport chain [7]. Excess ROS

activates protein kinase C and subsequently nuclear factor-κB (NF-κB), leading to myocardial injury [5, 6]. NF-κB is a redox-sensitive protein complexes with a central role in inflammation [8]. Activated NF-κB promotes the transcription and release of inflammatory mediators such as tumor necrosis factor-α (TNF-α) and thereby provokes myocardial inflammation [8].

Statins are hydroxymethylglutaryl coenzyme A (HMG-CoA) reductase inhibitors with lipid-lowering effect. Statins are the first-line treatment for coronary artery disease and are widely prescribed to prevent hypercholesterolemia [9]. Studies have shown the beneficial outcomes of statins on the cardiovascular system. In this context, Liu et al. [10] have recently reported that rosuvastatin postconditioning can protect isolated hearts against ischemia-reperfusion injury. Independently of their lipid-lowering effects, chronic pretreatment with statins preserved the integrity of microvasculature after acute myocardial infarction [11]. Improved myocardial perfusion and decreased infarction areas after ischemic reperfusion have been associated with early and chronic pretreatment with statins [11, 12]. The beneficial therapeutic outcomes of statins have been attributed to their ability to activate protein kinase B and endothelial nitric oxide synthase (eNOS) [13] and to attenuate oxidative stress [14, 15]. Previous studies have shown that simvastatin inhibits hypertrophy of cultured cardiomyocytes [16, 17] and in isoproterenol-induced rats [15]. In addition, simvastatin exerted protective effect against cardiac hypertrophy in a rat model of abdominal aortic constriction [18]. Recently, González-Herrera et al. [19] demonstrated that simvastatin can improve the pathophysiological condition in chronic Chagas cardiomyopathy experimental animal model. However, the protective effect of simvastatin against DCM has not yet been reported. Therefore, this study scrutinized the possible cardioprotective effect of simvastatin in a rat model of DCM.

2. Materials and Methods

2.1. Chemicals and Reagents. Simvastatin, streptozotocin (STZ), pyrogallol, reduced glutathione (GSH), malondialdehyde (MDA), thiobarbituric acid, and Griess reagent were supplied by Sigma-Aldrich (USA). Cholesterol, high-density lipoprotein (HDL) cholesterol, and triglyceride assay kits were supplied by Accurex (Mumbai, India). Antibodies for NF-κB p65 (Cat. number sc-372), caspase-3 (Cat. number sc-7148), and β-actin (Cat. number sc-47778) were purchased from Santa Cruz Biotechnology (USA). Other chemicals and reagents were supplied by Sigma-Aldrich or other standard suppliers.

2.2. Experimental Animals. Ten-week old male Wistar rats weighing 160–180 g were included in this investigation. The animals were supplied by the College of Pharmacy at King Saud University (Riyadh, Saudi Arabia) and were provided free access to standard laboratory diet of known composition and water ad libitum. The rats were maintained at normal atmospheric temperature ($23 \pm 2^{\circ}$C) on a 12 h light/dark cycle. The experimental protocol and all animal procedures were approved by the Institutional Research Ethics Committee, College of Pharmacy at King Saud University (Riyadh, Saudi Arabia).

2.3. Experimental Design and Treatments. Type 1 DM was induced by a single intraperitoneal (i.p.) injection of 55 mg/kg body weight STZ to overnight fasted rats. STZ solution was freshly prepared by dissolving in 0.1 M cold citrate buffer (pH 4.5). Diabetes was confirmed through the determination of blood glucose levels at 72 hr using MEDISAFE MINI blood glucose reader (TERUMO Corporation, Tokyo, Japan). Rats with blood glucose levels higher than 200 mg/dl were considered diabetic and selected for further experiments. Diabetes was further verified by measuring blood glucose levels 7 days after STZ injection. Normal control rats received a single i.p. dose of physiological saline.

Thirty-two rats (16 diabetic and 16 normal) were divided into 4 groups ($N = 8$) as follows:

Group I (control): Nondiabetic rats received physiological saline orally for 90 days.

Group II (SIM): Nondiabetic rats received simvastatin (10 mg/kg) [15] dissolved in saline by oral gavage for 90 days.

Group III (diabetic): Diabetic rats received physiological saline by oral gavage for 90 days.

Group IV (diabetic + SIM): Diabetic rats received simvastatin (10 mg/kg) for 90 days.

2.4. Sample Collection and Preparation. Twenty-four hours after the last treatment, overnight fasted rats were sacrificed by cervical dislocation. Blood was collected and processed to separate serum. Hearts were excised, washed, and weighed. Samples from the heart were homogenized in cold phosphate-buffered saline (10% *w*/*v*), and clear homogenate was collected to assay MDA, nitric oxide (NO), GSH, and superoxide dismutase (SOD). Other samples were collected on neutral buffered formalin for histological and immunohistochemical processing while others were kept at −80°C for Western blotting.

2.5. Biochemical Assays

2.5.1. Assay of Creatine Kinase MB (CK-MB) and Troponin I. Serum CK-MB and troponin I were determined using specific ELISA kits supplied by EIAab (Wuhan, China).

2.5.2. Assay of Serum Lipids and Cardiovascular Risk Indices. Total cholesterol [20], triglycerides [21], and HDL cholesterol [22] were assayed in serum of normal and diabetic rats using reagent kits purchased from Accurex (Mumbai, India). Low-density lipoprotein (LDL) cholesterol level was determined using the formula

$$\text{LDL cholesterol} = \text{total cholesterol} - \left(\left[\frac{\text{triglycerides}}{5} \right] + \text{HDL cholesterol} \right). \quad (1)$$

Very low-density lipoprotein (vLDL) cholesterol was calculated using the formula

$$\text{vLDL cholesterol} = \frac{\text{triglycerides}}{5}. \quad (2)$$

Cardiovascular risk indices [23] and atherogenic index of plasma (AIP) were calculated as follows:

$$\text{cardiovascular risk index 1} = \frac{\text{total cholesterol}}{\text{HDL cholesterol}},$$
$$\text{cardiovascular risk index 2} = \frac{\text{LDL cholesterol}}{\text{HDL cholesterol}},$$
$$\text{AIP} = \text{Log}_{10}\left(\frac{\text{triglycerides}}{\text{HDL cholesterol}}\right). \quad (3)$$

2.5.3. Assay of Tumor Necrosis Factor Alpha (TNF-α) and C-Reactive Protein (CRP). Serum TNF-α and CRP were determined using specific rat ELISA kits purchased from Merck Millipore (USA) and Abcam (USA), respectively.

2.5.4. Assay of Lipid Peroxidation, NO, GSH, and SOD. MDA, an index of lipid peroxidation, GSH, and SOD were assayed in the heart homogenates according to the methods described by Preuss et al. [24], Beutler et al. [25], Marklund and Marklund [26], respectively. NO in the heart homogenates was determined as nitrite content using Griess reagent [27].

2.6. Histopathology and Immunohistochemistry. Immediately after sacrifice, the hearts were excised, washed, and fixed in 10% neutral buffered formalin for 24 hr. Five μm-thick paraffin sections were prepared, cut, and stained with hematoxylin and eosin (H&E). Other sections were stained with Masson's trichrome. Stained heart sections were scanned and examined using light microscopy.

Other heart sections were blocked via incubation in 3% hydrogen peroxide and washed in Tris-buffered saline (TBS; pH 7.6). The slides were incubated with protein block (Novocastra) to prevent nonspecific binding of antibodies and probed with rabbit anti-caspase-3 (Santa Cruz Biotechnology, USA). The sections were then probed with anti-rabbit secondary antibody, washed, and counterstained with hematoxylin. Negative control sections were similarly processed with omission of incubation with the primary antibody.

2.7. Western Blot. To investigate the effect of simvastatin on NF-κB expression in the heart of normal and diabetic rats, Western blotting was applied as we recently reported [28]. Briefly, heart samples were homogenized in RIPA buffer containing proteinase inhibitors. Total protein content was assayed using Bradford reagent, and 40 μg proteins were separated on SDS-PAGE, electrotransferred onto nitrocellulose membranes and blocked in 5% skimmed milk in TBS Tween 20. The blocked membranes were probed with rabbit anti-NF-κB p65 and mouse anti-β-actin primary antibodies (Santa Cruz Biotechnology, USA). After washing, the membranes were incubated with the secondary antibodies and developed using enhanced chemiluminescence kit (Bio-Rad, USA). The blots were scanned and intensity of the obtained bands was quantified using ImageJ (NIH, USA). Results were normalized to β-actin and presented as percent of control.

2.8. Statistical Analysis. Results were presented as mean ± standard error of the mean (SEM). All statistical comparisons were made by means of the one-way ANOVA test followed by Tukey's test post hoc analysis using GraphPad Prism (GraphPad Software, CA, USA). A P value <0.05 was considered significant.

3. Results

3.1. Simvastatin Attenuates Body Weight Loss, Cardiac Hypertrophy, and Hyperglycemia in Diabetic Rats. Diabetic rats showed a significant ($P < 0.001$) body weight loss when compared with the control group (Figure 1(a)). Simvastatin significantly ($P < 0.01$) attenuated body weight loss in diabetic rats when supplemented for 90 days (Figure 1(a)). Normal rats that received simvastatin for 90 days showed nonsignificant ($P > 0.05$) changes in body weight when compared with the control group (Figure 1(a)).

Heart weight/body weight ratio (HW/BW) was significantly ($P < 0.01$) increased in diabetic rats when compared with the control group; an effect that was significantly ($P < 0.05$) repressed by simvastatin (Figure 1(b)). Simvastatin treatment for 90 days did not affect the HW/BW of normal rats as represented in Figure 1(b).

Blood glucose levels showed a significant ($P < 0.001$) increase when compared with the control rats (Figure 1(c)). Ninety days after, diabetic rats exhibited a significant ($P < 0.001$) increase in blood glucose when compared with the control rats. Simvastatin-treated diabetic rats showed a significant ($P < 0.001$) improvement in blood glucose levels when compared with the diabetic control rats (Figure 1(c)). Supplementation of simvastatin to normal rats did not affect blood glucose levels.

3.2. Simvastatin Prevents Hyperglycemia-Induced Damage and Collagen Deposition in the Diabetic Heart. To investigate hyperglycemia-induced myocardial injury and the possible protective role of simvastatin, we determined circulating CK-MB and troponin I levels and performed a histological study.

Diabetic rats showed significantly ($P < 0.001$) increased serum CK-MB. In contrast, diabetic rats treated with simvastatin exhibited a marked ($P < 0.001$) improvement in CK-MB (Figure 2(a)).

Similarly, diabetic rats showed a notable ($P < 0.001$) elevation in circulating levels of troponin I as showed in Figure 2(b). Treatment with simvastatin markedly ($P < 0.001$) improved serum troponin I levels in diabetic rats.

Treatment of normal rats with simvastatin did not induce significant changes in either CK-MB or troponin I.

Histopathological study of heart sections of normal control rats revealed normal histological appearance of both cardiomyocytes cytoplasm and nuclei (Figure 3(a)). Normal rats treated with simvastatin exhibited normal heart histology as showed in Figure 3(b). On the contrary, heart sections of diabetic rats showed myocardial degeneration

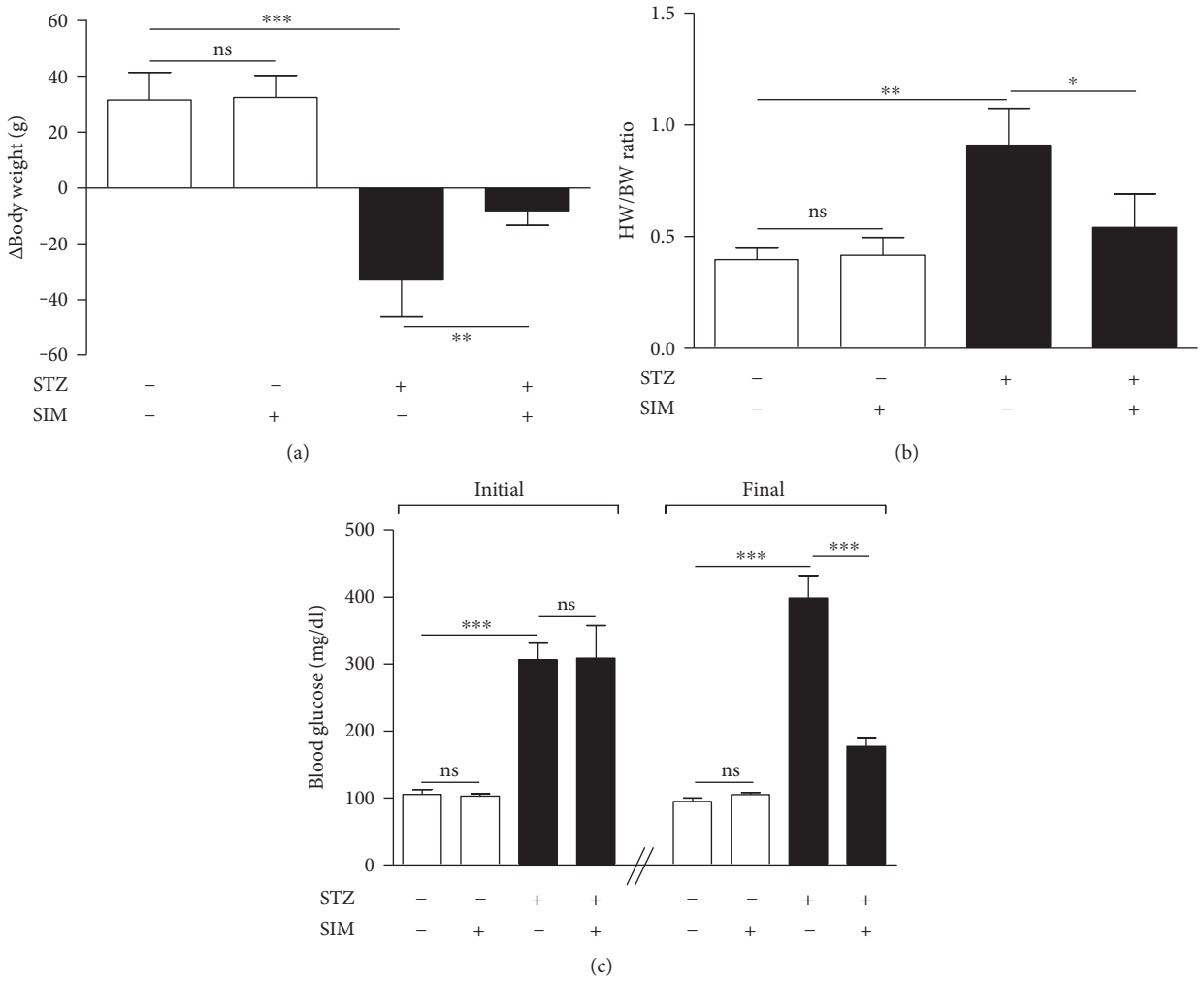

Figure 1: Simvastatin attenuates body weight loss (a), cardiac hypertrophy (b), and hyperglycemia (c) in STZ-induced diabetic rats. Data are $M \pm \text{SEM}$ ($N = 8$). $^{*}P < 05$, $^{**}P < 0.01$, and $^{***}P < 0.001$. STZ: streptozotocin; SIM: simvastatin; HW: heart weight; BW: body weight; ns: nonsignificant.

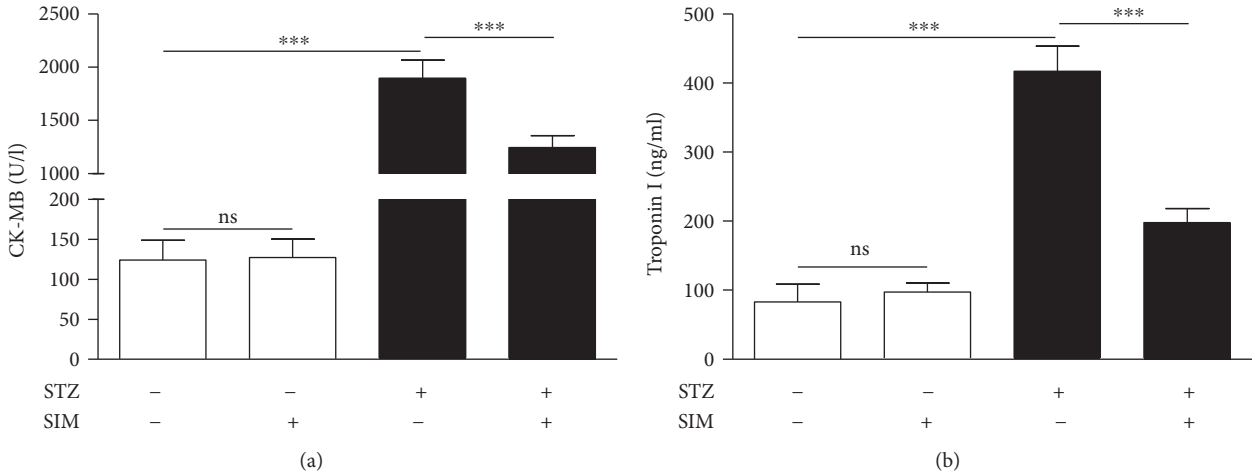

Figure 2: Simvastatin decreases serum CK-MB (a) and troponin I (b) levels in STZ-induced diabetic rats. Data are $M \pm \text{SEM}$ ($N = 8$). $^{***}P < 0.001$. STZ: streptozotocin; SIM: simvastatin; CK-MB: creatine kinase MB; ns: nonsignificant.

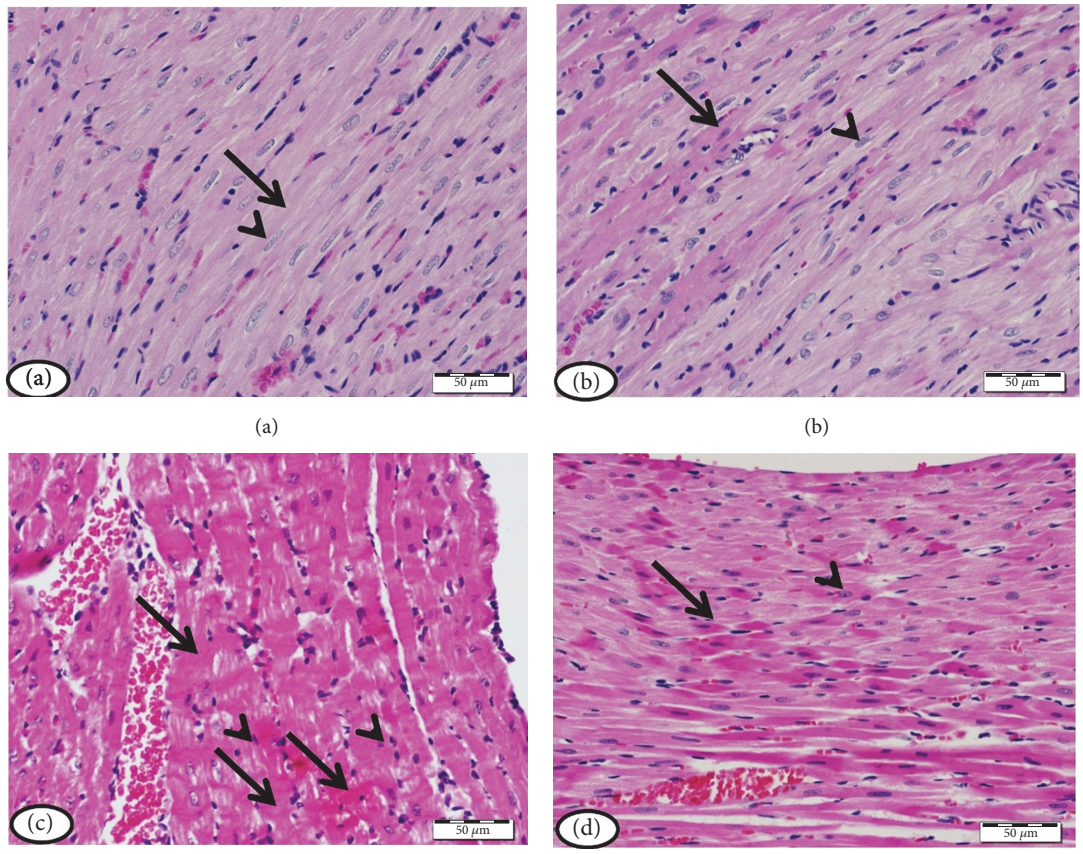

Figure 3: Heart of (a) normal control rats and (b) normal rats treated with simvastatin showing normal histological appearance of both myocardial cell cytoplasm (arrow) and nuclei (arrow head), (c) STZ-induced diabetic rats showing many myocardial cells with degenerated cytoplasm (arrow) and pyknotic nuclei (arrow head), and (d) diabetic rats treated with simvastatin showing decreased degeneration of myocardial cell cytoplasm (arrows) and nuclei (arrow heads). (H&E).

and pyknotic nuclei (Figure 3(c)). Simvastatin markedly prevented diabetes-induced myocardial damage as depicted in Figure 3(d).

The heart sections showing collagen deposition were represented in Figure 4. Control (Figure 4(a)) and simvastatin-treated rats (Figure 4(b)) showed normal interstitial collagen. Diabetic rats showed increased collagen deposition in the endomysium, especially surrounding blood vessels (Figure 4(c)). Diabetes-associated collagen deposition was markedly prevented in the heart of diabetic rats treated with simvastatin (Figure 4(d)).

3.3. Simvastatin Ameliorates Hyperlipidemia and Prevents Atherogenesis in Diabetic Rats. The impact of simvastatin on serum lipids and cardiovascular risk indices is depicted in Figure 5.

Diabetic rats showed an atherogenic lipid profile characterized by significant ($P < 0.001$) increase in serum triglycerides (Figure 5(a)) and total (Figure 5(b)), LDL (Figure 5(c)), and vLDL cholesterol (Figure 5(d)) when compared with the normal control rats. HDL cholesterol was significantly ($P < 0.001$) declined in serum of STZ-induced diabetic rats when compared with the control group (Figure 5(e)). Treatment of the diabetic rats with simvastatin significantly ($P < 0.001$) reversed these lipid profile derangements.

To evaluate the impact of hyperlipidemia on the heart and blood vessels and the protective effect of simvastatin, the cardiovascular risk indices and AIP were determined. Cardiovascular risk indices showed a pronounced ($P < 0.001$) increase in STZ-induced diabetic rats (Figures 5(f) and 5(g)) and AIP (Figure 5(h)). Treatment with simvastatin significantly ($P < 0.001$) decreased cardiovascular risk indices and AIP of the diabetic rats.

Normal rats that received simvastatin for 90 days showed nonsignificant ($P > 0.05$) changes in lipid profile, cardiovascular risk indices, and AIP.

3.4. Simvastatin Suppresses Diabetes-Induced Oxidative Stress in the Diabetic Heart. The effect of simvastatin on the myocardial redox status of normal and diabetic rats was investigated via assessment of MDA, NO, GSH, and SOD.

Diabetic animals exhibited a remarkable ($P < 0.001$) increase in the myocardial MDA (Figure 6(a)) and NO (Figure 6(b)). Treatment with simvastatin significantly ($P < 0.001$) decreased cardiac levels of MDA and NO in diabetic rats. In normal rats, simvastatin administration for 90 days did not affect MDA and NO levels.

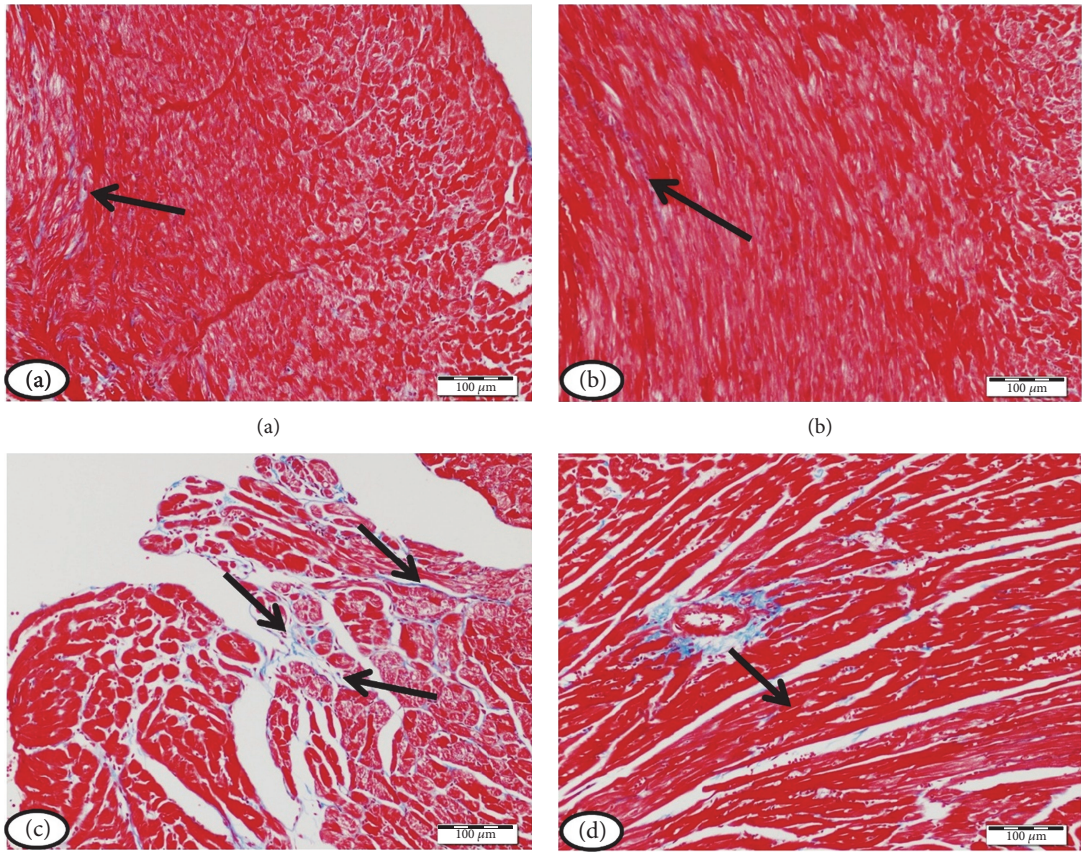

Figure 4: Heart of (a) control rats, (b) simvastatin-supplemented rats revealing normal amount and distribution of interstitial collagen (arrow), (c) STZ-induced diabetic rats with marked increase in the amount of collagen tissue in the endomysium especially surrounding blood vessels (arrows), and (d) diabetic rats treated with simvastatin showing decreased collagen deposition (arrow). (Masson's trichrome).

The antioxidant GSH was significantly ($P < 0.001$) declined in the heart of STZ-induced diabetic rats when compared with the control group (Figure 6(c)). In addition, diabetic rats showed a significant ($P < 0.01$) decrease in cardiac SOD activity (Figure 6(d)). Simvastatin, supplemented for 90 days, significantly ameliorated GSH content ($P < 0.001$) and SOD ($P < 0.05$) activity in the heart of diabetic rats while exerted nonsignificant ($P > 0.05$) effect in normal rats.

3.5. Simvastatin Inhibits Inflammation and Myocardial Apoptosis in Diabetic Rats. The ameliorative effect of simvastatin on diabetes-associated inflammation was explored via determination of serum TNF-α and CRP levels and cardiac NF-κB expression. TNF-α (Figure 7(a)) and CRP (Figure 7(a)) were significantly ($P < 0.001$) increased in diabetic rats. Simvastatin significantly decreased TNF-α and CRP in serum of the STZ-induced diabetic rats. Oral administration of simvastatin to control rats exerted nonsignificant ($P > 0.05$) effects on serum TNF-α and CRP.

Protein expression of NF-κB was significantly ($P < 0.001$) upregulated in the heart of STZ-induced diabetic rats (Figure 7(c)). Diabetic rats treated with simvastatin showed a significant ($P < 0.001$) downregulation of cardiac NF-κB expression. Simvastatin did not affect NF-κB expression levels in the heart of control rats (Figure 7(c)).

To investigate the protective effect of simvastatin on myocardial apoptosis in diabetes, the expression of caspase-3 was assessed by immunohistochemistry (Figure 7(d)). Heart sections of normal (Figure 7(d)-A) and simvastatin supplemented rats (Figure 7(d)-B) did not show caspase-3 immunopositive reaction of cardiomyocytes. STZ-induced diabetic rats showed marked increase in caspase-3 immunopositive stained cardiomyocytes (Figure 7(d)-C), an effect that was prevented by simvastatin (Figure 7(d)-D).

4. Discussion

Cardiomyopathy is an independent complication of DM which occurs in the absence of other heart diseases [29]. Hyperglycemia/hyperlipidemia-induced oxidative stress, inflammation, and apoptosis are probably involved in the pathogenesis of DCM [30, 31]. Here, we demonstrated the ameliorative potential of simvastatin on DCM in a rat model of STZ-induced diabetes. We provide the evidence that simvastatin ameliorates DCM via its ability to mitigate hyperglycemia, hyperlipidemia, oxidative stress, inflammation, and apoptosis.

The principal approach to control DM is lowering blood glucose levels. Here, STZ-induced diabetic rats exhibited a significant increase in blood glucose levels with

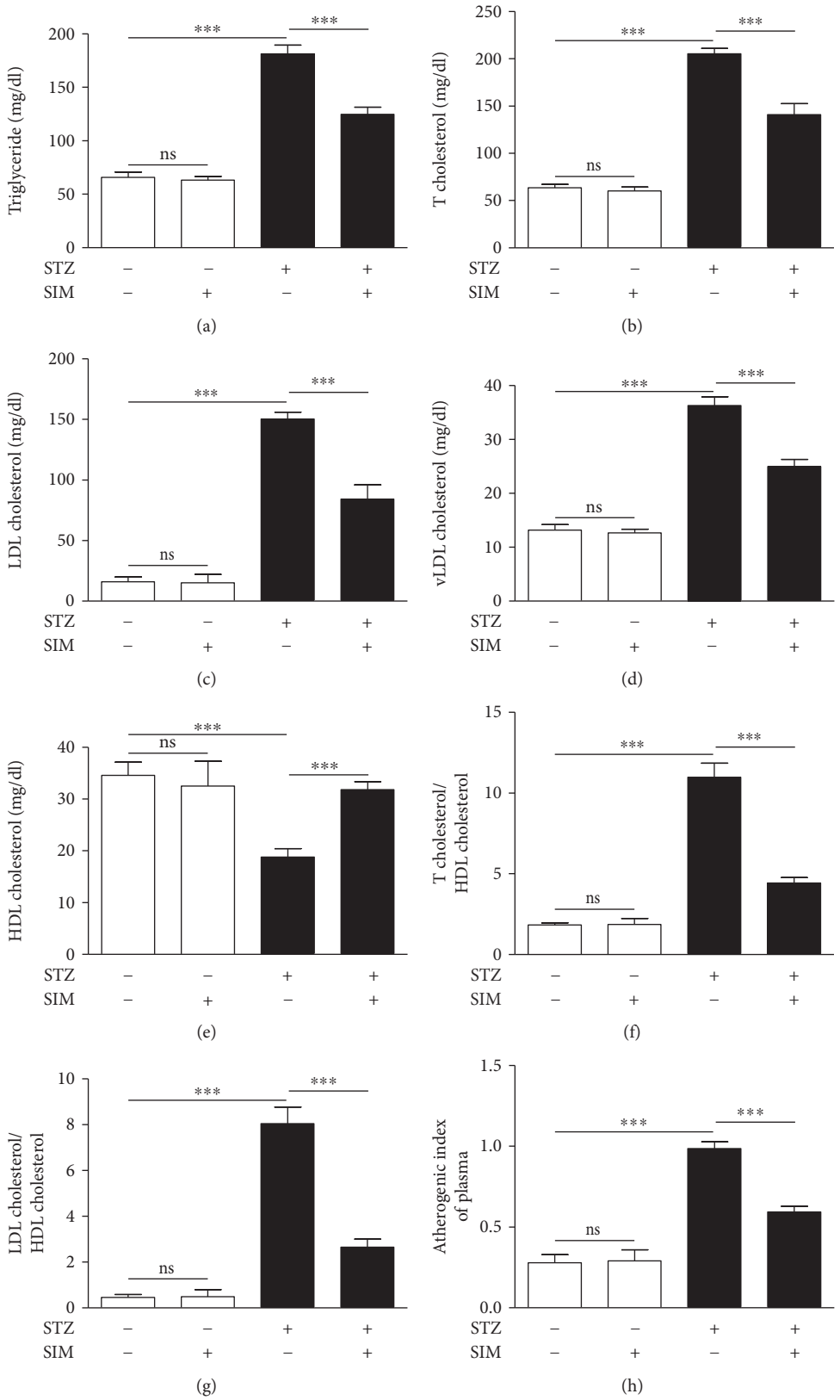

Figure 5: Simvastatin ameliorates hyperlipidemia and prevents atherogenesis in STZ-induced diabetic rats. Data are $M \pm \text{SEM}$ ($N = 8$). $^{***}P < 0.001$. STZ: streptozotocin; SIM: simvastatin; T cholesterol: total cholesterol; LDL: low-density lipoprotein; HDL: high-density lipoprotein; vLDL: very low density lipoprotein; ns: nonsignificant.

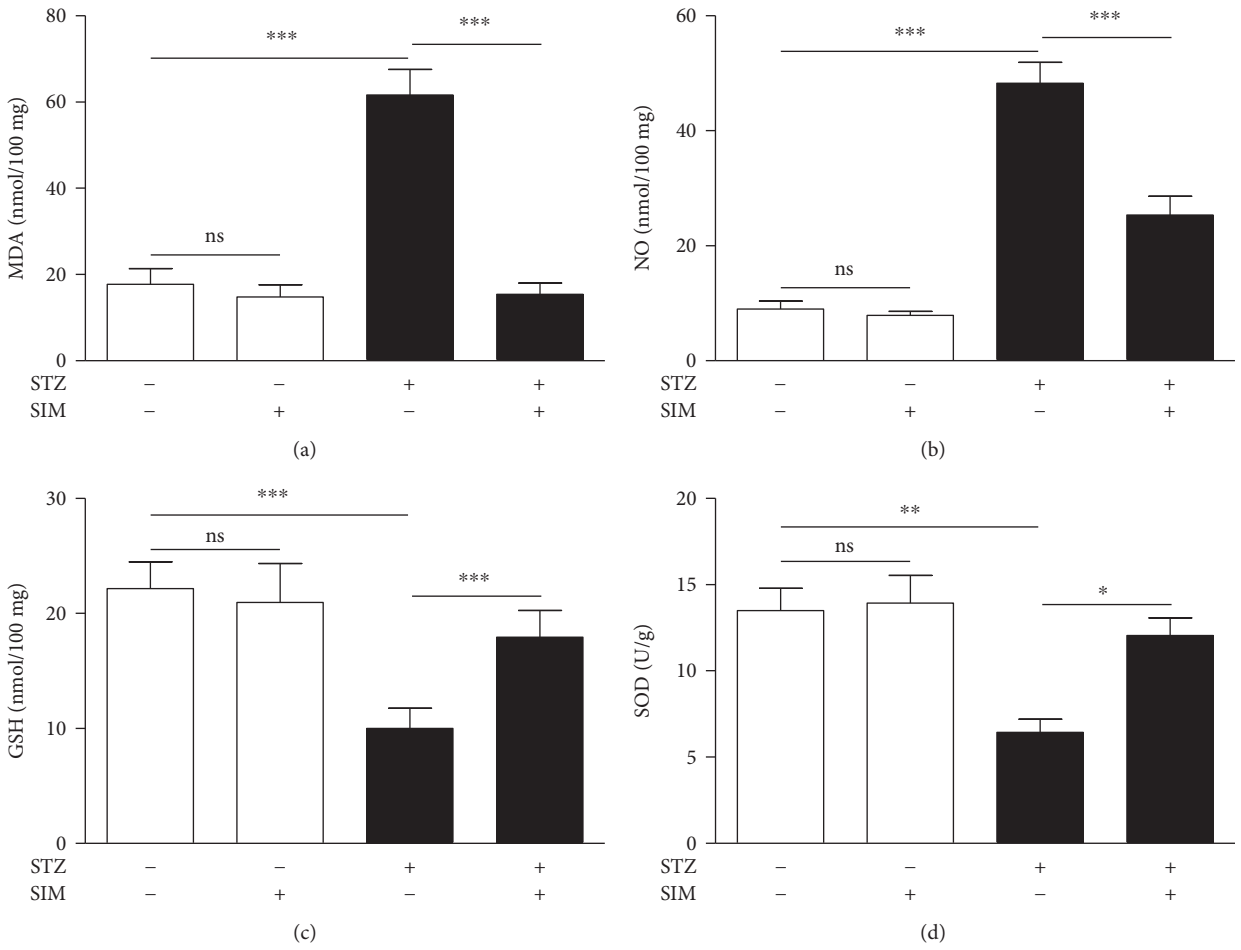

Figure 6: Simvastatin suppresses hyperglycemia-induced oxidative stress in the heart of STZ-induced diabetic rats. Data are $M \pm \text{SEM}$ ($N = 8$). $^{*}P < 0.05$, $^{**}P < 0.01$, and $^{***}P < 0.001$. STZ: streptozotocin; SIM: simvastatin; MDA: malondialdehyde; NO: nitric oxide; GSH: reduced glutathione; SOD: superoxide dismutase; ns: nonsignificant.

concomitantly declined body weight as we previously reported [32]. Treatment with simvastatin significantly improved blood glucose levels in diabetic rats. Similar findings have been described in type 1 [14] and type 2 diabetic rodent models [33]. The antihyperglycemic effect of statins may be attributed to their pleotropic effects, including increased insulin release and improved insulin signaling and protection of pancreatic β-cells from ROS [34, 35]. Additionally, statins have been proven to inhibit the activity of dipeptidyl peptidase IV (DPP-IV) [36]. In the same context, we have recently reported attenuated hyperglycemia and DCM in diabetic rats treated with the DPP-IV inhibitor sitagliptin [32]. The improved glycemic status following simvastatin treatment may have contributed to the alleviated body weight.

Oxidative stress and inflammation are known to promote cardiomyocyte hypertrophy in hyperglycemic conditions [37]. Here, diabetic rats exhibited cardiac hypertrophy evidenced by the increased HW/BW ratio. Similar findings have been reported in our recent study [32]. In our study, cardiac hypertrophy was associated with increased TNF-α and cardiac NF-κB expression. TNF-α has been reported to reduce degradation and increase synthesis of proteins in feline cardiomyocytes. These derangements occur through a mechanism involving preserved interaction between the extracellular matrix and cell integrins [38] and activation of NF-κB [39]. Increased rate of fatty acid (FA) oxidation in the diabetic myocardium results in lipid accumulation and subsequently cardiac hypertrophy [40]. Myocardial hypertrophy has also been reported to occur after 8 weeks of diabetes [41]. Simvastatin treatment prevented cardiac hypertrophy in the diabetic rats. This effect might be attributed to the attenuated inflammation and oxidative stress. In consistent with our findings, simvastatin has prevented isoproterenol-induced cardiac hypertrophy in rats as we previously reported [15]. In addition, Liu et al. [18] showed the capacity of simvastatin to prevent *in vitro* and *in vivo* myocardial hypertrophy.

Hyperglycemia provoked cardiomyocyte damage as evidenced by the myocardium degeneration and pyknotic nuclei and elevated serum CK-MB and troponin I. These derangements are direct consequences of hyperglycemia-induced oxidative stress, inflammation, and other alterations. Elevated serum level of CK-MB is a powerful and sensitive tool to predict the risk of cardiac complications [42]. The onset of myofibrillar disintegration and inflammation-

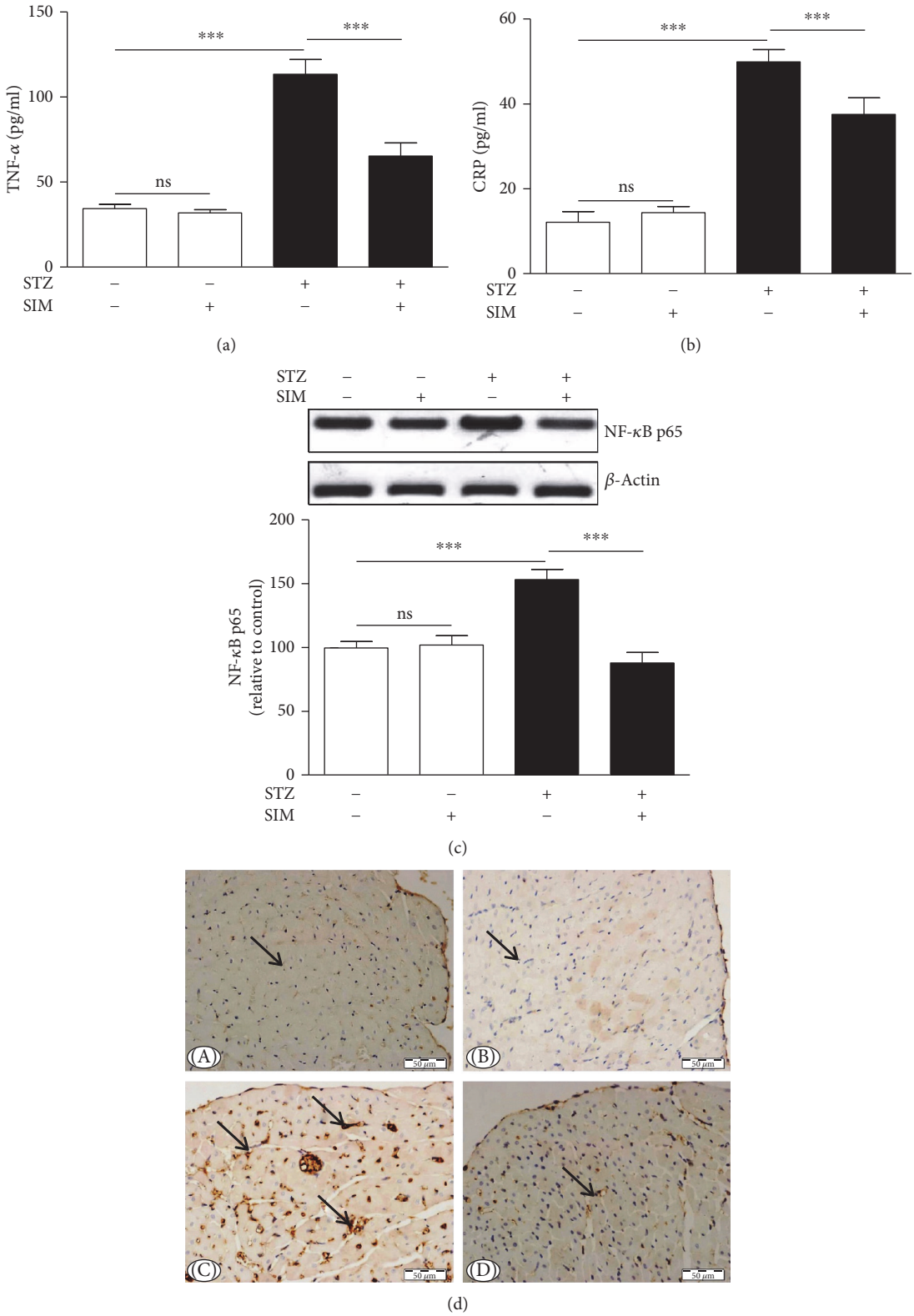

Figure 7: Simvastatin inhibits inflammation and myocardial apoptosis in STZ-induced diabetic rats. Simvastatin decreased serum levels of (a) TNF-α and (b) CRP and (c) NF-κB p65 expression in the heart of diabetic rats. Data are $M \pm \text{SEM}$ ($N = 8$). $^{***}P < 0.001$. STZ: streptozotocin; SIM: simvastatin; TNF-α: tumor necrosis factor alpha; CRP: C-reactive protein; NF-κB: nuclear factor kappaB; ns: nonsignificant. (d) Photomicrographs of caspase-3 immunostained sections in the heart of (A) control rats, (B) normal rats treated with simvastatin showing immune-negative reaction (arrow), (C) STZ-induced diabetic rats showing strong immunopositive reaction in many myocardial cells (arrows), and (D) diabetic rats treated with simvastatin showing marked decrease in caspase-3 immune-positivity of the myocardial cells (arrow).

induced increase in permeability are associated with elevated circulating CK-MB and troponin I [43]. Previous research from our lab showed increased CK-MB and troponin I in serum of rat models of myocardial hypertrophy [15] and DCM [32]. Hyperlipidemia is another factor that contributes to cell death and cardiac dysfunctions in diabetes. Hyperlipidemia promotes the deposition of triglycerides and cholesterol in the myocardium and influences cardiac toxicological consequences [44]. Simvastatin significantly ameliorated indices of myocardial damage in diabetic animals. Therefore, reduced CK-MB and troponin I in simvastatin-treated diabetic rats supports the role of lipid-lowering agents in reducing hyperglycemia/hyperlipidemia-induced myocardial damage.

Given its role in inducing the production of ROS [45] and deposition of lipids in the myocardium [44], hyperlipidemia exerts a direct impact on the myocardium and increases the risk of coronary heart disease [46]. Here, STZ-induced diabetic rats exhibited an atherogenic lipid profile characterized by significant increases in serum cholesterol, triglycerides, LDL cholesterol, and vLDL cholesterol. In contrast, the cardioprotective HDL cholesterol [47] was significantly declined in the diabetic rats. Moreover, diabetic rats showed significantly increased values of the cardiovascular risk indices and AIP which is a frequently used predictor of atherosclerosis [48]. Simvastatin significantly reduced hyperlipidemia, cardiovascular risk indices, and atherogenic index in diabetic rats, indicating its potent lipid-lowering, antiatherogenic, and cardioprotective effects.

Counteracting oxidative stress is another mechanism we assumed have mediated the protective effect of simvastatin on DCM. Hyperglycemia/hyperlipidemia-induced production of ROS and reactive nitrogen species (RNS) constitutes a major contributing factor in the development of DCM. Hyperglycemia promotes generation of ROS and RNS in the mitochondria [49], and increased cardiac FAs activate NADPH oxidases and induce leakage of the mitochondrial electron transport chain [7]. Excess ROS promote upsurges in lipid peroxidation and consequently alter membrane structure and enzyme activity [50]. In the present study, diabetic rats exhibited significantly elevated lipid peroxidation and NO in the myocardium. NO and superoxide radicals can react and produce peroxynitrite, leading to DNA fragmentation and protein damage [51]. Diabetic rats exhibited reduced cardiac GSH, indicating its overutilization in the redox-challenged cellular microenvironment. GSH depletion induces further oxidative damage and necrotic cell death [52, 53]. SOD, an enzyme catalyzing the dismutation of superoxide, showed declined activity in the diabetic heart. Simvastatin reduced lipid peroxidation and NO and alleviated antioxidants in the diabetic heart. Accordingly, simvastatin decreased lipid peroxidation and increased hepatic and renal GSH levels in diabetic rats [14]. We have previously demonstrated the ability of simvastatin to decrease ROS generation and enhance antioxidant defenses in a rodent model of cardiac hypertrophy [15]. Therefore, the efficacy of simvastatin to attenuate oxidative stress may mediate, at least in part, its protective effect against DCM.

Cardiac inflammation, apoptosis, and fibrosis have been defined in the diabetic heart [31]. Seddon et al. [54] reported that cardiac inflammation occurs as a consequence of hyperglycemia-induced excessive ROS generation in diabetes. In our study, diabetic rats showed a significant increase in circulating TNF-α and CRP. Previous experimental studies demonstrated the contributing role of chronic inflammatory status in DCM [55–57]. TNF-α has been reported to exert a crucial role in the development of myocardial hypertrophy and dysfunction [55–57]. In the study of Bozkurt et al. [58], exogenous administration of TNF-α induced *in vivo* cardiac inflammation and dysfunction. The role of TNF-α in DCM has been further supported through observing similar effects in a mouse model with cardiomyocyte-specific TNF-α overexpression [59]. Additionally, in a murine model of pressure overload, genetic disruption of TNF-α hampered cardiac hypertrophy, dysfunction, and fibrosis [60]. In STZ-induced DCM, TNF-α antagonism protected against myocardial inflammation, leukocyte infiltration, and fibrosis [61].

Elevated CRP in STZ-induced diabetic rats in the present investigation was in agreement with the findings of previous studies showing increased serum CRP levels in diabetic patients [62] and STZ-induced type 1 diabetic animals [63]. Interestingly, diabetic rats treated with simvastatin showed significantly reduced serum TNF-α and CRP levels. Therefore, the beneficial effect of simvastatin is connected to its ability to reduce inflammation. In accordance, we have previously reported attenuated inflammation in a rat model of cardiac hypertrophy following simvastatin administration [15].

Next, we demonstrated the effect of simvastatin on NF-κB expression in the diabetic heart. In consistent with the increased serum levels of TNF-α and CRP, cardiac NF-κB was upregulated in the diabetic rats. Different mechanisms implicated in the establishment of inflammation in the diabetic myocardium were reported to converge towards NF-κB activation. Hyperglycemia promotes NF-κB transcription through activation of NADPH oxidase and production of ROS [64], degradation of IκB [8], and activation of Erk1/2 [65] and mitogen-activated protein kinase (MAPK) [66]. Activated NF-κB induces the upregulation of TNF-α and other molecules contributing to cardiovascular damage [8]. Increased circulating lipids may also contribute to NF-κB activation in diabetes [67]. Treatment of the diabetic rats with simvastatin prevented NF-κB activation in the myocardium, confirming its anti-inflammatory efficacy. In an experimental model of cardiac hypertrophy, we have reported the ability of simvastatin to reduce NF-κB expression in the heart. This anti-inflammatory effect could be directly connected to its lipid-lowering mechanism.

Hyperglycemia-induced ROS generation can induce myocardial apoptosis and fibrosis [32, 54]. Myocardial inflammation promotes cardiomyocyte death and therefore contributes to cardiac remodeling [37]. Here, diabetic rats showed increased expression of the apoptosis marker caspase-3 in the myocardium. Apoptosis in the diabetic heart occurs as a direct result of sustained ROS production and inflammation. In this context, Haudek et al. [68] reported

that sustained TNF-α signaling provokes both intrinsic and extrinsic cell death pathways, increases caspase-3 activation, and promotes cardiomyocyte apoptosis. The proapoptotic effects of TNF-α are likely mediated via NF-κB activation [69]. Simvastatin markedly prevented hyperglycemia-induced cardiomyocyte apoptosis in STZ-induced diabetic rats via attenuating inflammation and ROS production.

Histological examination of the diabetic heart revealed myocardium degeneration and increased collagen deposition as we recently reported [32]. Oxidative stress, inflammation and cell injury are well-known causes of the cardiac fibrosis [61]. Cytokines and profibrotic factors released by cardiomyocytes and inflammatory cells stimulate fibrosis in the diabetic heart. Through its ability to activate WNT1 inducible-signaling pathway protein 1 (WISP1), TNF-α directly induces proliferation of cardiac fibroblast and production of collagen [70]. In addition, the profibrotic effects of cytokines have been shown to be boosted by ROS [55, 57]. Treatment with simvastatin markedly reduced collagen production and fibrosis, probably through its dual ability to enhance the antioxidant defenses and to reduce chronic inflammation in the heart of diabetic rats. Accordingly, statins have reduced cardiovascular events and mortality in diabetic patients [71]. Atorvastatin reduced myocardial inflammation and fibrosis in a diabetic rat model [72]. This effect was believed to be independent of atorvastatin's LDL cholesterol-lowering capacity [72]. Fluvastatin has also been reported to attenuate cardiac dysfunction and myocardial interstitial fibrosis in diabetes [73]. Therefore, lipid-lowering treatments seem to be effective in the attenuation of diabetes-associated cardiac fibrosis and cell injury together with a role in the primary prevention of the disease.

In conclusion, simvastatin has a protective effect on DCM. Simvastatin attenuated hyperglycemia/hyperlipidemia-induced oxidative stress and enhanced antioxidant defenses in the myocardium of diabetic rats. Simvastatin showed a strong modulatory effect against cardiac hypertrophy, inflammation, apoptosis, and fibrosis. Therefore, simvastatin and possibly other lipid-lowering agents can protect against DCM.

Conflicts of Interest

The authors declare that they have no conflicts of interest.

Acknowledgments

The authors extend their appreciation to the Deanship of Scientific Research at King Saud University for funding this work through research group no. RGP-1438-005.

References

[1] A. G. Bertoni, W. G. Hundley, M. W. Massing, D. E. Bonds, G. L. Burke, and D. C. Goff Jr, "Heart failure prevalence, incidence, and mortality in the elderly with diabetes," *Diabetes Care*, vol. 27, no. 3, p. 699, 2004.

[2] S. Boudina and E. D. Abel, "Diabetic cardiomyopathy revisited," *Circulation*, vol. 115, no. 25, pp. 3213–3223, 2007.

[3] A. Lorenzo-Almoros, J. Tunon, M. Orejas, M. Cortés, J. Egido, and Ó. Lorenzo, "Diagnostic approaches for diabetic cardiomyopathy," *Cardiovascular Diabetology*, vol. 16, no. 1, p. 28, 2017.

[4] Y. Saisho, "Glycemic variability and oxidative stress: a link between diabetes and cardiovascular disease?," *International Journal of Molecular Sciences*, vol. 15, no. 10, pp. 18381–18406, 2014.

[5] R. Khanra, S. Dewanjee, T. K Dua et al., "*Abroma augusta* L. (Malvaceae) leaf extract attenuates diabetes induced nephropathy and cardiomyopathy via inhibition of oxidative stress and inflammatory response," *Journal of Translational Medicine*, vol. 13, p. 6, 2015.

[6] N. Bhattacharjee, S. Barma, N. Konwar, S. Dewanjee, and P. Manna, "Mechanistic insight of diabetic nephropathy and its pharmacotherapeutic targets: an update," *European Journal of Pharmacology*, vol. 791, pp. 8–24, 2016.

[7] H. O. Steinberg, G. Paradisi, G. Hook, K. Crowder, J. Cronin, and A. D. Baron, "Free fatty acid elevation impairs insulin-mediated vasodilation and nitric oxide production," *Diabetes*, vol. 49, no. 7, pp. 1231–1238, 2000.

[8] M. S. Shah and M. Brownlee, "Molecular and cellular mechanisms of cardiovascular disorders in diabetes," *Circulation Research*, vol. 118, no. 11, pp. 1808–1829, 2016.

[9] N. K. Kapur and K. Musunuru, "Clinical efficacy and safety of statins in managing cardiovascular risk," *Vascular Health and Risk Management*, vol. 4, no. 2, pp. 341–353, 2008.

[10] C. W. Liu, F. Yang, S. Z. Cheng, Y. Liu, L. H. Wan, and H. L. Cong, "Rosuvastatin postconditioning protects isolated hearts against ischemia-reperfusion injury: the role of radical oxygen species, PI3K-Akt-GSK-3β pathway, and mitochondrial permeability transition pore," *Cardiovascular Therapeutics*, vol. 35, no. 1, pp. 3–9, 2017.

[11] K. Iwakura, H. Ito, S. Kawano et al., "Chronic pre-treatment of statins is associated with the reduction of the no-reflow phenomenon in the patients with reperfused acute myocardial infarction," *European Heart Journal*, vol. 27, no. 5, pp. 534–539, 2006.

[12] J. L. Zhao, Y. J. Yang, C. J. Cui, S. J. You, and R. L. Gao, "Pretreatment with simvastatin reduces myocardial no-reflow by opening mitochondrial K_{ATP} channel," *British Journal of Pharmacology*, vol. 149, no. 3, pp. 243–249, 2006.

[13] S. Manickavasagam, Y. Ye, Y. Lin et al., "The cardioprotective effect of a statin and cilostazol combination: relationship to Akt and endothelial nitric oxide synthase activation," *Cardiovascular Drugs and Therapy*, vol. 21, no. 5, pp. 321–330, 2007.

[14] A. M. Mohamadin, A. A. Elberry, H. S. Abdel Gawad, G. M. Morsy, and F. A. Al-Abbasi, "Protective effects of simvastatin, a lipid lowering agent, against oxidative damage in experimental diabetic rats," *Journal of Lipids*, vol. 2011, Article ID 167958, 13 pages, 2011.

[15] N. M. Al-Rasheed, M. M. Al-Oteibi, R. Z. Al-Manee et al., "Simvastatin prevents isoproterenol-induced cardiac hypertrophy through modulation of the JAK/STAT pathway," *Drug Design, Development and Therapy*, vol. 9, pp. 3217–3229, 2015.

[16] J. D. Luo, F. Xie, W. W. Zhang, X. D. Ma, J. X. Guan, and X. Chen, "Simvastatin inhibits noradrenaline-induced hypertrophy of cultured neonatal rat cardiomyocytes," *British Journal of Pharmacology*, vol. 132, no. 1, pp. 159–164, 2001.

[17] L. Wu, L. Zhao, Q. Zheng et al., "Simvastatin attenuates hypertrophic responses induced by cardiotrophin-1 via JAK-STAT pathway in cultured cardiomyocytes," *Molecular and Cellular Biochemistry*, vol. 284, no. 1-2, pp. 65–71, 2006.

[18] J. Liu, Q. Shen, and Y. Wu, "Simvastatin prevents cardiac hypertrophy in vitro and in vivo via JAK/STAT pathway," *Life Sciences*, vol. 82, no. 19-20, pp. 991–996, 2008.

[19] F. Gonzalez-Herrera, A. Cramer, P. Pimentel et al., "Simvastatin attenuates endothelial activation through 15-epi-lipoxin A4 production in murine chronic Chagas cardiomyopathy," *Antimicrobial Agents and Chemotherapy*, vol. 61, no. 3, 2017.

[20] C. C. Allain, L. S. Poon, C. S. Chan, W. Richmond, and P. C. Fu, "Enzymatic determination of total serum cholesterol," *Clinical Chemistry*, vol. 20, no. 4, pp. 470–475, 1974.

[21] P. Fossati and L. Prencipe, "Serum triglycerides determined colorimetrically with an enzyme that produces hydrogen peroxide," *Clinical Chemistry*, vol. 28, no. 10, pp. 2077–2080, 1982.

[22] M. Burstein, H. R. Scholnick, and R. Morfin, "Rapid method for the isolation of lipoproteins from human serum by precipitation with polyanions," *Journal of Lipid Research*, vol. 11, no. 6, pp. 583–595, 1970.

[23] R. Ross, "The pathogenesis of atherosclerosis," in *Heart Disease: A Textbook of Cardiovascular Medicine*, E. Braunwald, Ed., pp. 1106–1124, WB Saunders, Philadelphia, PA, 1992.

[24] H. G. Preuss, S. T. Jarrell, R. Scheckenbach, S. Lieberman, and R. A. Anderson, "Comparative effects of chromium, vanadium and Gymnema sylvestre on sugar-induced blood pressure elevations in SHR," *Journal of the American College of Nutrition*, vol. 17, no. 2, pp. 116–123, 1998.

[25] E. Beutler, O. Duron, and B. M. Kelly, "Improved method for the determination of blood glutathione," *The Journal of Laboratory and Clinical Medicine*, vol. 61, pp. 882–888, 1963.

[26] S. Marklund and G. Marklund, "Involvement of the superoxide anion radical in the autoxidation of pyrogallol and a convenient assay for superoxide dismutase," *European Journal of Biochemistry*, vol. 47, no. 3, pp. 469–474, 1974.

[27] M. B. Grisham, G. G. Johnson, and J. R. Lancaster Jr., "Quantitation of nitrate and nitrite in extracellular fluids," *Methods in Enzymology*, vol. 268, pp. 237–246, 1996.

[28] A. M. Mahmoud, M. O. Germoush, M. F. Alotaibi, and O. E. Hussein, "Possible involvement of Nrf2 and PPARγ up-regulation in the protective effect of umbelliferone against cyclophosphamide-induced hepatotoxicity," *Biomedicine & Pharmacotherapy*, vol. 86, pp. 297–306, 2017.

[29] K. Huynh, B. C. Bernardo, J. R. McMullen, and R. H. Ritchie, "Diabetic cardiomyopathy: mechanisms and new treatment strategies targeting antioxidant signaling pathways," *Pharmacology & Therapeutics*, vol. 142, no. 3, pp. 375–415, 2014.

[30] I. Falcao-Pires and A. F. Leite-Moreira, "Diabetic cardiomyopathy: understanding the molecular and cellular basis to progress in diagnosis and treatment," *Heart Failure Reviews*, vol. 17, no. 3, pp. 325–344, 2012.

[31] H. Suzuki, Y. Kayama, M. Sakamoto et al., "Arachidonate 12/15-lipoxygenase-induced inflammation and oxidative stress are involved in the development of diabetic cardiomyopathy," *Diabetes*, vol. 64, no. 2, pp. 618–630, 2015.

[32] N. M. Al-Rasheed, N. M. Al-Rasheed, I. H. Hasan, M. A. Al-Amin, H. N. Al-Ajmi, and A. M. Mahmoud, "Sitagliptin attenuates cardiomyopathy by modulating the JAK/STAT signaling pathway in experimental diabetic rats," *Drug Design, Development and Therapy*, vol. 10, pp. 2095–2107, 2016.

[33] S. Zhang, H. Xu, X. Yu, Y. Wang, F. Sun, and D. Sui, "Simvastatin ameliorates low-dose streptozotocin-induced type 2 diabetic nephropathy in an experimental rat model," *International Journal of Clinical and Experimental Medicine*, vol. 8, no. 4, pp. 6388–6396, 2015.

[34] S. I. McFarlane, R. Muniyappa, R. Francisco, and J. R. Sowers, "Clinical review 145: pleiotropic effects of statins: lipid reduction and beyond," *The Journal of Clinical Endocrinology and Metabolism*, vol. 87, no. 4, pp. 1451–1458, 2002.

[35] K. K. Ray and C. P. Cannon, "The potential relevance of the multiple lipid-independent (pleiotropic) effects of statins in the management of acute coronary syndromes," *Journal of the American College of Cardiology*, vol. 46, no. 8, pp. 1425–1433, 2005.

[36] T. Taldone, S. W. Zito, and T. T. Talele, "Inhibition of dipeptidyl peptidase-IV (DPP-IV) by atorvastatin," *Bioorganic & Medicinal Chemistry Letters*, vol. 18, no. 2, pp. 479–484, 2008.

[37] G. Frati, L. Schirone, I. Chimenti et al., "An overview of the inflammatory signalling mechanisms in the myocardium underlying the development of diabetic cardiomyopathy," *Cardiovascular Research*, vol. 113, no. 4, pp. 378–388, 2017.

[38] T. Yokoyama, M. Nakano, J. L. Bednarczyk, B. W. McIntyre, M. Entman, and D. L. Mann, "Tumor necrosis factor-α provokes a hypertrophic growth response in adult cardiac myocytes," *Circulation*, vol. 95, no. 5, pp. 1247–1252, 1997.

[39] G. Condorelli, C. Morisco, M. V. Latronico et al., "TNF-α signal transduction in rat neonatal cardiac myocytes: definition of pathways generating from the TNF-α receptor," *The FASEB Journal*, vol. 16, no. 13, pp. 1732–1737, 2002.

[40] T. Nishikawa, D. Edelstein, X. L. Du et al., "Normalizing mitochondrial superoxide production blocks three pathways of hyperglycaemic damage," *Nature*, vol. 404, no. 6779, pp. 787–790, 2000.

[41] G.-G. Wang, W. Li, X.-H. Lu, X. Zhao, and L. Xu, "Taurine attenuates oxidative stress and alleviates cardiac failure in type I diabetic rats," *Croatian Medical Journal*, vol. 54, no. 2, pp. 171–179, 2013.

[42] P. B. Taylor and Q. Tang, "Development of isoproterenol-induced cardiac hypertrophy," *Canadian Journal of Physiology and Pharmacology*, vol. 62, no. 4, pp. 384–389, 1984.

[43] A. Upaganlawar and R. Balaraman, "Protective effects of *Lagenaria siceraria* (Molina) fruit juice in isoproterenol induced myocardial infarction," *International Journal of Pharmacology*, vol. 6, no. 5, pp. 645–651, 2010.

[44] S. Boudina and E. D. Abel, "Diabetic cardiomyopathy, causes and effects," *Reviews in Endocrine & Metabolic Disorders*, vol. 11, no. 1, pp. 31–39, 2010.

[45] T. Inoguchi, P. Li, F. Umeda et al., "High glucose level and free fatty acid stimulate reactive oxygen species production through protein kinase C–dependent activation of NAD(P)H oxidase in cultured vascular cells," *Diabetes*, vol. 49, no. 11, pp. 1939–1945, 2000.

[46] A. C. Leite, T. G. Araujo, B. M. Carvalho, N. H. Silva, V. L. Lima, and M. B. Maia, "Parkinsonia aculeata aqueous extract fraction: biochemical studies in alloxan-induced diabetic rats," *Journal of Ethnopharmacology*, vol. 111, no. 3, pp. 547–552, 2007.

[47] P. Keul, K. Sattler, and B. Levkau, "HDL and its sphingosine-1-phosphate content in cardioprotection," *Heart Failure Reviews*, vol. 12, no. 3-4, pp. 301–306, 2007.

[48] M. Hemmati, E. Zohoori, O. Mehrpour et al., "Anti-atherogenic potential of jujube, saffron and barberry: anti-diabetic and antioxidant actions," *EXCLI Journal*, vol. 14, pp. 908–915, 2015.

[49] S. Boudina, S. Sena, B. T. O'Neill, P. Tathireddy, M. E. Young, and E. D. Abel, "Reduced mitochondrial oxidative capacity and increased mitochondrial uncoupling impair myocardial energetics in obesity," *Circulation*, vol. 112, no. 17, pp. 2686–2695, 2005.

[50] T. Silambarasan and B. Raja, "Diosmin, a bioflavonoid reverses alterations in blood pressure, nitric oxide, lipid peroxides and antioxidant status in DOCA-salt induced hypertensive rats," *European Journal of Pharmacology*, vol. 679, no. 1–3, pp. 81–89, 2012.

[51] S. E. McKim, E. Gäbele, F. Isayama et al., "Inducible nitric oxide synthase is required in alcohol-induced liver injury: studies with knockout mice," *Gastroenterology*, vol. 125, no. 6, pp. 1834–1844, 2003.

[52] A. M. Mahmoud, M. B. Ashour, A. Abdel-Moneim, and O. M. Ahmed, "Hesperidin and naringin attenuate hyperglycemia-mediated oxidative stress and proinflammatory cytokine production in high fat fed/streptozotocin-induced type 2 diabetic rats," *Journal of Diabetes and its Complications Journal of Diabetes and its Complications*, vol. 26, no. 6, pp. 483–490, 2012.

[53] A. M. Mahmoud and H. S. A. Dera, "18β-Glycyrrhetinic acid exerts protective effects against cyclophosphamide-induced hepatotoxicity: potential role of PPARγ and Nrf2 upregulation," *Genes & Nutrition*, vol. 10, no. 6, pp. 1–13, 2015.

[54] M. Seddon, Y. H. Looi, and A. M. Shah, "Oxidative stress and redox signalling in cardiac hypertrophy and heart failure," *Heart*, vol. 93, no. 8, pp. 903–907, 2007.

[55] R. A. Frieler and R. M. Mortensen, "Immune cell and other noncardiomyocyte regulation of cardiac hypertrophy and remodeling," *Circulation*, vol. 131, no. 11, pp. 1019–1030, 2015.

[56] D. L. Mann, "Innate immunity and the failing heart: the cytokine hypothesis revisited," *Circulation Research*, vol. 116, no. 7, pp. 1254–1268, 2015.

[57] S. D. Prabhu and N. G. Frangogiannis, "The biological basis for cardiac repair after myocardial infarction: from inflammation to fibrosis," *Circulation Research*, vol. 119, no. 1, pp. 91–112, 2016.

[58] B. Bozkurt, S. B. Kribbs, F. J. Clubb Jr et al., "Pathophysiologically relevant concentrations of tumor necrosis factor-α promote progressive left ventricular dysfunction and remodeling in rats," *Circulation*, vol. 97, no. 14, pp. 1382–1391, 1998.

[59] T. Kubota, C. F. McTiernan, C. S. Frye et al., "Dilated cardiomyopathy in transgenic mice with cardiac-specific overexpression of tumor necrosis factor-α," *Circulation Research*, vol. 81, no. 4, pp. 627–635, 1997.

[60] M. Sun, M. Chen, F. Dawood et al., "Tumor necrosis factor-α mediates cardiac remodeling and ventricular dysfunction after pressure overload state," *Circulation*, vol. 115, no. 11, pp. 1398–1407, 2007.

[61] D. Westermann, S. V. Linthout, S. Dhayat et al., "Tumor necrosis factor-alpha antagonism protects from myocardial inflammation and fibrosis in experimental diabetic cardiomyopathy," *Basic Research in Cardiology*, vol. 102, no. 6, pp. 500–507, 2007.

[62] M. K. Rutter, J. B. Meigs, L. M. Sullivan, R. B. D'Agostino Sr., and P. W. Wilson, "C-reactive protein, the metabolic syndrome, and prediction of cardiovascular events in the Framingham offspring study," *Circulation*, vol. 110, no. 4, pp. 380–385, 2004.

[63] S. K. Gupta, S. Dongare, R. Mathur et al., "Genistein ameliorates cardiac inflammation and oxidative stress in streptozotocin-induced diabetic cardiomyopathy in rats," *Molecular and Cellular Biochemistry*, vol. 408, no. 1-2, pp. 63–72, 2015.

[64] T. J. Guzik, S. Mussa, D. Gastaldi et al., "Mechanisms of increased vascular superoxide production in human diabetes mellitus: role of NAD(P)H oxidase and endothelial nitric oxide synthase," *Circulation*, vol. 105, no. 14, pp. 1656–1662, 2002.

[65] Y. Tan, T. Ichikawa, J. Li et al., "Diabetic downregulation of Nrf2 activity via ERK contributes to oxidative stress-induced insulin resistance in cardiac cells in vitro and in vivo," *Diabetes*, vol. 60, no. 2, pp. 625–633, 2011.

[66] H. C. Volz, C. Seidel, D. Laohachewin et al., "HMGB1: the missing link between diabetes mellitus and heart failure," *Basic Research in Cardiology*, vol. 105, no. 6, pp. 805–820, 2010.

[67] F. Kim, M. Pham, I. Luttrell et al., "Toll-like receptor-4 mediates vascular inflammation and insulin resistance in diet-induced obesity," *Circulation Research*, vol. 100, no. 11, pp. 1589–1596, 2007.

[68] S. B. Haudek, G. E. Taffet, M. D. Schneider, and D. L. Mann, "TNF provokes cardiomyocyte apoptosis and cardiac remodeling through activation of multiple cell death pathways," *The Journal of Clinical Investigation*, vol. 117, no. 9, pp. 2692–2701, 2007.

[69] R. G. Baker, M. S. Hayden, and S. Ghosh, "NF-kappaB, inflammation, and metabolic disease," *Cell Metabolism*, vol. 13, no. 1, pp. 11–22, 2011.

[70] K. Venkatachalam, B. Venkatesan, A. J. Valente et al., "WISP1, a pro-mitogenic, pro-survival factor, mediates tumor necrosis factor-α (TNF-α)-stimulated cardiac fibroblast proliferation but inhibits TNF-α-induced cardiomyocyte death," *The Journal of Biological Chemistry*, vol. 284, no. 21, pp. 14414–14427, 2009.

[71] Y. H. Chen, B. Feng, and Z. W. Chen, "Statins for primary prevention of cardiovascular and cerebrovascular events in diabetic patients without established cardiovascular diseases: a meta-analysis," *Experimental and Clinical Endocrinology & Diabetes*, vol. 120, no. 2, pp. 116–120, 2012.

[72] S. V. Linthout, A. Riad, N. Dhayat et al., "Anti-inflammatory effects of atorvastatin improve left ventricular function in experimental diabetic cardiomyopathy," *Diabetologia*, vol. 50, no. 9, pp. 1977–1986, 2007.

[73] Q. M. Dai, J. Lu, and N. F. Liu, "Fluvastatin attenuates myocardial interstitial fibrosis and cardiac dysfunction in diabetic rats by inhibiting over-expression of connective tissue growth factor," *Chinese Medical Journal*, vol. 124, no. 1, pp. 89–94, 2011.

Hindawi
Oxidative Medicine and Cellular Longevity
Volume 2017, Article ID 8095825, 13 pages
https://doi.org/10.1155/2017/8095825

Research Article

Febuxostat Modulates MAPK/NF-κBp65/TNF-α Signaling in Cardiac Ischemia-Reperfusion Injury

Sana Irfan Khan,[1] Rajiv Kumar Malhotra,[1] Neha Rani,[1] Anil Kumar Sahu,[1] Ameesha Tomar,[1] Shanky Garg,[1] Tapas Chandra Nag,[2] Ruma Ray,[3] Shreesh Ojha,[4] Dharamvir Singh Arya,[1] and Jagriti Bhatia[1]

[1]*Department of Pharmacology, Cardiovascular Research Laboratory, All India Institute of Medical Sciences, New Delhi, India*
[2]*Department of Anatomy, All India Institute of Medical Sciences, New Delhi, India*
[3]*Department of Pathology, All India Institute of Medical Sciences, New Delhi, India*
[4]*Department of Pharmacology and Therapeutics, College of Medicine and Health Sciences, United Arab Emirates University, Abu Dhabi, UAE*

Correspondence should be addressed to Shreesh Ojha; shreeshojha@uaeu.ac.ae and Jagriti Bhatia; jagriti2012@gmail.com

Received 12 May 2017; Accepted 2 July 2017; Published 24 August 2017

Academic Editor: Mohamed M. Abdel-Daim

Xanthine oxidase and xanthine dehydrogenase have been implicated in producing myocardial damage following reperfusion of an occluded coronary artery. We investigated and compared the effect of febuxostat and allopurinol in an experimental model of ischemia-reperfusion (IR) injury with a focus on the signaling pathways involved. Male Wistar rats were orally administered vehicle (CMC) once daily (sham and IR + control), febuxostat (10 mg/kg/day; FEB10 + IR), or allopurinol (100 mg/kg/day; ALL100 + IR) for 14 days. On the 15th day, the IR-control and treatment groups were subjected to one-stage left anterior descending (LAD) coronary artery ligation for 45 minutes followed by a 60-minute reperfusion. Febuxostat and allopurinol pretreatment significantly improved cardiac function and maintained morphological alterations. They also attenuated oxidative stress and apoptosis by suppressing the expression of proapoptotic proteins (Bax and caspase-3), reducing TUNEL-positive cells, and increasing the level of antiapoptotic proteins (Bcl-2). The MAPK-based molecular mechanism revealed suppression of active JNK and p38 proteins concomitant with the rise in ERK1/ERK2, a prosurvival kinase. Additionally, a reduction in the level of inflammatory markers (TNF-α, IL-6, and NF-κB) was also observed. The changes observed with febuxostat were remarkable in comparison with those observed with allopurinol. Febuxostat protects relatively better against IR injury than allopurinol by suppressing inflammation and apoptosis mediating the MAPK/NF-κBp65/TNF-α pathway.

1. Introduction

Ischemic heart disease is the major cause of morbidity and mortality worldwide. Ischemia stimulates metabolic and ionic disturbance in the myocardium and leads to rapid deterioration of cardiac function. Hence, thrombolytic therapy or primary percutaneous coronary intervention is imperative for salvaging the myocardium and improving clinical outcome [1]. However, restoration of blood flow to the ischemic myocardium termed reperfusion unavoidably leads to a number of complications such as stunning (diminished contractile function), rhythm abnormalities, and sequentially heart failure. Paradoxically, reperfusion may also induce death of cardiomyocytes which were viable prior to therapeutic procedure and can worsen infarct size, an entity termed myocardial ischemia-reperfusion (IR) injury [2]. Therefore, developments of effective therapeutic strategies are necessary to protect heart against the inimical consequences of reperfusion injury.

There are substantial evidences that oxidative stress plays a crucial role in IR injury [3]. Oxidative stress in turn produces mitochondrial impairment which leads to the

release of inflammatory cytokines and subsequent cell death [4, 5]. Subsequently, there is stimulation of intracellular signaling pathways such as mitogen-activated protein kinases (MAPKs) [6]. The subfamilies of MAPKs identified in the cardiomyocyte are c-Jun NH-terminal kinases (JNKs), extracellular signal-regulated kinase-1/2 (ERK1/2, also known as p42/p44 MAPK), and p38 MAPKs [7]. The activation of MAPKs may further activate transcription factors, inducing exaggerated synthesis of proinflammatory cytokines, subsequently triggering inflammatory responses and institution of the apoptotic cascade [8]. NF-κB is a nuclear transcription factor which regulates gene expression critical to inflammation and apoptosis during various pathologies including IR injury [9–11]. NF-κB, when inactive, is sequestered in the cytoplasm, where it is bound by the IκB family proteins including IκB-α. Upon stimulation, NF-κB gets phosphorylated and IκB-α is degraded by IKK. The NF-κB subunits translocate from the cytoplasm to the nucleus where they induce gene expression of inflammatory cytokines [11]. The role of NF-κB subunit p65 has been demonstrated in different ischemic reperfusion injuries including cardiac injury [12–14].

Xanthine oxidase (XO) is involved in free radical generation following hypoxia as well as during reperfusion [15, 16]. Under normal physiological conditions, XO occurs mainly in the dehydrogenase form (XDH), while during reperfusion, the dehydrogenase form is converted to XO by posttranslational modifications [17]. Both XDH and XO are important enzymes that produce oxidative stress during reperfusion injury [18]. Allopurinol and its metabolites are structural analogues of both purines and pyrimidines, whereas febuxostat is a nonpurine inhibitor of XO. In contrast to allopurinol, febuxostat suppresses both oxidized and reduced forms of XO which may contribute to its superiority in limiting oxidative stress [17, 18]. Xanthine oxidase inhibitors (XOI) have demonstrated beneficial effects on myocardial IR injury [19]. The mitigation of oxidative stress, apoptosis, and inflammation by febuxostat has been extensively studied and documented [18, 19]. Febuxostat has also been shown to affect the MAPK pathway by inhibiting JNK phosphorylation in macrophages [20]. Since febuxostat has also demonstrated favorable outcomes in heart failure patients and ischemia-reperfusion injury is one of the precursors of heart failure, we proposed a hypothesis of the utility of febuxostat in reducing ischemia-reperfusion injury; thereby, febuxostat can be clinically translated as a preventive measure in heart failure. We have focused on the molecular pathways because to the best of our knowledge, there is no study depicting the role of XOI on MAPK modulation in the heart. Therefore, this study was conducted in order to investigate and delineate the downstream and upstream components of febuxostat- and allopurinol-mediated MAPK modulation in cardiac IR injury in rats.

2. Materials and Methods

2.1. Animals. Healthy adult male Wistar albino rats, 10 to 12 weeks old, weighing 150 to 200 g were used in the present study. The rats were maintained at standard laboratory conditions and provided food and water ad libitum. The experiments were conducted following the animal ethics approval from the Institutional Animal Ethics Committee of the All India Institute of Medical Sciences, New Delhi, India, with reference number IAEC No. 893/IAEC/15. The handling of the animals during experiments was carried out in accordance with the Indian National Science Academy Guidelines for the use and care of experimental animals.

2.2. Chemicals. Febuxostat (Febutaz) was purchased from Sun Pharma, Sikkim, India, and allopurinol (Zyloric) was purchased from GlaxoSmithKline, Mumbai, India. The drugs were suspended in carboxymethyl cellulose (0.5% CMC). The kits for TNF-α and IL-6 were purchased from RayBiotech Inc., Norcross, GA. The CK-MB kit was purchased from Logotech Private Limited, India.

The primary antibodies for caspase-3 (#9662S), Bcl-2 (#2876S), and β-actin (#4967S) were procured from Cell Signaling Technology, MA, USA, and those for Bax (#7480), NF-κBp65 (#109), p-NF-κBp65 (Ser536) (#101752), JNK (#572), p-JNK (#6254) (Thr 183/Tyr 185), ERK1/2 (#135900), p-ERK1/2 (#16982) (Thr 202/Tyr 204), and p-p38 (#17852) (Thr 180/Tyr 182) as well as anti-rabbit (#2004) and anti-goat (#2020) secondary antibodies were procured from Santa Cruz, California, USA. Antibody for p38 (#197348) was purchased from Abcam Technologies, USA.

2.3. Experimental Protocol. A total of 38 rats were randomly distributed into 4 groups. The doses of febuxostat and allopurinol were chosen based on a dose-response study in our laboratory [21] and previous studies [22]:

Group 1 (sham; $n = 8$): administered 0.5% CMC (2 mL/kg/day; p.o.) for 14 days. On day 15, IR surgery was performed and thread was passed beneath the left anterior descending (LAD) coronary artery but the coronary artery was not occluded.

Group 2 (IR-control; $n = 10$): administered 0.5% CMC (2 mL/kg/day; p.o.) for 14 days. On day 15, surgery was performed for LAD coronary artery ligation for 45 min following reperfusion for 60 min.

Group 3 (FEB10 + IR; $n = 10$): administered febuxostat (10 mg/kg/day; p.o.) for 14 days. On day 15, surgery was performed for LAD coronary artery ligation for 45 min following reperfusion for 60 min.

Group 4 (ALL100 + IR; $n = 10$): administered allopurinol (100 mg/kg/day; p.o.) for 14 days. On day 15, surgery was performed for LAD coronary artery ligation for 45 min following reperfusion for 60 min. There was no effect of febuxostat and allopurinol on normal heart (per se) in our preliminary morphological assessment (data not shown) which is in keeping with previous studies [19, 23].

2.4. Experimental Procedure for Myocardial Injury Induction and Hemodynamic Parameter Measurement. The experimental procedure followed for induction of ischemia and reperfusion and assessment of hemodynamic and ventricular function has been described by Agrawal et al. [24]. Briefly, following anesthesia with intraperitoneal injection of pentobarbitone sodium (60 mg/kg), monitoring and maintenance of body temperature were carried out at 37°C throughout the experiment. A ventral midline incision was made after opening the neck, a tracheostomy was performed, and the rats were ventilated with room air from a positive pressure respirator (TSE animal respirator, Germany) using compressed air at the rate of 70 strokes per minute and a tidal volume of 10 mL/kg. 0.9% saline was infused continuously through a polyethylene tube with which the left jugular vein was cannulated. After that, the right carotid artery was cannulated, and the cannula filled with heparinised saline was connected to a pressure transducer (Gould Statham P231D, USA) for the assessment of blood pressure (mean arterial pressure (MAP) and heart rate (HR)). A left thoracotomy was then performed at the fifth intercostal space, and the heart was exposed after opening the pericardium. After that, the LAD coronary artery was ligated using a 5-0 silk suture 4-5 mm from its origin with an atraumatic needle, and ends of this ligature were passed through a small vinyl tube to form a snare. Upon completion of this step, the heart was then returned back into the thorax. After stabilization of the animals for 15 minutes, LAD coronary artery ligation was carried out and myocardial ischemia was induced by one-stage occlusion of the LAD coronary artery by pressing the polyethylene tubing against the ventricular wall and then fixing it in place by clamping it with a hemostat (except in IR-sham rats). In addition to the above parameters, the maximum rates of rise and fall of left ventricular pressure (peak +LVdP/dt and peak −LVdP/dt) as well as of preload, that is, left ventricular end-diastolic pressure (LVEDP), were recorded using Biopac system software BSL 4.0 MP36 by introducing a sterile metal cannula into the cavity of the left ventricle. The ischemic region appeared grossly as an area of epicardial cyanosis. After 45 minutes, the snare was released gently thereby allowing reperfusion to commence which was evident from an area of hyperaemia in the previously cyanosed region. After 60 minutes of reperfusion, blood was drawn from the heart and rats were sacrificed with an overdose of pentobarbitone sodium (150 mg/kg; i.p.). Blood was withdrawn from the heart and centrifuged at 5000 rpm (Heraeus Biofuge, Germany) for 10 min to obtain serum for biochemical analysis. Hearts were then excised, rinsed in ice-cold saline, and stored for biochemical, histopathological, and ultrastructural evaluation; terminal deoxynucleotide transferase dUTP nick end labeling (TUNEL) assay; immunohistochemistry (IHC); and Western blot analysis. For biochemical estimations, hearts were stored in liquid nitrogen, whereas for immunohistochemistry, hearts were fixed in 10% buffer formalin.

2.5. Assessment of Biochemical Parameters. A 10% homogenate of the heart was prepared in ice-cold phosphate buffer (0.1 M, pH 7.4), and an aliquot was used to estimate thiobarbituric acid reactive substance (TBARS) and reduced glutathione (GSH). The supernatant obtained following the centrifugation of homogenate at 4930g for 15 minutes was used for the estimation of catalase and superoxide dismutase (SOD) activities. Serum samples were used for the estimation of lactate dehydrogenase (LDH) and creatine kinase-MB (CK-MB) isoenzyme activities and interleukin-6 (IL-6) and tumor necrosis factor-α (TNF-α) levels.

2.6. Measurement of MDA Level and Reduced GSH Content. Tissue MDA level was measured by the method published by Ohkawa et al. [25]. This method assesses the ability of MDA to react with thiobarbituric acid in acidic conditions leading to the development of pink color adducts whose absorbance was read at 532 nm.

Reduced GSH level was assessed by the method described by Moron et al. [26]. This method is based on the generation of yellow color when 5,5′-dithiobis(2-nitrobenzoic acid) (DTNB) is added to compounds containing sulfhydryl group like glutathione. The homogenate was centrifuged with equal parts of 10% tricarboxylic acid (TCA) at 5000 rpm for 10 min. The supernatant containing glutathione (which has a thiol (-SH) group) reacted with DTNB at pH 8.0 to produce a yellow-colored ion whose concentration was measured at 412 nm.

2.7. Measurement of Activities of Enzymes SOD and CAT. The activity of SOD was determined by the method described by Marklund S and Marklund G [27] measuring the extent of inhibition of pyrogallol autoxidation at pH 8.4. The activity of CAT was determined by the method described by Aebi measuring difference in H_2O_2 extinction per unit time [28].

2.8. CK-MB and LDH Enzyme Activities. The activities of myocardial enzymes, CK-MB isoenzyme and LDH, were determined in serum according to the manufacturer's instructions which have been extensively described previously [29].

2.9. Estimation of Serum TNF-α and IL-6 Levels. The levels of proinflammatory cytokines, TNF-α and IL-6, were estimated in serum following the manufacturer's instructions as previously described [29].

2.10. Histopathological Evaluation. The protocol followed for histopathological studies was described previously [30]. The formalin-fixed and paraffin-embedded heart tissues were cut to get cross sections of 5 μm thick. The sections were stained with hematoxylin and eosin (H&E) and examined by a pathologist using a light microscope (DeWinter Technologies, Italy). The pathologist was unaware of the experimental groups and treatments. Three hearts from each group were examined for histological examination and graded for the severity of changes using a score on a scale of severe (+++), moderate (++), mild (+), and nil (−).

2.11. Ultrastructural Evaluation. The protocol followed for ultrastructural studies was described previously [30]. Karnovsky's fixed heart tissues were processed and embedded in araldite CY212 to cut thin sections (70–80 nm) using an

ultracut microtome (Reichert, Australia) and stained with uranyl acetate and lead acetate. The visualization was performed using a transmission electron microscope (Morgagni 268D, Fei Company, the Netherlands) operated at 80 kV and evaluated by a cytologist masked to the experimental groups and treatments.

2.12. Immunostaining for Myocardial Apoptosis Markers. The protocol followed for immunostaining for detection of apoptosis markers in the heart was described previously [30]. The sections after deparaffinization were processed for immunostaining using primary rabbit monoclonal antibodies (mAb) against Bax, Bcl-2, and caspase-3 for 48 h followed by incubation with horse radish peroxidase- (HRP-) conjugated secondary antibodies. 3,3-Diaminobenzidine (DAB) was added for the initiation of colorimetric reaction and assessment under the light microscope (DeWinter Technologies, Italy) following the methods described [30].

2.13. Terminal Deoxynucleotidyl Transferase dUTP Nick End Labeling. The TUNEL assay for analysis of apoptosis in heart sections was performed using the ApoBrdU DNA fragmentation assay kit (Biovision, USA; #K403-50), and the steps for the assessment are described previously [9]. The sections were deparaffinized and processed to visualize the antigen-antibody interaction, and the counterstaining was then done with hematoxylin visualized under a light microscope. At least 5 fields in each slide were examined for any TUNEL-positive cells in each group by the pathologist unaware of the experimental groups and treatments.

2.14. Assessment by Western Blot. The heart tissue homogenate was prepared using RIPA buffer supplemented with protease inhibitor cocktail. The protein concentration was measured by the method described by Bradford [31]. The protocol followed for Western blotting has been described previously [32]. Briefly, each well was loaded with equal amounts of proteins (40 μg) in 10% sodium dodecyl sulfate polyacrylamide gel electrophoresis (SDS-PAGE) and then transferred to the nitrocellulose transfer membrane (Bio-Trace™ NT, Pall Corporation, USA) which was blocked for 1 h with 3% bovine serum albumin or 5% nonfat dried milk and incubated for 12 h at 4°C with primary antibodies. The primary antibodies used were against β-actin, total and phosphorylated IKK-β, total and phosphorylated NF-κBp65, total and phosphorylated p38, total and phosphorylated JNK, and total and phosphorylated ERK1/2 which were detected with HRP-conjugated anti-rabbit/anti-goat secondary antibodies. The antibody-antigen complexes were visualized using an enhanced chemiluminescence kit (Thermo Fischer Scientific Inc., USA) under the FluorChem M Protein Imaging System (ProteinSimple, USA) and were quantified using ImageJ software.

2.15. Statistical Analysis. The data were expressed as mean ± SEM. Statistical analysis was performed by ANOVA followed by the multiple comparison post hoc Bonferroni test which was done using GraphPad InStat 3 software (GraphPad Software Inc., San Diego, USA). The value of $p < 0.05$ was considered statistically significant.

3. Results

3.1. Mortality. During the course of this study, 4 out of 38 rats (translating to a mortality of 11%) died; one rat died in the IR-control group, two died in the FEB10 + IR group, and one died in ALL100 + IR group. The rats that died were not considered during statistical analysis, and the reason of the death was excessive bleeding during either carotid artery cannulation or coronary artery ligation.

3.2. XOI Improved Hemodynamic and Ventricular Dysfunction after IR. Reperfusion following cardiac ischemia in rats led to a significant fall in heart rate and mean arterial pressure (MAP) as compared to the sham group at all time points. Pretreatment with febuxostat (10 mg/kg) or allopurinol (100 mg/kg) significantly improved heart rate and MAP as compared to IR-control rats during reperfusion (Figure 1). The induction of IR also significantly depressed ventricular function as depicted by elevated LVEDP and reduced +LVdP/dtmax as well as −LVdP/dtmax as compared to the sham group at all time points (Figure 2). This was ameliorated by febuxostat and allopurinol during reperfusion. There was no significant difference between the improvements by allopurinol and febuxostat.

3.3. XOI Augmented Antioxidants, Improved Cardiac Injury, and Reduced Inflammatory Markers after IR. As depicted in Figure 3, there was a significant ($p < 0.001$) rise in oxidative stress as evidenced by an increase in the lipid peroxidation product, MDA, with a significant ($p < 0.001$) fall in the antioxidant system, that is, GSH, SOD, and catalase levels in the IR-control group when compared to the sham group. Febuxostat and allopurinol pretreatment in IR-injured rats significantly ($p < 0.001$, $p < 0.01$) reduced the level of MDA concomitant with the significant ($p < 0.001$, $p < 0.01$) rise in GSH level and also increased the activities of the endogenous antioxidants SOD and catalase in comparison to the IR-control group. Improvement by febuxostat was more significant ($p < 0.05$) when compared to that by allopurinol.

As illustrated in Figure 4, there was a significant ($p < 0.001$) increase in the CK-MB isoenzyme and LDH in the IR-control group when compared to the sham group. The XOIs also significantly ($p < 0.01$, $p < 0.05$) preserved the level of the CK-MB isoenzyme and LDH, respectively. Improvement by febuxostat was more significant ($p < 0.05$) when compared to that by allopurinol. Since inflammation is a critical point in IR injury, we assessed TNF-α and IL-6 in the serum as these are usually low in normal heart. As anticipated, we observed a significant ($p < 0.001$) increase in cytokines TNF-α and IL-6 in the IR-control group when compared to the sham group, while febuxostat and allopurinol treatment significantly downregulated TNF-α ($p < 0.001$ and $p < 0.05$) and IL-6 ($p < 0.001$ and $p < 0.05$) (Figure 4). Improvement by febuxostat was more significant ($p < 0.05$) when compared to that by allopurinol with TNF-α but not with IL-6.

3.4. XOI Preserved Myocardial Architecture Histologically and Ultrastructurally after IR. The light microscopic examination of heart sections from the myocardial IR group showed myofibrillar membrane damage with extensive

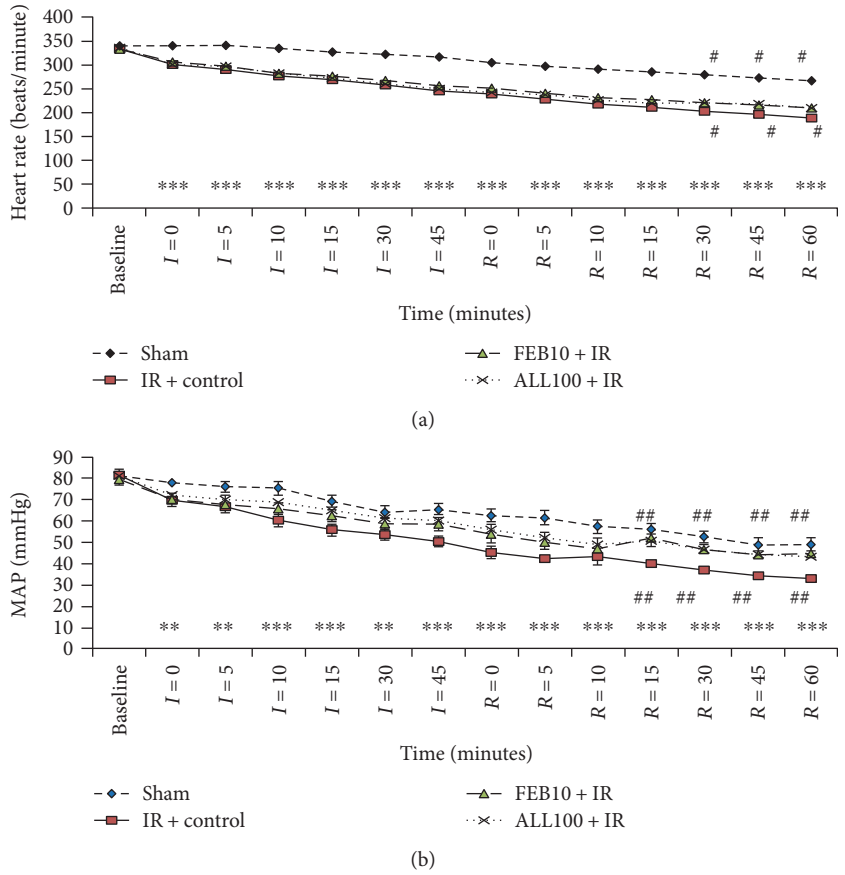

Figure 1: Effect of XOI on arterial pressure and heart rate. IR + control: ischemia-reperfusion control; FEB10 + IR: febuxostat 10 mg/kg/day + ischemia-reperfusion; ALL100 + IR: allopurinol 100 mg/kg/day + ischemia-reperfusion. Data are expressed as the mean ± SEM; $n = 6$ in each group. $^{**}p < 0.01$ and $^{***}p < 0.001$ versus sham; $^{\#}p < 0.05$ and $^{\#\#}p < 0.01$ versus IR + control.

myonecrosis, edema, and inflammatory cell infiltration as compared to the light microscopic examination of heart sections from the sham group (Figure 5). On the other hand, XOI pretreatment in the IR rats showed scanty areas of myofibril loss with necrosis with little edema and inflammatory cell infiltration. However, the degree of myofibril loss, necrosis, edema, and inflammatory cell infiltration seen with allopurinol was higher than that seen with febuxostat (Table 1). Ultrastructural examination by electron microscopy revealed cardiomyocytes with intact myofibrils, mitochondria with well-preserved cristae, and nucleus with uniformly dispersed chromatin in the sham group (Figure 5). Loss of cytoplasmic organelles, myofibril disintegration, presence of lipid droplets, mitochondrial damage, and chromatin condensation were observed in the IR-control group. Pretreatment with febuxostat and allopurinol displayed lesser mitochondrial swelling and cristae disruption and fewer vacuoles with a better preservation seen with febuxostat as compared to allopurinol.

3.5. XOI Modulated Apoptosis, MAPKs, and Inflammation after IR. The underlying molecular mechanism through which XOI exerts protection following cardiac IR was evaluated. The expression of various key regulatory proteins (caspase-3, Bax, and Bcl-2) in apoptosis was studied using immunohistochemistry studies. The TUNEL assay was also carried out to detect DNA fragmentation in apoptotic nuclei. Photomicrographs represented in Figure 5 demonstrate the effect of febuxostat and allopurinol on caspase-3, Bax, and Bcl-2 proteins and TUNEL-positive cells, respectively. As anticipated, expressions of caspase-3 and Bax proteins were increased and that of Bcl-2 was decreased in the IR-control group as compared to the sham group. Moreover, TUNEL-positive cells were increased in the IR-control rats as compared to the sham group (Figure 5). The XOI pretreatment decreased caspase-3 and Bax and increased Bcl-2 levels. Further, it also reduced TUNEL-positive cells when compared with IR-control group. It was remarkable that the changes produced in the febuxostat group were more marked in comparison to those produced in the allopurinol group. We further demonstrated the role of inflammation in IR injury by assessing the expression of NF-κBp65 in the myocardium using Western blot. In rats subjected to IR, we observed significantly ($p < 0.001$) increased expression of NF-κBp65 in the myocardium, whereas XOI pretreatment significantly reduced its expression when compared to IR-control (Figure 7(b)). The levels of inflammatory markers were reduced more significantly by febuxostat ($p < 0.05$) as compared to allopurinol. We further assessed whether the cardioprotective effect of XOI was MAPK dependent by

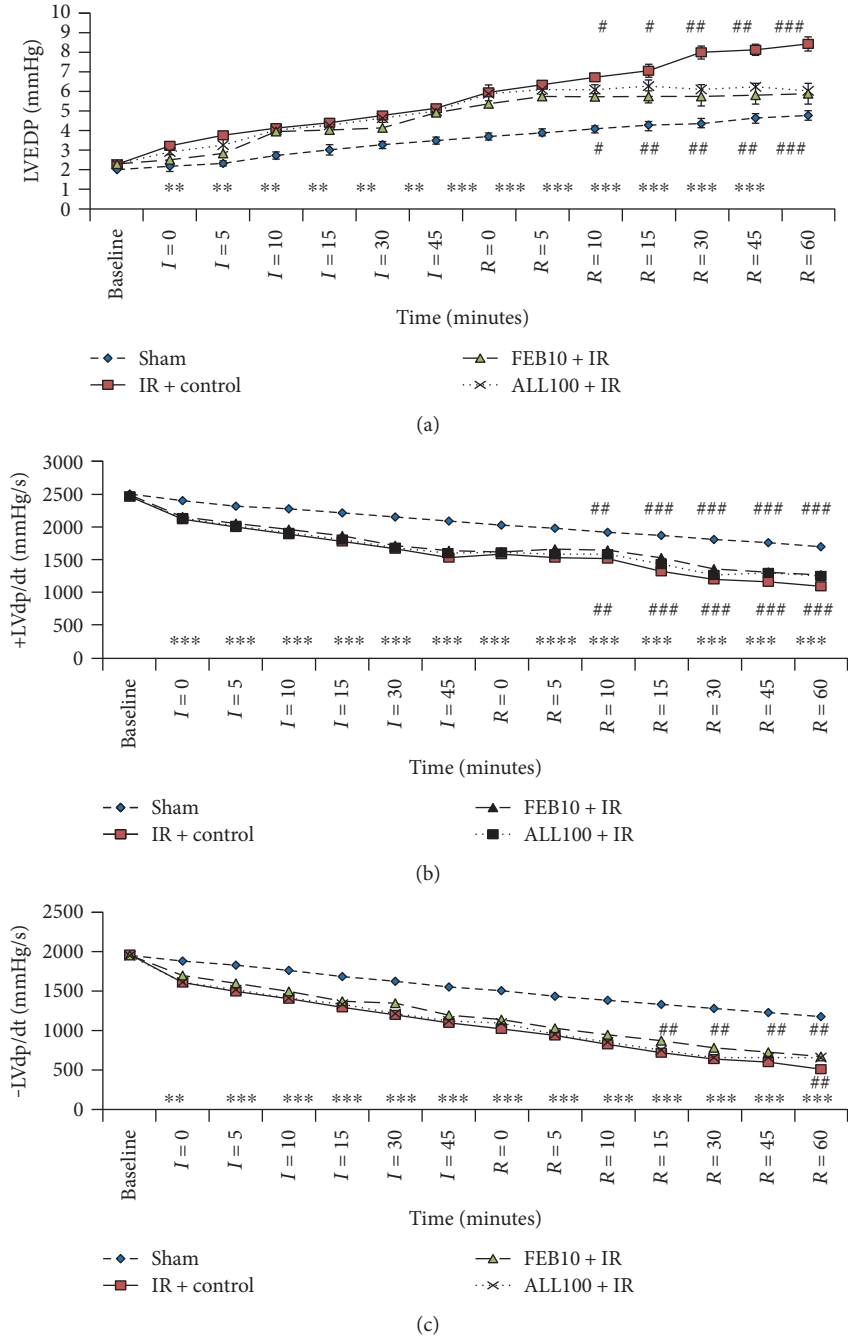

Figure 2: Effect of XOI on ventricular function. (a) LVEDP, (b) maximal positive rate of the left ventricular pressure (+LVdP/dtmax), and (c) maximal negative rate of the left ventricular pressure (−LVdP/dtmax). IR + control: ischemia-reperfusion control; FEB10 + IR: febuxostat 10 mg/kg/day + ischemia-reperfusion; ALL100 + IR: allopurinol 100 mg/kg/day + ischemia-reperfusion. Data are expressed as the mean ± SEM; $n = 6$ in each group. $^{**}p < 0.01$ and $^{***}p < 0.001$ versus sham; $^{\#}p < 0.05$, $^{\#\#}p < 0.01$, and $^{\#\#\#}p < 0.001$ versus IR + control.

investigating their effect on phosphorylation of MAPK proteins. We did not observe any significant change in total p38, JNK, and ERK protein expressions in any of the groups. Though there was a significant ($p < 0.001$) decrease in expression of p-ERK and increase in expressions of p-p38 and p-JNK in the IR-control group as compared to the sham group. These findings were normalized by febuxostat (p-ERK: $p < 0.01$, p-JNK: $p < 0.001$, and p-p38: $p < 0.001$) and allopurinol ($p < 0.05$) pretreatment. Interestingly, febuxostat increased p-ERK and decreased p-p38 and JNK more significantly ($p < 0.05$) as compared to allopurinol (Figures 7(a) and 7(b)).

4. Discussion

Although numerous studies have described the fundamental role of XO in IR injury, however, the molecular mechanisms underlying the inhibition of XO in cardiac IR injury are not

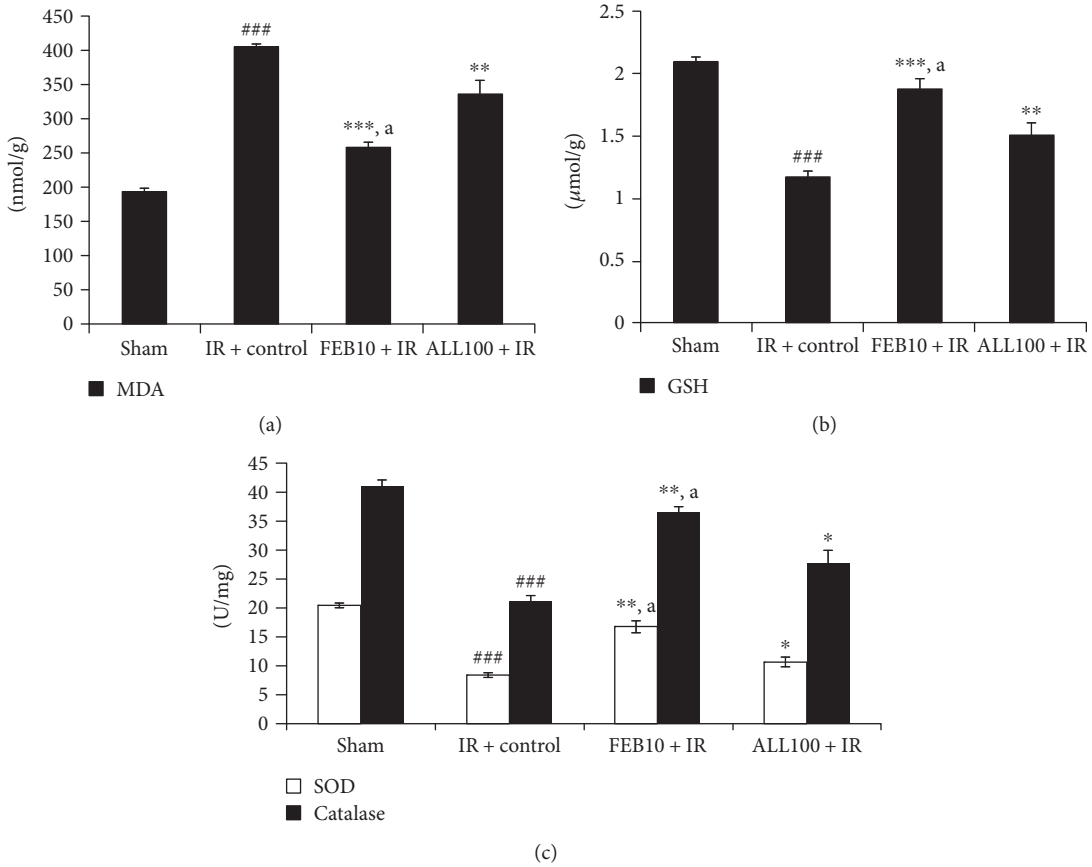

Figure 3: Effect of XOI on oxidative stress markers. (a) GSH; (b) MDA; (c) SOD and catalase. IR + control: ischemia-reperfusion control; FEB10 + IR: febuxostat 10 mg/kg/day + ischemia-reperfusion; ALL100 + IR: allopurinol 100 mg/kg/day + ischemia-reperfusion. Data are expressed as the mean ± SEM; $n = 6$ in each group. $^{*}p < 0.05$, $^{**}p < 0.01$, and $^{***}p < 0.001$ versus IR + control; $^{###}p < 0.001$ versus sham. $^{a}p < 0.05$ versus ALL100 + IR.

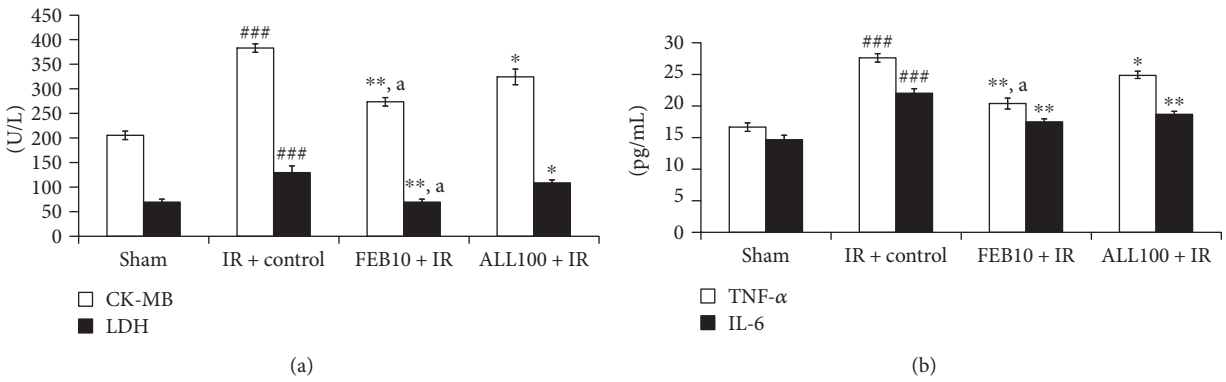

Figure 4: Effect of XOI on cardiac injury and inflammatory markers. (a) CK-MB and LDH; (b) TNF-α and IL-6. IR + control: ischemia-reperfusion control; FEB10 + IR: febuxostat 10 mg/kg/day + ischemia-reperfusion; ALL100 + IR: allopurinol 100 mg/kg/day + ischemia-reperfusion. Data are expressed as the mean ± SEM; $n = 6$ in each group. $^{*}p < 0.05$ and $^{**}p < 0.01$ versus IR + control; $^{###}p < 0.001$ versus sham. $^{a}p < 0.05$ versus ALL100 + IR.

known. Thus, our study design attempted to examine the effects of selective and potent inhibitor of XO, febuxostat, in comparison to the classical XOI, allopurinol, in a rat model of myocardial infarction. In this study, we observed that febuxostat significantly diminished ischemia-reperfusion-induced myocardial injury and the effect was superior to that of allopurinol. This was evident from suppression of oxidative stress and apoptosis in the febuxostat treatment group. We further explored the effect of febuxostat pretreatment on MAPK-mediated inflammation and observed that

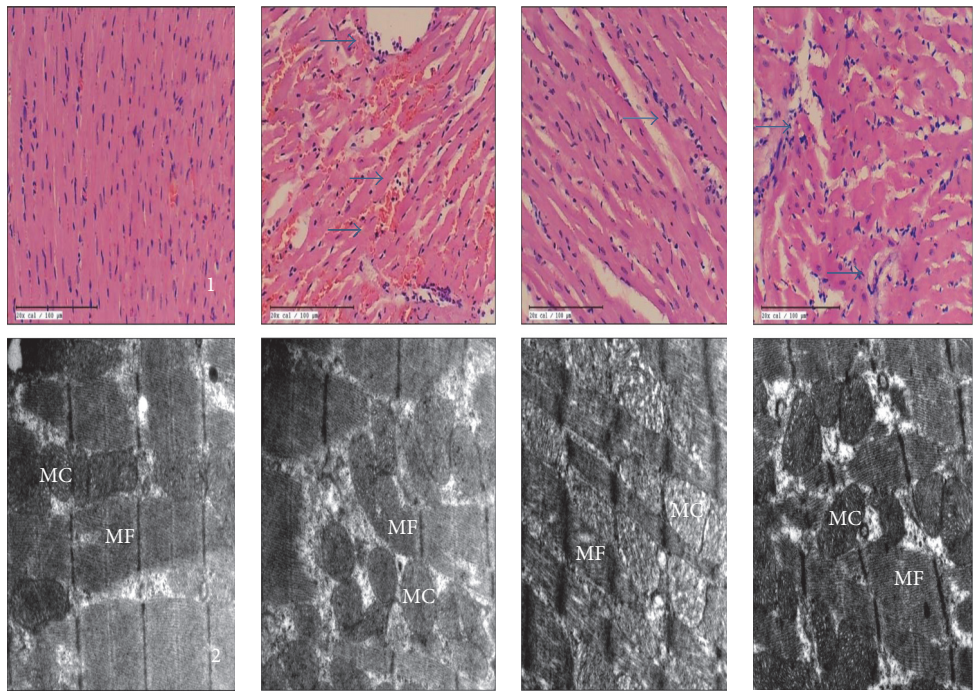

Figure 5: Effect of XOI on (a1–d1) histopathology ($n = 3$) (20x; scale bar 100 μm) and (a2–d2) ultrastructure ($n = 3$). (a) Sham; (b) IR + control: ischemia-reperfusion control; (c) FEB10 + IR: febuxostat 10 mg/kg/day + ischemia-reperfusion; (d) ALL100 + IR: allopurinol 100 mg/kg/day + ischemia-reperfusion.

Table 1: Effect of XOI on histological scoring of cardiac tissue.

	Myonecrosis	Inflammatory cells	Edema
Sham	neg	neg	neg
IR-C	3+	3+	4+
FEB10 + IR	1+	1+	1+
ALL100 + IR	2+	2+	2+

(3+) severe; (2+) moderate; (+) mild; (neg) nil. IR-C: ischemia-reperfusion control; FEB10 + IR: febuxostat 10 mg/kg/day + ischemia-reperfusion; ALL100 + IR: allopurinol 100 mg/kg/day + ischemia-reperfusion.

febuxostat pretreatment ameliorated the cardiac dysfunction induced by reperfusion injury, primarily via the activation of the ERK1/2 pathway and suppression of the p38/JNK/NF-κBp65/TNF-α pathway. Further, febuxostat modulated these regulatory proteins more markedly than allopurinol.

The rat model of myocardial IR injury is a clinically relevant model and mimics the human pathophysiological condition. This IR model has been standardized as ischemia for 45 min followed by reperfusion for 60 min in our laboratory [9, 30, 33]. The occlusion of the LAD coronary artery results in myocardial ischemia which initiates complex cascade of cellular events leading to myocardial cell death. Reperfusion (restoration of blood flow), on the other hand, aggravates myocardial injury, induces metabolic derangement, and diminishes cardiac contractile function. In the present study, the IR group exhibited significant impairment of systolic and diastolic function, depicted by a decrease in MAP, as well as by impaired inotropic and lusitropic state, represented by a fall in +LVdP/dtmax and −LVdP/dtmax, respectively, along with increased LVEDP which characterizes increased preload on the compromised heart. These hemodynamic changes were improved by pretreatment with febuxostat or allopurinol. A more pronounced and earlier onset of improvement was observed in the febuxostat group. This improvement could be attributed to the faster acting property of febuxostat. Additionally, the histological examination of heart sections in the IR group revealed inflammatory cells, necrosis, edema, and replacement of myofibrils by interfibrillar spaces. The pretreatment with XOI mitigated these changes. Further, pretreatment with febuxostat showed more marked restoration as compared to that with allopurinol. In the IR group, ultrastructural findings further corroborated the myocardial injury and swollen as well as irregular mitochondria with loss of cristae and chromatin condensation, whereas pretreatment with febuxostat showed only mild separation of the mitochondrial cristae with negligible swelling and vacuolation. This cardioprotective effect was less pronounced in the allopurinol group. The plausible reason for the cardioprotective effect of febuxostat is the inhibition of XO-mediated oxidative stress and inflammation and augmented mitochondrial protection.

XO-mediated oxidative stress has been extensively demonstrated by numerous investigators [1, 15, 33]. Its levels have also been found to increase in heart tissue during reperfusion following myocardial ischemia [15, 17]. Ischemic injury leads to energy charge depletion from the cell that subsequently results in accumulation of hypoxanthine from ATP

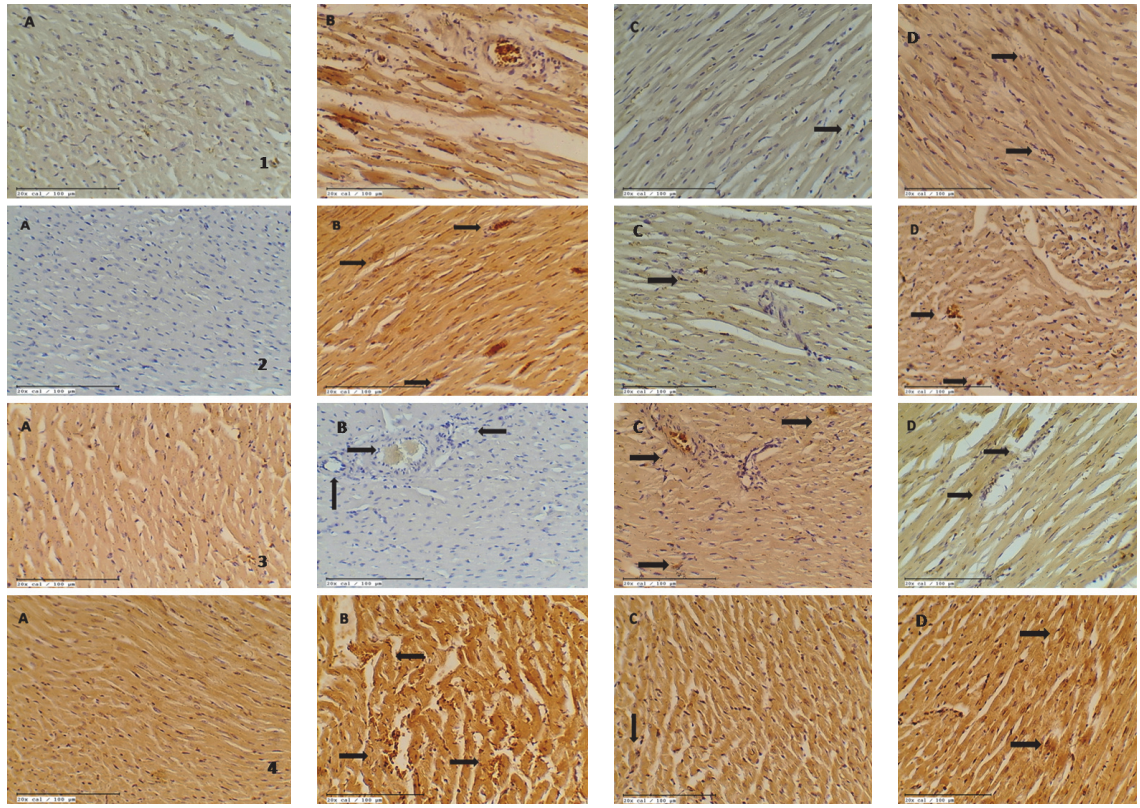

Figure 6: Effect of XOI on (a1–d1) caspase-3 immunohistochemistry ($n = 3$) (20x; scale bar 100 μm), (a2–d2) Bax immunohistochemistry ($n = 3$) (20x; scale bar 100 μm), (a3–d3) Bcl-2 immunohistochemistry ($n = 3$) (20x; scale bar 100 μm), and (a4–d4) TUNEL positivity (20x; scale bar 100 μm). (a) Sham; (b) IR + control: ischemia-reperfusion control; (c) FEB10 + IR: febuxostat 10 mg/kg/day + ischemia-reperfusion; (d) ALL100 + IR: allopurinol 100 mg/kg/day + ischemia-reperfusion.

breakdown as well as concomitant conversion of xanthine dehydrogenase (XDH) to its XO isoform, a reaction which is mediated by sulfhydryl oxidation [17]. XDH exhibits NADH oxidase activity under acidic conditions like ischemia and XDH oxidizes NADH rather than xanthine, it has also been shown that a tissue likely remains in a reductive state (low NAD+-to-NADH ratio) in the early reperfusion period which favors oxidative stress in terms of ROS generation by XDH. Therefore, accumulated hypoxanthine as well as a reductive state (higher NADH relative to NAD+) during reperfusion produces a burst in superoxide production [17, 34]. Interestingly, while allopurinol can inhibit the generation of superoxide by XO, the drug has no effect on the NADH oxidase activity of XDH. Therefore, we hypothesized that febuxostat should be superior to allopurinol in ameliorating myocardial IR injury. Febuxostat has been shown to attenuate pressure overload in the left ventricle as well as it protects the kidneys from IR injury via suppression of oxidative stress [19, 35]. From our study, it is evident that febuxostat alleviated oxidative stress by restoring the antioxidant enzymes SOD and catalase and preventing depletion of GSH concomitant with the inhibition of lipid peroxidation as evidenced by decreased MDA formation. Febuxostat exerted a significantly better antioxidant effect than allopurinol. Oxidative stress-mediated lipid peroxidation also denatures cellular proteins and DNA resulting in loss of membrane integrity. Consequently, cardiac enzymes such as LDH and CK-MB are released from the intracellular compartment to the extracellular fluid [36, 37]. In our study, we observed that cardiac enzyme levels were raised in the IR-control group. However, febuxostat pretreatment reduced the serum LDH and CK-MB levels more potently as compared to allopurinol pretreatment. This further validates that febuxostat has a superior antioxidant property. Studies have proposed that MAPK pathway activation is mediated via oxidative stress by the inactivation of MAPK phosphatases (MKPs). It has been demonstrated that ERK is responsible for promoting cell survival, while p38 MAPKs/JNKs are involved in cell death and a tight regulation of these pathways is an important determinant of cell survival [37–39].

The free radicals generated from the mitochondria induces DNA damage and membrane peroxidation that promotes outer membrane permeabilization and facilitates translocation of Bax and cytochrome C from the mitochondria to the cytosol with subsequent activation of caspases to initiate and execute apoptosis [32, 40]. The antiapoptotic protein, Bcl-2, maintains the external mitochondrial membrane integrity and thereby prevents the release of cytochrome C from the mitochondria. On the contrary, the proapoptotic protein, Bax, induces mitochondrial injury that

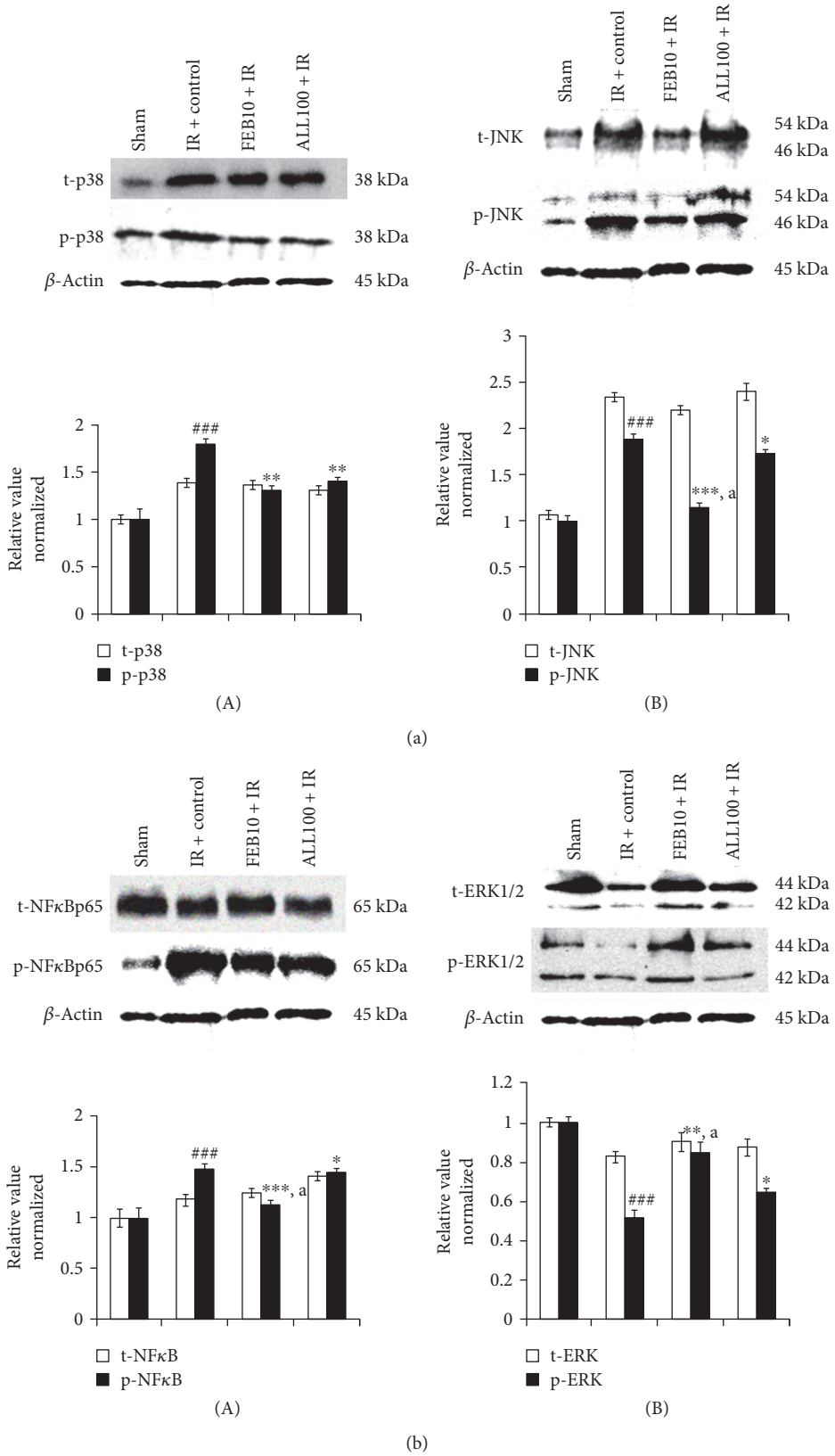

Figure 7: Effect of XOI on MAPK protein expressions. (a) (A) p38 and p-p38 and (B) JNK and p-JNK; (b) (A) NFκBp65 and p-NFκBp65 and (B) ERK1/2 and p-ERK1/2. Protein expressions are normalized with β-actin. All the values are expressed as mean ± SEM; $n = 3$ in each group. $^{*}p < 0.05$, $^{**}p < 0.01$, and $^{***}p < 0.001$ versus IR + control; $^{\#\#\#}p < 0.001$ versus sham. $^{a}p < 0.05$ versus ALL100 + IR.

results in cell death [41, 42]. MAPK also arbitrates apoptosis directly by activating Bax during reperfusion. The apoptosis-induced cardiac damage following IR is halted by the activation of ERK1/ERK2 [43]. There is substantial evidence regarding improvement of cardiac function following IR injury by suppressing cardiomyocyte apoptosis through targeted inhibition of p38 MAPK [36, 39, 44]. The present study findings reveal for the first time that febuxostat modulates the MAPK in the heart tissue as evidenced by enhanced activities of ERK1/ERK2, increased Bcl-2, decreased Bax, reduced caspase-3, and fewer DNA fragments in febuxostat-treated groups relative to the untreated group. This observation is in affirmation with the MAPK-regulating property of febuxostat explored previously in the macrophages [20], whereas allopurinol, on the other hand, demonstrated a milder effect when compared to febuxostat. It appears from the present study that MAPK is a downstream component of oxidative stress and an upstream component of apoptosis. Furthermore, we can convincingly state that oxidative stress can activate apoptosis directly as well as indirectly by modulation of the MAPK pathway.

The components of the MAPK pathway are known to induce nuclear factor kappa-light-chain-enhancer of activated B cells (NF-κB), an important inflammatory transcription factor [10, 17, 34]. NF-κB plays a key role in the process of inflammation and apoptosis induced by IR injury [10]. Previous studies have shown that the NF-κB subunit p65 is activated during IR injury in the rat steatotic liver [13]. This has been further supported by the suppression of NF-κB using its inhibitor BAY 11-7802 or the inhibition of IκB phosphorylation which has been shown to reduce the inflammation and apoptosis induced by myocardial as well as cerebral IR injury [12, 14]. Previous studies have also shown that NF-κB activation is associated with the release of proinflammatory cytokines such as TNF-α [9, 13, 18]. In addition, the TNF-α-induced secretion of IL-6 is mediated by NF-κB signaling as evidenced by reduced expression of IL-6 when NF-κB is inhibited [45]. It was also evident from our study that upon reperfusion, there was increased phosphorylation of NF-κB and IκB, along with increased expression of TNF-α and IL-6. This transcription factor phosphorylation and cytokine increase were significantly diminished by febuxostat pretreatment. This is in agreement with the previously documented NF-κB inhibitory effect of febuxostat [34]. In the present study, however, a significantly lower protection was observed with allopurinol. These two drugs have been previously compared in intestinal IR injury where febuxostat emerged superior to allopurinol in ameliorating the reperfusion injury [22]. Wang and colleagues have also demonstrated the antioxidant and antiapoptotic effect of XOI on cardiac ischemia-reperfusion injury *in vitro* and *in vivo* [19]. To our knowledge, the present study for the first time focused on the signaling pathway through which XOI mediated their cardioprotective effect. A convincing reason for the superior effect of febuxostat as a cardioprotective agent in IR injury is the ability of this drug to inhibit both XDH and XO thereby abolishing the NADH-derived as well as hypoxanthine-derived sources of free radical-mediated cell damage.

To conclude, using an experimental model of cardiac IR injury, our study provides convincing data on the improved efficacy of febuxostat in ameliorating the cardiac damage induced by IR injury following LAD coronary artery occlusion. The effect of febuxostat appears to be mediated by attenuation of XO-mediated oxidative stress as well as suppression of apoptosis and inflammation mediating the MAPK signaling pathway. In view of the favorable properties of febuxostat vis a vis allopurinol, the former may be further evaluated for its usefulness in halting the damage produced in the heart by revascularization procedures in humans.

Conflicts of Interest

The authors declare that they have no conflicts of interest.

Authors' Contributions

Sana Irfan Khan and Rajiv Kumar Malhotra contributed equally to this work.

Acknowledgments

The authors are thankful to Mr. B.M. Sharma and Mr. Deepak Sharma for their technical assistance. The research in the laboratory of Shreesh Ojha is supported by the University Program for Advanced Research and Center-Based Interdisciplinary grants from the Office of the Deputy Vice Chancellor of Research and Graduate Studies of United Arab Emirates University, Al Ain, UAE.

References

[1] A. Frank, M. Bonney, S. Bonney, L. Weitzel, M. Koeppen, and T. Eckle, "Myocardial ischemia reperfusion injury: from basic science to clinical bedside," *Seminars in Cardiothoracic and Vascular Anesthesia*, vol. 16, pp. 123–132, 2012.

[2] K. Raedschelders, D. M. Ansley, and D. D. Chen, "The cellular and molecular origin of reactive oxygen species generation during myocardial ischemia and reperfusion," *Pharmacology & Therapeutics*, vol. 133, pp. 230–255, 2012.

[3] Y. Li, D. Zhong, L. Lei, Y. Jia, H. Zhou, and B. Yang, "Propofol prevents renal ischemia-reperfusion injury via inhibiting the oxidative stress pathways," *Cellular Physiology and Biochemistry*, vol. 37, pp. 14–26, 2015.

[4] W. Du, Z. Pan, X. Chen et al., "By targeting Stat3 microRNA-17-5p promotes cardiomyocyte apoptosis in response to ischemia followed by reperfusion," *Cellular Physiology and Biochemistry*, vol. 34, pp. 955–965, 2014.

[5] T. Zhou, C. C. Chuang, and L. Zuo, "Molecular characterization of reactive oxygen species in myocardial ischemia-reperfusion injury," *BioMed Research International*, vol. 2015, Article ID 864946, 9 pages, 2015.

[6] G. Vassalli, G. Milano, and T. Moccetti, "Role of mitogen-activated protein kinases in myocardial ischemia-reperfusion injury during heart transplantation," *Journal of Transplantation*, vol. 2012, Article ID 928954, 16 pages, 2012.

[7] C. M. Walshe, J. G. Laffey, L. Kevin, and D. O'Toole, "Sepsis protects the myocardium and other organs from subsequent ischaemic/reperfusion injury via a MAPK-dependent

mechanism," *Intensive Care Medicine Experimental*, vol. 3, p. 35, 2015.

[8] X. Guo, J. Shang, Y. Deng, X. Yuan, D. Zhu, and H. Liu, "Alterations in left ventricular function during intermittent hypoxia: possible involvement of O-GlcNAc protein and MAPK signaling," *International Journal of Molecular Medicine*, vol. 36, pp. 150–158, 2015.

[9] K. Suchal, S. Malik, N. Gamad et al., "Kaempferol attenuates myocardial ischemic injury via inhibition of MAPK signaling pathway in experimental model of myocardial ischemia-reperfusion injury," *Oxidative Medicine and Cellular Longevity*, vol. 2016, Article ID 7580731, 10 pages, 2016.

[10] L. Ma, H. Liu, Z. Xie et al., "Ginsenoside Rb3 protects cardiomyocytes against ischemia-reperfusion injury via the inhibition of JNK-mediated NF-kappaB pathway: a mouse cardiomyocyte model," *PloS One*, vol. 9, article e103628, 2014.

[11] S. E. Stokes and L. M. Winn, "NF-kappaB signaling is increased in HD3 cells following exposure to 1,4-benzoquinone: role of reactive oxygen species and p38-MAPK," *Toxicological Sciences*, vol. 137, pp. 303–310, 2014.

[12] Y. S. Kim, J. S. Kim, J. S. Kwon et al., "BAY 11-7082, a nuclear factor-kappaB inhibitor, reduces inflammation and apoptosis in a rat cardiac ischemia-reperfusion injury model," *International Heart Journal*, vol. 51, pp. 348–353, 2010.

[13] S. Ramachandran, J. M. Liaw, J. Jia et al., "Ischemia-reperfusion injury in rat steatotic liver is dependent on NFkappaB P65 activation," *Transplant Immunology*, vol. 26, pp. 201–206, 2012.

[14] J. H. Gu, J. B. Ge, M. Li, F. Wu, W. Zhang, and Z. H. Qin, "Inhibition of NF-kappaB activation is associated with anti-inflammatory and anti-apoptotic effects of ginkgolide B in a mouse model of cerebral ischemia/reperfusion injury," *European Journal of Pharmaceutical Sciences*, vol. 47, pp. 652–660, 2012.

[15] N. Ozbek, E. B. Bali, and C. Karasu, "Quercetin and hydroxytyrosol attenuates xanthine/xanthine oxidase-induced toxicity in H9c2 cardiomyocytes by regulation of oxidative stress and stress-sensitive signaling pathways," *General Physiology and Biophysics*, vol. 34, pp. 407–414, 2015.

[16] Y. S. Zhang, B. Liu, X. J. Luo et al., "A novel function of nuclear nonmuscle myosin regulatory light chain in promotion of xanthine oxidase transcription after myocardial ischemia/reperfusion," *Free Radical Biology & Medicine*, vol. 83, pp. 115–128, 2015.

[17] D. N. Granger and P. R. Kvietys, "Reperfusion injury and reactive oxygen species: the evolution of a concept," *Redox Biology*, vol. 6, pp. 524–551, 2015.

[18] J. Saban-Ruiz, A. Alonso-Pacho, M. Fabregate-Fuente, and G.-Q. C. Puertade la, "Xanthine oxidase inhibitor febuxostat as a novel agent postulated to act against vascular inflammation," *Anti-Inflammatory & Anti-Allergy Agents in Medicinal Chemistry*, vol. 12, pp. 94–99, 2013.

[19] S. Wang, Y. Li, X. Song et al., "Febuxostat pretreatment attenuates myocardial ischemia/reperfusion injury via mitochondrial apoptosis," *Journal of Translational Medicine*, vol. 13, p. 209, 2015.

[20] J. Nomura, N. Busso, A. Ives et al., "Febuxostat, an inhibitor of xanthine oxidase, suppresses lipopolysaccharide-induced MCP-1 production via MAPK phosphatase-1-mediated inactivation of JNK," *PloS One*, vol. 8, article e75527, 2013.

[21] B. Krishnamurthy, N. Rani, S. Bharti et al., "Febuxostat ameliorates doxorubicin-induced cardiotoxicity in rats," *Chemico-Biological Interactions*, vol. 237, pp. 96–103, 2015.

[22] A. N. Shafik, "Febuxostat improves the local and remote organ changes induced by intestinal ischemia/reperfusion in rats," *Digestive Diseases and Sciences*, vol. 58, pp. 650–659, 2013.

[23] J. D. Gladden, B. R. Zelickson, J. L. Guichard et al., "Xanthine oxidase inhibition preserves left ventricular systolic but not diastolic function in cardiac volume overload," *American Journal of Physiology. Heart and Circulatory Physiology*, vol. 305, pp. H1440–H1450, 2013.

[24] Y. O. Agrawal, P. K. Sharma, B. Shrivastava et al., "Hesperidin produces cardioprotective activity via PPAR-gamma pathway in ischemic heart disease model in diabetic rats," *PloS One*, vol. 9, article e111212, 2014.

[25] H. Ohkawa, N. Ohishi, and K. Yagi, "Assay for lipid peroxides in animal tissues by thiobarbituric acid reaction," *Analytical Biochemistry*, vol. 95, pp. 351–358, 1979.

[26] M. S. Moron, J. W. Depierre, and B. Mannervik, "Levels of glutathione, glutathione reductase and glutathione S-transferase activities in rat lung and liver," *Biochimica et Biophysica Acta*, vol. 582, pp. 67–78, 1979.

[27] S. Marklund and G. Marklund, "Involvement of the superoxide anion radical in the autoxidation of pyrogallol and a convenient assay for superoxide dismutase," *European Journal of Biochemistry / FEBS*, vol. 47, pp. 469–474, 1974.

[28] H. Aebi, "Catalase in vitro," *Methods in Enzymology*, vol. 105, pp. 121–126, 1984.

[29] K. Suchal, S. Malik, S. I. Khan et al., "Molecular pathways involved in the amelioration of myocardial injury in diabetic rats by kaempferol," *International Journal of Molecular Sciences*, L. Speranza, J. L. Quiles and S. Franceschelli, Eds., vol. 18, no. 5, p. 1001, 2017.

[30] N. Rani, S. Bharti, M. Manchanda et al., "Regulation of heat shock proteins 27 and 70, p-Akt/p-eNOS and MAPKs by naringin dampens myocardial injury and dysfunction in vivo after ischemia/reperfusion," *PloS One*, vol. 8, article e82577, 2013.

[31] M. M. Bradford, "A rapid and sensitive method for the quantitation of microgram quantities of protein utilizing the principle of protein-dye binding," *Analytical Biochemistry*, vol. 72, pp. 248–254, 1976.

[32] E. Hochhauser, E. Lahat, M. Sultan et al., "Ultra low dose delta 9-tetrahydrocannabinol protects mouse liver from ischemia reperfusion injury," *Cellular Physiology and Biochemistry*, vol. 36, pp. 1971–1981, 2015.

[33] S. Malik, A. K. Sharma, S. Bharti et al., "In vivo cardioprotection by pitavastatin from ischemic-reperfusion injury through suppression of IKK/NF-kappaB and upregulation of pAkt-eNOS," *Journal of Cardiovascular Pharmacology*, vol. 58, pp. 199–206, 2011.

[34] H. J. Lee, K. H. Jeong, Y. G. Kim et al., "Febuxostat ameliorates diabetic renal injury in a streptozotocin-induced diabetic rat model," *American Journal of Nephrology*, vol. 40, pp. 56–63, 2014.

[35] H. Tsuda, N. Kawada, J. Y. Kaimori et al., "Febuxostat suppressed renal ischemia-reperfusion injury via reduced oxidative stress," *Biochemical and Biophysical Research Communications*, vol. 427, pp. 266–272, 2012.

[36] L. T. Retamoso, M. E. J. Silveira, F. D. Lima et al., "Increased xanthine oxidase-related ROS production and TRPV1

synthesis preceding DOMS post-eccentric exercise in rats," *Life Sciences*, vol. 152, pp. 52–59, 2016.

[37] D. Yu, M. Li, Y. Tian, J. Liu, and J. Shang, "Luteolin inhibits ROS-activated MAPK pathway in myocardial ischemia/ reperfusion injury," *Life Sciences*, vol. 122, pp. 15–25, 2015.

[38] C. Li, J. He, Y. Gao, Y. Xing, J. Hou, and J. Tian, "Preventive effect of total flavones of Choerospondias axillaries on ischemia/ reperfusion-induced myocardial infarction-related MAPK signaling pathway," *Cardiovascular Toxicology*, vol. 14, pp. 145–152, 2014.

[39] X. F. Gao, Y. Zhou, D. Y. Wang, K. S. Lew, A. M. Richards, and P. Wang, "Urocortin-2 suppression of p38-MAPK signaling as an additional mechanism for ischemic cardioprotection," *Molecular and Cellular Biochemistry*, vol. 398, pp. 135–146, 2015.

[40] M. L. Circu and T. Y. Aw, "Reactive oxygen species, cellular redox systems, and apoptosis," *Free Radical Biology & Medicine*, vol. 48, pp. 749–762, 2010.

[41] C. Y. Chien, C. T. Chien, and S. S. Wang, "Progressive thermopreconditioning attenuates rat cardiac ischemia/ reperfusion injury by mitochondria-mediated antioxidant and antiapoptotic mechanisms," *The Journal of Thoracic and Cardiovascular Surgery*, vol. 148, pp. 705–713, 2014.

[42] J. Huang, X. Zhang, F. Qin et al., "Protective effects of Millettia pulchra flavonoids on myocardial ischemia in vitro and in vivo," *Cellular Physiology and Biochemistry*, vol. 35, pp. 516–528, 2015.

[43] H. Wang, Q. W. Zhu, P. Ye et al., "Pioglitazone attenuates myocardial ischemia-reperfusion injury via up-regulation of ERK and COX-2," *Bioscience Trends*, vol. 6, pp. 325–332, 2012.

[44] C. J. Thomas, D. C. Ng, N. Patsikatheodorou et al., "Cardioprotection from ischaemia-reperfusion injury by a novel flavonol that reduces activation of p38 MAPK," *European Journal of Pharmacology*, vol. 658, pp. 160–167, 2011.

[45] C. Lee, J. I. Oh, J. Park et al., "TNF alpha mediated IL-6 secretion is regulated by JAK/STAT pathway but not by MEK phosphorylation and AKT phosphorylation in U266 multiple myeloma cells," *BioMed Research International*, vol. 2013, Article ID 580135, 8 pages, 2013.